Late transition metal Fischer carbene complexes of group 9 and 11: synthesis and application

by

Granny Kabelo Ramollo

Submitted in partial fulfilment of the requirements for the degree

PHILOSOPHIAE DOCTOR

In the Faculty of Science

School of Chemistry

University of the Witwatersrand

Johannesburg

December 2020

Supervisor: Prof. D. I. Bezuidenhout

Co-Supervisors: Dr. J. L. van Wyk

Dr. I. Kotze

Declaration

I, Granny Kabelo Ramollo, declare that the thesis, which I hereby submit for the degree PhD Chemistry at the University of the Witwatersrand, is my own work and has not been previously submitted by me for a degree at this or any other tertiary institution.

The study is a continuation of the MSc project preceding this degree, and all data from my MSc. dissertation have been clearly referenced and cited in this thesis.

The hydroformylation catalysis was completed by Mr. Sthephen De Doncker, Dr. Sheperd Siangwata, and Dr. Tshegofatso L. Mashabane in the laboratories of Prof. Gregory S. Smith at University of Cape Town.

The transfer hydrogenation catalysis was completed by me in collaboration with Dr. Stephen O. Ojwach, University of KwaZulu-Natal and Dr. Juanita L. van Wyk, at the University of the Witwatersrand.

Collection and refinement of single crystal X-ray diffraction data were performed by Prof. Andreas Lemmerer, Dr. Manuel A. Fernandes, and Dr. George Kleinhans at the University of the Witwatersrand.

The cyclic voltammetry measurements, computational calculations, and EPR spectroscopy experiments reported in Chapter 4, were completed by Mr. Maurice P. Schrick and Ms. Cristina-Maria Hirshbiegel in the laboratories of Prof. Katja Heinze, Johannes Gutenberg University of Mainz, Germany.

The expertise of Dr. George Kleinhans and Dr. María J. López-Gómez, in the synthesis and crystallization of highly reactive organometallic complexes, is hence acknowledged.

Results obtained from this study have been published in:

Tunable Rh(I) Fischer Carbene Complexes for Application in the Hydroformylation of 1-octene

T. L. Mashabane, G. K. Ramollo, G. Kleinhans, S. De Doncker, S. Siangwata, M. A. Fernandes, A. Lemmerer, G. S. Smith and D. I. Bezuidenhout, *J. Organomet. Chem.*, **2020**, 920, 121341.

Fischer Carbene Complexes of Iridium(I) for Application in Catalytic Transfer Hydrogenation

G. K. Ramollo, I. Strydom, M. A. Fernandes, A. Lemmerer, S. O. Ojwach, J. L. van Wyk and D. I. Bezuidenhout, *Inorg. Chem.*, **2020**, 59, 4810–4815.

Signature: 

Date: 13 December 2020

Acknowledgements

First and foremost, I would like to thank my grandfather, my mother, my aunt and her husband, for their collective efforts in fostering a healthy and happy environment for my upbringing, and for their constant support and encouragement throughout the arduous journey that led to this point of my life.

I hereby gratefully acknowledge Sasol Technology R&D Pty. Ltd. South Africa for Financial support in the form of a bursary.

The financial assistance of the National Research Foundation (NRF) towards this research is hereby acknowledged. Opinions expressed and conclusions arrived at, are those of the author and are not necessarily to be attributed to the NRF.

To my supervisor Prof. Daniela I. Bezuidenhout, thank you for taking a chance on a village-girl, and for being a patient guiding hand throughout the last eight years and even more so recently. Thank you for encouraging me to do my absolute best and for entrusting me with the implementation of the varied research projects presented in this thesis.

Special thanks to my co-supervisors Dr. Juanita L. van Wyk and Dr. Izak Kotze, for always being willing to help with GC and NMR experiments at a moment's notice, and thank you for your constant encouragement and advice.

I am immensely grateful to my landlord Mr. Darko Skrbinsek for his understanding of my situation, thusly demonstrated by his constant encouragement to "Deal with the already stressful enough process of writing a thesis…". Words cannot express my gratitude, I will forever be in your debt.

Thank you to Danielle and Johan (Mrs. and Dr. van der Westhuizen) for always being there for me and for providing much needed financial and emotional support during this difficult period. Friends like you are hard to come by :)

To the rest of my friends and cheerleaders, especially to Mrs. Keletso Mabeba, Mr. Gustaff Koopa, Mr. Wynand Louw and Ms. Morongwa Mokgawa; thank you for cheering me on throughout the years, more so over the past few months.

My sincerest thanks to all the teachers of Makgopele High School, especially to Ms. Manketla J. Makhurupetsi and Mr. S. Alfred Sedulawese, for selflessly going far and beyond to help me achieve my academic goals. With additional thanks to Mrs. Lebea, Mrs. Mohale and Mr Kubayi for their collective efforts in getting me started on the journey that lead here.

Finally, from the bottom of my heart, thank you to Mr. Benny Mojela for being there and helping me through the tears and frustrations. Thank you for providing enough support and books to keep me sane, and for all the listening…so much listening.

Abstract

Carbene ligand transfer from tungsten(0) pentacarbonyl (hetero)aryl-ethoxy Fischer carbene complexes (FCCs) to rhodium(I) and gold(I) metal precursors, results in new examples of rare class of mono-heteroatom stabilized rhodium(I) and gold(I) FCCs, respectively. Analogously, a series of novel iridium(I) FCCs were accessed *via* transmetallation reactions of the relevant tungsten(0) FCCs with the selected iridium(I) precursor. The (hetero)aryl substituents included 2-thienyl (Th), 2-furyl (Fu), *para*-N,N-dimethylaniline (*p*-DMA), cyclopentadienylmetalcarbonyls $Cp'Fe(CO)_2Me$, $Cp'Mn(CO)_3$, and $Cp'Re(CO)_3$, as well as ruthenocenyl (Rc), and ferrocenyl (Fc) entities. The isolated Rh^I, Ir^I, and Au^I ethoxy-FCCs were modified by either aminolysis- or carbonylation reactions, for direct- or remote fine-tuning of the electron- donating ability of the carbene ligand. The electronic properties were monitored by spectroscopic and structural characterization methods. Tolman electronic parameters (TEPs) of Rh^I and Ir^I complexes were calculated, and the relative electron donating strength of the FC ligands were determined as increasing in the order $:C(OEt)(Cp'Re(CO)_3) < :C(OEt)Fc \approx :C(OEt)Rc < :C(OEt)$*p*-DMA $\leq :C(NH^nPr)Fc < :C(NH^nPr)$*p*-DMA $< :C(NH(CH_2)_2NMe_2)Fc$, with the unexpected implication that *p*-DMA-substituted FC ligands are more electron donating than Fc and Rc analogues.

The isolated Rh^I FCCs $[Rh(LL')\{C(OEt)Ar\}Cl]$ ($LL' = cod, (CO)_2$; Ar = *p*-DMA, Rc) were evaluated as precatalysts in the hydroformylation of 1-octene. The best catalytic activity was observed for metallocenyl-substituted complexes, where the possibility of bimetallic-activity at the central rhodium- and metallocenyl- substituent (iron- or, to a larger extent, ruthenium-) metal atom, cannot be ruled out. Chemical oxidation of the previously reported Rh^I Fc-FCC was also achieved, resulting in a significantly more electrophilic ferroceniumyl-substituted rhodium(I) FCC, which indicated improved regioselectivity in catalytic hydroformylation, at the expense of both catalytic activity and chemoselectivity.

Iridium(I) FCCs $[Ir(LL')\{(NR)Ar\}Cl]$ ($LL' = cod, (CO)_2$; XR = OEt, NH^nPr, $NH(CH_2)_2NMe_2$; Ar = $Cp'Re(CO)_3$, *p*-DMA, Fc), were used as precatalysts in the base-assisted transfer hydrogenation of acetophenone with the solvent *iso*-propanol acting as the sacrificial hydrogen atom donor. This study details the first report of the use of classical acyclic mono-heteroatom stabilized FCCs in molecular catalysis, results of which indicated an increase in catalytic activity with increasing electron-donating strength of the corresponding FC ligand. Excellent catalytic activities were observed for the *p*-DMA- mono-amino (-NH^nPr) and Fc-substituted diamino (-$NH(CH_2)_2NMe_2$) carbene complexes, with high turnover frequencies (TOFs) of 273 and 445 hr^{-1}, respectively.

Finally, Au^{I} aminocarbene complexes [Au{(NR)Ar}Cl] (R = ^{n}Pr, $(CH_2)_2NMe_2$; Ar = Th, *p*-DMA, Fc) were evaluated in redox-switchable catalytic reactions mediated by the oxidant Magic Blue (MB). Significantly improved catalytic activity of the Fc- aryl-carbene complexes as compared to the Fu- and *p*-DMA analogues were observed. The use of diamino-substituted carbene ligands (-$NH(CH_2)_2NMe_2$) instead of the monoamino analogues (-$NH^{n}Pr$), also yielded enhanced catalytic activity. The catalytic mechanism was investigated by means of experimental electron paramagnetic resonance (EPR) spectroscopy and computational density functional theory (DFT) studies. In all cases, the formation of catalytically active Au^{II} species upon the addition of MB is implicated. For the organic- (Fu-, *p*-DMA-) aryl-substituted carbene complexes, MB directly (and irreversibly) oxidizes the Au^{I} metal atom, resulting in the catalytically active Au^{II} intermediate, which instantaneously decomposes to carbene ligand oxidation products and elemental gold. For the Fc-substituted precatalysts however, reversible oxidation of the Fe^{II} metal atom with subsequent *in situ* inter- and intramolecular transformations upon addition of MB, results in ferrocenophane-substituted active Au^{II} species, and the Au^{I} precatalysts could be regenerated by addition of a suitable reductant to the respective Au^{I}-FCC/MB mixtures.

Table of Content

List of Complexes

Chapter 2

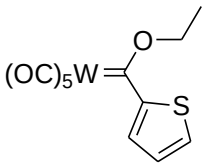

1

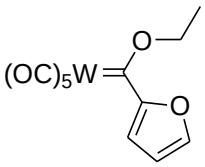

2

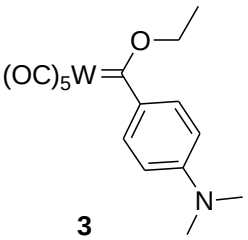

3

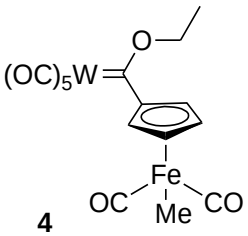

4

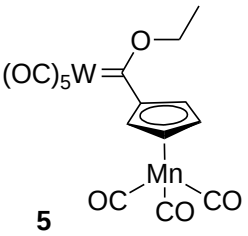

5

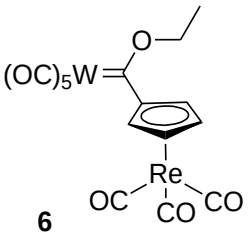

6

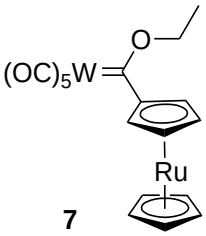

7

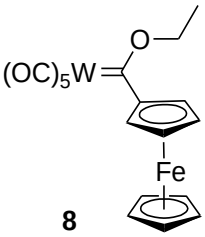

8

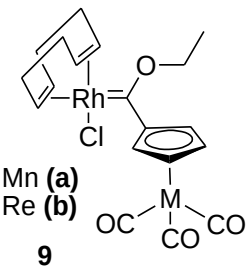

Mn **(a)**
Re **(b)**

9

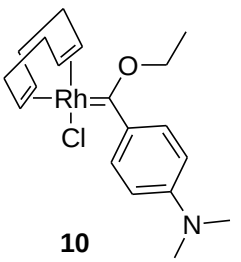

10

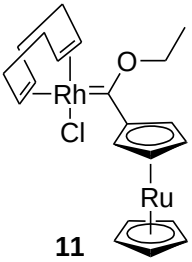

11

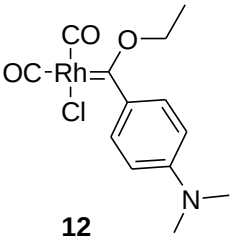

12

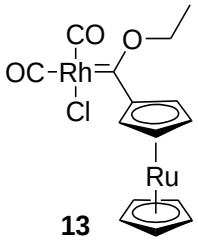

13

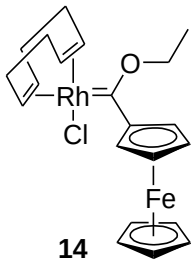

14

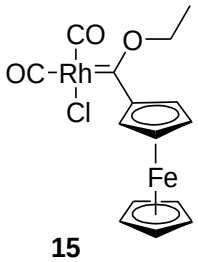

15

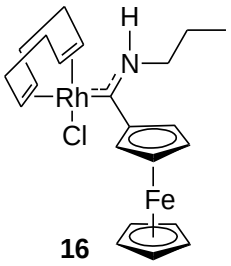

16

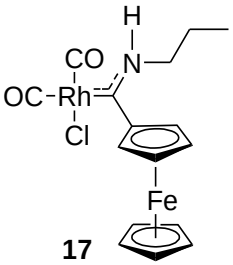

17

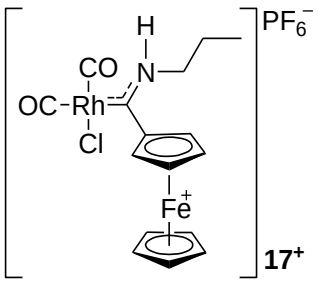

17⁺

Chapter 3

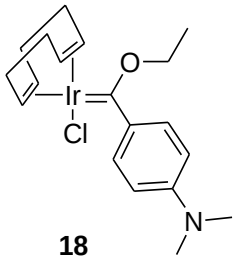

18

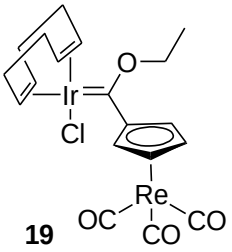

19

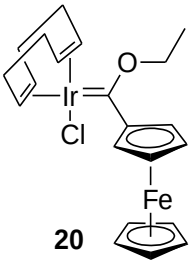

20

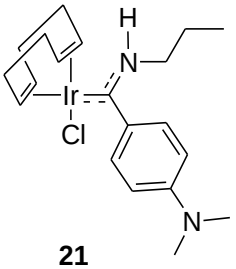

21

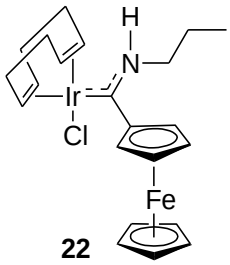

22

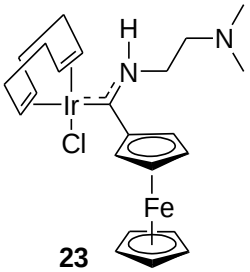

23

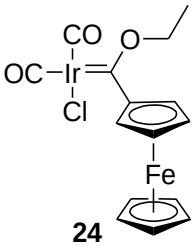

24

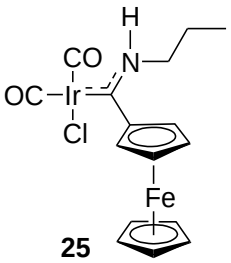

25

Chapter 4

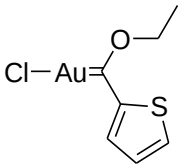

26

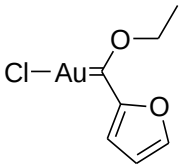

27

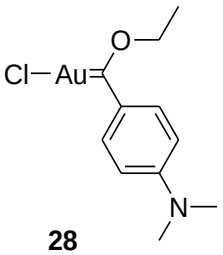

28

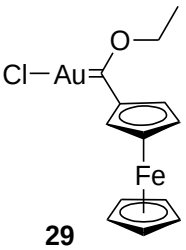

29

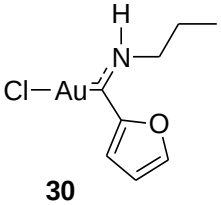

30

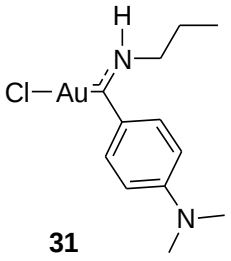

31

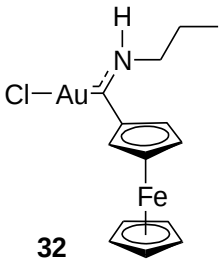

32

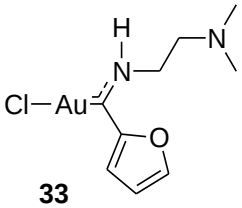

33

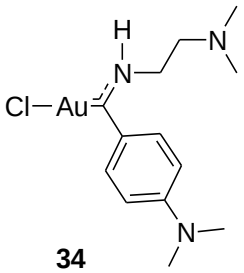

34

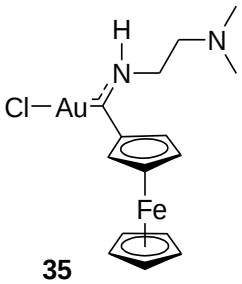

35

List of Abbreviations

Ar	aryl
br	broad (NMR)
Bu	butyl
CAAC	cyclic(alkyl)(amino)carbene
cod	1, 5-cyclooctadiene
Cp	cyclopentadienyl
Cp'	mono-substituted cyclopentadienyl
Cp*	pentamethylcyclopentadienyl
CV	cyclic voltammetry
DCM	dichloromethane
dd	doublet of doublets
DFT	density function theory
DMA	*N*,*N*-dimethylaniline
DMEN	*N*,*N*-dimethylethylenediamine
E	electrophile
EPR	electron paramagnetic resonance
Fc	ferrocenyl
Fc'	ferrocenophane
Fc^+	ferroceniumyl
FT-IR	Fourier-transform infrared
Fu	furyl
m	medium (IR)
m	multiplet (NMR)
Me	methyl
MS	mass spectrometry
NHC	*N*-heterocyclic carbene
NMR	Nuclear Magnetic Resonance
n.o.	not observed
Nu	nucleophile
Ph	phenyl
ppm	parts per million
Rc	ruthenocenyl

rt	room temperature
s	singlet (NMR)
s	strong (IR)
TEP	Tolman Electronic Parameter
Th	Thienyl
TH	Transfer hydrogenation
THF	tetrahydrofuran
tht	tetrahydrothiophene
TLC	thin layer chromatography
TOF	turnover frequency
vs	very strong (IR)
XRD	X-ray diffraction

Chapter 1: Introduction

In this introductory chapter, a short overview of Fischer carbene complexes is presented, including their electronic structure and bonding, as well as general preparative methods and applications. In addition, the catalytic transformations targeted as applications of the synthesized complexes in this study, are introduced as a preface to the outlining of the aims and objectives of the study. A detailed literature evaluation of the state-of-the-art of each topic of this study is presented as background introduction in each of the subsequent chapters.

1.1 Carbene structure and binding

1.1.1 Definition

A carbene can be best described as a neutral divalent carbon atom, instead of a tetravalent carbon, resulting in a highly reactive carbon species with six valence electrons as depicted in Figure 1.1 below.[1] When the carbene ligand is coordinated to a metal center, a carbene complex is formed.

Figure 1.1 General representation of a free carbene.[1]

1.1.2 Main classes of carbene complexes

Carbene complexes are mainly classified as singlet- or triplet-type, according to the electronic nature of the metal-carbene bond as effected by the accompanying carbene carbon substituents, with presence of a heteroatom (such as an oxygen- or nitrogen-atom) adjacent to the carbene carbon atom in the former class and lack thereof in the latter as the most commonly recognisable distinguishing factor. The first spectroscopically characterized singlet carbene complex was reported by Fischer and Maasböl in 1964,[2] while such an example of a triplet carbene complex was reported by Schrock a decade later[3] (see Figure 1.2 (a)). In both cases, the metal-carbene bond is characteristic of both σ- and π interactions between the metal- and carbene carbon-atoms, as outlined in Figure 1.2 (b).[4] A Fischer-type singlet-carbene carbon atom features a doubly-occupied sp^2 orbital and an empty p_z orbital, and offers stronger sigma-interaction with the accompanying metal fragment than does the

Schrock-type triplet-counterpart, wherein the parallel-spin electrons each occupies the sp^2 and p_z orbitals. These divalent-carbon species are thus more isolable when complexed to transition metal-atoms. The resultant metal-carbene bond is characteristic of carbene-to-metal dative donation of sp^2-electrons into the empty d_σ orbital with concurrent metal-to-carbene dative electron donation (from d_π to p_z) in Fischer-type carbene complexes. In Schrock-type carbene complexes, the metal-carbene bond is characteristic of two covalent bonds in a d_σ-sp^2 and d_π-p_z orbital-interactions, each polarised towards the carbene carbon atom.

Additionally, while Schrock carbene complexes feature both σ- and π-interactions (at the metal-carbene site) in an equal capacity, the metal-carbene bond in Fischer carbene complexes entails a predominantly (carbene-to-metal) σ-interaction with variable (metal-to-carbene) π-backbonding. Due to the mostly insufficient π-backbonding and carbene-bound heteroatom stabilization in Fischer carbene complexes, a partial positive charge resides on the carbene carbon atom, whereas the covalent-bonding nature of Schrock-type carbene complexes effects a partial negative charge on the carbene carbon atom. Consequently, Fischer-type singlet-carbene complexes are generally electrophilic at the carbon atom site while the Schrock-type triplet-counterpart is of nucleophilic character. Furthermore, singlet-state carbene ligands are more variable than their triplet-counterparts, which reasons for the vast majority of carbene literature reviews generally focusing on singlet-carbene ligands and associated complexes.[1,4–7]

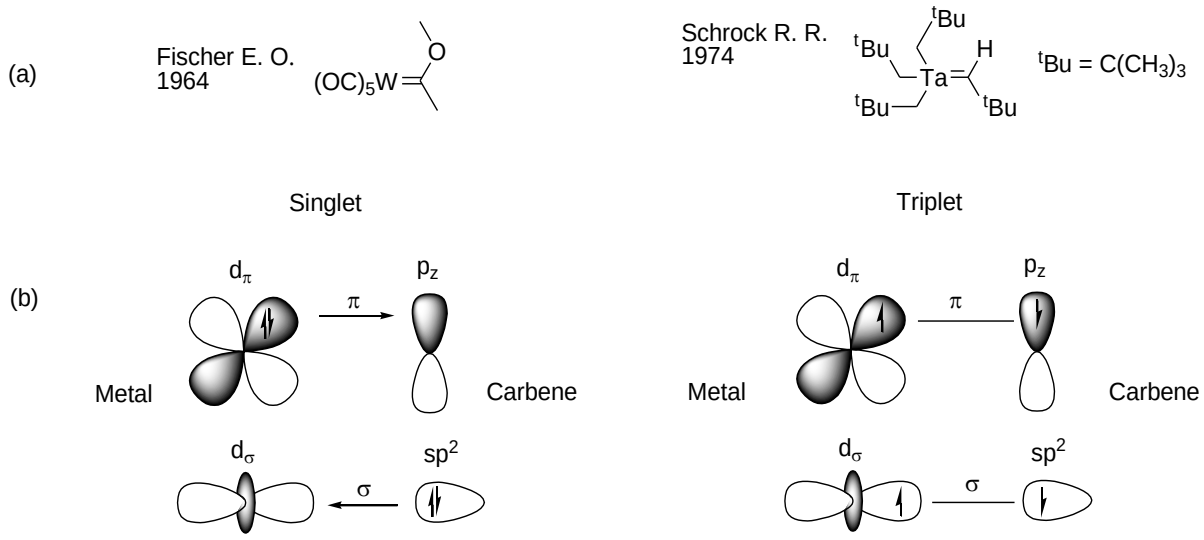

Figure 1.2 The bonding in singlet and triplet transition metal-carbene complexes in literature.

1.1.3 Singlet-state carbene ligand modification

As stated above, singlet-state carbene ligands inherently feature π-donor heteroatoms directly bound to the carbene carbon atom. Experimental and computational studies of simple (acyclic mono-heteroatom-stabilized) Fischer carbene complexes in literature agree that alkoxy-substituted carbene complexes exhibit reduced sigma-donor strength compared to their amino-analogues, as effected by lessened oxygen-to-carbene electron-density donation in the former in comparison to stronger nitrogen-to-carbene donation in the latter.[4,8,9] Due to the resultant robust nature of aminocarbene complexes compared to their alkoxy-analogues, *N*-atom stabilized variations of singlet-carbene ligands have emerged over the past two decades.[4,10,11] As depicted in Figure 1.3 below,[4] subclasses of Fischer-type carbene ligands arise due to different reactivity patterns brought about by the overall π-donor effect of the nitrogen atom. Classical acyclic (aryl-substituted) aminocarbene ligands (a) are said to exhibit lesser sigma-donor strength than the cyclic (alkyl)(amino) carbene (CAAC) ligand (b), whereby the carbene carbon- and nitrogen-atoms are interlinked through a saturated 5-membered ring effecting an isolable carbene ligand (b).[12,13] Indeed, acyclic aryl- Fischer carbenes (FCs) have not been reported in their free form to date. However, an acyclic analogues of (b), featuring stabilizing *tert*-butyl and *iso*propyl substituents at the carbene carbon- and nitrogen-atoms, respectively, reportedly exhibits enhanced σ-donor strength which results in an isolable acyclic (alkyl)(amino) carbene ligand.[14] Inclusion of a second nitrogen-atom in place of the alkyl carbene substituent in the CAAC ligand (b), yields a di-heteroatom stabilized *N*-heterocyclic carbene (NHC) ligand (c), and the overall electron donor strength of the NHC ligand is notably higher than in the FC and CAAC ligands. In this case, flanking of the carbene carbon atom by two π-donor σ-acceptor *N*-atoms effects a synergic electron-density push-pull system throughout the NHC ligand which stabilized said uncoordinated carbene carbon, and the free NHC can consequently be isolated.[15–17] Acyclic versions of NHCs have also been reported in literature[18] as viable ancillary ligands, and can be isolated in their free-carbene[19] form. Thus, cyclic carbene (CAAC and NHC) ligands exhibit stronger σ-character (and hence increased stability) than their acyclic (FC) counterparts, while saturated NHCs are stronger σ-donors and π-acceptors than their unsaturated analogues.

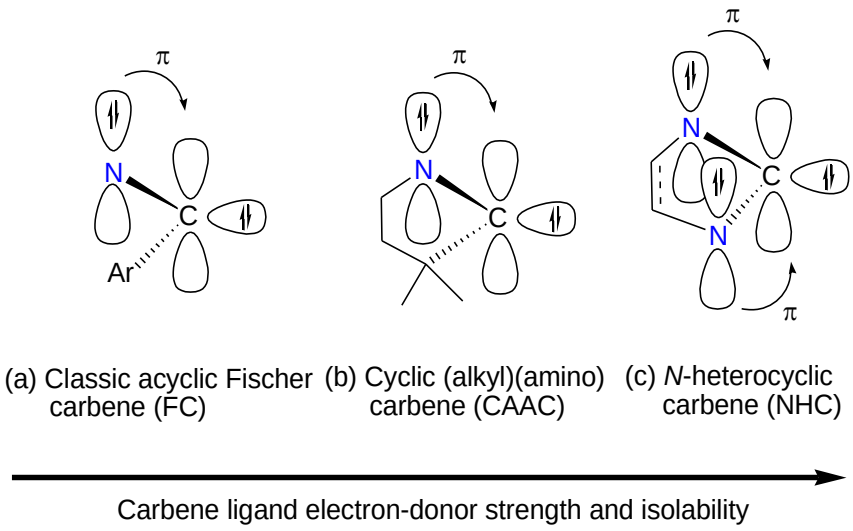

Figure 1.3 Selected examples of *N*-atom stabilized singlet-carbenes.

While metal-carbene complexes featuring stronger σ-donor ligands such as CAACs[20] and NHCs[21–24] are continually reported to exhibit excellent catalytic activity towards various organic transformations, such literature reports of classical acyclic Fischer carbene complexes (FCCs) are comparatively scarce. As such, this thesis will focus on acyclic(aryl) mono-heteroatom stabilized FCCs and their application in homogeneous catalysis. In addition, all alkoxy- and aminocarbene complexes discussed in this thesis will be depicted as in Figure 1.4 (a) and (b), respectively, to illustrate the above-mentioned stronger electron-donor nature and overall stabilization effect of amino *vs* alkoxy substituents. This depiction will however be limited to mono-heteroatom stabilized FCCs, with multi-heteroatom stabilized analogues to be depicted as featuring M-$C_{carbene}$ single bonds to emphasize the stronger sigma-character of metal-(NHC) and -acyclic diaminocarbene complexes (Figure 1.4 (c)).

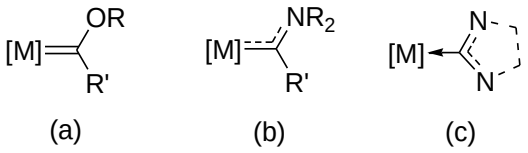

Figure 1.4 General depiction of heteroatom-stabilized metal-carbene complexes with variable M-C bond order.

1.2 Synthesis and application of Fischer carbene complexes

Fischer carbene complexes (FCCs), named after their discoverer, are traditionally accessed *via* reaction of metal-carbonyls with an organolithium reagent followed by alkylation of the resultant metal acylate as depicted in Scheme 1.1 (a).[2,25,26] This synthetic strategy was first reported by Fischer and Maasböl

and is commonly known as the Fischer route. The isolated carbene complex is usually of early-transition metal fragments in low oxidation state, such as chromium(0) or tungsten(0) carbonyls. Alternatively, FCCs can be accessed by modification of an existing carbene- or co-ligand,[9,27,28] or by transmetallation to catalytically useful late transition metals such as rhodium(I) as depicted in Scheme 1.1 (b). These post-synthesis complex-modification studies, wherein the structural characteristics of the metal-carbene bond are retained, were first reported by Fischer in 1970.[29] This strategy has been utilized in literature since then for approaches to more complex and structurally versatile FCCs.[30–33]

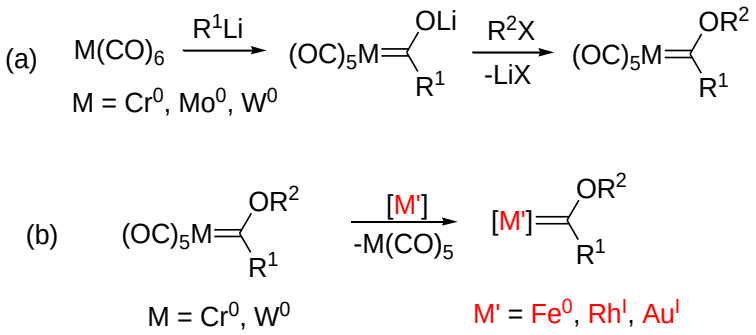

Scheme 1.1 Synthetic routes towards previously isolated Fischer carbene complexes *via* (a) the traditional Fischer and (b) transmetallation methods.

FCCs are generally highly reactive and prone to various carbene ligand-modification or ligand-substitution reactions, a few of which are depicted in Figure 1.5 below.[9] Nucleophilic attack of the carbene carbon atom readily occurs, especially in more electrophilic complexes (pathway **A**), wherein reaction with primary and secondary amines results in an aminocarbene complex and accompanying alcohol.[27,28] Reaction pathway **B** depicts electrophilic attack at the stabilizing-heteroatom center, which is sometimes a key step in metal-carbyne synthesis.[34,35] Deprotonation at α-CH of methylcarbene can also occur due to elevated acidity of α-CH proton, resulting in a functionalized carbene complex (pathway **C**).[9] Additionally, metal-carbonyl FCCs undergo nucleophilic substitution reactions (pathway **D**) wherein replacement of a CO-ligand in metal-carbonyl FCCs by tertiary pnictogens such as phosphines results in a new metal-pnictogen interaction, remotely fine-tuning the accompanying carbene ligand.[36,37]

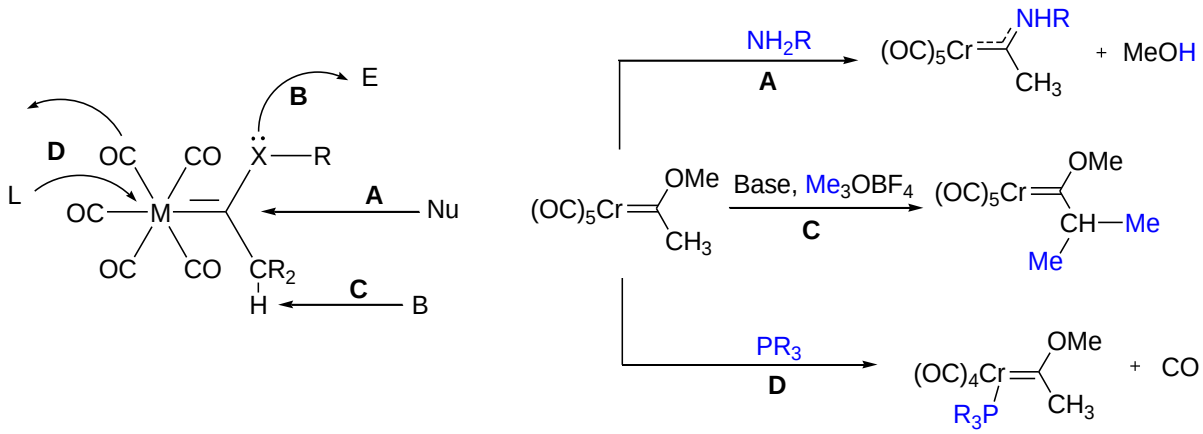

Figure 1.5 Possible reactivity pathways of FCCs[38] (left) with selected example reaction schemes[9] (right)

This inherent "high reactivity" and resulting general instability of FCCs are key to the application of these complexes in template organic reactions (generalized in Figure 1.6 below).[38] FCCs in literature have primarily been utilized in organic cyclization reactions whereby the carbene ligand forms part of the targeted products.[39] For example, group 6 alkynyl FCCs react (in a [2 + 2] cyclization pathway) with alkynes or alkenes to result in cyclobutenylcarbene intermediates, and the metal-carbene fragment is retained in the final organic product.[40–42] Generally, reaction of terminal carbon- and heteroatom nucleophiles with group 6 alkenyl FCCs, usually in the presence of a late transition metal complex and/or under thermal conditions, results in loss of the carbene-metal fragment and formation of a [2 + 3] cyclization product incorporating the carbene ligand.[43–47] This metal-assisted thermal decomposition of FCCs is thus a powerful tool towards synthesis of complex heterocycles in literature.[39] Additionally, other possible reaction pathways between FCCs and organic substrates (such as alkenylation, cycloaddition, and self-dimerization)[48–53] have been implicated in the synthesis of natural products such as antibiotics, vitamins, and peptides.[26,54–57]

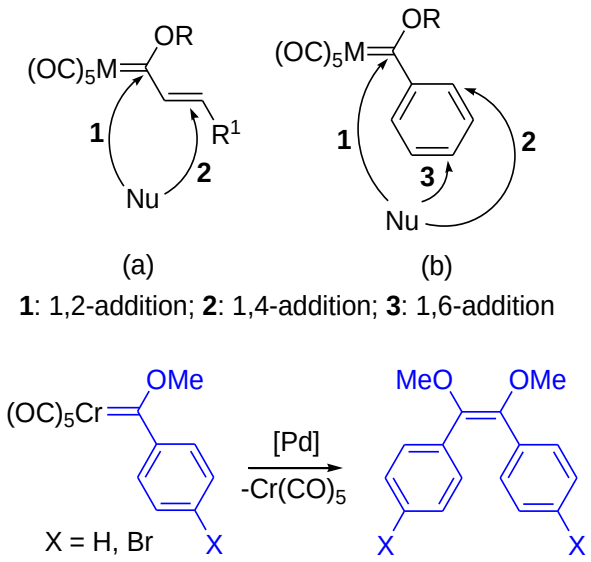

Figure 1.6 Possible reaction pathways (top) of alkenyl- (a) or phenyl- (b) Fischer carbene complexes with nucleophiles, and (bottom) metal-assisted self-dimerization of a Cr^0 FCC.[52,58]

While group 6 FCCs are traditionally employed in stoichiometric organic C-C bond formation reactions, applications of these complexes as catalysts are limited. This is due to the requirement of modifiable carbonyl or *iso*nitrile ligands in the coordination sphere of the group 6 metal precursors, for nucleophilic attack to prepare the metal acylates as FCC precursors. This means that the group 6 metal must be in a low oxidation state, and also precludes the possibility of halido co-ligands susceptible to attack by nucleophiles. To the best of our knowledge, a literature search of FCCs utilized as catalysts yielded only two recent reports, namely rhodium-catalyzed alkene hydroformylation and gold-mediated intramolecular oxazoline synthesis.[37,59] In both cases, carbene transfer reactions from the group 6 FCC to the catalytically-relevant late transition metal complex, was prerequisite. In contrast to the two reported metal-FCC catalyzed olefin hydroformylation and oxazoline synthesis transformations, FCCs have not hitherto been utilized in other important catalytic reactions such as transfer hydrogenation of ketones, wherein relevant metal-NHCs have found wide application.[60] A brief summary of these homogeneous catalytic reactions is outlined below to emphasize their industrial and commercial applications. The effect of NHC ligands on these organic transformations as catalyzed by the corresponding metal-NHCs, and the prospects of comparison to envisaged analogous metal-FCCs will be elaborated upon in later chapters (2, 3, and 4), wherein the specific catalytic process (hydroformylation, transfer hydrogenation, and oxazoline synthesis, respectively) will be further expanded upon.

1.3 Late transition metal catalyzed organic transformations

All late transition metal FCCs reported in this thesis will be utilized as catalyst precursors (precatalysts) towards relevant organic reactions, where FCCs have previously found little to no application. These metal-catalyzed reactions are briefly summarized in this section and their industrial importance thus highlighted.

1.3.1 Olefin hydroformylation

Hydroformylation reactions typically involve the net addition of syn-gas (synthesis gas, CO/H_2 mixture) across a terminal alkene C=C bond in the presence of a crucial transition metal catalyst, resulting in linear and branched aldehydes, and occasionally, internal alkenes and alcohols (Scheme 1.2).[61] Catalytic performance of the utilized metal-catalyst is then evaluated in terms of activity rate (complete conversion of olefin substrate to any possible product), chemo- (conversion of olefin to aldehydes), and regio-selectivity (favoured formation of linear or branched aldehydes). Under ideal conditions, the reaction proceeds to the exclusive formation of commercially preferred linear aldehydes, which are useful precursors for the industrial production of plasticizers, detergents, flavours and perfumes.[62–64] Ru-, Co-, and Rh-metal centered complexes are commonly utilized catalyst precursors for the hydroformylation of olefins,[65–68] with the latter steadily gaining more popularity over the past few decades.[69–71] While cobalt is the cheaper of the listed metals, rhodium-catalyzed hydroformylation reactions in literature proved significantly more active under ambient conditions (thus catalyst turnover is improved) and are generally more chemoselective towards aldehydes,[65,72,73] justifying the ubiquity of Rh-based catalyst precursors in this regard.

The formation of chiral branched aldehydes *via* asymmetric hydroformylation for stereoselectivity control is also a possibility. Such chiral aldehydes are commonly employed in the organic synthesis of chiral alcohols, amines, or esters and in fine chemical synthesis.[74,75] Additionally, the design of a suitable precatalyst (precursor to a catalytically active species, usually generated in situ during the catalytic cycle) is envisaged around rhodium metal-complexes resembling the best precatalysts reported in literature. As such, rhodium complexes of the form $[Rh^{I}(CO)_2LX]$, reminiscent of Wilkinson's catalyst,[76] have been reported as good hydroformylation precatalysts in literature, wherein chemo- and stereoselective control is improved by carbonyl-ligand substitution, or by varying the electron-donor strength and steric parameters of the investigated ligand L.[61,70,74] Furthermore, catalytic activity can be improved by inclusion of an additional active site in the catalyst-system, such that the resulting bimetallic precatalyst exhibits dinuclear cooperative catalysis.[77–79] Finally, while Rh^{I}

complexes of both saturated and unsaturated NHCs have been utilized as precatalysts for the hydroformylation of olefins,[11,80] with chemo- and stereoselectivity controlled experiments exhibiting excellent results, [81–84] literature examples of traditional acyclic Rh^{I}-FCC towards hydroformylation of alkenes are limited,[37] leaving room for comparable Rh-FCC catalyzed reactions to be discussed in Chapter 2.

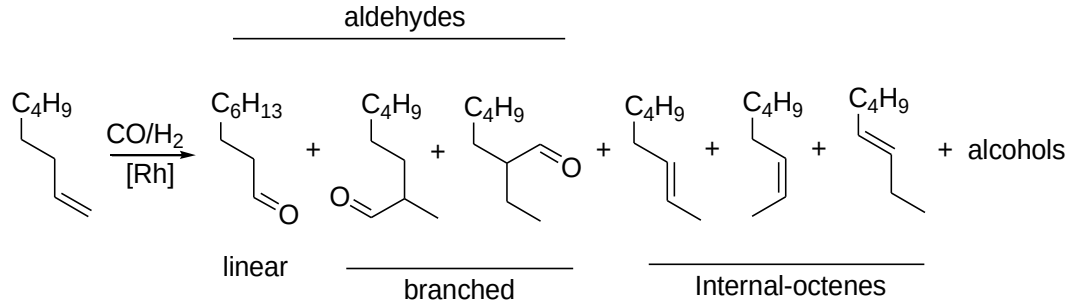

Scheme 1.2 Catalytic hydroformylation of 1-octene towards nonanal and related side products.

1.3.2 Transfer hydrogenation

The transfer hydrogenation (TH) process involves the metal-catalyzed transfer of molecular hydrogen from a non-H_2 hydrogen source to an unsaturated bond in substrates like alkenes, alkynes, imines, ketones, etc.[85–87] This TH process dates back to 1903, when Knoevenagel first reported that elemental palladium easily enabled intermolecular self-hydrogenation of a diester compound,[88] and serves as a less hazardous hydrogenation pathway than the more common gaseous H_2-promoted direct hydrogenation.[89] Consequently, this TH process has since been utilized and adapted in literature studies of transition metal catalyzed TH transformations. In this regard, Rh, Ru, and Ir complexes are the most common precatalysts.[90–93] Especially prominent is the TH/ reduction of ketones by *iso*-propanol as both solvent and sacrificial hydrogen donor (Scheme 1.3),[94–96] resulting in chiral and/ or achiral alcohols for use in organic reactions and pharmaceutical synthesis.[97,98] As with the olefin hydroformylation reactions described above, catalytic efficiency of the utilized metal complex is defined in terms of complete conversion of the unsaturated ketone substrate towards the desired alcohol product in a relatively short period of time. Thus design of Ir-FCC precatalysts towards efficient reduction of ketones will allow for the inauguration of FCCs in iridium-mediated catalysis, and will allow for comparison to abundant literature examples of Ir-NHCs in catalytic TH of ketones (*vide infra*, Chapter 3).[11,99–101]

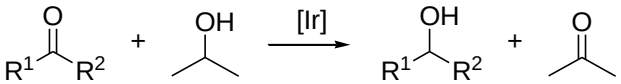

Scheme 1.3 Iridium-catalyzed transfer hydrogenation of ketones by *iso*-propanol

1.3.3 Oxazoline synthesis

Oxazolines are 5-membered cyclic compounds incorporating both a nitrogen- and oxygen-atom, and are present in a variety of biologically active compounds.[102,103] These heterocycles are credited with inducing activity in the antifungal, antiviral, and antibacterial behaviour of oxazoline-containing compounds.[104–106] Consequently, the synthesis of functionalized oxazolines has provided quick access to a variety of biologically useful compounds in literature, such as the synthesis of the naturally occurring amino acid hydroxysyline [an important intermediate in the synthesis of balanol (fungal metabolite effective in protein kinase C inhibition)] depicted in Scheme 1.4 below.[107] As such, numerous synthetic approaches towards oxazolines have been reported in literature,[108,109] wherein inter- and intramolecular cyclization reactions between 1,2-amino-alcohols and carboxylic acids, aromatic aldehydes, or *iso*nitriles are commonplace.[110–113] Additionally, these cyclization reactions usually occur in the presence of organo- or metal-catalysts.[114] While literature reports of metal-catalyzed oxazoline synthesis highlight a variety of Lewis-acid precatalysts (eg: $Cu^{I/II}$, Zn^{II}, Fe^{III}, etc),[106,115,116] gold-based complexes are usually preferred presumably due to potential aurophilic-stabilization of the gold (pre)catalyst in the catalytic cycle.[106,107,117–119] Au-FCCs will therefore be targeted for application in oxazoline synthesis reactions (in Chapter 4) under mild catalytic conditions comparable to reported Au-NHCs in literature (low precatalyst-loading, ambient temperature, exclusion of co-catalysts/ additives, etc).

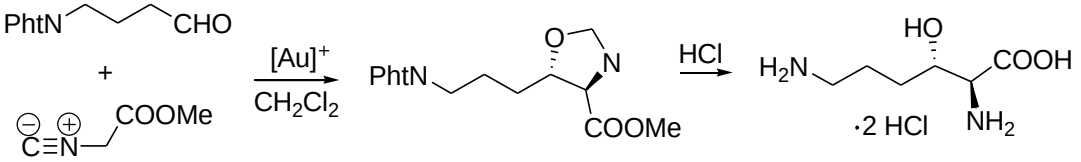

Scheme 1.4 Gold-catalyzed oxazoline synthesis and subsequent utilization for synthesis of hydroxylysine.

1.4 Aim

Accessibility of late transition metal FCCs is limited, and their catalytic applications consequently underexplored. The requirement of carbonyl or *iso*nitrile ligands, and preclusion of halido co-ligands in the transition metal's coordination sphere for FCC synthesis *via* the Fischer route (*vide supra*), hinders the direct synthesis of FCCs of catalytically relevant late transition metals. In addition, the carbene ligand transfer reaction, usually employed for synthesis of late transition metal FCCs, has been shown to result in self-dimerization of the carbene ligand. In this case, the (seldom isolated) late transition metal carbene complex undergoes unprecedented decomposition resulting in an olefinic carbene-dimer (Scheme 1.5). This self-dimerization can however be circumvented by inclusion of strongly electron donating carbene substituents.[37]

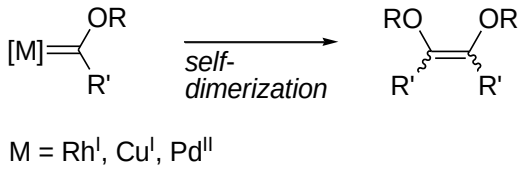

Scheme 1.5 Self-dimerization decomposition of late transition metal FCCs.

On the contrary, group 6 FCCs have been thoroughly explored and reviewed, and their application in organic transformation reactions highlights the usefulness of the FC ligand. As such, the main aim of this project is the synthesis of known FCCs of group 6 transition metals *via* the Fischer route, as precursors for subsequent transmetallation to catalytically important group 9 and 11 metals. To this effect, the objectives of this study include (i) the synthesis of group 6 FCCs followed by (ii) the synthesis of new group 9 (Rh, Ir) and 11 (Au) FCCs *via* transmetallation, and complete characterization by means of spectroscopic and structural techniques of the steric and electronic properties of the novel complexes. Finally (iii) catalytic screening of all late metal FCCs towards relevant organic transformation reactions are targeted, specifically (1) rhodium-catalyzed alkene hydroformylation, (2) iridium-catalyzed transfer hydrogenation and (3) gold-catalyzed oxazoline synthesis.

1.5 References

1 P. de Frémont, N. Marion and S. P. Nolan, *Coord. Chem. Rev.*, 2009, **253**, 862–892.

2 E. O. Fischer and A. Maasböl, *Angew. Chem. Int. Ed.*, 1964, **3**, 580–581.

3 R. R. Schrock, *J. Am. Chem. Soc.*, 1974, **96**, 6796–6797.

4 D. Munz, *Organometallics*, 2018, **37**, 275–289.

5 S.-T. Liu and K. R. Reddy, *Chem. Soc. Rev.*, 1999, **28**, 315–322.

6 R. R. Schrock, *J. Chem. Soc. Dalton Trans.*, 2001, 2541–2550.

7 J. W. Herndon, *Coord. Chem. Rev.*, 2014, **272**, 48–144.

8 R. H. Grubbs, T. M. Trnka and M. S. Sanford, in *Fundamentals of Molecular Catalysis*, eds. H. Kurosawa and A. B. T.-C. M. in I. C. Yamamoto, Elsevier, 2003, vol. 3, pp. 187–231.

9 E. O. Fischer, *Pure Appl. Chem.*, 1970, **24**, 407–424.

10 T. Dröge and F. Glorius, *Angew. Chem. Int. Ed.*, 2010, **49**, 6940–6952.

11 E. Peris, *Chem. Rev.*, 2018, **118**, 9988–10031.

12 G. D. Frey, R. D. Dewhurst, S. Kousar, B. Donnadieu and G. Bertrand, *J. Organomet. Chem.*, 2008, **693**, 1674–1682.

13 J. Chu, D. Munz, R. Jazzar, M. Melaimi and G. Bertrand, *J. Am. Chem. Soc.*, 2016, **138**, 7884–7887.

14 V. Lavallo, J. Mafhouz, Y. Canac, B. Donnadieu, W. W. Schoeller and G. Bertrand, *J. Am. Chem. Soc.*, 2004, **126**, 8670–8671.

15 A. J. Arduengo, R. L. Harlow and M. Kline, *J. Am. Chem. Soc.*, 1991, **113**, 361–363.

16 A. J. Arduengo, M. Kline, J. C. Calabrese and F. Davidson, *J. Am. Chem. Soc.*, 1991, **113**, 9704–9705.

17 P. Bazinet, T.-G. Ong, J. S. O'Brien, N. Lavoie, E. Bell, G. P. A. Yap, I. Korobkov and D. S. Richeson, *Organometallics*, 2007, **26**, 2885–2895.

18 V. P. Boyarskiy, K. V Luzyanin and V. Y. Kukushkin, *Coord. Chem. Rev.*, 2012, **256**, 2029–2056.

19 R. W. Alder, P. R. Allen, M. Murray and A. G. Orpen, *Angew. Chem. Int. Ed. Engl.* 1996, **35**, 1121–1123.

20 M. Melaimi, R. Jazzar, M. Soleilhavoup and G. Bertrand, *Angew. Chem. Int. Ed.*, 2017, **56**, 10046–10068.

21 G. C. Fortman and S. P. Nolan, *Chem. Soc. Rev.*, 2011, **40**, 5151–5169.

22 W. Gil and A. M. Trzeciak, *Coord. Chem. Rev.*, 2011, **255**, 473–483.

23 F. Wang, L. Liu, W. Wang, S. Li and M. Shi, *Coord. Chem. Rev.*, 2012, **256**, 804–853.

24 F. Lazreg, F. Nahra and C. S. J. Cazin, *Coord. Chem. Rev.*, 2015, **293**–**294**, 48–79.

25 E. O. Fischer and A. Maasböl, *Chem. Ber.*, 1967, **100**, 2445–2456.

26 K. Weiß and E. O. Fischer, *Chem. Ber.*, 1976, **109**, 1868–1886.

27 B. van der Westhuizen, P. J. Swarts, I. Strydom, D. C. Liles, I. Fernández, J. C. Swarts and D. I. Bezuidenhout, *Dalton Trans.*, 2013, **42**, 5367–5378.

28 B. van der Westhuizen, P. J. Swarts, L. M. van Jaarsveld, D. C. Liles, U. Siegert, J. C. Swarts, I. Fernández and D. I. Bezuidenhout, *Inorg. Chem.*, 2013, **52**, 6674–6684.

29 E. O. Fischer and H.-J. Beck, *Angew. Chem. Int. Ed. Engl.* 1970, **9**, 72–73.

30 H. G. Raubenheimer and S. Cronje, *Chem. Soc. Rev.*, 2008, **37**, 1998–2011.

31 J. Barluenga, R. Vicente, L. A. López and M. Tomás, *J. Organomet. Chem.*, 2006, **691**, 5654–5659.

32 J. C. Del Amo, M. J. Mancheño, M. Gómez-Gallego and M. A. Sierra, *Organometallics*, 2004, **23**, 5021–5029.

33 D. I. Bezuidenhout, B. van der Westhuizen, A. J. Rosenthal, M. Wörle, D. C. Liles and I. Fernández, *Dalton Trans.*, 2014, **43**, 398–401.

34 F. R. Hartley and S. Patai, *The Chemistry of the Metal-Carbon Bond*, Wiley, Chichester, 1982.

35 E. O. Fischer, F. J. Gammel, J. O. Besenhard, A. Frank and D. Neugebauer, *J. Organomet. Chem.*, 1980, **191**, 261–282.

36 M. Landman, R. Liu, R. Fraser, P. H. van Rooyen and J. Conradie, *J. Organomet. Chem.*, 2014, **752**, 171–182.

37 G. K. Ramollo, M. J. López-Gómez, D. C. Liles, L. C. Matsinha, G. S. Smith and D. I. Bezuidenhout, *Organometallics*, 2015, **34**, 5745–5753.

38 K. H. Dötz and J. Stendel, *Chem. Rev.*, 2009, **109**, 3227–3274.

39 J. Barluenga, J. Santamaría and M. Tomás, *Chem. Rev.*, 2004, **104**, 2259–2283.

40 K. L. Faron and W. D. Wulff, *J. Am. Chem. Soc.*, 1988, **110**, 8727–8729.

41 R. Aumann, B. Hildmann and R. Fröhlich, *Organometallics*, 1998, **17**, 1197–1201.

42 R. Aumann, Z. Yu and R. Fröhlich, *Organometallics*, 1998, **17**, 2897–2905.

43 J. Barluenga, R. Vicente, L. A. López and M. Tomás, *J. Am. Chem. Soc.*, 2006, **128**, 7050–7054.

44 J. Barluenga, R. Vicente, P. Barrio, L. A. López and M. Tomás, *J. Am. Chem. Soc.*, 2004, **126**, 5974–5975.

45 J. Barluenga, P. Barrio, L. Riesgo, L. A. López and M. Tomás, *Tetrahedron*, 2006, **62**, 7547–7551.

46 J. Barluenga, R. Vicente, L. A. López and M. Tomás, *Tetrahedron*, 2005, **61**, 11327–11332.

47 J. Barluenga, R. Vicente, L. A. López, E. Rubio, M. Tomás and C. Álvarez-Rúa, *J. Am. Chem. Soc.*, 2004, **126**, 470–471.

48 E. O. Fischer and K. H. Dötz, *Chem. Ber.*, 1972, **105**, 3966–3973.

49 C. P. Casey and T. J. Burkhardt, *J. Am. Chem. Soc.*, 1972, **94**, 6543–6544.

50 C. P. Casey, T. J. Burkhardt, C. A. Bunnell and J. C. Calabrese, *J. Am. Chem. Soc.*, 1977, **99**, 2127–2134.

51 E. O. Fischer and K. Heinz Dötz, *Chem. Ber.*, 1970, **103**, 1273–1278.

52 M. A. Sierra, M. J. Mancheño, E. Sáez and J. C. del Amo, *J. Am. Chem. Soc.*, 1998, **120**, 6812–6813.

53 M. L. Lage, D. Curiel, I. Fernández, M. J. Mancheño, M. Gómez-Gallego, P. Molina and M. A. Sierra, *Organometallics*, 2011, **30**, 1794–1803.

54 A. S. Kende, Y. geng Tsay and J. E. Mills, *J. Am. Chem. Soc.*, 1976, **98**, 1967–1969.

55 W. D. Wulff and P. C. Tang, *J. Am. Chem. Soc.*, 1984, **106**, 434–436.

56 K. H. Dötz, I. Pruskil and J. Mühlemeier, *Chem. Ber.*, 1982, **115**, 1278–1285.

57 K. H. Dötz and I. Pruskil, *J. Organomet. Chem.*, 1981, **209**, C4–C6.

58 J. Barluenga, J. Flórez and F. J. Fañanás, *J. Organomet. Chem.*, 2001, **624**, 5–17.

59 P. Veit, C. Volkert, V. Förster, Christoph Ksenofontov, S. Schlicher, M. Bauer and K. Heinze, *Chem. Commun.*, 2019, **55**, 4615–4618.

60 S. Díez-González, N. Marion and S. P. Nolan, *Chem. Rev.*, 2009, **109**, 3612–3676.

61 R. Franke, D. Selent and A. Börner, *Chem. Rev.*, 2012, **112**, 5675–5732.

62 M. G. Mura, L. De Luca, M. Taddei, J. M. J. Williams and A. Porcheddu, *Org. Lett.*, 2014, **16**, 2586–2589.

63 C. M. Fairchild, *Anal. Chem.*, 1967, **39**, 22A-34A.

64 S. R. Derrington, N. J. Turner and S. P. France, *J. Biotechnol.*, 2019, **304**, 78–88.

65 C. M. Crudden and H. Alper, *J. Org. Chem.*, 1994, **59**, 3091–3097.

66 A. Van Rooy, P. C. J. Kamer, P. W. N. M. Van Leeuwen, K. Goubitz, J. Fraanje, N. Veldman and A. L. Spek, *Organometallics*, 1996, **15**, 835.

67 C. A. Tolman, *Chem. Rev.*, 1977, **77**, 313–348.

68 N. C. Antonels, J. R. Moss and G. S. Smith, *J. Organomet. Chem.*, 2011, **696**, 2003–2007.

69 M. Vilches-Herrera, L. Domke and A. Börner, *ACS Catal.*, 2014, **4**, 1706–1724.

70 S. S. Nurttila, P. R. Linnebank, T. Krachko and J. N. H. Reek, *ACS Catal.*, 2018, **8**, 3469–3488.

71 J. M. Marinkovic, A. Riisager, R. Franke, P. Wasserscheid and M. Haumann, *Ind. Eng. Chem. Res.*, 2019, **58**, 2409–2420.

72 A. Stefani, G. Consiglio, C. Botteghi and P. Pino, *J. Am. Chem. Soc.*, 1977, **99**, 1058–1063.

73 P. Pino, G. Consiglio, C. Botteghi and C. Salomon, in *Homogeneous Catalysis—II*, American Chemical Society, 1974, vol. 132, pp. 20–295.

74 F. Agbossou, J.-F. Carpentier and A. Mortreux, *Chem. Rev.*, 1995, **95**, 2485–2506.

75 B. Breit, *Acc. Chem. Res.*, 2003, **36**, 264–275.

76 D. Evans, J. A. Osborn and G. Wilkinson, *J. Chem. Soc. A Inorg. Phys. Theor.*, 1968, 3133–3142.

77 M. A. Rida and A. K. Smith, *J. Mol. Catal. A Chem.*, 2003, **202**, 87–95.

78 M. E. Broussard, B. Juma, S. G. Train, W.-J. Peng, S. A. Laneman and G. G. Stanley, *Science* 1993, **260**, 1784 – 1788.

79 D. G. H. Hetterscheid, S. H. Chikkali, B. de Bruin and J. N. H. Reek, *ChemCatChem*, 2013, **5**, 2785–2793.

80 M. T. Zarka, M. Bortenschlager, K. Wurst, O. Nuyken and R. Weberskirch, *Organometallics*, 2004, **23**, 4817–4820.

81 M. Bortenschlager, J. Schütz, D. von Preysing, O. Nuyken, W. A. Herrmann and R. Weberskirch, *J. Organomet. Chem.*, 2005, **690**, 6233–6237.

82 W. Gil, A. M. Trzeciak and J. J. Ziółkowski, *Organometallics*, 2008, **27**, 4131–4138.

83 M. V. Jiménez, J. Fernández-Tornos, J. J. Pérez-Torrente, F. J. Modrego, S. Winterle, C. Cunchillos, F. J. Lahoz and L. A. Oro, *Organometallics*, 2011, **30**, 5493–5508.

84 R. Laï, J.-C. Daran, A. Heumann, A. Zaragori-Benedetti and E. Rafii, *Inorg. Chim. Acta*, 2009, **362**, 4849–4852.

85 D. Wang and D. Astruc, *Chem. Rev.*, 2015, **115**, 6621–6686.

86 F. Foubelo, C. Nájera and M. Yus, *Tetrahedron: Asymmetry*, 2015, **26**, 769–790.

87 F. Foubelo and M. Yus, *Chem. Rec.*, 2015, **15**, 907–924.

88 E. Knoevenagel and B. Bergdolt, *Ber. Dtsch. Chem. Ges.,* 1903, **36**, 2857–2860.

89 F. Rigas and S. Sklavounos, *Int. J. Hydrog. Energy*, 2005, **30**, 1501–1510.

90 O. Prakash, P. Singh, G. Mukherjee and A. K. Singh, *Organometallics*, 2012, **31**, 3379–3388.

91 M. Bianchi, U. Matteoli, G. Menchi, P. Frediani, S. Pratesi, F. Piacenti and C. Botteghi, *J. Organomet. Chem.*, 1980, **198**, 73–80.

92 S. Hohloch, L. Suntrup and B. Sarkar, *Organometallics*, 2013, **32**, 7376–7385.

93 A. Azua, M. Finn, H. Yi, A. Beatriz Dantas and A. Voutchkova-Kostal, *ACS Sustain. Chem. Eng.*, 2017, **5**, 3963–3972.

94 M. Albrecht, J. R. Miecznikowski, A. Samuel, J. W. Faller and R. H. Crabtree, *Organometallics*, 2002, **21**, 3596–3604.

95 L. Yang, A. Krüger, A. Neels and M. Albrecht, *Organometallics*, 2008, **27**, 3161–3171.

96 A. C. Hillier, H. M. Lee, E. D. Stevens and S. P. Nolan, *Organometallics*, 2001, **20**, 4246–4252.

97 R. Akkari, M. Calmes, N. Mai, M. Rolland and J. Martinez, *J. Org. Chem.*, 2001, **66**, 5859–5865.

98 M. Wolberg, M. V. Filho, S. Bode, P. Geilenkirchen, R. Feldmann, A. Liese, W. Hummel and M. Müller, *Bioproc. Biosyst. Eng.*, 2008, **31**, 183–191.

99 M. V. Jiménez, J. Fernández-Tornos, J. J. Pérez-Torrente, F. J. Modrego, P. García-Orduña and L. A. Oro, *Organometallics*, 2015, **34**, 926–940.

100 A. Azua, J. A. Mata and E. Peris, *Organometallics*, 2011, **30**, 5532–5536.

101 J. R. Miecznikowski and R. H. Crabtree, *Polyhedron*, 2004, **23**, 2857–2872.

102 D. C. Palmer and S. Venkatraman, in *Oxazoles: Synthesis, Reactions, and Spectroscopy*, John Wiley & Sons, Ltd, 2003, pp. 1–390.

103 J. A. Frump, *Chem. Rev.*, 1971, **71**, 483–505.

104 J.-P. Genet, S. Thorimbert and A.-M. Touzin, *Tetrahedron Lett.*, 1993, **34**, 1159–1162.

105 L. Fan, E. Lobkovsky and B. Ganem, *Org. Lett.*, 2007, **9**, 2015–2017.

106 C. Jin, J. P. Burgess, J. A. Kepler and C. E. Cook, *Org. Lett.*, 2007, **9**, 1887–1890.

107 P. F. Hughes, S. H. Smith and J. T. Olson, *J. Org. Chem.*, 1994, **59**, 5799–5802.

108 M. Roy, C. H. R. M. Wilsens, N. Leoné and S. Rastogi, *ACS Sustain. Chem. Eng.*, 2019, **7**, 8842–8852.

109 J. D. Haupt, M. Berger and S. R. Waldvogel, *Org. Lett.*, 2019, **21**, 242–245.

110 H. Jiang, L. Yan, M. Xu, W. Lu, Y. Cai, W. Wan, J. Yao, S. Wu, S. Zhu and J. Hao, *J. Org. Chem.*, 2013, **78**, 4261–4269.

111 C. L. Zhong, B. Y. Tang, P. Yin, Y. Chen and L. He, *J. Org. Chem.*, 2012, **77**, 4271–4277.

112 A. R. Katritzky, C. Cai, K. Suzuki and S. K. Singh, *J. Org. Chem.*, 2004, **69**, 811–814.

113 S. Hajra, S. Bar, D. Sinha and B. Maji, *J. Org. Chem.*, 2008, **73**, 4320–4322.

114 G. S. K. Wong and W. Wu, in *Oxazoles: Synthesis, Reactions, and Spectroscopy*, John Wiley & Sons, Ltd, 2004, pp. 331–528.

115 G. C. Senadi, W.-P. Hu, J.-S. Hsiao, J. K. Vandavasi, C.-Y. Chen and J.-J. Wang, *Org. Lett.*, 2012, **14**, 4478–4481.

116 M. Trose, F. Lazreg, M. Lesieur and C. S. J. Cazin, *J. Org. Chem.*, 2015, **80**, 9910–9914.

117 A. S. K. Hashmi, *Chem. Rev.*, 2007, **107**, 3180–3211.

118 S. Klenk, S. Rupf, L. Suntrup, M. Van Der Meer and B. Sarkar, Organometallics, 2017, **36**, 2026–2035.

119 D. Canseco-Gonzalez, A. Petronilho, H. Mueller-Bunz, K. Ohmatsu, T. Ooi and M. Albrecht, *J. Am. Chem. Soc.*, 2013, **135**, 13193–13203.

Chapter 2: Synthesis and characterization of rhodium(I) Fischer carbene complexes as precatalysts for olefin hydroformylation

2.1 Literature review

Traditional acyclic (mono-heteroatom stabilized) Fischer carbene complexes (FCCs) of early transition metals are abundant in literature, with applications thereof predominantly in organic template reactions.[1,2] These stoichiometric reactions typically involve the formation of new carbon-carbon or carbon-heteroatom (C-C or C-X) bonds between an organic substrate and the selected FCC, whereby the carbene ligand of the investigated FCC reacts with the nucleophilic organic substrate and forms part of the targeted products, with thermal- or additive-induced carbene-decomplexation as part of the reaction cycle. In many such cases, FCCs bearing the strongly electron withdrawing metalpentacarbonyl fragment ($M(CO)_5$, M = Cr, W) have shown exceptional reactivity towards carbon- and nitrogen-nucleophiles in comparison to their organic ester analogues.[1,3] In addition, the [4 + 2] cycloaddition of isoprene and an alkenyl-carbene chromium(0) complex is completed after 3 hours, whereas analogous reaction with methyl acrylate instead of the FCC proceeds over several months with reduced selectivity between the *meta*- and *para*-substituted cyclohexene products (see Scheme 2.1).[4] As such, Fischer carbene complexes can serve as vital substrates towards the synthesis of complex carbocyclic and heterocyclic compounds for application in synthetic organic and organometallic chemistry.

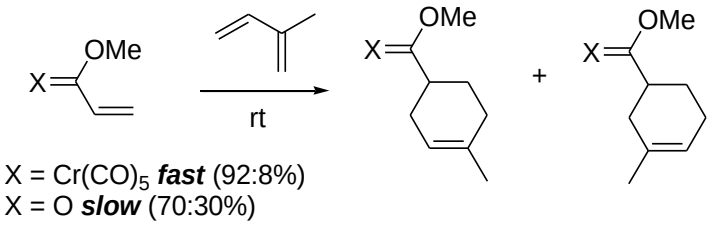

Scheme 2.1 Comparative synthesis of functionalized cyclohexene; FCC- *vs* ester-substrate.

2.1.1 Carbene templated carbon-carbon bond formation

FCCs synthesized from chromium(0) and tungsten(0) hexacarbonyls are the most dominant of the FCC series, resulting in a plethora of metal-pentacarbonyl alkyl-, alkenyl-, alkynyl-, and aryl-carbene complexes ([$M(CO)_5$Carbene], M = Cr^0, W^0) applicable as building blocks or as carbene ligand carriers

for the formation of novel complexes and useful organic fragments. Cycloaddition reactions are more commonplace in this regard (see Scheme 2.1 for selected examples). Group 6 FCCs bearing α,β-unsaturated alkenyl-carbene substituents are the most dominant in these cycloadditions, wherein Cr^0 complexes are prefered due to their relative ease of isolation and enhanced reactivity (providing higher yields of targeted products) in comparison to their W^0 analogues. The Dötz benzannulation for example – Cr^0 carbene-templated synthesis of a benzene ring across a C-C triple bond – was first reported by Dötz and co-workers in 1975 and 1983 for phenyl- and alkenyl-carbene complexes, respectively (Scheme 2.2).[5,6] During this unprecedented [3 + 2 + 1] cyclization, a chromium(0) pentacarbonyl alkenylmethoxycarbene complex is decarbonylated and simultaneously coordinated to the alkyne at the vacant chromium tetracarbonyl site. Subsequent reorganization of the modified $Cr(CO)_4$-FCC intermediate *via* migratory insertion of both the chromium-coordinated alkyne substrate and carbonyl ligand, 1,2-shift of the $Cr(CO)_3$ fragment, and ultimate ring-closure results in a new benzene ring incorporating the original alkenyl carbene substituent. Demetallation of the chromium tricarbonyl fragment (which is π-coordinated to the benzannulated site) can easily be achieved by reaction with carbon monoxide to liberate chromium(0) hexacarbonyl from the desired aromatic product. Additionally, the use of aminocarbene complexes (instead of their alkoxy-analogues) in this regard was reported to generally result in [3 + 2] cycloaddition products such as cyclopentene derivatives, as a result of unpermitted carbonyl-migratory insertion towards benzannulation.[7]

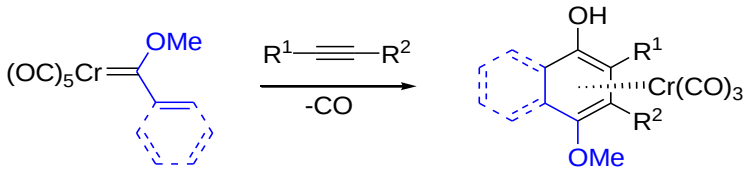

Scheme 2.2 Dötz benzannulation of a Cr^0 alkenyl- or phenylmethoxy FCC.

While the above-mentioned [3 + 2 + 1] and [3 + 2] annulations were achieved in the absence of a catalytic species, the use of late transition metal catalysts in these reactions forgoes the benzannulation route, resulting instead in heptannulation and pentannulation products (among a wide range of linear and (hetero)cyclic possibilities) depending on the nature of the catalyst and choice of substrate. These metal-assisted carbocyclizations have been thoroughly explored, especially by the research group of Barluenga since 2002,[8] examples of which are depicted in Scheme 2.3 (a – d) below. The application of a nickel(0) precatalyst in the cycloaddition of Cr^0 alkenylmethoxy-FCC and a terminal alkyne yielded a [3 + 2 + 2] cyclization of the carbene ligand and two molecules of the alkyne, as reported by Barluenga and co-workers (a).[9] However, use of the same alkenyl FCC and Ni^0 precatalyst

in the presence of an internal alkyne yielded the [3 + 2] cycloaddition product (d).[10] This cyclopentenone derivative could also be synthesized when the nickel(0) precatalyst was substituted for a rhodium(I) precatalyst for cycloadditions on terminal and internal alkynes respectively depicted as (c) and (d).[11,12] Additionally, the use of activated allenes instead of the internal and terminal alkynes was also reported to yield methylenecyclopentene derivatives (b).[13]

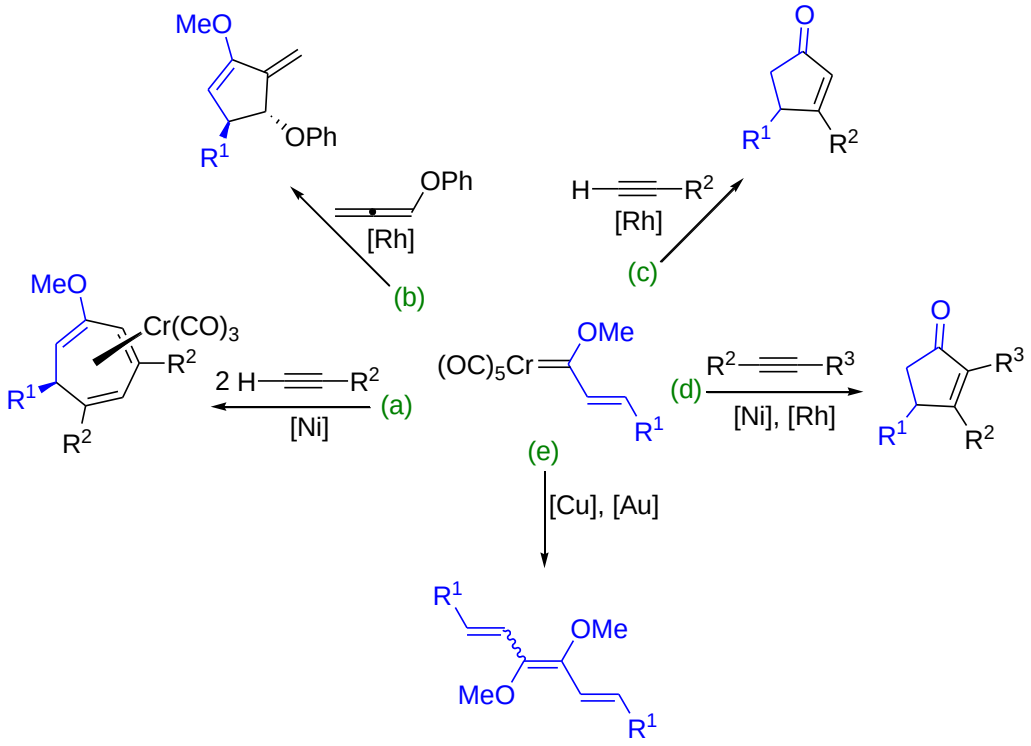

Scheme 2.3 Selected examples of late transition metal catalyzed- cycloadditions (a) – (d) and dimerization (e) of a Cr^0 alkenyl carbene complexes.

FCCs bearing alkenyl carbene substituents have also been reported to undergo carbene-dimerization in the absence of a substrate, with the aid of a metal precatalysts and under ambient conditions. Scheme 2.3 (e) depicts rare examples of alkenyl-FCCs self-dimerization as catalysed by copper or gold precatalysts at room temperature towards conjugated trienes.[14,15] This metal-assisted self-dimerization of the carbene ligand has been thoroughly studied, especially by the research group of Sierra and co-workers.[16–19] Additionally, these self-dimerization reactions usually require temperatures greater than 80 °C in the absence of a catalytic species, and generate major unwanted side-products in the process.[16,20] Catalytic self-dimerization of the carbene ligand is generally considered to proceed as depicted in Scheme 2.4 below. During the catalytic cycle, the exemplary chromium(0) FCC (**I**) reacts with the late transition metal catalyst, forming a highly reactive metallacycle which rearranges to expel the chromium pentacarbonyl moiety and results in a new late

transition metal FCC (**II**). A second molecule of **I** then reacts with the new FCC (**II**) to form the unstable mononuclear biscarbene complex (**III**), followed by C-C coupling of both carbene ligands resulting in the stereoselective formation of the targeted olefinic dimer (a). In the presence of an activated alkene (Scheme 2.4, half-cycle), the late transition metal FCC (**II**) forms a [2 + 2] cycloaddition intermediate, which also rearranges to form a [1 + 2] cyclopropanation product (b) and regenerates the late transition metal compound ML_n. It is important to note that the vast majority of reported catalytic self-dimerization and cycloaddition reactions of FCCs consistently agree with the respective mechanistic routes depicted in Scheme 2.4 below. That is, catalytic C-C bond-formation FCC-templated reactions proceed through a late transition metal FCCs as per Scheme 2.4 (**II**), and the intermediary complex **II** in turn acts as the active species for the intended transformation.[13,14,16,21–27]

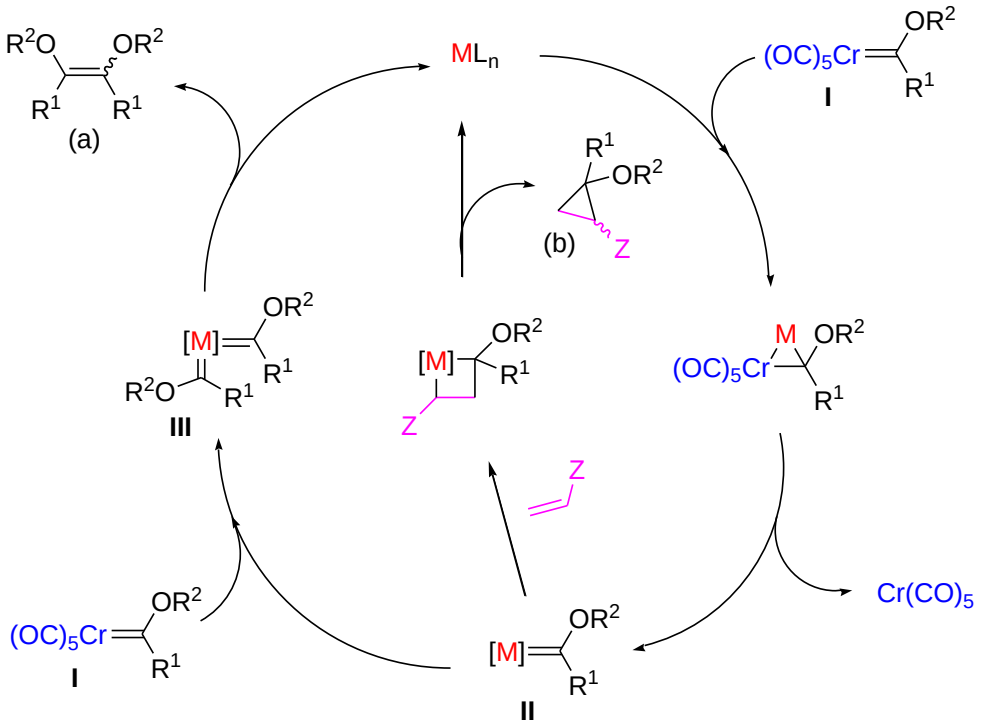

Scheme 2.4 The role of group 6 FCCs in metal-assisted self-dimerization (major) and cyclopropanation (minor) reactions.

These metal-assisted self-dimerization reactions are commonly studied with alkenyl or aryl FCCs as carbene-ligand carriers, whereas methylcarbene complexes result exclusively in vinyl ethers instead of the intended dimeric species.[16] The cyclization-type reactions are however exclusive to α,β-unsaturated alkenyl- and alkynyl-FCCs, with saturated methyl FCCs avoided due to potential β-hydride elimination, thus finding limited and often restricted applicability in carbene-templated reactions. For example, Cr^0 methylethoxy- and aminocarbene complexes undergo aldol-condensation[28] and Michael-

addition[29] transformations respectively, with α-deprotonation as the key step in both cases, resulting in functionalized complexes bearing alkenyl- and remote keto-carbene substituents respectively.[30,31]

2.1.2 Carbene ligand transfer to late transition metals

FCCs of catalytically relevant late transition metals (such as palladium or rhodium) are not readily accessible *via* the traditional Fischer route. The reaction of an organolithium reagent with a metal-carbonyl or -*iso*cyanide entity as a starting point of the Fischer route, would require the absence of any competing metal-halogen site, preventing the direct synthesis of late transition metal FCCs by metal-acylation of late transition metal precursors such as rhodium, palladium, or gold to name a few (which are typically available in +1 or +2 oxidation states stabilized by halogen co-ligands). As such, late transition metal FCCs are usually accessed *via* direct metal-metal ligand transfer reactions between an existing FCC and the relevant late metal precursor in a transmetallation process.

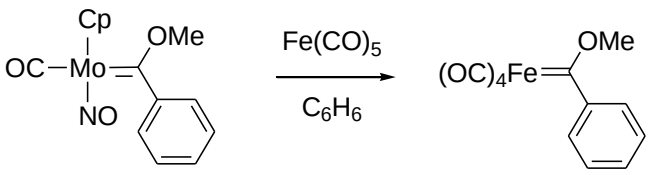

Scheme 2.5 The first reported transmetallation of a Fischer carbene complex.

The atom-economic transmetallation of a FCC was first reported by Fischer and Beck four decades ago (Scheme 2.5), who demonstrated the phenylmethoxycarbene ligand transfer from a molybdenum(I) FCC to an iron(0) metal center,[32] resulting in the air sensitive Fe^0 FCC depicted in Figure 2.1 (a), which was inaccessible through the conventional Fischer route. This reaction was accelerated by the photodecarbonylation of the iron pentacarbonyl precursor and proceeded within five hours. The authors therein postulated the similar formation of a volatile (non-isolable) trimeric nickel(II) phenylmethoxycarbene complex (Figure 2.1 (b)). A limited number of late transition metal FCCs have since been reported by various research groups utilizing this transmetallation approach (Figure 2.1 and 2.2), with complete characterization commonly prevented by the highly reactive nature of these rarely isolated FCCs. Barluenga and co-workers reported the Cu^I complex depicted in Figure 2.1 (c) in 2001, *via* a simple Cr^0-Cu^I transmetallation reaction.[33] Additionally, the simple FCC-acetonitrile ligand exchange between a W^0 aminocarbene complex and a Pd^{II} *trans*-dichloro precursor produced the Pd^{II} FCC at room temperature as reported by Meana and co-workers (Figure 2.1 (d)).[34] However, transmetallation from the same W^0 FCC and a Pd^{II} aryl-*trans*-chloro precursor instead of the dichloro

analogue yields a dinuclear metallacyclic biscarbene complex, which could be converted into the mononuclear Pd^{II} FCC by reaction with a tertiary phosphine (Figure 2.1 (e)).[35] The base-assisted transmetallation of a Cr^0 alkenyl FCC (with a primary enaminyl- carbene substituent) to a palladium(II) or platinum(II) precursor was reported to yield mononuclear metalacyclic biscarbene complexes depicted in Figure 2.1 (f).[36] Lastly, the reaction of a Cr^0 styryl FCC and Au^I complex bearing strong electron donor *N*-heterocyclic carbene or tertiary phosphine (NHC or PR_3) ligands, in the presence of a halogen-scavenger, yielded cationic Au^I FCCs stabilized by electron rich NHC or PR_3 co-ligands (Figure 2.1 (g)).[15] Examples of rhodium FCCs are briefly discussed below, and the gold FCCs will be further elaborated upon in Chapter 4.

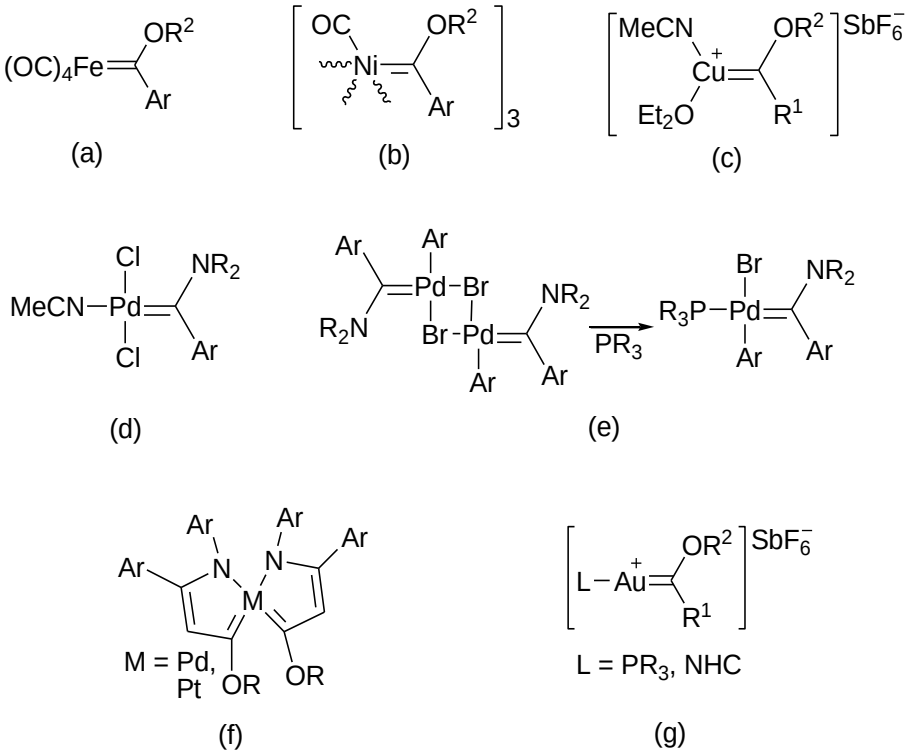

Figure 2.1 Selected examples of transmetallated FCCs

The Rh^I FCCs depicted in Figure 2.2 below were found to be the only examples of such complexes strictly synthesized *via* the transmetallation route between Cr^0 or W^0 FCCs and the relevant Rh^I precursor, to the best of our knowledge. The first spectroscopically characterized Rh^I alkenylcarbene complex (a) was isolated by Göttker-Schnetmann and co-workers in 2001[37] after postulating its intermediary existence in rhodium-catalyzed W^0 carbene-templated organic transfomations.[38] Barluenga later reported (in 2004) the successful transmetallation of Cr^0 alkenylmethoxycarbene complexes to a cationic rhodium metal centre in moderate to high yields ((b), 60 – 72%).[12] Additionally,

Barluenga and co-workers reported the mononuclear Rh^{I}-NHC-FCC mixed-carbene complex in 2006 (c), synthesized by direct transmetallation of a Cr^{0} FCC and Rh^{I} NHC complex, and the resulting Rh^{I} acyclic FCC is *trans*-stabilized by the electron rich NHC co-ligand.[11] Finally, transmetallation of a Cr^{0} ferrocenylcarbene complex and a Rh^{I} precursor was reported by our research group in 2015 (d).[39] Incidentally, Barluenga's mixed-carbene complex (c) is the only reported successful transfer of an acyclic (mono)aminocarbene ligand to a rhodium centre, while the latter report specifies post-complexation aminolysis for access to aminocarbene analogues of (d).

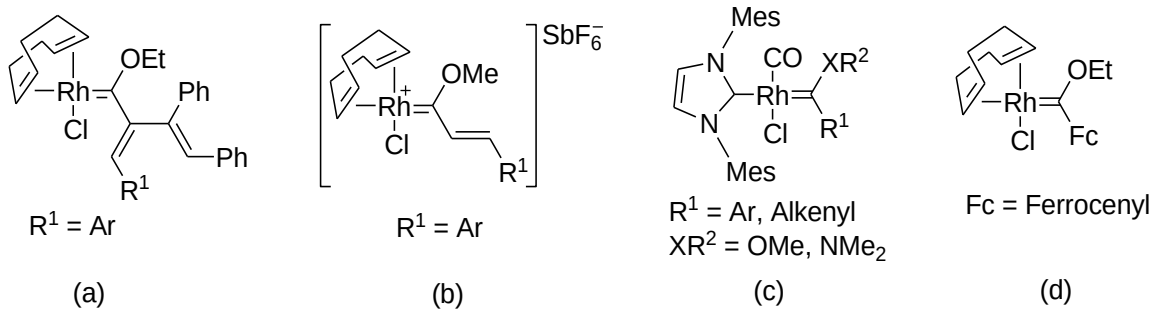

Figure 2.2 Rare examples of transmetallated Rh^{I} FCCs.

In addition to these transmetallated examples (Figure 2.2), literature reports of otherwise synthesized rhodium acyclic FCCs in both common oxidation states are also available (Figure 2.3 below). Specifically, direct complexation of a free alkyl(amino)carbene ligand to a rhodium metal centre readily proceeds to yield the stable Rh^{I} complex (a).[40] However, this more straight-forward approach requires the design of a stable aminocarbene ligand, yielding a significantly more electron rich complex than traditional FCCs, and provides limited options for carbene-ligand modification. The Rh^{I} heptyl(amino)carbene complex (b) could be accessed *via* ligand modification of a vinylidene-bridged dirhodium precursor, by reaction of the rhodium dimer with a secondary amine to yield a Rh^{I} FCC bearing an electron rich pincer (ONP) co-ligand.[41] Finally, a Rh^{III} FCC could also be synthesized by reaction of a square planar cationic Rh^{III} precursor and activated alcohols, resulting in the stable monocationic Rh^{III} complex (c) as depicted.[42]

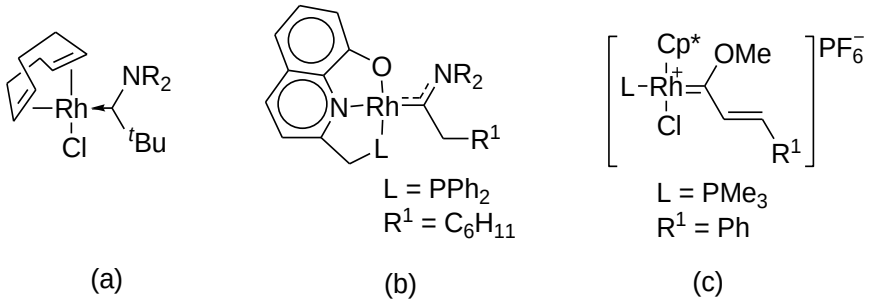

Figure 2.3 Selected examples of Rh^{I} (a), (b) and Rh^{III} (c) FCCs accessed *via* non-transmetallation methods.

2.1.3 Reactivity and stability of rhodium(I) Fischer carbene complexes

Rhodium(I) FCCs have been successfully utilized in stoichiometric cycloaddition of terminal electron poor alkynes[12] and self -dimerization[11] reactions, albeit with limited FC ligand variation in both cases as compared to their group 6 metal analogues. The inherent reactivity of rhodium FCCs and the ease of ligand decomplexation is the main reason for this pigeonholed applicability of said complexes. Utilization of an electron rich carbene ligand is thus necessary for catalytic applicability of the resultant stable rhodium complex.

Scheme 2.6 below depicts self-dimerization of electron rich Rh^{I} FCCs featuring heteroaryl carbene substituents or NHC co-ligands. The Rh^{I} *trans*-NHC-FCC accessed *via* Cr^{0}-Rh^{I} transmetallation, wherein carbonyl- and FC ligands were instantaneously transferred from the Cr^{0}- to the Rh^{I} -metal centres as reported by Barluenga and co-workers, proved thermally unstable at 60 °C, resulting in self-dimerization of the FC ligand while the Rh^{I}-NHC-(CO) moiety remains intact in its dimeric form (a).[11] Attempts at circumventing this self-dimerization, undertaken by our research group a decade later were initially unsuccessful. Cr^{0}-Rh^{I} transmetallation of 2-thienyl and 2-furyl FCCs resulted in unstable heteroaryl Rh^{I} FCCs which exhibited the carbene ligand self-dimerization discussed above, at ambient temperatures (b), and could therefore not be isolated and characterized.[39] Thus the strong inductive electron-donating nature of the heteroaryl carbene substituents [deduced from theoretical and experimental trends of chromium(0),[43] molybdenum(0),[44] tungsten(0),[45] and manganese(I)[46] FCCs in literature, wherein the investigated FC ligand features alkoxy- (and amino-) thienyl, furyl, *N*-methylpyrrolyl, or ferrocenyl carbene substituents] proved insufficient towards stabilization of the envisioned Rh^{I} FCCs, especially in the absence of electron rich co-ligands.

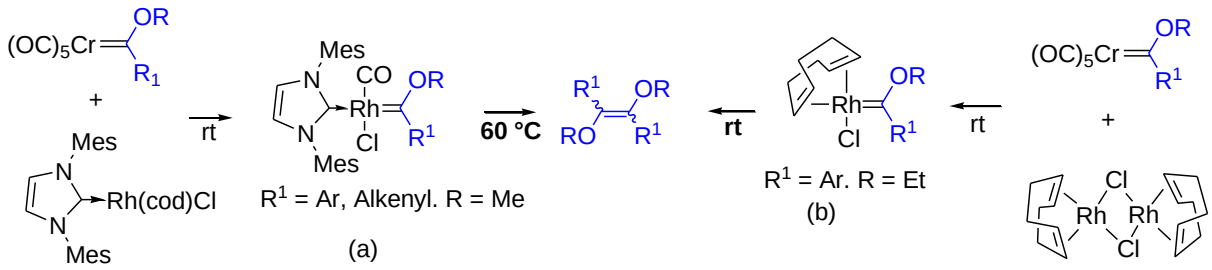

Scheme 2.6 Transmetallation and subsequent self-dimerization of rhodium(I) FCCs.

Inclusion of a ferrocenyl carbene substituent in the precursor Cr^0 FCC however yielded a stable rhodium(I) 1,5-cyclooctadienyl ferrocenylethoxycarbene complex which was spectroscopically and structurally characterized.[39] The electron rich nature of the ferrocenyl substituent[47,48] and its stronger electron-donor effect in comparison to the thienyl and furyl substituents[46,49] aid in the stabilization of the resultant complex. The Rh-carbene bond of the ferrocenyl complex also withstood the self-dimerization test, whereby thermal decomposition (80 °C) of a benzene solution of the complex saturated with gaseous carbon monoxide resulted instead in a (postulated) dimeric Rh^{I}-FCC-(CO) species where the Rh-$C_{carbene}$ bond was retained (Scheme 2.7 (a)), reminiscent of Barluenga's Rh^{I}-NHC-(CO) dimer discussed above. The thermally stable monomeric Rh^{I} FCC was then utilized as a precursor for fine-tuning. Access to modified ferrocenylcarbene complexes was accomplished by inclusion of carbonyls, phosphines, or arsines in the rhodium coordination sphere, and by variation of *O*- or *N*-heteroatoms, *via* simple co-ligand substitution or aminolysis of the alkoxycarbene complex, respectively (Scheme 2.7 (b)). Specifically, reaction of the transmetallated ethoxycarbene complex with excess *n*-propylamine in diethyl ether yielded the desired aminocarbene complex. Additionally, the transmetallated Rh^{I} ferrocenylcarbene complexes could be converted to their respective dicarbonyl analogues, which allowed for further subsequent modification by carbonyl substitution with various tertiary pnictogens such as triphenyl- phosphine, phosphite, or arsine, and tricyclohexylphosphine (Scheme 2.7 (b)). The resultant series of Rh^{I} complexes could then be utilized in the catalytic hydroformylation of olefins.

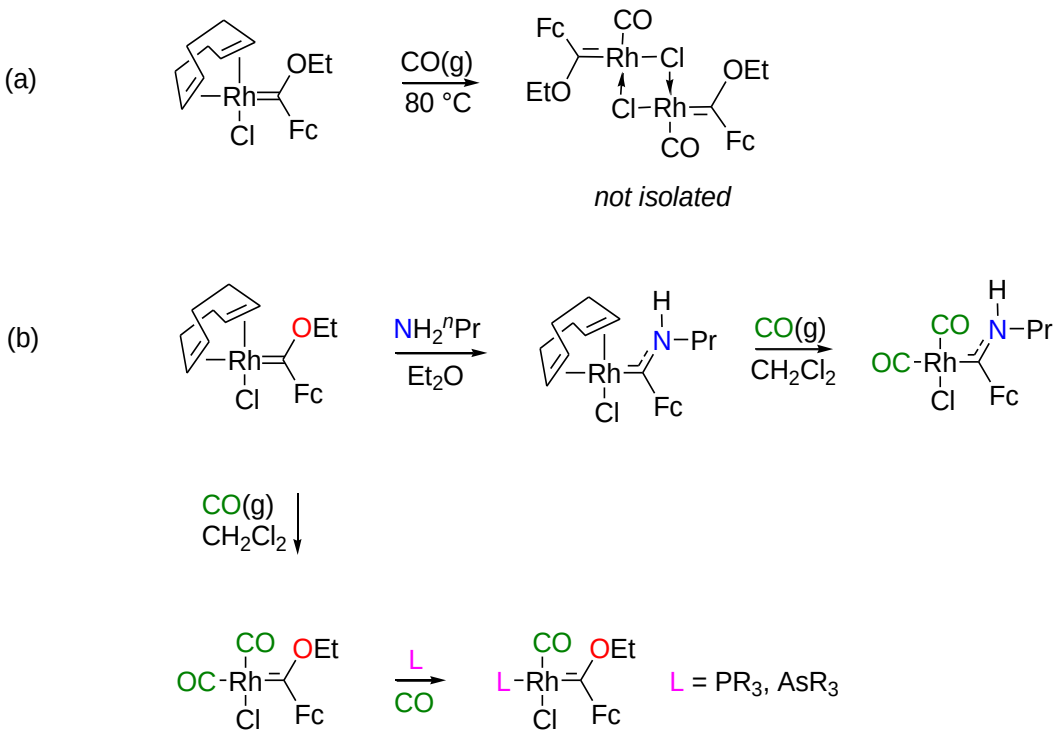

Scheme 2.7 Thermal self-dimerization (a) and post-transmetallation modification (b) of a Rh^{I} ferrocenylcarbene complex.

2.2 Aim

The successfully isolated rhodium(I) FCCs reported in the author's Masters studies featuring; ethoxy- or amino ferrocenylcarbene ligands and 1,5-cyclooctadiene (cod), dicarbonyl $(CO)_2$, or carbonyl-pnictogen {$(CO)PR_3$/ $(CO)AsR_3$} co-ligands, were found to be excellent precatalysts in the hydroformylation of 1-octene as depicted in Scheme 2.8 below.[39] During the catalytic study, excellent conversions of 1-octene (> 99%) were achieved utilizing all Rh^{I} FCCs described above, with varied chemo- and regioselectivities dependent on the electronic nature of the precatalyst and presented as turnover frequency (TOF) and *n*/*iso* ratios, respectively. TOFs in the range 343 – 418 hr^{-1} and *n*/*iso* ratios 0.79 – 1.33 were achieved under optimum catalytic conditions (0.06 mol% Rh^{I} FCC with respect to 1-octene, 40 bar syn-gas pressure, 80 °C for 4 hours). Comparison of alkoxy- *vs* amino carbene (*O*-, *vs* *N*-atom) substituent effects indicated consistent increase in catalytic activity (TOF) as electron-donor strength decreased from amino- to ethoxycarbene complexes. The effects of co-ligand electron-donating or withdrawing ability was also evident in catalytic activity of the cod- *vs* -$(CO)_2$ co-ligands, exhibiting consistent increase in turnover frequencies as electron donor strength increased from $(CO)_2$- to cod -carbene complexes. Similarly, monocarbonyl complexes indicated the same co-ligand

electron-donating effect as discussed above. Regioselectivity of the tested precatalysts however showed a consistently inverted relationship to catalytic activity in comparable complexes across the board. As TOF increases from less to more electrophilic carbene ligands, *n*/*iso* ratios respectively decrease from amino- to ethoxycarbene complexes. The same trend was observed for cod *vs* $(CO)_2$ co-ligands and for the phosphine-, phosphite-, and arsine-substituted monocarbonyl series. Therefore, electronic fine tuning of the Rh^I FCCs by varying stabilizing heteroatoms *O vs N* and co-ligands in a constant ferrocenyl-carbene environment effected isolable, thermally stable, and catalytically efficient novel Rh^I FCCs thusly reported in the prior study.

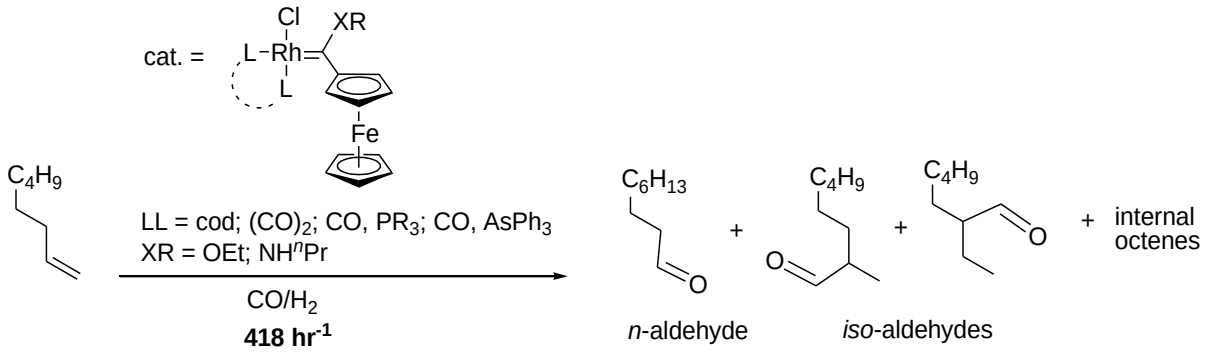

Scheme 2.8 The first reported rhodium-FCC-catalyzed hydroformylation.

Variation of the aryl (ferrocenyl) substituent, other than our failed 2-thienyl and -furyl attempts, is still unexplored to date, while a variety of Cr^0 and W^0 (hetero)aryl FCCs have been reported. Examples of the featured carbene substituent include organic entities such as an *ortho*- or *para*-substituted aniline ring, as well as other organometallic compounds such as metallocenes or piano stool cyclopentadienylmetalcarbonyls, to name a few. This leaves ample opportunity for access to new examples of Rh^I FCCs *via* the simple transmetallation route. The main aim of this study was thus to synthesize new Rh^I FCCs from W^0 precursors featuring electron-donating or withdrawing carbene substituents. To this effect, the facile transmetallation method (depicted in Scheme 2.9 below) will be employed to investigate (i) the possibility of preparing rhodium FCCs with organic substituents such as *ortho*- or *para*-*N,N*-dimethylaniline (*o*-, *p*-DMA), as electron-donating aryl carbene substituents to stabilize late transition metal FCCs, and (ii) the viability of including a different electron donating organometallic metallocenyl carbene substituent, such as a ruthenocenyl entity (Rc) for preparation of another electron rich rhodium FCC, whereby the organometallic fragment proves more electron donating than accessible *via* traditional organic moieties. The final aim (iii) is to explore the possibility of using organometallic moieties that are known to act as electron-sinks (i.e. electron withdrawing substituents such as cyclopentadienylmetalcarbonyls ($Cp'M(CO)_n$)), to prepare isolable rhodium FCCs.

All isolated Rh^{I} FCCs will subsequently be employed as precatalysts towards the hydroformylation of 1-octene, wherein the effect of electron- donating and withdrawing carbene substituents will be investigated and contrasted with the reported ferrocenyl (Fc) analogues. Finally, the known redox-activity of a reported Rh^{I} Fc-FCC will be exploited for selective chemical oxidation at the iron(II) centre, to synthesize a ferroceniumyl- (Fc^{+}) carbene complex wherein the Fc^{+} substituent is electron withdrawing (instead of donating in the neutral ferrocenyl form) for further fine-tuning and rationalization of previously reported results. The objectives of this chapter were thus (1) Synthesis of new and known tungsten(0) FCCs as precursors for carbene ligand transfer to late transition metals, (2) Synthesis and characterization of new rhodium(I) FCCs, and (3) Catalytic hydroformylation of 1-octene using new Rh^{I} FCCs, and comparison with known Rh^{I} Fc-FCCs.

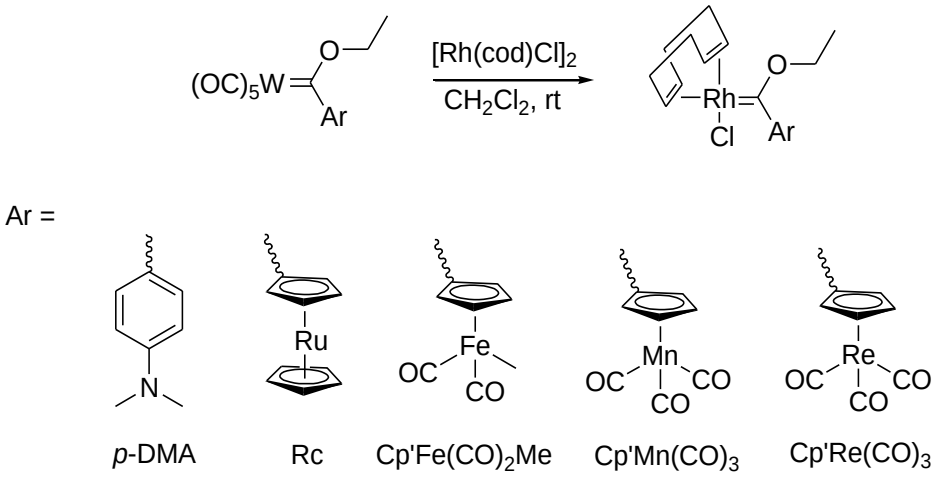

Scheme 2.9 Envisioned synthesis of new Rh^{I} FCCs

2.3 Results and discussion

2.3.1 Synthetic strategy

In this section, a summary of the synthesis of known tungsten(0) pentacarbonyl ethoxycarbene complexes featuring (hetero)aryl carbene substituents is outlined, followed by a detailed report on the synthesis and characterization of rhodium(I) FCCs [1,5-cyclooctadienechlorido{arylethoxycarbene}rhodium(I)] from precursor tungsten(0) analogues. While tungsten(0) and rhodium(I) FCCs have been previously isolated following various synthetic routes in both cases, the classic Fischer- and transmetallation reaction pathways were employed for the synthesis of W^{0}- and Rh^{I} FCCs, respectively.

2.3.1.1 Synthesis and characterization of tungsten(0) Fischer carbene complexes

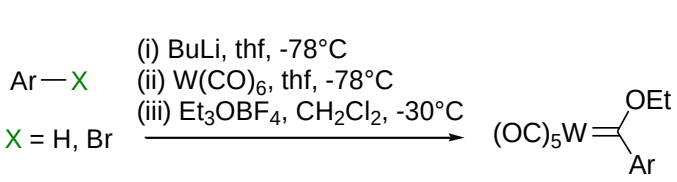

1 Ar = 2-thienyl (65%)
2 Ar = 2-furyl (63%)
3 Ar = *p*-DMA (37%)
4 Ar = Cp'Fe(CO)$_2$Me (15%)
5 Ar = Cp'Mn(CO)$_3$ (76%)
6 Ar = Cp'Re(CO)$_3$ (56%)
7 Ar = Ruthenocenyl (28%)
8 Ar = Ferrocenyl (15%)

Scheme 2.10 Synthesis of W^0 (hetero)aryl FCCs **1** – **8** *via* the classic Fischer route[50]

While both chromium(0) and tungsten(0) alkenyl FCCs have been reported as equally excellent substrates in carbene ligand-transfer reactions,[24,37,51] Cr^0-analogues of complexes **1** – **8** were excluded herein due to the low-yielding nature of Cr^0 heteroaryl FCCs compared to W^0 analogues towards synthesis of Rh^I complexes, in our previous endeavours.[52] As such, only W^0 FCCs were prepared as precursors for efficient carbene ligand transfer reactions to be discussed in this and later chapters. W^0 FCCs **1**,[53] **2**,[54] **4**,[55] **5**,[56] **7**,[57] and **8**[57–59] (outlined in Scheme 2.10 above) have been previously reported, while a methoxy-analogue of the ethoxycarbene complex **6**[19,60] has also been reported. Complex **3** however was recently thoroughly characterized within our research group,[61] since Fischer reported only the infrared spectroscopic characterization of this compound in 1970.[50]

The complexes were synthesized by equimolar reaction of *n*-butyllithium with thiophene, furan, 4-bromo-*N*,*N*-dimethylaniline, or cyclopentadienylmetalcarbonyl precursors [CpFe(CO)$_2$Me], [CpMn(CO)$_3$], and [CpRe(CO)$_3$], while *tert*-butyllithium was employed for analogous reaction with ruthenocene and ferrocene, resulting in the desired organolithium intermediates bearing 2-thienyl (Th), 2-furyl (Fu), *p*-DMA, Cp'Fe(CO)$_2$Me, Cp'Mn(CO)$_3$, Cp'Re(CO)$_3$, Rc, and Fc moieties. Addition of tungsten(0) hexacarbonyl and subsequent alkylation results, after column chromatographic purification (employing aluminium oxide or silica gel as resin and *n*-hexane as eluent), in the targeted W^0 FCCs **1** – **8** (Scheme 2.10). Inclusion of (hetero)aryl carbene substituents result in carbene complexes stabilized by π-bond delocalization (see Figure 2.4 below). Specifically, organic substituents such as *p*-DMA offer π-resonance stabilization of the ensuing complex (a),[62] while metal-containing (π-bound) substituents such as ferrocene exhibit π-resonance interaction between the cyclopentadienyl ring and the carbene-metal center (b).[63] Thus overall electron donation from metallocenyl substituents is generally accepted as inductive (c), while cyclopentadienyl-π-metalcarbonyl substituents exhibit an overall electron withdrawing effect (d).[47]

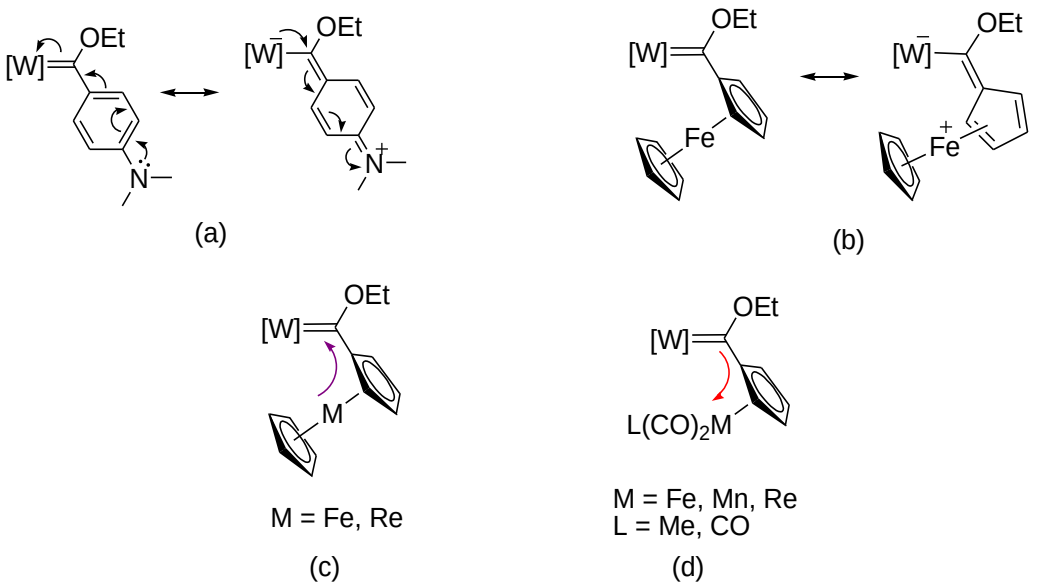

Figure 2.4 π-resonance effects of organic *p*-DMA (a) and organometallic-cyclopentadienyl (b) carbene substituents, and electron-inductive effects of metallocenyl (c) and cyclopentadienylmetal carbonyl (d) carbene substituents.

The targeted W^0 FCCs **1** – **8** (depicted in Figure 2.5 below) were synthesized *via* the Fischer route as described above. The indicated atom-labelling system will henceforth be used when referring to the characterization of the (hetero)aryl Th, Fu, *p*-DMA, and metal-cyclopentadienyl ($Cp'Fe(CO)_2Me$, $Cp'Mn(CO)_3$, $Cp'Re(CO)_3$, Fc, and Rc) carbene substituents.

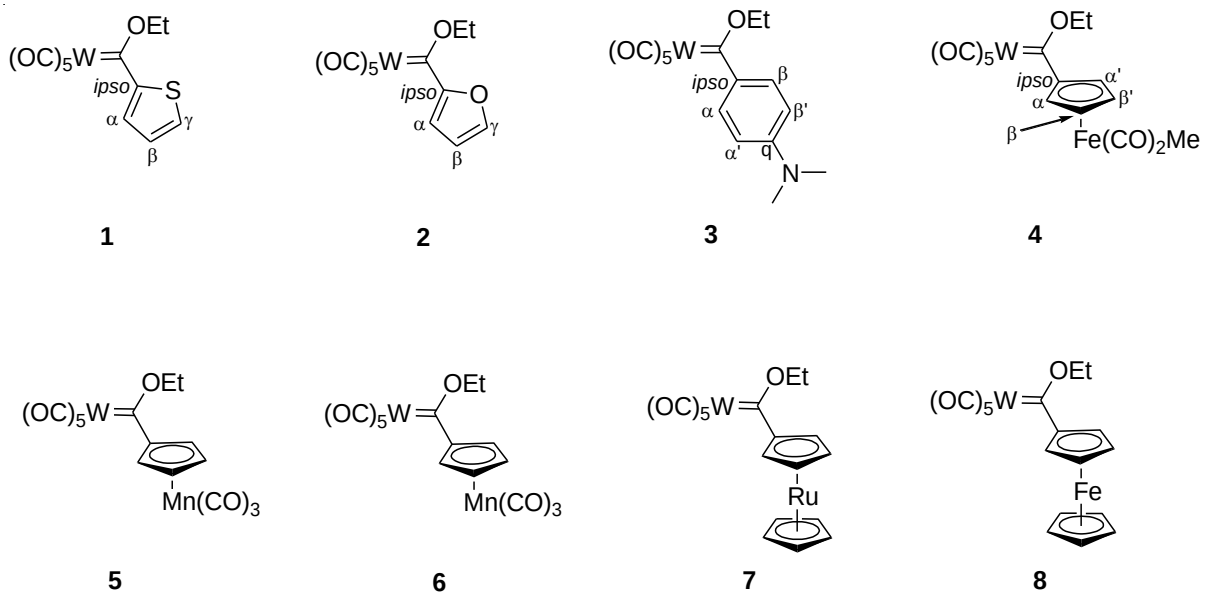

Figure 2.5 Successfully synthesized W^0 FCCs for carbene ligand transfer reactions reported in this thesis, with atom-labelling scheme employed for the (hetero)aryl carbene substituents.

Spectroscopic characterization of W^0 ethoxycarbene complexes **1** – **8** was in agreement with literature reports of these complexes. Nuclear Magnetic Resonance (NMR) spectroscopy[64] of the isolated complexes consistently indicated expected chemical resonances of the α and α' C- and H-atoms, and β and β' C/H atoms, respectively, for *p*-DMA (**3**) and cyclopentadienyl carbene substituents in **5** – **8**. For example, ^1H and $^{13}C\{^1H\}$ NMR spectra of complex **6** presented in Figure 2.6 below clearly show this symmetry pattern, wherein $H_{\alpha,\alpha'}$ and $H_{\beta,\beta'}$ resonate at 5.37 and 4.28 ppm, respectively (a). $^{13}C\{^1H\}$ NMR chemical shifts of $C_{\alpha,\alpha'}$ and $C_{\beta,\beta'}$ accordingly resonate at 90.1 and 85.6 ppm, respectively (b), again indicating that $C_{carbene}$-C_{ipso} bond rotation in the isolated W^0 FCCs is observed.

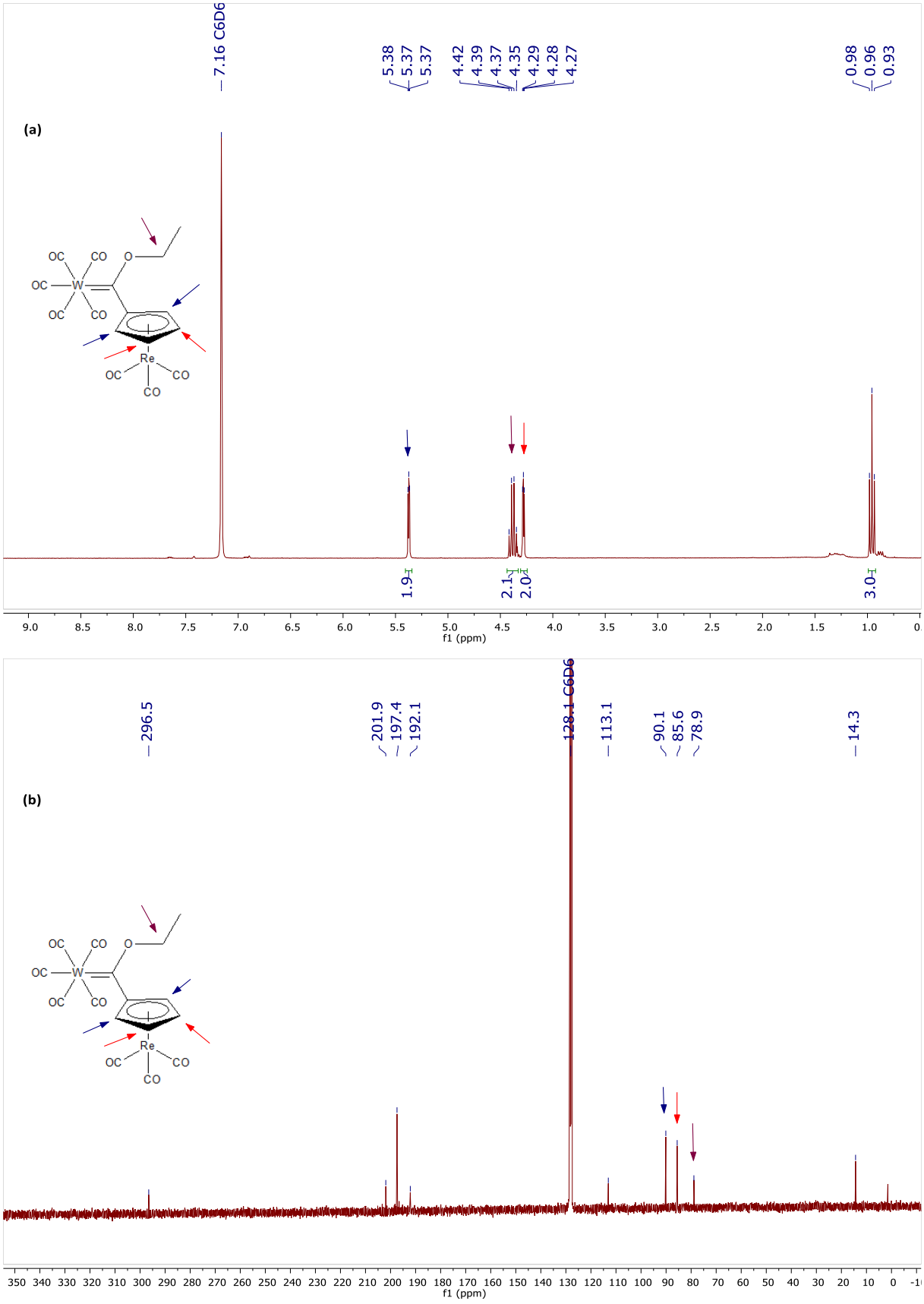

Figure 2.6 ^{1}H- (a) and ^{13}C{^{1}H}- (b) NMR spectra of **6** indicating the symmetry observed for the cyclopentadienyl carbene substituent resonances.

$^{13}C\{^{1}H\}$ NMR spectroscopy of the complexes indicated a downfield shift of the carbene carbon atom resonances from heteroaryl to metal-cyclopentadienyl carbene ligands. Less significant differences are observed among comparable organic and organometallic substituents. Specifically, for the Th-, Fu- and *p*-DMA-substituted carbene complexes **1**, **2**, and **3**, the δ $C_{carbene}$ resonances are observed at 285, 291, and 299 ppm, respectively. This suggests that the *p*-DMA substituent is less electron donating than the Th and Fu substituents, although later experimental evidence (*vide infra*) provides contrasting results. For the bimetallic complexes, the corresponding δ $C_{carbene}$ chemical shifts are observed at 304, 303, 296, 297, and 304 ppm for W^0 metalcarbonyl- and metallocenyl-FCCs **4** ($Cp'Fe(CO)_2Me$), **5** ($Cp'Mn(CO)_3$), **6** ($Cp'Re(CO)_3$), **7** (Rc), and **8** (Fc), respectively. The downfield δ $C_{carbene}$ resonance observed for Rc-substituted **7** in comparison to $Cp'M(CO)_2L$-substituted **5** and **6** was unexpected, as strongly electron withdrawing $Cp'M(CO)_2L$ substituents are expected to exhibit more downfield δ $C_{carbene}$ resonances compared to the strongly electron donating metallocenyl substituents. This is however not unusual, as it is known that $^{13}C\{^{1}H\}$ NMR spectroscopy is not a reliable method to determine substituent electron donating effect on the C-atom under investigation. Therefore, the relative electrophilicity of W^0 FCCs **1** – **8** could not be determined unambiguously from $^{13}C\{^{1}H\}$ NMR spectral shifts.

Fourier-transform infrared (FT-IR) spectroscopy of the isolated complexes could be used to tentatively categorize the electron-donor or -withdrawal extent of complexes **1** – **8**. The carbonyl (C-O) vibrational frequencies of metal-carbonyls are said to be independent of other vibrations in the complex under investigation, thus C-O vibrational frequencies and bond orders can be directly correlated.[65] FC ligands are weak π-acceptors in comparison to carbonyl ligands, therefore π-backbonding ability of the metal is stronger towards carbonyl ligands as compared to FC ligands. Thus when weak π-acceptors are complexed to metal-carbonyls as in $M(CO)_nL$-, electron donation from the ligand L to central metal M to the π* orbital of CO co-ligands is supported by consistent lowering of the carbonyl vibrational stretching frequencies with an increase in the electron donor strength of L.[66] The M-C bond order of metal carbonyls increases with an increase in backbonding, with a consequent decrease in the C-O bond length and lowering of the carbonyl stretching vibrational frequency. The recorded IR spectra of all W^0 FCCs **1** – **8** exhibit a pattern of four bands in the carbonyl region as shown in Figure 2.7 and Table 2.1 below. This IR spectroscopic pattern is common for the pseudo-C_{4v} symmetry observed for octahedral monosubstituted metal-pentacarbonyl complexes $[M(CO)_5L]$ (L = carbene).[49,50,58,63]

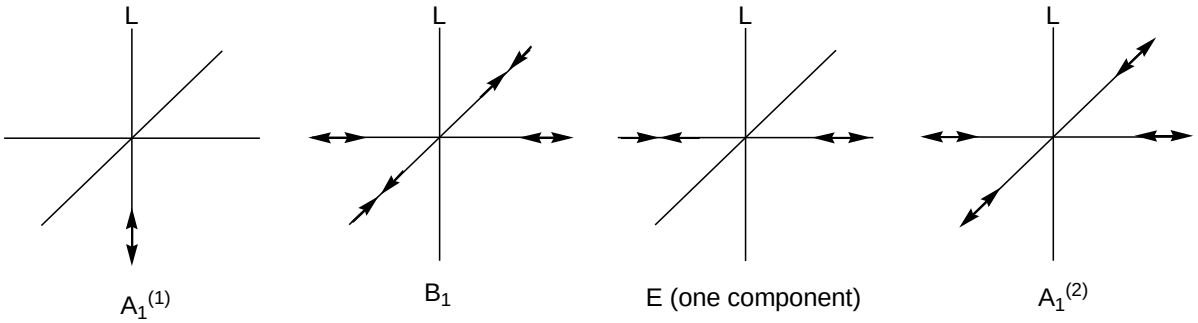

Figure 2.7 IR active modes observed for complexes of the general formula $[M(CO)_5L]$

Table 2.1 FT-IR tungsten-carbonyl stretching frequencies of **1** – **8** recorded in hexane

Complex	**Carbonyl stretching frequencies (cm^{-1})**			
	$A_1^{(1)}$	**$A_1^{(2)}$**	**B_1**	**E**
1	2069	1988	1963	1948
2	2072	1979	1960	1949
3	2062	1960	1955	1933
4	2069	1982	1960	1943
5	2070	1982	1957	1943
6	2071	1982	1951	1942
7	2063	1972	1940	1933
8	2066	1976	1948	1936

For the recorded IR spectra, a weak $A_1^{(1)}$ vibrational band is consistently observed at the highest frequencies (2062 – 2072 cm^{-1}), followed by an intense E band with a medium $A_1^{(2)}$ shoulder band. The typically IR-inactive B mode appears as a weak vibrational band due to lifting of symmetry rules by the non-monatomic carbene ligands. The high-frequency $A_1^{(1)}$ vibrational band (*trans* to the carbene ligand) can be utilized as an IR-probe to organize the W^0 complexes in order of electron- donor or withdrawal effect of FC ligands featured in **1** – **8**. In this case, *p*-DMA-substituted complex **3** exhibits the lowest $A_1^{(1)}$ frequency at 2062 cm^{-1}, followed by metallocenyl complexes **7** and **8** (2063, 2066 cm^{-1}). Higher vibrational frequencies are observed for complexes **1**, **2**, **4**, **5** and **6** at 2069, 2072, 2069, 2070, and 2071 cm^{-1}, respectively. Thus the *p*-DMA ethoxycarbene ligand is the most electron donating within the reported series according to $A_1^{(1)}$ frequency trends, followed by the Rc analogue as a close second. The Fc-ethoxycarbene ligand then follows as more electron donating than the piano

stool electron-sink and heteroaryl carbene ligands (2066 *vs* 2069 – 2072 cm^{-1}). The isolated W^0 FCCs can therefore be arranged in order of increasing electrophilicity as **3** (p-DMA) < **7** (Rc) < **8** (Fc) < **1** (Th) ≈ **4** ($Cp^{'}Fe(CO)_2Me$) < **5** ($Cp^{'}Mn(CO)_3$) < **6** ($Cp^{'}Re(CO)_3$) < **2** (Fu). Additional carbonyl vibrational bands also appear for the iron, manganese, and rhenium carbonyl moieties in complexes **4** ($Cp^{'}Fe(CO)_2Me$), **5** ($Cp^{'}Mn(CO)_3$), and **6** ($Cp^{'}Re(CO)_3$), respectively, and have been appropriately assigned in the experimental section.

2.3.1.2 Tungsten(0)-rhodium(I) transmetallation

Tungsten(0) FCCs **3** – **7** were utilized as precursor complexes for the synthesis of new examples of Rh^{I} complexes as summarized in Scheme 2.11 below. As previously reported, carbene transfer reactions with **1** and **2** resulted in carbene dimerization.[39] All transmetallation reactions were carried out under moisture- and oxygen-free conditions, and were monitored by thin layer chromatography (TLC). Regrettably, all attempts at synthesizing Rh^{I} FCCs from W^0 complexes **4**, **5**, and **6** proved futile. Reaction of complex **4** with the Rh^{I} precursor $[Rh(cod)Cl]_2$ resulted in unidentified (insoluble) side product formation upon complete conversion of the starting material as observed on a TLC plate. The targeted Rh^{I} FCC depicted in Scheme 2.11 (a) could therefore not be isolated. Scheme 2.11 (b), (c), and (d) depicts W^0-Rh^{I} transmetallations where formation of the Rh^{I} FCC (**9** – **11**, and **14**) could be observed on the TLC plate. After complete conversion of starting W^0 FCCs **3**, **5**, **6**, and **7** was observed on the TLC plate, the product Rh^{I} FCCs (**10**, **9a**, **9b**, and **11** respectively) were purified by column chromatography and were isolated in high yields (72 – 84%). However, spectroscopic characterization of complexes **9a** and **9b** indicated decomposition to dimeric products over time (*vide supra*). Carbene ligand transfer from complexes **3** and **7** yielded stable [Rh(cod){carbene}Cl] complexes **10** and **11** respectively (route (c), Scheme 2.11). Further co-ligand modification *via* reaction with gaseous carbon monoxide yielded the corresponding dicarbonyl carbene complexes $[Rh(CO)_2\{carbene\}Cl]$, **12** and **13** respectively. Known Fc-carbene complexes **14** – **17** (route (d),[39] were also included in the study for comparison of the previously reported catalytic performance with the new examples.

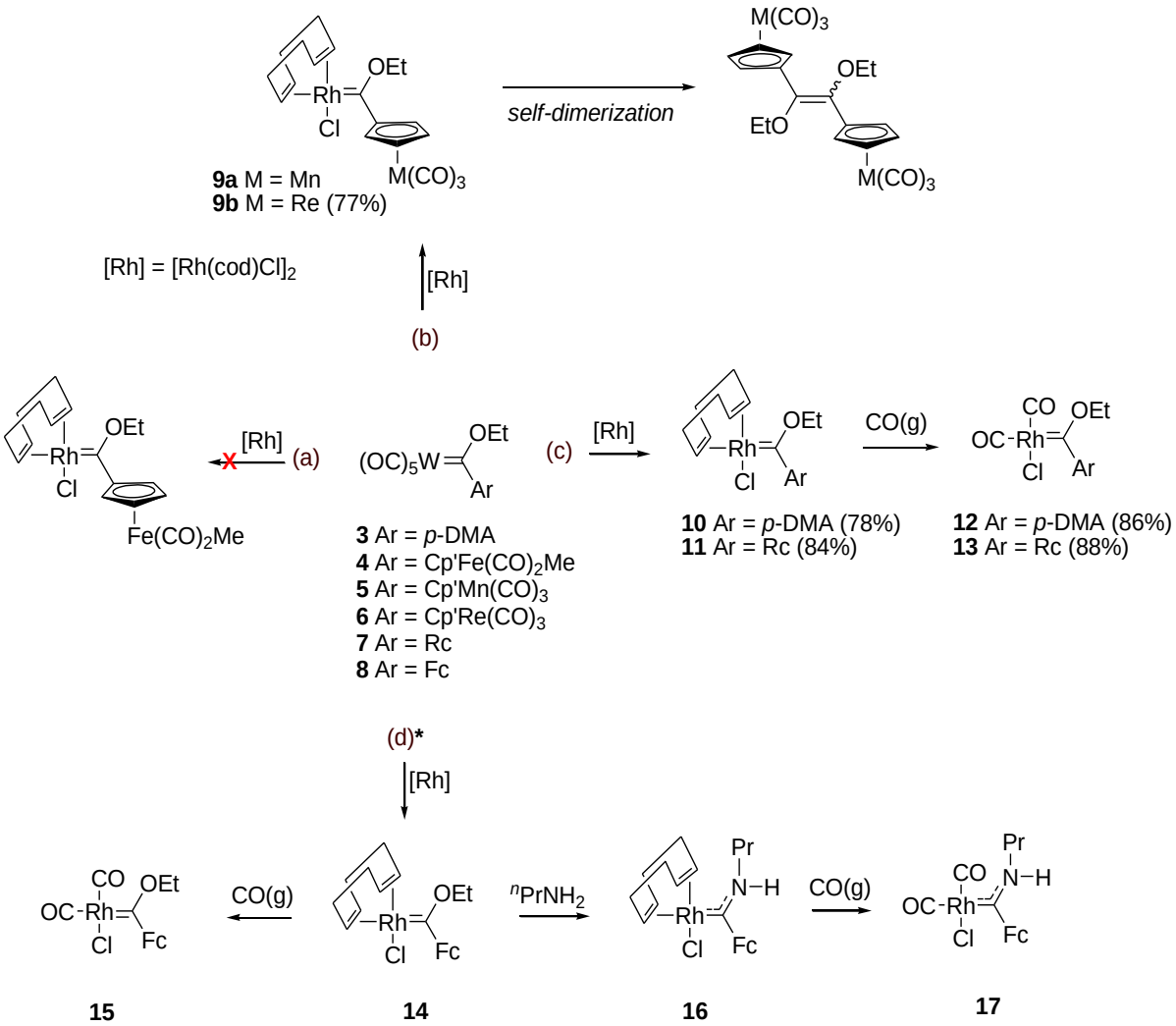

Scheme 2.11 Synthesis of Rh^{I} FCCs *via* simple transmetallation and ligand modification. *This route has been previously reported.[39]

While transmetallation from W^0 FCCs **5** and **6** indicated successful carbene ligand transfer as observed on the TLC plate, the resulting Rh^{I} FCCs **9a** and **9b** proved unstable in solution. NMR spectroscopy of these complexes indicated the undesired carbene-ligand dissociation reported for Rh^{I} alkenyl-[11] and heteroaryl-FCCs[39] in literature. The ^{1}H NMR spectrum of **9a** was poorly resolved, and could not be unambiguously assigned. Evidence for the presence of the decomposition alkene (carbene-dimer), along with the targeted Rh^{I} FCC, was present immediately upon dissolving in solvent. This includes the duplication of the upfield shifted ethoxy-CH_2 and -$CpMn(CO)_3$ $H_{\alpha,\alpha'}/H_{\beta,\beta'}$ signals. Complex **9a** could therefore not be characterized, even by ^{1}H NMR spectroscopy. For complex **9b**, the purified carbene complex is initially observed as the only species in the ^{1}H NMR spectrum (see Figure 2.8 below). The observed NMR spectrum indicates a symmetry/chemical equivalency pattern similar to reported Rh(cod) FCCs in literature, where each of the ethoxy-CH_2 protons resonate at distinct chemical shifts. Different chemical environments are also observed for each of the $Cp'Re(CO)_3$ $H_{\alpha,\alpha',\beta,\beta'}$ protons, with

an average 1 ppm downfield shift in comparison to W^0 precursor **6**. Decomposition ensues in solvent over time, as observed in the $^{13}C\{^1H\}$ NMR spectrum in Figure 2.9, where the FCC **9b** is still observed as evidenced by the carbene carbon resonance at 300 ppm. After approximately 16 hours in solution, another ^1H NMR spectrum of **9b** was recorded, showing extensive decomposition to the carbene-dimer alkene and the corresponding Rh-cod dimer (Figure 2.10). Due to the evident instability **9b**, the complex could not be completely characterized, and only the NMR characterization is reported in the experimental section.

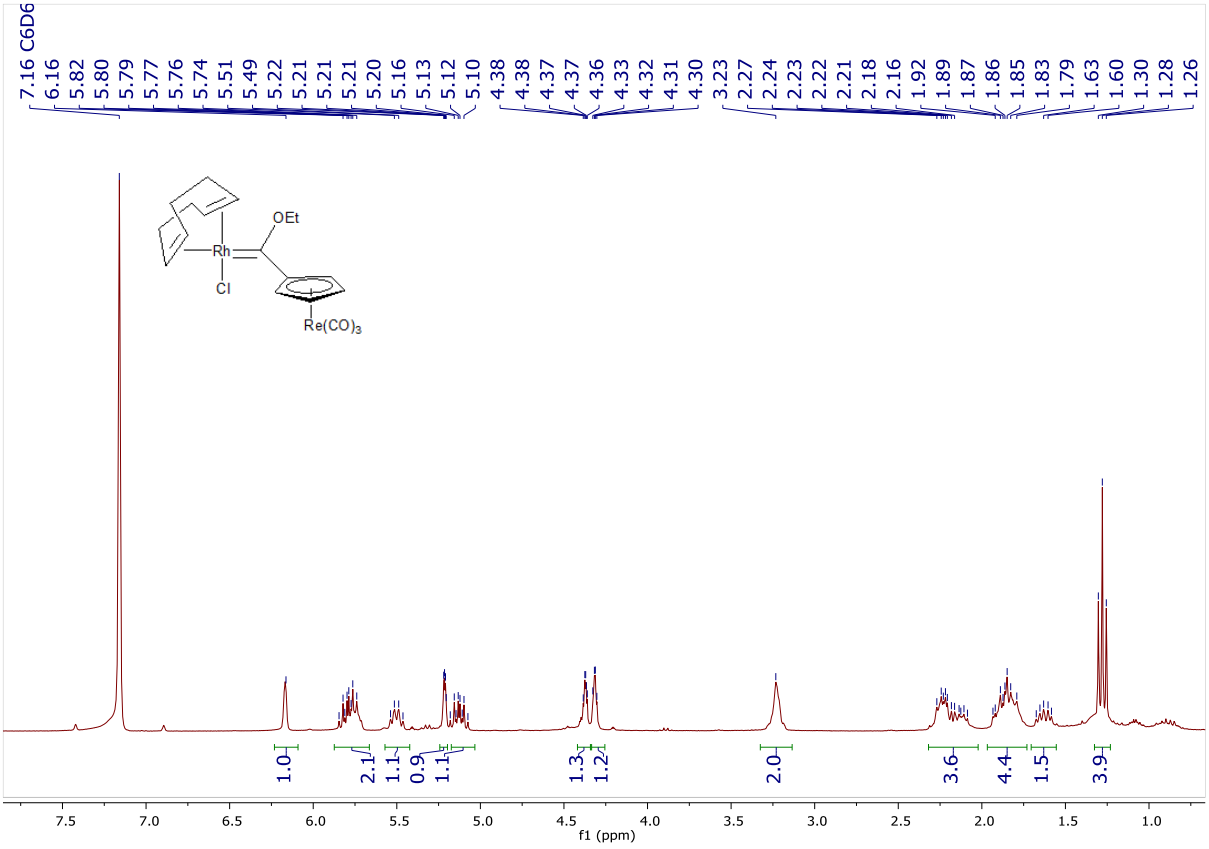

Figure 2.8 ^1H NMR spectrum of **9b** in C_6D_6 before decomposition

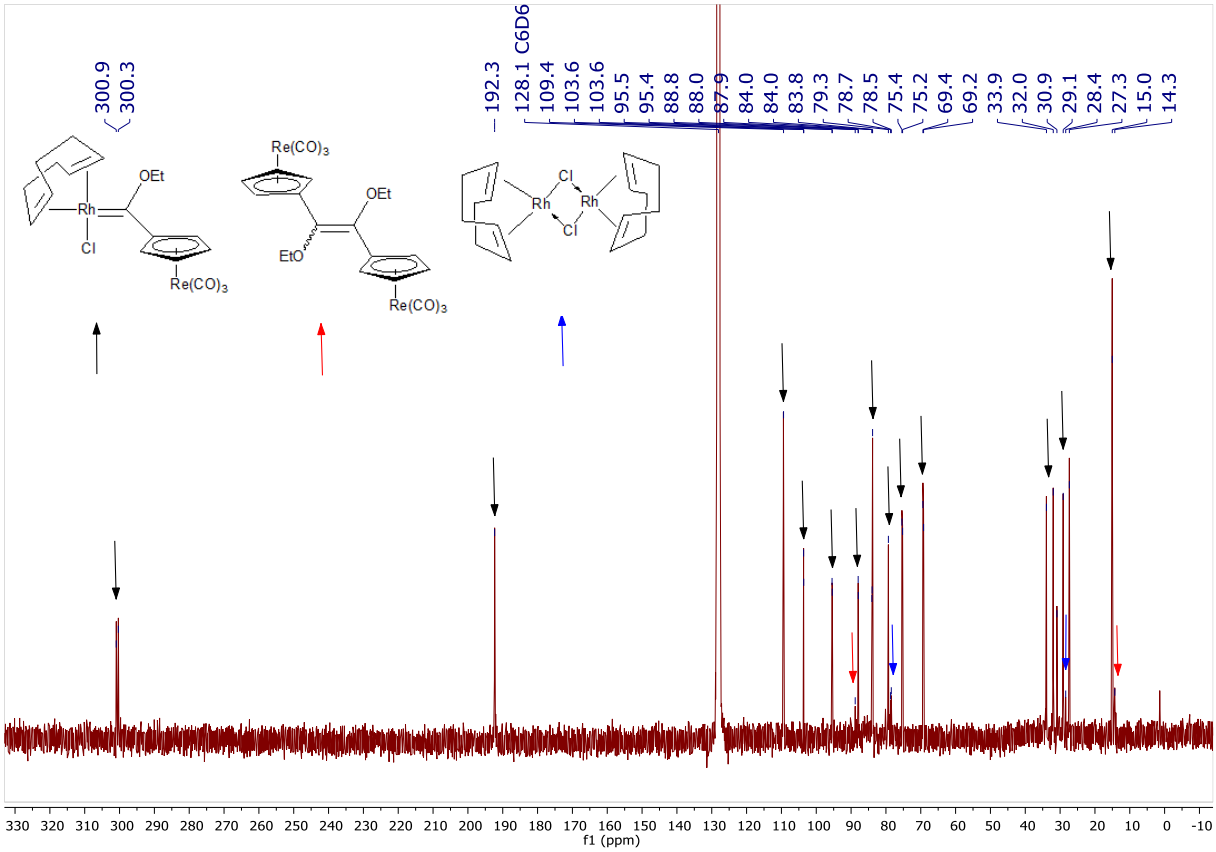

Figure 2.9 $^{13}C\{^{1}H\}$ NMR spectrum of **9b** (and minor decomposition-product signals) in C_6D_6 after a time lapse of 2 hours.

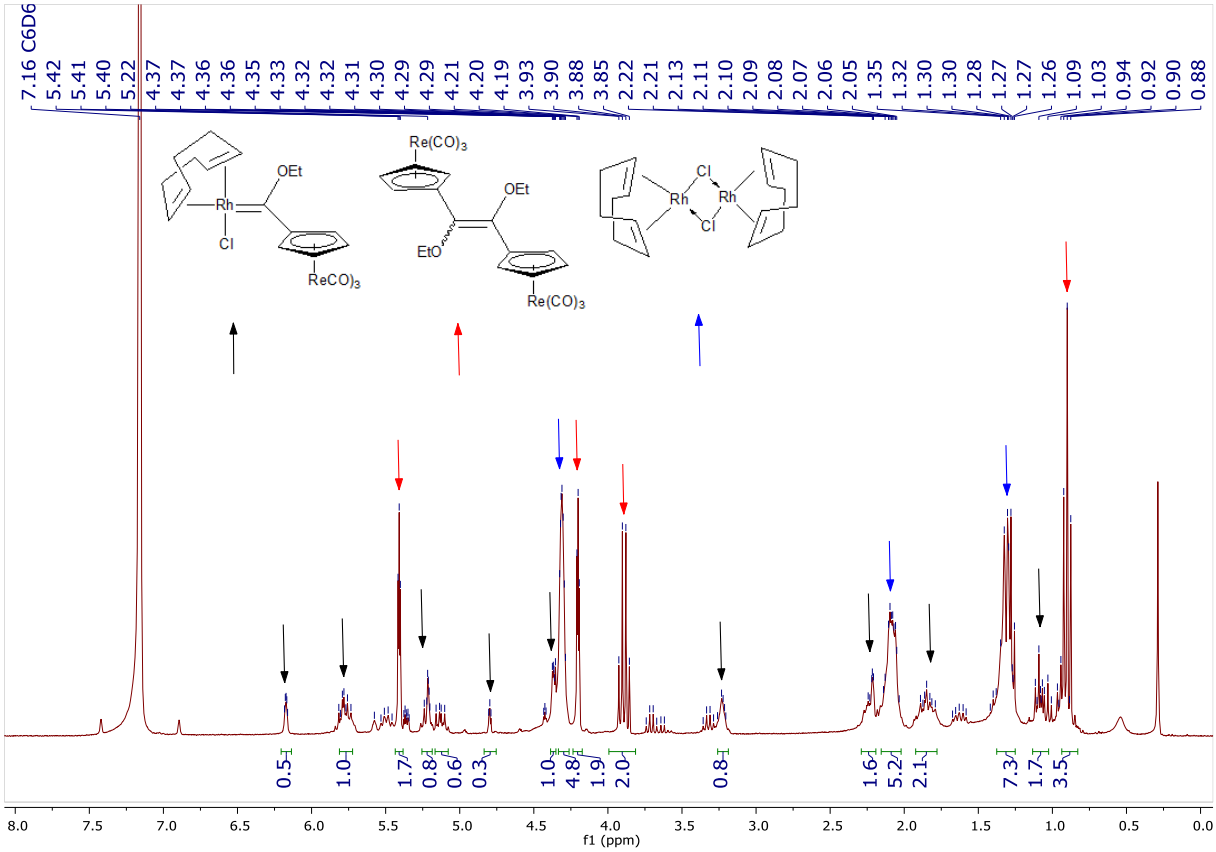

Figure 2.10 ^{1}H NMR spectrum of **9b** (and major decomposition-product signals) in C_6D_6 after a time lapse of 16 hours.

2.3.2 Characterization of stable rhodium(I) Fischer carbene complexes

In this section, spectroscopic (NMR, MS, and FT-IR), electrochemical (cyclic voltammetric), and structural (single-crystal XRD) characterization of successfully isolated complexes **10** – **13** are discussed. Important NMR spectroscopic details of each complex are first discussed in brief, followed by comparative characterization of the new Rh^{I} *p*-DMA- and Rc-FCCs and previously reported Fc-analogues **14** – **17**.

2.3.2.1 1,5-cyclooctadienechlorido{*p*-(*N,N*-dimethylaniline)ethoxycarbene}rhodium(I) complex 10

^{1}H and ^{13}C{^{1}H} NMR spectra of complex **10** (depicted as Figure 2.11 and 2.12, respectively) indicated loss of symmetry in the carbene- and cod ligand environments, in comparison to the precursors W^{0} FCC **3** and [Rh(cod)Cl]$_2$, respectively. This asymmetry pattern is common for Rh^{I}-cod FCCs in literature,[12,39] and was evidenced by splitting of the ethoxy-CH_2 protons of **10** into distinct chemical environments (Figure 2.11 insert). When coordinated to a tungsten metal center, ethoxy-CH_2 protons

consistently resonate as one quartet signal (see W^0 FCCs **1** – **8**). This characteristic loss of symmetry also extends to cod-CH proton and carbon signals, and is the first spectroscopic evidence of successful transmetallation in the synthesis of complex **10**, in addition to the presence of characteristic carbene carbon atom doublet (*vide supra*) observed in the $^{13}C\{^1H\}$ NMR spectrum.

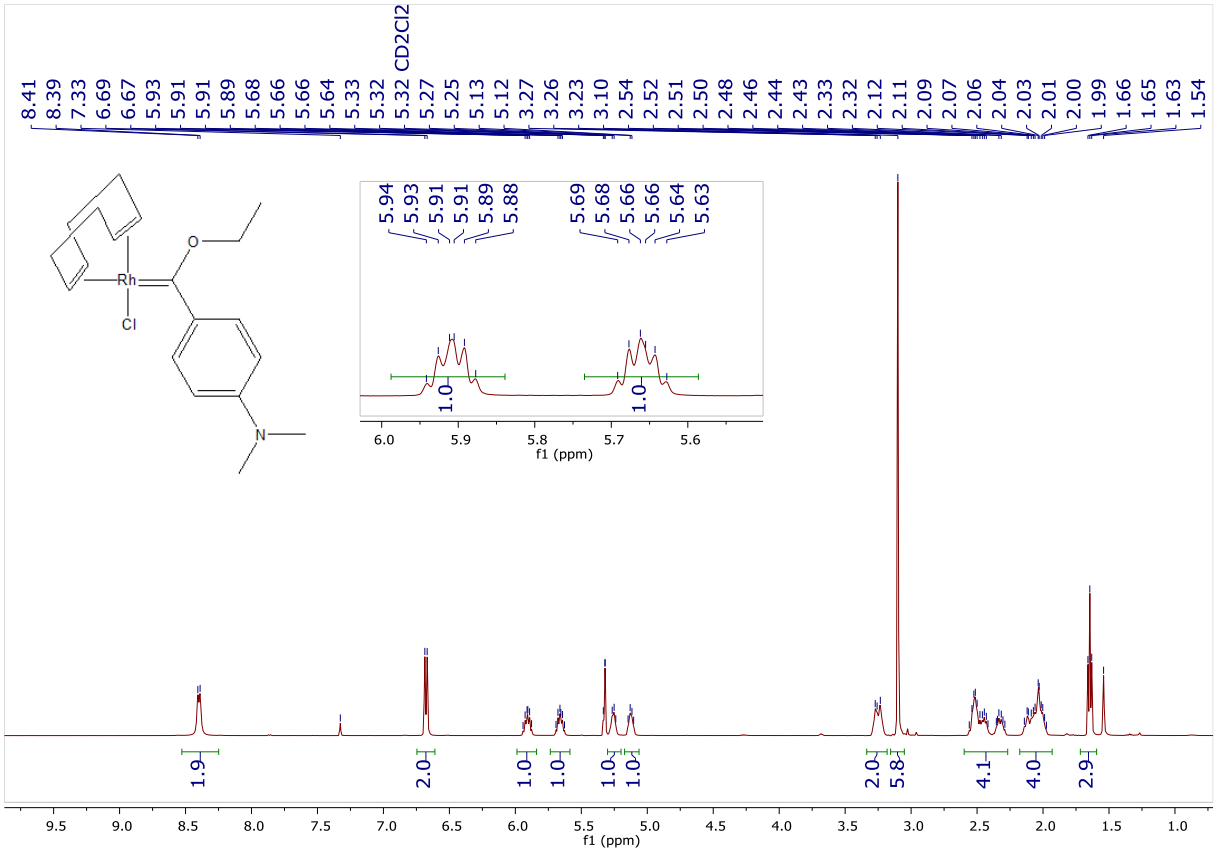

Figure 2.11 ^1H NMR spectrum of **10** in CD_2Cl_2

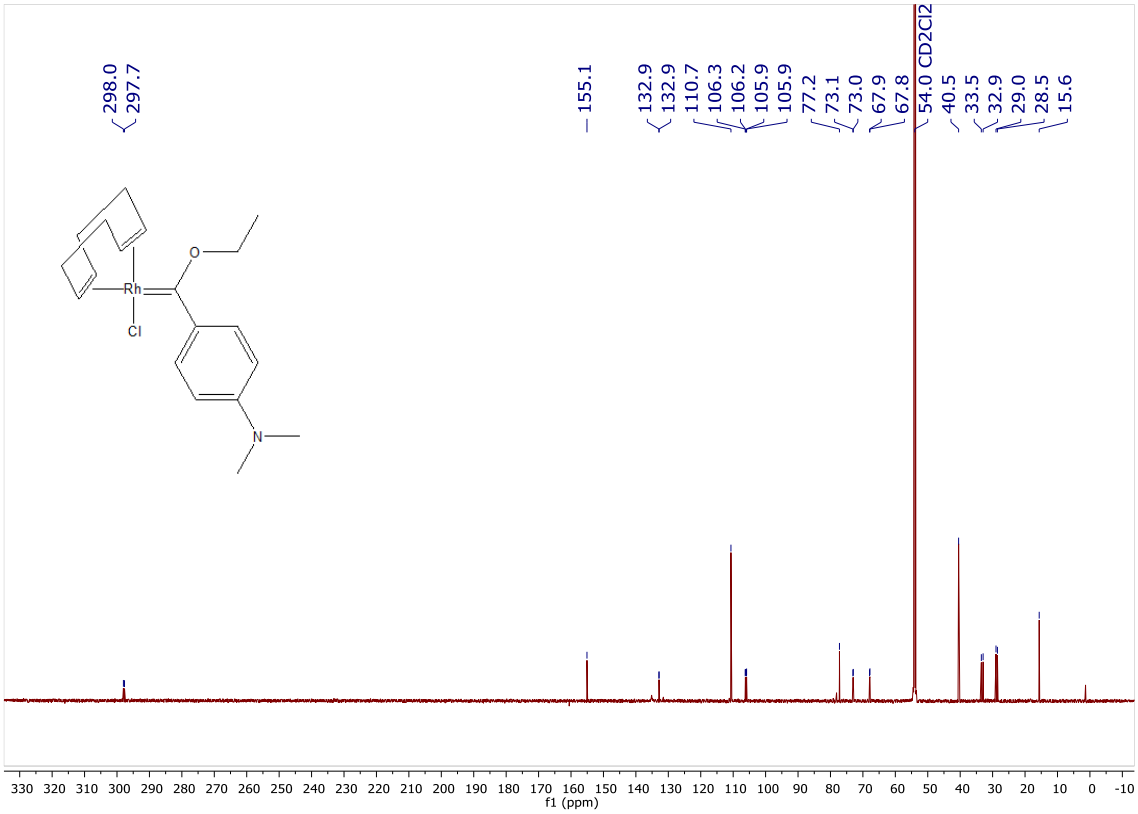

Figure 2.12 $^{13}C\{^{1}H\}$ NMR spectrum of **10** in CD_2Cl_2

2.3.2.2 1,5-cyclooctadienechlorido{(ruthenocenyl)ethoxycarbene}rhodium(I) complex 11

Similarly to complex **10** above, NMR spectroscopy of Rc-ethoxycarbene complex **11** also indicated a loss of symmetry around the rhodium-carbene center, compared to what was observed for **10**. Both the ^{1}H and $^{13}C\{^{1}H\}$ NMR spectra of complex **11** (Figure 2.13 and 2.14 below) display a duplication of the ethoxy-CH_2 and cod-CH chemical shifts. The sterically bulky Rc substituent also exhibits this asymmetric pattern, as each of the Rc-Cp' protons/carbons resonate at different chemical shifts in the $^{1}H/^{13}C\{^{1}H\}$ NMR spectra. This asymmetry of the carbene ligand, as opposed to completely symmetrical W^0 FCC **7**, is the first spectroscopic evidence of successful synthesis of complex **11**.

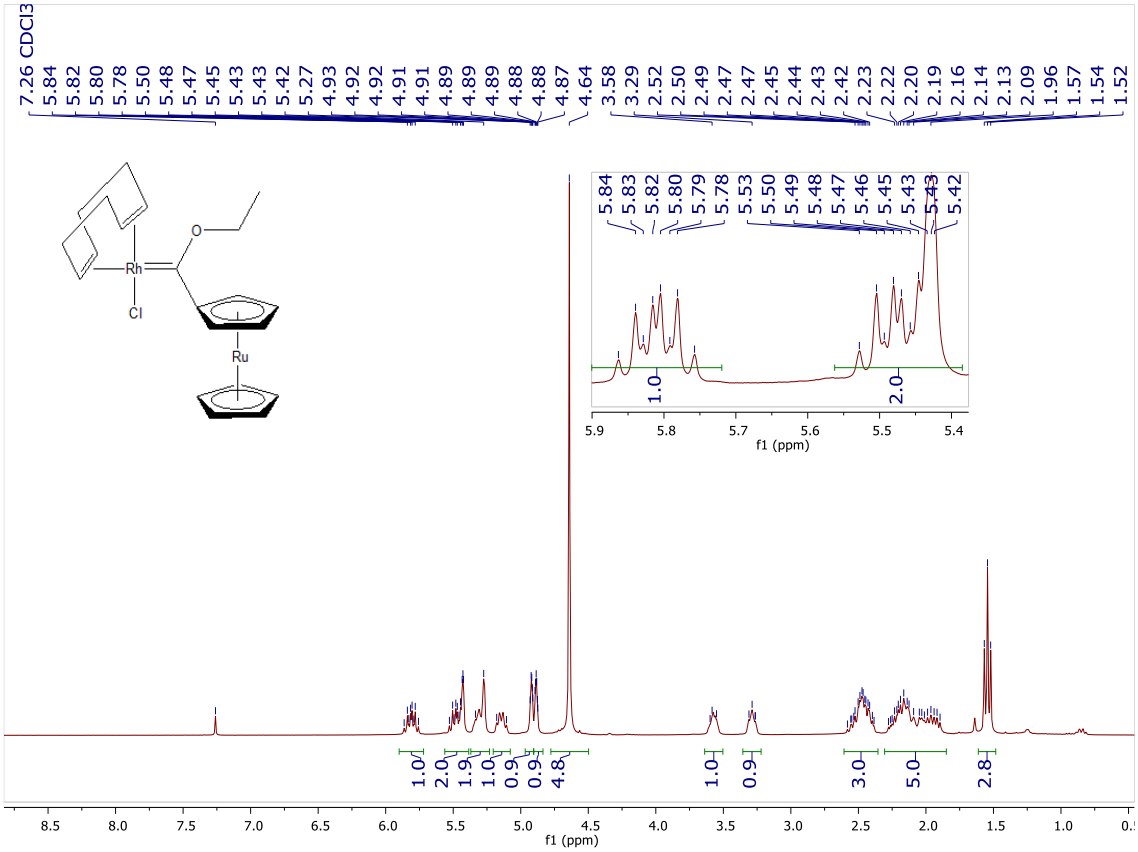

Figure 2.13 ^{1}H NMR spectrum of **11** in $CDCl_3$

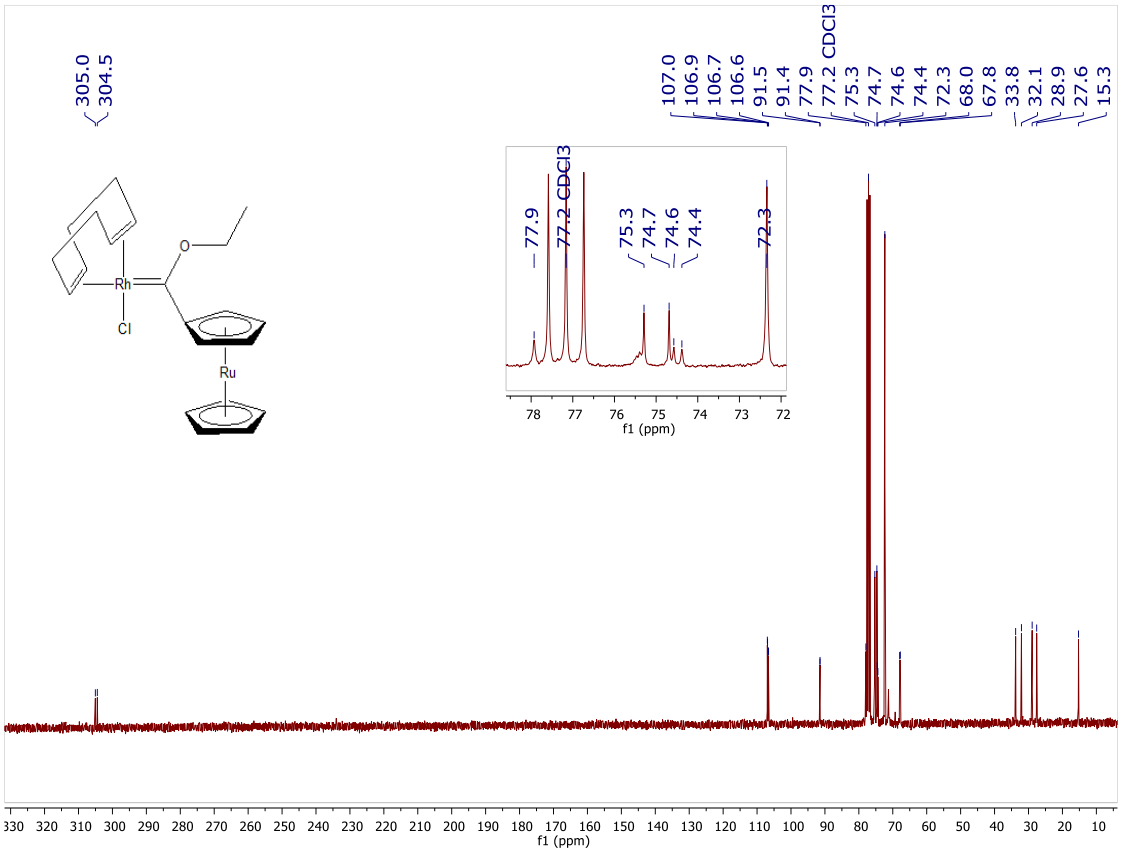

Figure 2.14 $^{13}C\{^{1}H\}$ NMR spectrum of **11** in $CDCl_3$

2.3.2.3 *cis*-(dicarbonyl)chlorido{(*p*-(*N,N*-dimethylaniline)ethoxycarbene}rhodium(I) complex 12

In contrast to complex **10** with the sterically hindered cod co-ligand, the dicarbonyl complex **12** displays again a completely symmetrical chemically equivalent environment around the rhodium-carbene center. As evident in the ^{1}H NMR spectrum of **12** (Figure 2.15), ethoxy-CH_2 protons resonate as one multiplet signal which appears to be an overlap of two quartet signals (Figure 2.15 insert), effected by the removal of the sterically bulky chelating cod ligand from the rhodium coordination sphere. Additionally, complete disappearance of all cod-ligand signals in both the ^{1}H and ^{13}C{^{1}H} NMR spectra of **12** (Figure 2.15 and 2.16 respectively) in comparison to spectra of **10** is also evident, and was thus indicative of successful cod-to-$(CO)_2$ ligand substitution in the synthesis of **12**.

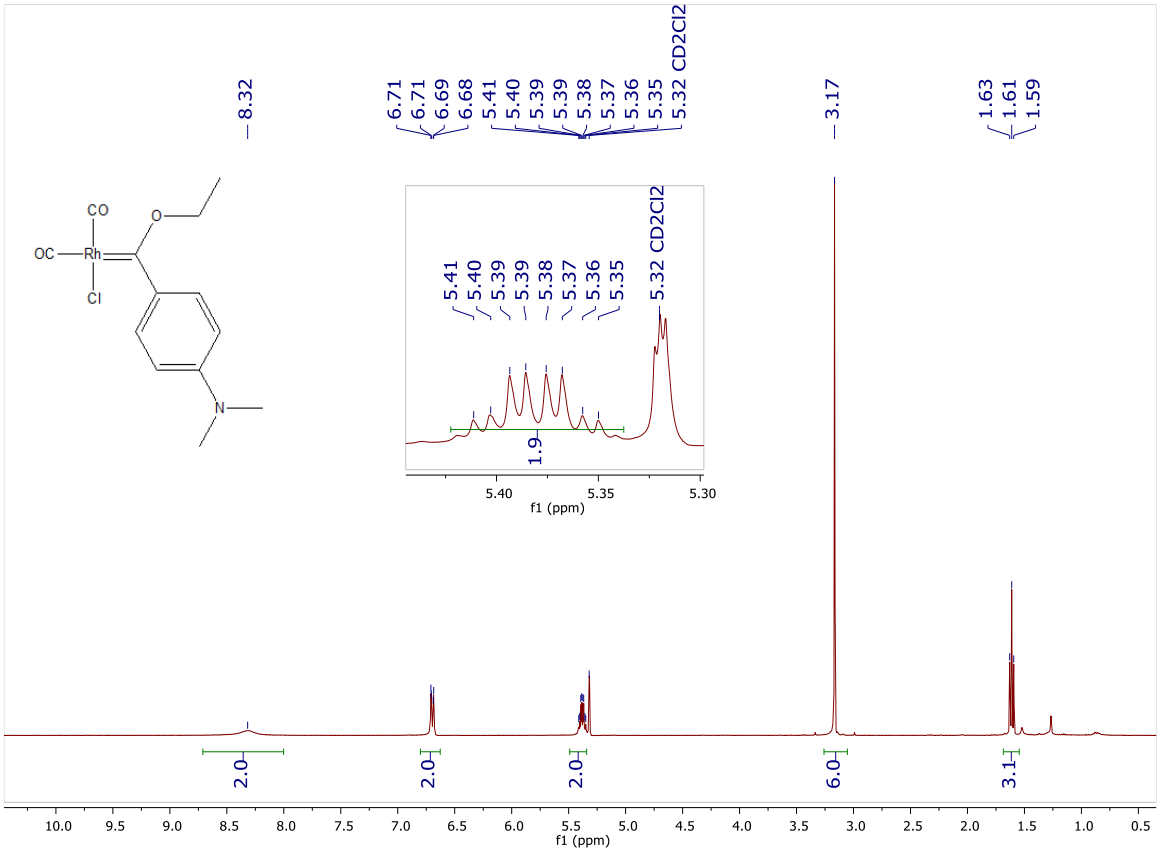

Figure 2.15 ^{1}H NMR spectrum of **12** in CD_2Cl_2

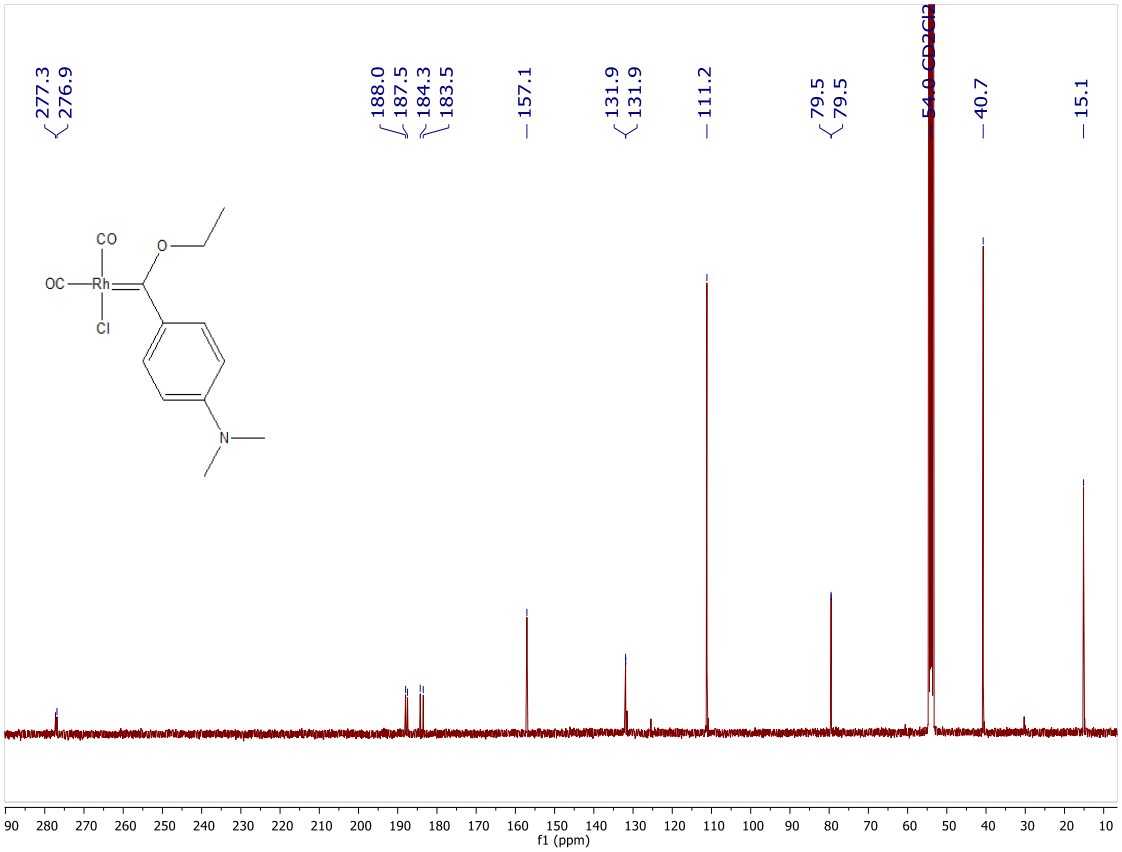

Figure 2.16 $^{13}C\{^{1}H\}$ NMR spectrum of **12** in CD_2Cl_2

2.3.2.4 *cis*-(dicarbonyl)chlorido{(ruthenocenyl)ethoxycarbene}rhodium(I) complex 13

Substitution of the bulky cod ligand by two carbonyl ligands from complex **11** to **13** respectively did not result in a regaining of the symmetrical chemical environment around the rhodium-carbene center as seen for **12**. The Rc carbene substituent proved a steric hindrance as the ^{1}H NMR spectrum of **13** indicates different chemical shifts for ethoxy-CH_2 protons and Rc-$H_{\alpha,\alpha'}$ protons (Figure 1.17 insert). ^{1}H and $^{13}C\{^{1}H\}$ NMR spectra of **13** (Figure 2.17 and 2.18 respectively) also indicate disappearance of all cod-ligand signals as compared to the Rh-cod analogue **11**, indicative of the successful formation of complex **13**.

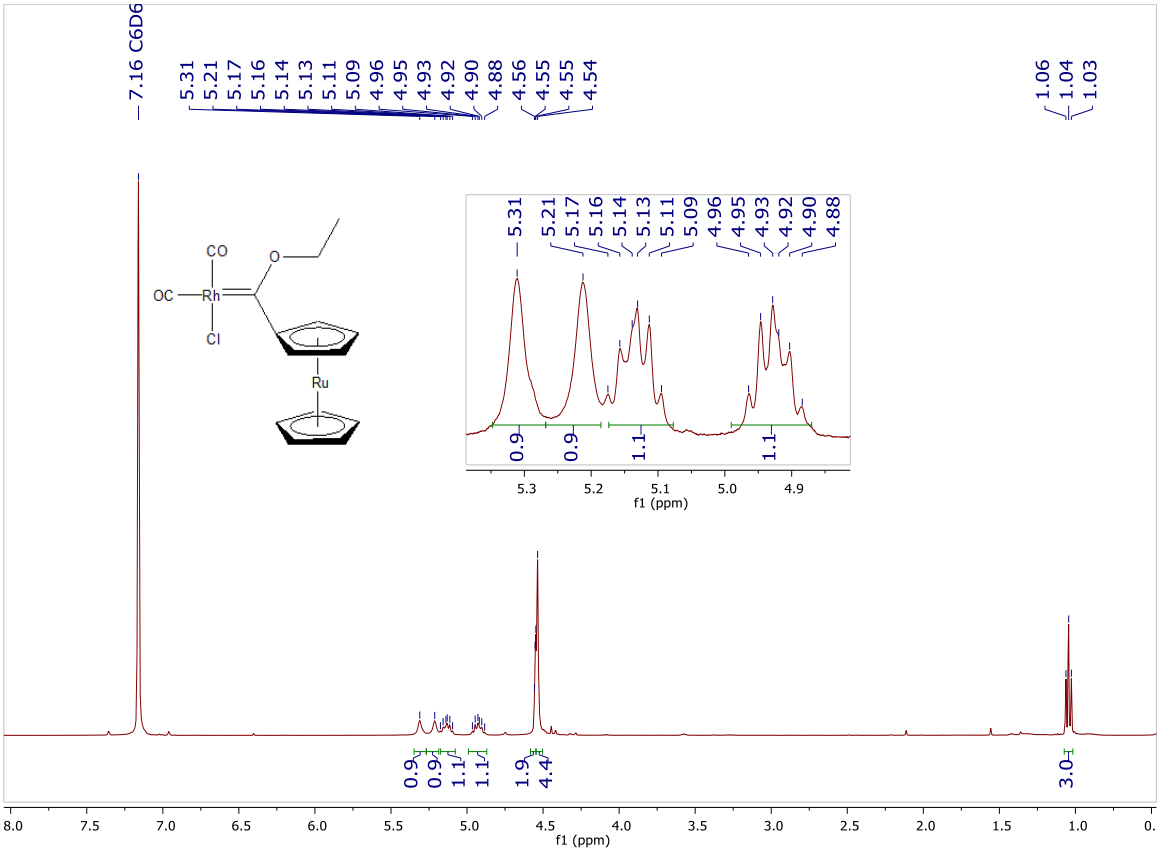

Figure 2.17 ^{1}H NMR spectrum of **13** in C_6D_6

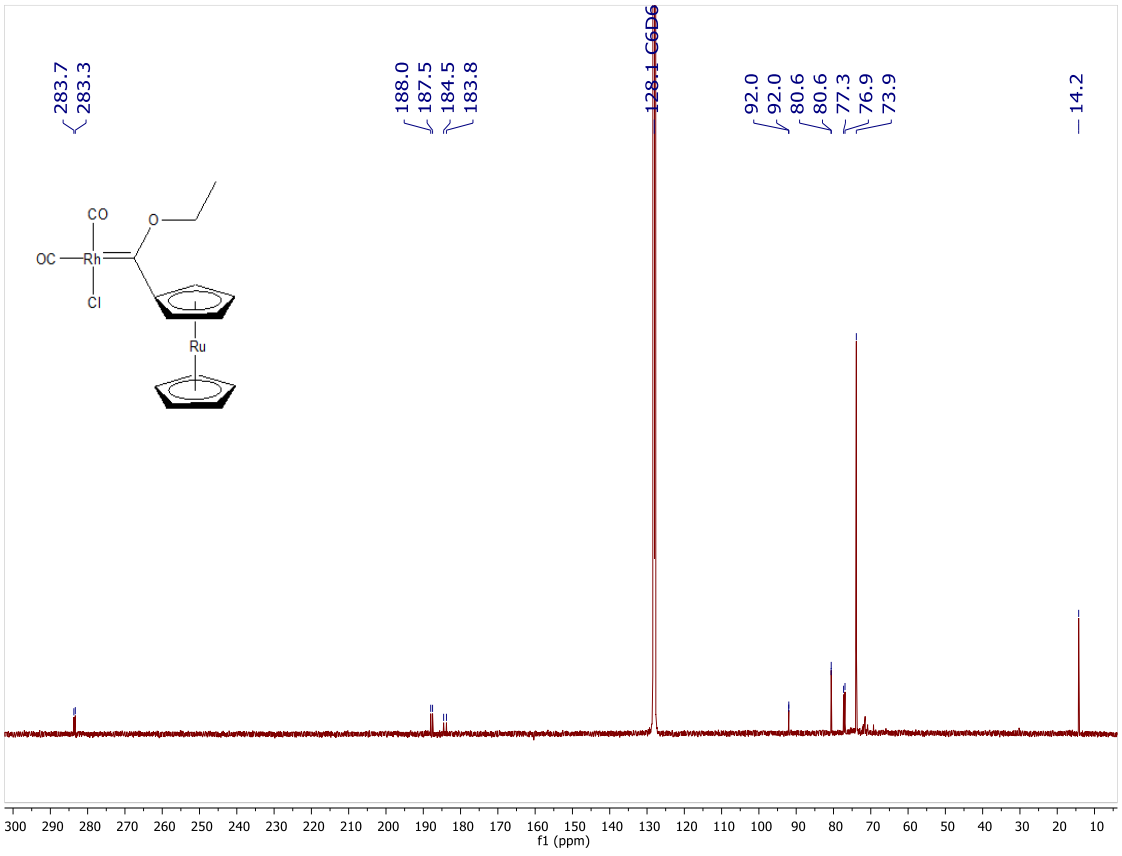

Figure 2.18 $^{13}C\{^{1}H\}$ NMR spectrum of **13** in C_6D_6

2.3.2.5 NMR and FT-IR spectroscopic trends of rhodium(I) Fischer carbene complexes

A characteristic feature of the $^{13}C\{^1H\}$ NMR spectra of all the Rh^I FCCs, is the presence of the carbene carbon atom resonance, presenting as a doublet with Rh-C coupling constants ranging from 35 – 43 Hz. As summarized in Table 2.2 below, $^{13}C\{^1H\}$ NMR spectroscopic data indicate a general upfield-shift of $C_{carbene}$ signals in *p*-DMA- as compared to analogous Rc-carbene complexes. Specifically, Rh(cod) *p*-DMA- and Rc-substituted complexes **10** and **11** exhibit a 25 ppm difference in $C_{carbene}$ chemical shifts (280 and 305 ppm respectively). However, carbene carbon chemical shifts for the dicarbonyl complexes resonate at 277 (*p*-DMA-substituted **12**) or 284 ppm (Rc-substituted **13**) respectively, with a minor 7 ppm difference. Comparison of analogous metallocenyl-carbene complexes indicated insignificant differences in $C_{carbene}$ resonances, suggesting similar inductive effects of Rc and Fc carbene substituents for Rh^I- cod and $(CO)_2$ complex pairs **11**/**14** and **13**/**15** (3 and 5 ppm δ $C_{carbene}$ differences respectively). In conjunction with $C_{carbene}$ chemical shifts of W^0- complexes **3**, **7**, and **8** (299, 297, 304 ppm respectively), the negligible differences in δ $C_{carbene}$ of Rh^I- analogues (**10**, **11**, and **14** for -cod; **12**, **13**, and **15** for -$(CO)_2$) suggests similar electron-donor strengths of the respective carbene substituents *p*-DMA, Rc, and Fc, with apparent interchangeability dependent on the carbene-metal centre and/or co-ligand environment. In addition, although it is known that stronger donor ligands coordinated *trans* to a carbonyl ligand should result in small *J*(RhC) coupling constants for the corresponding carbonyl carbon atom, virtually no change is observed for the series of Rh^I FCCs. Thus as observed for the group 6 precursors,[67] $^{13}C\{^1H\}$ NMR spectroscopy is not a viable tool to assess electrophilicity trends for the isolated Rh^I FCCs with variable aryl carbene substituents.

Table 2.2 Spectroscopic data for complexes **10** – **14**.

Complex	$^{13}C\{^1H\}$ δ($C_{carbene}$), (^1J(RhC))	$^{13}C\{^1H\}$ δ(CO), (^1J(RhC))	IR[a] ν(CO) (cm^{-1})	IR[a] ν_{av}(CO), TEP[d] (cm^{-1})
10	280 (d, 43)	-	-	
11	305 (d, 43)	-	-	
12	277 (d, 37)	188 (d, 50)[b]	1995[c]	2037
		184 (d, 78)[c]	2078[b]	2049[d]
13	284 (d, 39)	188 (d, 50)[b]	2001[c]	2043
		184 (d, 76)[c]	2084[b]	2054[d]
14	302 (d, 43)			
15	289 (d, 38)	187 (d, 50)[b]	2001[c]	2043
		183 (d, 77)[c]	2084[b]	2054[d]
16	258 (d, 40)			
17	238 (d, 35)	187 (d, 51)[b]	1995[c]	2036
		183 (d, 78)[c]	2077[b]	2049[d]

[a]Recorded in CH_2Cl_2. [b]CO-ligand trans to carbene. [c]CO-ligand trans to Cl. [d]Calculated using the linear regression model TEP = 0.8001ν_{av}(CO)**Rh** + 420 cm^{-1}.

While W^0 FCCs utilize the $A_1^{(1)}$ mode (CO_{trans}) as an IR-probe to measure relative ligand electron donor strength, Rh^I-dicarbonyl analogues can be employed to estimate the Tolman Electronic Parameter (TEP); a measure of electron donor-withdrawal effects of different phosphine- and carbon-ligands of nickel-, rhodium-, and iridium-carbonyl complexes. Tolman first reported the electronic effect ν (TEP) of phosphine ligands in 1969 *via* IR spectroscopic characterization of a series of $[Ni(CO)_3L]$ complexes bearing a variety of phosphine ligands (L). A_1 frequencies of the Ni^0 complexes were correlated as a measure of basicity or acidity of L, and a linear regression formula for ν (TEP_{Ni} = 2056.1 + $\sum_{i=1}^{3} Xi$) was established *via* predictable substituent contribution (Xi) of tri-substituted phosphorous ligands relative to P^tBu_3 (Xi = 0 cm^{-1}).[68,69] This method was later modified and adapted for easier-to-handle group 9 metal-chlorides $[M(CO)_2LCl]$ (M = Ir, Rh), utilizing both the CO_{trans} (A_1) and CO_{cis} (E) stretching frequencies recorded for the $[M(CO)_2LCl]$ complexes as an average value. Crabtree and co-workers reported a linear correlation between Tolman's calculated ν(TEP_{Ni}) and the average carbonyl stretching frequency ν_{av}(CO) of $[Ir(CO)_2(PR_3)Cl]$ complexes bearing the corresponding phosphine ligands. Consequently, the new linear regression equation TEP_{Ir} = 0.722ν_{av}(CO) + 593 cm^{-1} utilizing

ν_{av}(CO) of [Ir(CO)$_2$LCl] (L = PR$_3$, NHC) complexes was reported, and the relative electron-donor strength of NHCs and PR$_3$ ligands could be more readily determined without the use of toxic [Ni(CO)$_4$] precursors.[70] This formula was later corrected by the research group of Nolan to the now-widely-employed version $TEP_{Ir} = 0.847\nu_{av}(CO) + 366$ cm^{-1}.[71] Plenio and Wolf similarly correlated experimental ν_{av}(CO) values of [Rh(CO)$_2$LCl] complexes to iridium analogues bearing comparable NHC ligands,[72] thus the formula $TEP_{Rh} = 0.8001\nu_{av}(CO) + 420$ cm^{-1} was developed.[66]

TEPs of NHC ligands have been extensively reported in literature, where apparent ease of preparation of [M(CO)$_2$(NHC)Cl] (M = Rh, Ir) complexes provides a wide array of saturated and unsaturated NHC ligands with relatively quantified electron-donor strengths comparable to known PR$_3$ ligands. In this way, ease of design for new NHC complexes resembling existent analogues with predetermined stability and spectro-electronic properties is provided for. Fc ethoxy- and propylaminocarbene ligands were reported to exhibit TEPs comparable to saturated and unsaturated NHCs in the previous study of complexes **14** – **17**, consequences of which will be discussed in comparison to new additions reported below and in Chapter 3. Other than these limited examples, literature reports of classical FC ligand-TEPs are non-existent, presumably due to the dearth of reports on [M(CO)$_2$(FC)Cl] (M = Rh, Ir) complexes available for traditional FC ligands.

IR spectra of complexes **12** and **13** were measured in solvent CH_2Cl_2 and displayed the expected two distinct carbonyl stretching bands (Table 2.2). The average ν_{av}(CO) frequencies are 2037 and 2043 cm^{-1}, respectively, from which respective TEPs 2049 and 2054 cm^{-1} were calculated using the TEP_{Rh} regression formula. The TEPs clearly indicate that the *p*-DMA-substituted FC ligand is more electron donating towards the central Rh^{I} metal as compared to the analogous Rc-FC ligand (Δ5 cm^{-1}). Thus the metallocenyl-FC ligand :C(OEt)Rc (**12**) is less electron donating than the organic counterpart :C(OEt)*p*-DMA (**13**). The calculated TEP values for **12** and **13** are reminiscent of the Fc-ethoxycarbene- and Fc-aminocarbene ligands :C(OEt)Fc (**15**) and :C(NH^{n}Pr)Fc (**17**); 2054 and 2049 cm^{-1}, respectively. This suggests an unprecedented equal electron-donor strength of *p*-DMA-ethoxycarbene- and Fc-aminocarbene ligands. In addition, an equivalent electron-donor capacity of analogous metallocenyl-carbene ligands :C(OEt)Rc (**13**) and :C(OEt)Fc (**15**) is also implied. Therefore electron-donor strength of FC ligands reported previously[39] and herein can be arranged as :C(OEt)*p*-DMA (**12**) ≈ :C(NH^{n}Pr)Fc (**17**) **>** :C(OEt)Rc (**13**) ≈ :C(OEt)Fc (**15**), according to NMR and IR spectroscopic findings, and are comparable to similarly determined values for saturated and unsaturated NHCs in literature (TEP = 2049 – 2068).[71]

2.3.2.6 Single-crystal XRD crystallography

Molecular structures of complexes **10**, **11**, and **12** were determined by X-ray diffraction of suitable crystals, which were obtained *via* slow-diffusion of *n*-hexane into concentrated CH_2Cl_2 solutions of the complexes and are displayed as Figures 2.19 (a), (b), and (c), respectively. These complexes display *pseudo*-square planar (for Rh(cod)- **10**, **11**) or square planar (for $Rh(CO)_2$- **12**) geometries around the central Rh^I metal, and the structures are comparable with those of Fc analogues **14** and **15** (depicted as Figures 2.19 (c) and (d), respectively). Crystallographic data for complexes **14**[39] and **15**[73] are reproduced from published results for comparative purposes.

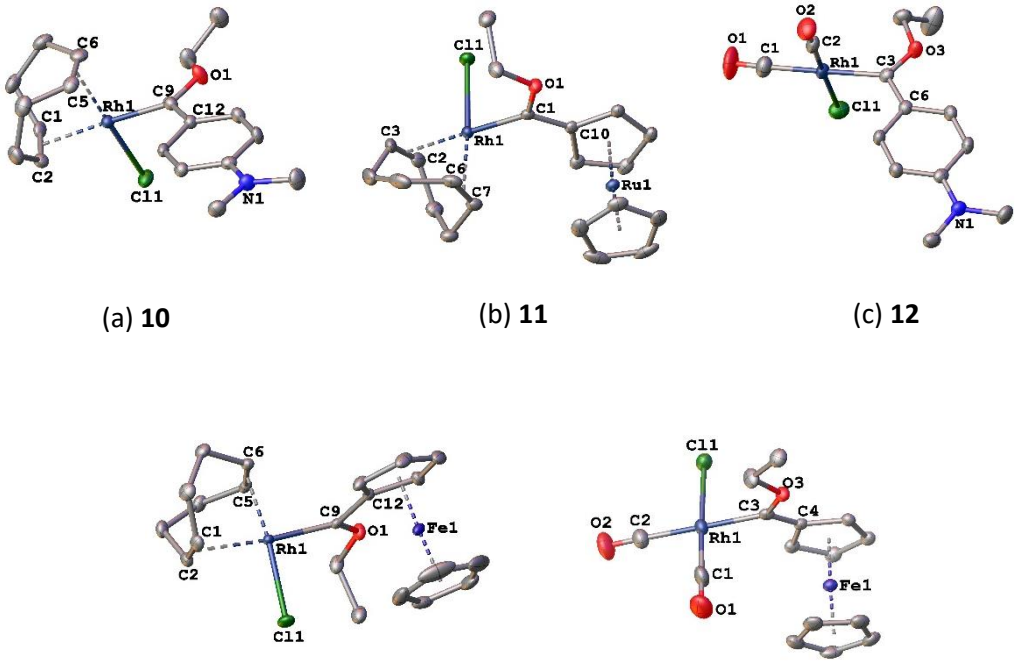

(a) **10** (b) **11** (c) **12**

(d) **14** (e) **15**

Figure 2.19 Partially labelled crystal structures of new Rh^I FCCs **10** – **12** ((a) – (c)) and previously reported analogues **14** (d) and **15** (e).

Table 2.3 Selected bond lengths (Å) and angles (°) for complexes **10** – **12**, **14**, and **15**.

	10	**11**	**12**	**14***	**15***
			Bond lengths		
Rh-$C_{carbene}$	1.970(3)	1.953(18)	2.046(3)	1.958(2)	2.032(2)
$C_{carbene}$-O	1.332(3)	1.311(2)	1.318(3)	1.322(3)	1.306(2)
$C_{carbene}$-C_{ipso}	1.436(4)	1.451(3)	1.421(4)	1.448(3)	1.442(3)
Rh-Cl	2.383(8)	2.381(5)	2.353(8)	2.375(1)	2.356(6)
Rh-Y[a,b] or Rh-CO_{trans}	2.118(3)[a]	2.159(19)[b]	1.929(3)	2.005(1)[c]	1.933(3)
Rh-Y[c,d] or Rh-CO_{cis}	1.990(3)[d]	2.002(19)[e]	1.833(3)	2.166(1)[f]	1.833(3)
			Bond angles		
$C_{carbene}$-Rh-Cl	88.09(8)	87.58(5)	86.02(8)	94.90 (7)	85.78(6)
O-$C_{carbene}$-C_{ipso}	111.7(2)	110.23(15)	112.8(2)	109.3(2)	111.87(18)
			Torsion angles		
C_{α}-C_{ipso}-$C_{carbene}$-O	7.79(4)	1.93(3)	4.1(4)	1.8(3)	35.3(3)

*Data was obtained from literature.[39,73] [a]Y = midpoint of C(1)-C(2). [b]Y = midpoint of C(2)-C(3). [c]Y = midpoint of C(6)-C(7). [d]Y = midpoint of C(5)-C(6). [e]Y = midpoint of C(6)-C(7). [f]Y = midpoint of C(1)-C(2).

Selected bond lengths, bond angles and torsion angles of new complexes **10** – **12** and comparable literature analogues **14** and **15** are summarized in Table 2.3 above. As with TEP (IR spectroscopy) trends discussed above, Rh-$C_{carbene}$ bond lengths are also indicative of π-backbonding ability of the metal towards the carbene carbon atom; strongly electron-donating FC ligands effect longer Rh-$C_{carbene}$ bond distances as indication of less π-backbonding required for Rh-$C_{carbene}$ bond stabilization. Likewise, shorter Rh-$C_{carbonyl}$ bond lengths indicate stronger Rh-$C_{carbonyl}$ π-backbonding due to strongly electron donating FC ligands through the generally accepted sequential electron-density flow from the FC (*via* σ-donation) to the carbonyl ligand (π*-acceptance through Rh),[66] and the emerging Rh-$C_{carbene}$ distances are consequently longer. Rh-$C_{carbene}$ distances of -cod complexes **10**, **11** and **14** (1.970(3), 1.953(18) and 1.958(2) Å, respectively) increase in the order **11** < **14** < **10**. In addition, the Rh-$C_{carbene}$ distance of -$(CO)_2$ complexes is longer in *p*-DMA FCC **12** than observed for Fc analogue **15** (1.953(18) Å and 1.958(2) Å respectively). The accompanying Rh-$C_{CO\text{-}trans}$ distance slightly increases from **12** to **15** (1.929(3) Å and 1.933(3) Å respectively) while the Rh-$C_{CO\text{-}cis}$ bond length is 1.833(3) Å for both **12** and **15**. The $C_{carbene}$-*O* bond length also increases with an increase in the Rh-$C_{carbene}$ distances of -cod complexes **10**, **11**, and **14**. This trend is evident in -$(CO)_2$ complexes **13** and **15** alike. Additionally, the observed $C_{carbene}$-Rh-Cl bond angles for Rh- cod and dicarbonylcarbene complexes indicate a square planar geometry around the Rh-metal atom (86.02 – 94.90°). The C_{α}-C_{ipso}-$C_{carbene}$-*O* torsion angles for

-cod complexes are smaller in Rc- and Fc-substituted complexes as compared to the *p*-DMA analogue (**11**, 1.93(3)°; **14**, 1.8(3)°; **10**, 7.79(4)°, respectively). However for the -$(CO)_2$ complexes, a smaller torsion angle is evident in *p*-DMA-substituted **12** as compared to the Fc-substituted analogue **15** (4.1(4)° and 35.3(3)° respectively). This suggests a planar orientation of the FC ligands in **11**, **12**, and **14**, while the FC ligands in **10** and **15** are distorted. The C_{ipso}-$C_{carbene}$-*O* angles for these complexes are unaffected by variations in aryl carbene substituents and co-ligand environment. Thus the proposed relative electron-donor strength of FC ligands determined by TEP calculations was corroborated by single-crystal X-ray data. As before, it was found that the *p*-DMA ethoxycarbene ligand is superior in stabilization of the electrophilic carbene carbon atom to yield a FC ligand that is notably more electron donating than the metallocenyl analogues when complexed to metals with comparable co-ligand environments.

2.3.2.7 Mass spectrometry of rhodium(I) Fischer carbene complexes

Mass spectral analyses were performed to confirm identity of the isolated complexes. The common mass fragment ions (*m/z*) $[M - Cl]^+$ and $[M - Cl - CO]^+$ were obtained for Rh- cod (**10** and **11**) and -$(CO)_2$ complexes (**12** and **13**), in accordance with literature data for respective Fc analogues **14** and **15**. The experimental *m/z* values were found at 388.1146, 499.0085, 308.0155, and 418.9021 for complexes **10**, **11**, **12**, and **13** respectively. The absence of any tungsten carbonyl *m/z* fragments was indication of successful transmetallation and purification of the reported complexes.

2.3.2.8 Electrochemical analysis

The previously isolated Rh^I Fc-carbene complexes (**14** – **17**) have been electrochemically characterized.[39] Cyclic voltammetry (CV) measurements (at a glassy carbon electrode in CH_2Cl_2) generally indicated the electrochemical processes specified in Scheme 2.12 below. Irreversible reduction of the carbene bond (negative reduction potentials range 1.95 – 2.60 V), reversible oxidation of the Fc moiety ($E^{\circ\prime}$ $Fe^{II/III}$ = 0.13 – 0.36 V), and irreversible oxidation waves related to the $Rh^{I/II}$ and $Rh^{II/III}$ couples at higher oxidation potentials (E_p^{ox} 0.52 – 1.02 V), were observed for the isolated [Rh(LL')\{C(XR)Fc\}Cl] complexes (*vs.* Ag/Ag^+, $E^{\circ\prime}$= -0.54 V for the couple $[Fe(\eta^5\text{-}C_5Me_5)_2]^{+1/0}$ as an internal standard, referenced to the ferrocene/ferrocenium couple at 0 V). Of importance to note is the fact that cyclic voltammogram of [Rh(cod)\{C(OEt)Fc\}Cl] complex **14** clearly indicated the two redox events, with no evident overlap of any electrochemical processes. Additionally, the $Fe^{II/III}$ (Fc) redox event was

reversible for all Fc-carbene complexes, thus chemical oxidation of the Fe^{II} could potentially be achieved for any of the complexes under ideal suitable (air- and moisture-free) conditions.

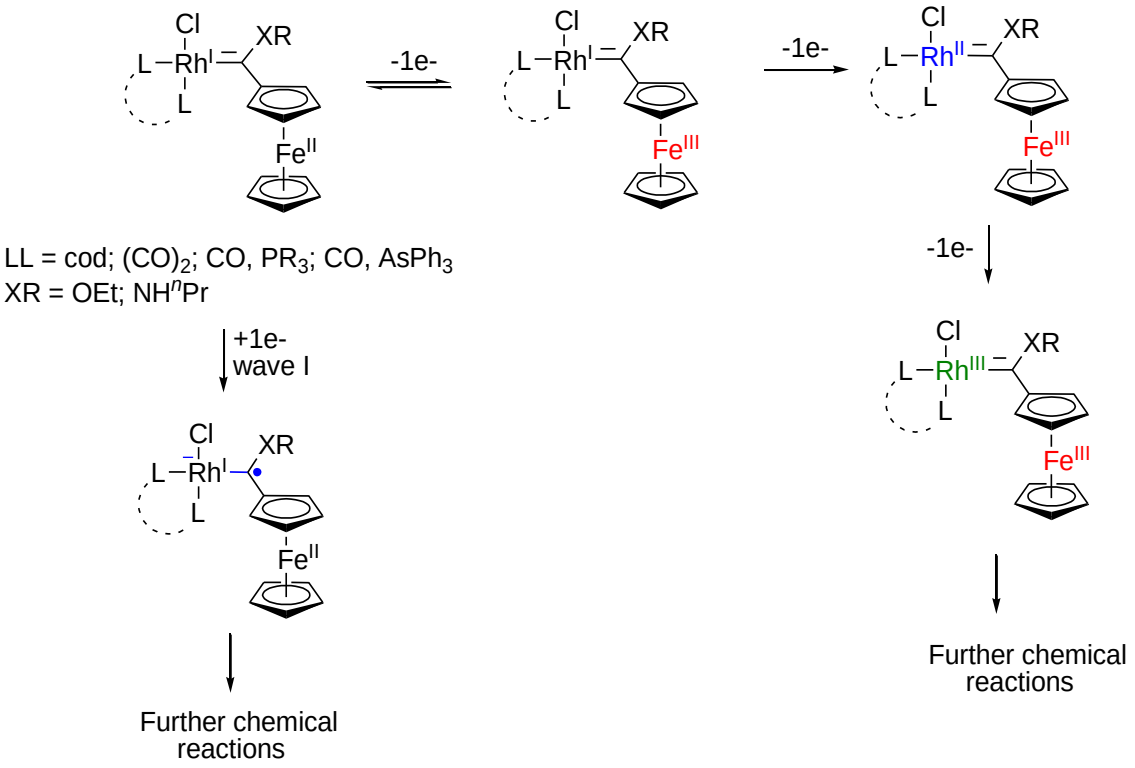

Scheme 2.12 Electrochemical processes reported for Rh^{I} Fc-carbene complexes in literature.

Electrochemical analysis of the new [Rh(cod){C(OEt)Ar}Cl] (Ar = *p*-DMA, Rc) complexes **10** and **11** however, provided no definitive information towards further electronic characterization of these complexes. Cyclic voltammograms of **10** and **11** indicated overlap of redox events as presented in Table 2.4, and deconvolution of the oxidation waves were not possible without the aid of computational molecular orbital calculations. Presumably, the two waves observed at the most positive potentials can be assigned to the $Rh^{I/II}$ and $Rh^{II/III}$ couples for both complexes (as per Fc-analogues above), and the remaining redox potential is assigned to redox events at *p*-DMA-nitrogen and Rc-ruthenium atoms of complexes **10** and **11**, respectively ($E^{\circ\prime}$; [NMe_2/NMe_2^+] ~ -0.24 V, [$Ru^{II/III}$] ~ -0.22 V). The redox behaviour of ruthenocene is well-known,[74] and the [NMe_2/NMe_2^+] redox behaviour of the *p*-DMA substituent[61] is also documented. These extensively overlapping irreversible redox processes of complexes **10** and **11** could therefore not be compared to the fully reversible Fc-analogue **14**. Inherently, the convoluted nature of all redox events of complexes **10** and **11,** and exclusion of the carbene bond reduction wave (presumed to fall outside the solvent window employed in the study; Table 2.4, E_p^{red} [Rh=C/$^{-}$Rh-C$^{\cdot}$]) is clear indication that these complexes exhibit electronic properties

distinct from the previously reported Rh^{I}- cod and $(CO)_2$ Fc-carbene complexes. No Density Functional Theory (DFT) calculations were done to identify spin-densities of each oxidized intermediate, and thus the tabulated electrochemical events cannot be unambiguously assigned to the redox couples [NMe_2/NMe_2^+], [$Rh^{I/II}$], and [$Rh^{II/III}$] (for **10**) or to [$Ru^{II/III}$], [$Rh^{I/II}$], and [$Rh^{II/III}$] (for **11**). The obtained CVs of **10** and **11** are depicted in Figure 6.1 (Chapter 6).

Table 2.4 Cyclic voltammetry results for rhodium carbene complexes **10** and **11**

Complex	E_p^{red} (V) [Rh=C/$^{-}$Rh-C$^{\cdot}$]	$^{b}E_p^{ox}$ (V) [$Ru^{II/III}$] or [NMe_2/NMe_2^+]	$^{b}E_p^{ox}$ (V) [$Rh^{I/II}$], [$Rh^{II/III}$]
10	[a]	-0.24	0.12, 0.64
11	[a]	-0.22	0.24, 0.88

[a]Not observed in the solvent window employed. [b]Overlapping and irreversible waves.

2.3.3 Chemical oxidation to yield a rhodium(I) ferroceniumyl Fischer carbene radical cation

The redox reversibility of ferrocene has been exploited in literature.[75] Electrochemical analysis of Fc-compounds provides useful information for fine-tuning the electronic characteristics of said compounds, where chemical oxidation of the Fe^{II} metal to Fe^{III} results in measurable and calculable changes in the spectro-electronic behavior of the emerging ferroceniumyl (Fc^+) compound. Such electronic manipulations have proven viable for FCCs in literature, where for example, reaction of silver hexafluorophosphate ($AgPF_6$) and a W^0 FCC [$W(CO)_5${C(OEt)Fc}] (**8**) yielded the targeted W^0 Fc^+-FCC salt **8**$^+$ as depicted in Scheme 2.13 (a) below.[76] Initially, cyclic voltammetry of **8**, supported by DFT calculations, had indicated $Fe^{II/III}$ as the first (reversible one-electron) oxidation event followed by irreversible oxidation of the central W^0 metal to W^{III}. Selective chemical oxidation of **8** could therefore be achieved in the isolation of cationic **8**$^+$, where the unaltered $W^0(CO)_5$- moiety was subsequently utilized as an IR-probe to measure the effects of switching from electron- donating Fc to -withdrawing Fc^+ carbene substituents. FT-IR spectroscopy of **8**$^+$ indicated an 11 cm^{-1} increase of the $A_1^{(1)}$ vibration mode from **8**. On the contrary, selective oxidation of Fc FCCs can also occur at the carbene-metal, while subsequent oxidation at more positive potentials are recorded for the $Fe^{II/III}$. As depicted in Scheme 2.13 (b), chemical oxidation of Mn^{I} Fc-ethoxycarbene complex [$Mn(CO)_2Cp${(OEt)Fc}] resulted in the radical cation Mn^{II} complex wherein the Fe^{II} metal remained unoxidized.[46] In this case, chemical oxidation of the central metal bound to the carbonyl ligands, instead of a terminal metal substituent, has a much more significant effect on the carbonyl stretching frequencies, with a substantial increase

(Δ116 cm^{-1}) in ν_{av}(CO) on going from neutral Mn^{I}- to the radical cation $[Mn^{+}(CO)_2Cp\{C(OEt)Fc\}]$ complex.

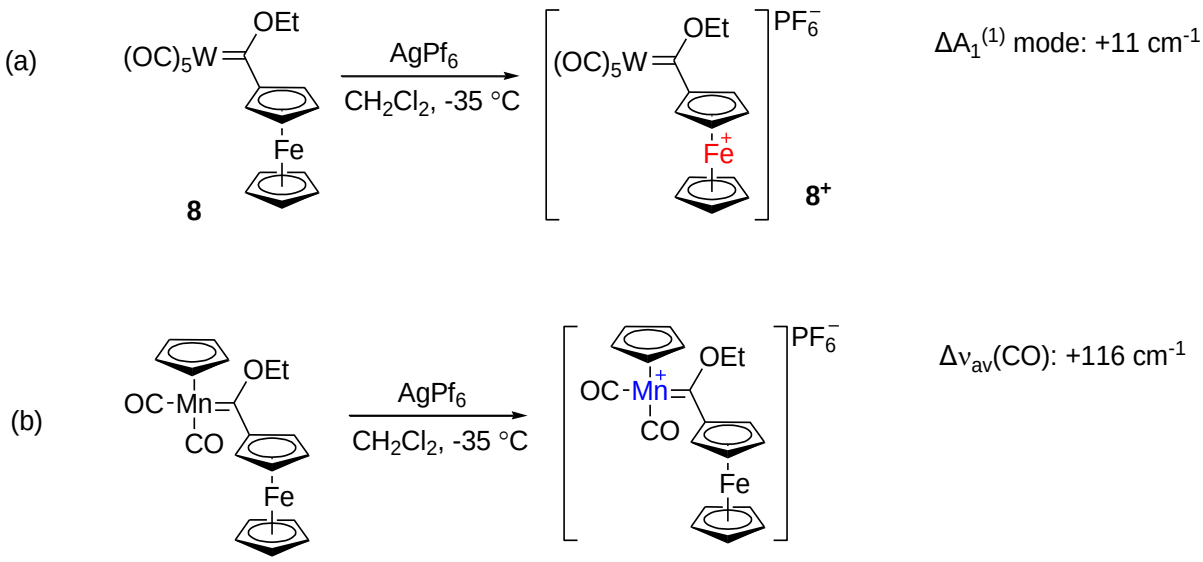

Scheme 2.13 Selective chemical oxidation of Fc-carbene complexes at the substituent- Fe^{II} (a) or carbene- Mn^{I} (b) metal centres.

Selective chemical oxidation of Fc-functionalized Rh^{I} NHCs has also been explored in literature. Most recently in our research group, chemical oxidation of a $[Rh(CO)_2(NHC\text{-}Fc)Cl]$ complex at the Fe^{II} atom of the Fc substituent, to Fe^{III} was reported to afford the corresponding $[Rh(CO)_2(NHC\text{-}Fc^{+})Cl]$ cationic complex, where a higher-frequency TEP of 2057 cm^{-1} (ν_{av}(CO) increased of 13 cm^{-1}) confirmed successful synthesis of the $Rh^{I}(CO)_2$- NHC-Fc^{+} complex.[77] The authors therein reported the catalytic behaviour of the Rh^{I} NHC-Fc^{+} in contrast to its neutral Fc-analogue towards hydroformylation of 1-octene. The effects of this redox-non-innocent substituent were evidenced by a slight increase in catalytic activity (conversion +4%), enhanced chemoselectivity and catalytic efficiency (+10% and +19 hr^{-1} for percentage aldehydes and TOF respectively), and reduced regioselectivity (*n*/*iso* ratio -0.83) from Fc- to Fc^{+}-functionalized aminocarbene complexes, respectively. These results prompted us to exploit the possibility of redox-switchable catalysis utilizing our previously reported Rh^{I} Fc FCCs, wherein available CV results provide the oxidation potential for the $Fe^{II/III}$ couple to aid in the selection of a suitable oxidizing agent. Due to the more electron-rich nature of Rh^{I} Fc-aminocarbene complexes in comparison to ethoxy-analogues, the $[Rh(CO)_2\{C(NH^{n}Pr)Fc\}Cl]$ complex **17** was chosen as starting complex for chemical oxidation of the Fc group ($E^{\circ\prime}$ $Fe^{II/III}$ = 0.24 V in solvent CH_2Cl_2).[39] This complex includes the presence of carbonyl ligands as IR probes of the Rh and Fe oxidation states following

oxidation, due to the NMR-silent behaviour of the envisioned Rh^{I}-Fe^{III} complex. The use of halide-scavengers (for example, $AgPF_6$) as chemical oxidants has to be avoided due to potential rhodium-dechlorination and decomposition of the targeted one-electron oxidation product of **17**. Instead, acetylferrocenium hexafluorophosphate ([FcOAc][PF_6]) was identified as a suitable oxidant ($E^{\circ\prime}$ $Fe^{II/III}$ of 0.27 V in solvent CH_2Cl_2).[75] Thus the synthesis and characterization of Rh^{I} Fc^{+}-carbene complex **17**$^{+}$ was undertaken as follows:

Equimolar amounts of **17** and [FcOAc][PF_6] were reacted in deoxygenated CH_2Cl_2 under inert argon gas atmosphere at room temperature (see Scheme 2.14 below), and the reaction was monitored by IR spectroscopy. An immediate colour change from orange to brown was observed, however, the reaction was stirred for 24 hours as required for complete oxidation of all **17**-Fe^{II} species. Recorded IR spectrum of the crude reaction solution indicated a ν_{av}(CO) increase of 18 cm^{-1} from the original spectrum of **17** (Figure 2.20 below), and the high-frequency TEP of the :C(NH^{n}Pr)Fc^{+} ligand was calculated at 2063 cm^{-1} (+14 cm^{-1} from **17** to **17**$^{+}$). The CH_2Cl_2 solvent was removed *in vacuo* and the paste was washed with diethyl ether followed by CH_2Cl_2 extraction *via* cannula filtration methods, and the oxidized complex **17**$^{+}$ was isolated as a brown powder. No useful ^{1}H, $^{13}C\{^{1}H\}$, and ^{31}P NMR spectroscopic information was obtained. However, the ^{19}F NMR spectrum of **17**$^{+}$ (Figure 2.21) could be recorded, and indicated an upfield chemical shift of -82.7 ppm with a large coupling constant (^{1}J(PF) = 712 Hz). This is comparable to literature reports of counterion hexafluorophosphate (PF_6^{-}) in a paramagnetic system, where the PF_6^{-} counterion of Fc^{+} complexes resonates at -85.4[76] and -85.1[77] ppm. For a PF_6^{-} counterion in a diamagnetic (NMR-active) environment, ^{19}F NMR resonance was reported at -72.9 ppm in literature.[77] Additionally, the 14 cm^{-1} ν_{av}(CO) shift from **17** to **17**$^{+}$ falls within the expected range of $Fe^{II/III}$ oxidation of the remote Fc group of the FC and NHC complexes (10 – 20 cm^{-1}), and is out of range for oxidation of the carbene-metal ($Rh^{I/II/III}$ where the ν_{av}(CO) shift would increase by 50 – 100 cm^{-1} for carbonyl ligands bonded directly to the oxidized metal). Thus Rh^{I} Fc^{+}-FCC **17**$^{+}$ was successfully synthesized as a mono-cationic system complex salt.

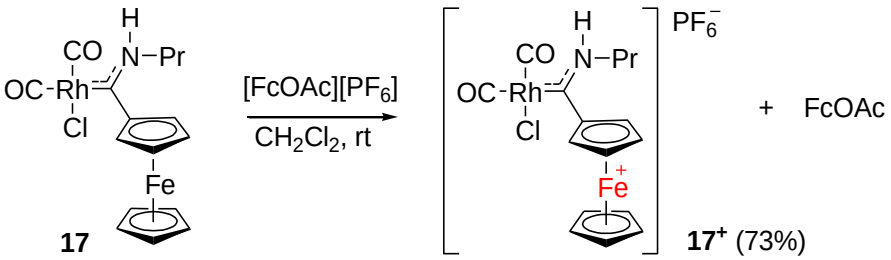

Scheme 2.14 Selective chemical oxidation at Fe^{II} metal to afford Rh^{I} Fc^{+}-FCC **17**$^{+}$

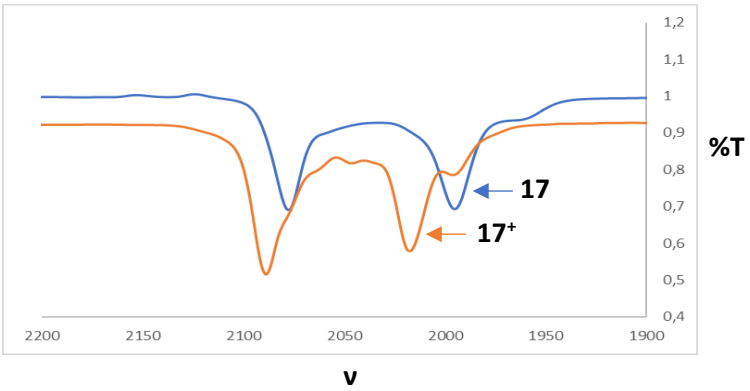

Figure 2.20 Stacked IR spectra of **17** and **17**$^{+}$

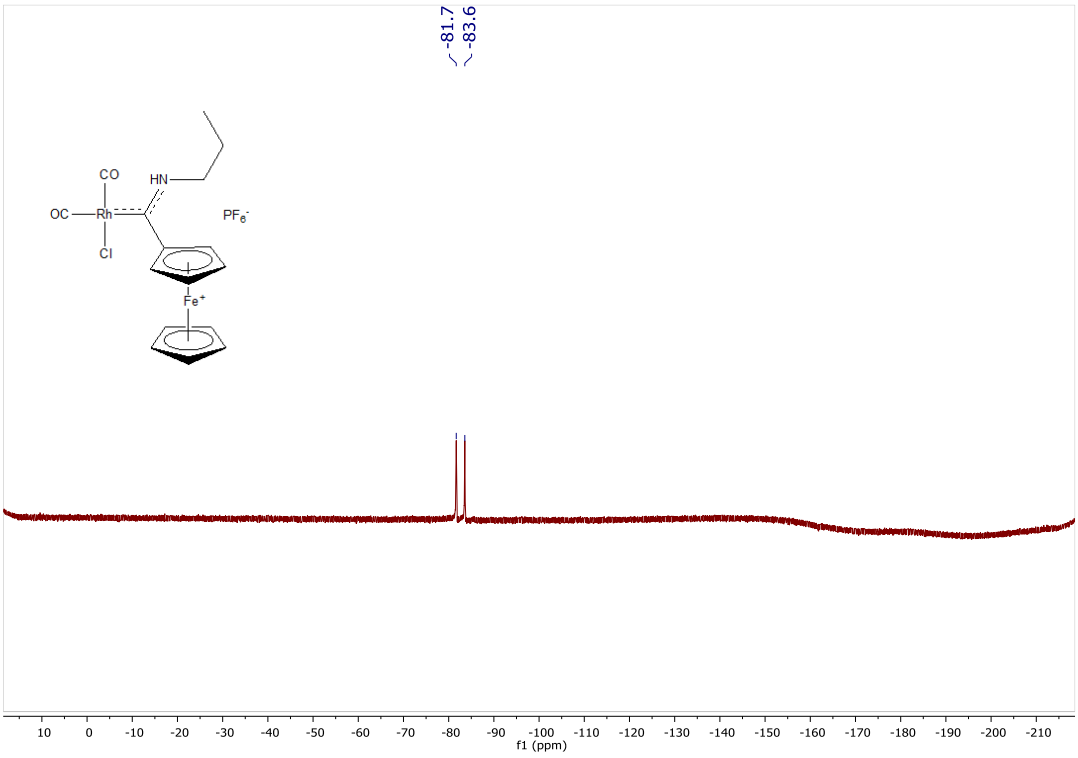

Figure 2.21 $^{19}F\{^{1}H\}$ NMR spectrum of **17**$^{+}$ in CD_2Cl_2

2.3.4 Catalytic application of rhodium(I) carbene complexes in the hydroformylation of 1-octene

All isolated Rh^{I} FCCs **10** – **13**, and **17**$^{+}$ were utilized as catalyst precursors for Rh-catalyzed hydroformylation of 1-octene as depicted in Scheme 2.15 below, results of which are summarized in Table 2.5. Previously reported Fc-carbene complexes **14** – **17** are included herein for comparison to new results.

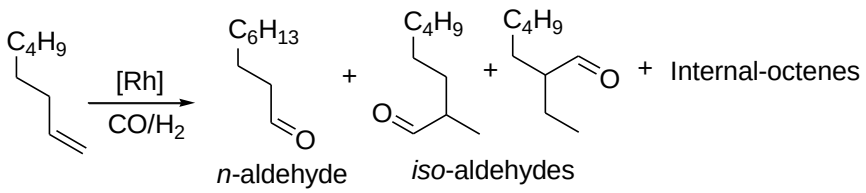

Scheme 2.15 Rhodium-catalyzed hydroformylation of 1-octene utilizing Rh^{I} FCCs **10** – **17**, and **17^{+}**

Table 2.5 Rhodium-assisted hydroformylation of 1-octene by precatalysts **10** – **17** and **17^{+}** under previously optimized conditions.[a]

Entry	Complex	Conv. (%)	Total aldehydes (%)	*n*-aldehydes (%)	*iso*-octenes (%)	TOF[c] (h^{-1})	*n*/*iso*
1	**10**	99(1.1)	99(0.7)	47(1.1)	1(0.7)	543	0.89
2	**11**	100(0.1)	98(0.6)	47(1.5)	2(0.6)	608	0.89
3	**12**	79(10.2)	64(3.9)	71(1.1)	35(3.9)	318	2.44
4	**13**	100(0.1)	98(1.3)	47(2.9)	2(1.3)	615	0.88
5	**14**	100	100	44(4.0)	0	418	0.79
6	**15**	100	100	50(1.2)	0	379	0.98
7	**16**	100	90(2.3)	55(3.0)	10(2.3)	366	1.25
8	**17**	99(0.1)	85(0.5)	57(3.8)	15(0.5)	343	1.33
[b]9	**17^{+}**	55(13.2)	68(1.8)	69(0.1)	32(1.8)	167	2.25

[a]Hydroformylation of 1-octene (6.37 mmol) in toluene (5 mL) at a temperature of 75 °C, with a syngas (1:1, $CO:H_2$) pressure of 40 bar, reaction time of 4 hours and a (pre)catalysts loading of 5.096 x 10^{-3} mmol. All reactions were carried out in triplicate, and averages are reported in entries 1 – 9 with standard deviations indicated in brackets. Conversions were monitored by gas chromatography, and *n*-decane was used as internal standard. [b]Precatalyst employed was generated *in situ* by reaction of equimolar amounts of $[FcOAc][PF_6]$ and **17** in the reaction vessel. [c]Average turnover frequency [(mmol of product) / (mmol of precatalyst)] determined after 4 hours.

The acyclic Rh^{I}-FCCs **10** – **13** were employed as precatalysts under the previously optimized catalytic conditions (40 bar syngas pressure, 75 °C, over 4 hours) for comparable Fc-substituted analogues **14** – **17**. Excellent conversions were observed for the Rh(cod)- complexes **10** and **11** featuring *p*-DMA- and Rc-substituted FC ligands respectively (99 and 100%, respectively), and are comparable to the

previously reported Fc-analogue **14** (100%). However, replacement of the cod-ligand with carbonyl co-ligands resulted in a significant decrease in the catalytic activity and chemoselectivity of $Rh(CO)_2$-*p*-DMA complex **12** (79% conversion, 64% total aldehydes) as compared to its Rh(cod)-analogue **10** (100% conversion, 99%total aldehydes). For metallocenyl-substituted precatalysts **11**, **13**, **14**, and **15**, no change in the conversions and total aldehyde yields were observed as a result of cod- or dicarbonyl-co-ligand effects (compare entry 2 to 4 for Rc-substituted **11** and **13**, respectively, and entry 5 to 6 for Fc-analogues **14** and **15**, respectively). Comparison of the catalytic efficiency of the new Rh^{I} *p*-DMA- and Rc-substituted complexes **10** – **13** to Fc-analogues **14** and **15**, in terms of turnover frequencies (TOFs) of the aforementioned complexes, indicated a significant increase in the order **14** (Fc) < **10** (*p*-DMA) < **11** (Rc) for Rh(cod)- complexes (418, 543, and 608 hr^{-1} for complexes **14**, **10**, and **11**, respectively). However, a different trend is observed for $Rh(CO)_2$-analogues, where TOFs increase in the order **12** (*p*-DMA) < **15** (Fc) < **13** (Rc) (318, 379, and 615 hr^{-1} for complexes **12**, **15**, and **13**, respectively). Thus the effects of aryl carbene substituents *p*-DMA, Rc, and Fc in precatalysts **10 – 15** are equivocal. Consequently, correlations of TOFs to calculated TEPs of analogous *p*-DMA-, Rc-, and Fc-substituted Rh^{I} FCCs reported herein is not unambiguous. The highest TOFs (over 600 hr^{-1}) were observed for Rc-substituted precatalysts **11** and **13**, presumably due in part to the catalytic activity at the secondary Ru^{II}-metal site, in accordance with literature reports of the synergic effects of bimetallic cooperative hydroformylation.[78–80]

Comparison of co-ligand effects on TOFs also does not provide conclusive results. The catalytic turnovers observed, decrease from Rh(cod)- complexes **10** (*p*-DMA, 543 hr^{-1}) and **14** (Fc, 418 hr^{-1}) to $Rh(CO)_2$-analogues **12** (318 hr^{-1}) and **15** (379 hr^{-1}), respectively, while a slight increase was observed for the Rc-substituted analogues **11** and **13** (608 and 615 hr^{-1}, for Rh- cod and $(CO)_2$ complexes, respectively). This finding of increased activity for the Rc-substituted precatalyst **13** was consistent with our previous observation that an increase in the electrophilicity of the FCCs results in higher TOFs. Regioselectivity trends (*n/iso* ratio) of the employed precatalysts were in agreement with accompanying chemoselectivities, where 98 – 100% total aldehydes were observed alongside *n/iso* ratios of 0.79 – 0.89 for Rh- cod and $(CO)_2$ precatalysts alike. Complimentary, the lowest percentage total aldehydes recorded for *p*-DMA-substituted pracatalyst **12** (64%) corresponds to the highest *n/iso* ratio (2.44). These results are again consistent with our previous observation for Fc-substituted precatalysts that an increase in chemoselectivity is accompanied by a decrease in regioselectivity. Results reported herein are comparable to olefin hydroformylation utilizing Rh^{I}-NHC precatalysts in literature, where TOFs ranging from 480 to 3540 hr^{-1} were reported alongside *n/iso* ratios lower than 0.5.[81–85]

Finally, *in situ* chemical oxidation of the Fc-substituted precatalyst **17** was achieved by equimolar reaction with oxidant [FcOAc][PF_6] in the reaction vessel. The resultant more electrophilic Fc^+-substituted precatalyst **17**$^+$ effected a notable decrease in the catalytic activity and chemoselectivity as compared to **17** (compare entry 8 to 9). A low TOF of 167 hr^{-1} is observed for precatalyst **17**$^+$, and the percentage conversion of 1-octene was halved from 99% to 55% when utilizing precatalysts **17** or **17**$^+$, respectively. While chemoselectivity towards the formation of aldehydes was also reduced with decreased electron-donor strength of the FC ligand (85% and 68% for **17** or **17**$^+$ respectively), regioselectivity towards linear aldehydes was doubled in reverse order (*n/iso* ratio = 2.25 and 0.98 for **17**$^+$ and **17**, respectively). The increase in regioselectivity at the expense of chemoselectivity was consistent with our previously reported observations of Rh-FCC catalyzed hydroformylation.

2.4 Conclusion

Literature abundant W^0 FCCs **1** – **8** were successfully synthesized *via* the Fischer route as precursors to rhodium(I) FCCs. A transmetallation strategy was employed for the selected complexes, and subsequent minor ligand modification yielded the new Rh^I FCCs **10** – **13**. In accordance with our previous study, it was found that FC ligands that are not electron-donating enough to stabilize the Rh-carbene bond, lead to carbene-dimerization, and the corresponding Rh^I FCCs could not be isolated from the carbene transfer reactions. For the isolated Rh^I complexes, the calculation of TEP values as an established quantifiable method to establish the relative electron-donating capacity of the FC ligands, was employed to determine the electrophilicity of the FC ligands, where it was found that the :C(OEt)*p*-DMA ligand is more electron-donating than the :C(OEt)Rc and :C(OEt)Fc ligands.

The isolated Rh^I complexes bearing *p*-DMA and Rc FC ligands were evaluated as precatalysts in the hydroformylation of 1-octene, and compared to previously reported Fc-analogues. The highest TOF was observed for Rc-substituted precatalysts **11** and **13**, while the highest regioselectivity and accompanying lowest chemoselectivity were achieved for the *p*-DMA-substituted precatalyst **12**. An increase in the overall electrophilicity of the Fc-substituted FCC *via* chemical oxidation yielded the monocationic Fc^+-aminocarbene complex **17**$^+$. Catalytic evaluation of the *in situ* generated **17**$^+$ demonstrated a significantly improved regioselectivity at the expense of both catalytic activity and chemoselectivity, as compared to the neutral Fc-analogue.

2.5 Experimental

The synthesis and purification of W^0 and Rh^I FCCs described herein were carried out *via* standard Schlenk techniques, under an atmosphere of dry and oxygen-free nitrogen or argon gas. Further details are provided in Section 6.1 (Chapter 6).

W^0 FCCs **1** – **5**, **7**, and **8** have been previously reported and were thus prepared according to literature procedures.[19,50,55,56,58,60–63,76,86–88] The methoxycarbene-analogue of W^0 ethoxycarbene complex **6** has also been reported, thus the synthesis of unreported **6b** is discussed in detail (*vide infra*). New Rh^I FCCs **10** – **13** , and **17**$^+$ were synthesized according to procedures described in Sections 2.5.9 – 2.5.13.

2.5.1 [W(CO)$_5${C(OEt)(2-thienyl)}] 1[45,63]

Yield = 65%. ^{1}H NMR (300 MHz, $CDCl_3$) δ 8.16 (dd, ^3J(HH) = 4.1 Hz, ^4J(HH) = 1.0 Hz, 1H, Th-H_α), 7.82 (dd, ^3J(HH) = 5.0 Hz, ^4J(HH) = 1.0 Hz, 1H, Th-H_γ), 7.22 (dd, ^3J(HH) = 5.0 Hz, ^3J(HH) = 4.1 Hz, 1H, Th-H_β), 5.00 (q, ^3J(HH) = 7.1 Hz, 2H, O$\underline{CH_2}CH_3$), 1.66 (t, ^3J(HH) = 7.1 Hz, 3H, $OCH_2\underline{CH_3}$). $^{13}C\{^1H\}$ NMR (75 MHz, $CDCl_3$) δ 291.1 ($C_{carbene}$), 202.9 (CO_{trans}), 198.0 (CO_{cis}), 158.7 (Th-C_{ipso}), 141.9 (Th-C_α), 136.3 (Th-C_γ), 129.3 (Th-C_β), 78.9 (O$\underline{CH_2}CH_3$), 15.3 ($OCH_2\underline{CH_3}$). IR (dcm) ν(CO/cm^{-1}): 2069 (w), 1988 (w), 1963 (m), 1948 (s).

2.5.2 [W(CO)$_5${C(OEt)(2-furyl)}] 2[54,86]

Yield = 63%. ^{1}H NMR (300 MHz, $CDCl_3$) δ 7.88 (dd, ^3J(HH) = 3.6 Hz, ^4J(HH) = 0.7 Hz, 1H, Fu-H_γ), 7.15 (dd, ^3J(HH) = 3.7 Hz, ^4J(HH) = 0.6 Hz, 1H, Fu-H_α), 6.62 (dd, ^3J(HH) = 3.7 Hz, ^3J(HH) = 1.7 Hz, 1H, Fu-H_β), 4.96 (q, ^3J(HH) = 7.1 Hz, 2H, O$\underline{CH_2}CH_3$), 1.64 (t, ^3J(HH) = 7.1 Hz, 3H, $OCH_2\underline{CH_3}$). $^{13}C\{^1H\}$ NMR (75 MHz, $CDCl_3$) δ 285.2 ($C_{carbene}$), 203.7 (CO_{trans}), 197.7 (CO_{cis}), 166.5 (Fu-C_{ipso}), 150.3 (Fu-C_γ), 115.2 (Fu-C_α), 113.8 (Fu-C_β), 78.7 (O$\underline{CH_2}CH_3$), 15.4 ($OCH_2\underline{CH_3}$). IR (dcm) ν(CO/cm^{-1}): 2072 (w), 1979 (w), 1960 (m), 1945 (s).

2.5.3 [W(CO)$_5${C(OEt)*p*-DMA}] 3[61]

Yield = 37%. ^{1}H NMR (300 MHz, $CDCl_3$) δ 8.02 (d, ^3J(HH) = 9.3 Hz, 2H, DMA-$\underline{H_{\alpha,\alpha'}}$), 6.62 (d, , ^3J(HH) = 9.3 Hz, 2H, DMA-$\underline{H_{\beta,\beta'}}$), 4.99 (q, ^3J(HH) = 7.0 Hz, 2H, O$\underline{CH_2}CH_3$), 3.11 (s, 6H, DMA-N$\underline{(CH_3)_2}$), 1.66 (t, ^3J(HH) = 7.0 Hz, 3H, $OCH_2\underline{CH_3}$). $^{13}C\{^1H\}$ NMR (75 MHz, $CDCl_3$) δ 299.7 ($C_{carbene}$), 203.3 (CO_{trans}), 198.6 (CO_{cis}), 154.4 (DMA-$\underline{C_q}$), 141.0 (DMA-C_{ipso}), 134.4 (DMA-$\underline{C_{\alpha,\alpha'}}$), 110.2 (DMA-$\underline{C_{\beta,\beta'}}$), 78.4 (O$\underline{CH_2}CH_3$), 40.2 (DMA-N$\underline{(CH_3)_2}$), 15.3 ($OCH_2\underline{CH_3}$). IR (hexane) ν(CO/cm^{-1}): 2062 (w), 2060 (w), 2055 (m), 1933 (s).

2.5.4 [W(CO)$_5${C(OEt)(Cp'Fe(CO)$_2$Me)}] 4[55]

Yield = 15%. ^{1}H NMR (300 MHz, $CDCl_3$) δ 5.47 (s, 2H, FeCp'-$\underline{H_{\alpha,\alpha'}}$), 5.15 (s, br, 2H, FeCp'-$\underline{H_{\beta,\beta'}}$), 4.74 (s, br, 2H, O$\underline{CH_2}CH_3$), 1.65 (s, br, 3H, $OCH_2\underline{CH_3}$), 0.29 (s, 3H, $FeCH_3$). $^{13}C\{^1H\}$ NMR (75 MHz, $CDCl_3$) δ 304.4 ($C_{carbene}$), 215.1 (CO_{trans}), 202.5 (CO_{cis}), 197.6 (FeCO), 109.0 (FeCp'-C_{ipso}), 90.9 (O$\underline{CH_2}CH_3$), 87.7 (FeCp'-

$C_{\alpha,\alpha'}$), 79.3 (FeCp'-$C_{\beta,\beta'}$), 15.5 (OCH_2CH_3), -20.4 ($FeCH_3$). IR (hexane) ν(CO/cm^{-1}): 2069 (s), 2021 (s), 1982 (m), 1973 (s), 1960 (s), 1943 (s), 1930 (w).

2.5.5 [W(CO)$_5${C(OEt)(Cp'Mn(CO)$_3$)}] 5[56]

Yield = 76%. ^{1}H NMR (300 MHz, C_6D_6) δ 4.92 (s, 2H, MnCp'-$H_{\alpha,\alpha'}$), 4.40 (q, ^3J(HH)= 7.0 Hz, 2H, OCH_2CH_3), 3.89 (s, 2H, MnCp'-$H_{\beta,\beta'}$), 1.00 (t, ^3J(HH)= 7.0Hz, 3H, OCH_2CH_3). $^{13}C\{^1H\}$ NMR (75 MHz, C_6D_6) δ 303.9 ($C_{carbene}$), 222.7 (Mn-$\{CO\}_3$), 202.7 (W-CO_{trans}), 197.0 (W-CO_{cis}), 108.8 (MnCp'-C_{ipso}), 88.8 (MnCp'-$C_{\alpha,\alpha'}$), 84.0 (MnCp'-$C_{\beta,\beta'}$), 77.2 (OCH_2CH_3), 14.8 (OCH_2CH_3). IR (hexane) ν(CO/cm^{-1}): 2070 (m), 2030 (s), 1982 (w), 1965 (w), 1957(m), 1943 (s), 1928 (w).

2.5.6 [W(CO)$_5${C(OEt)(Cp'Re(CO)$_3$)}] 6[19,60]

The methoxy- analogue of this complex has been previously reported.[19,60] ^{n}BuLi (3.30 mmol, 2.2 mL) was slowly added to a solution of $CpRe(CO)_3$ (3.00 mmol, 1.006 g) in THF and stirred at -78 °C for 2 hours. The reaction was warmed up to -50 °C, at which point $W(CO)_6$ was added in one portion and stirred for 1 hour while slowly warming to room temperature. The THF solvent was removed *in vacuo* and the resulting residue dissolved in DCM (30 mL) and cooled down to -30 °C. A DCM solution of $Et_3O^+BF_4^-$ (3.00 mmol, 0.570 g in 10 mL) was then slowly added at -30 °C and stirred for 1 hour while warming to room temperature. The resulting dark-red solution was reduced *in vacuo* and added to a silica chromatography column. Elution with *n*-hexane gave the only red band, which was collected and reduced under vacuum to give bright-red crystals. Yield = 1.20 g, 56%. ^{1}H NMR (300 MHz, C_6D_6) δ 5.36 (s, 2H, ReCp'-$H_{\alpha,\alpha'}$), 4.37 (q, ^3J(HH)= 7.0 Hz, 2H, OCH_2CH_3), 4.27 (s, 2H, ReCp'-$H_{\beta,\beta'}$), 0.94 (t, ^3J(HH)= 7.0Hz, 3H, OCH_2CH_3). $^{13}C\{^1H\}$ NMR (75 MHz, C_6D_6) δ 296.2 ($C_{carbene}$), 201.5 (W-CO_{trans}), 197.1 (W-CO_{cis}), 191.8 (Re-$\{CO\}_3$), 112.7 (ReCp'-C_{ipso}), 89.7 (ReCp'-$C_{\alpha,\alpha'}$), 85.2 (ReCp'-$C_{\beta,\beta'}$), 78.5 (OCH_2CH_3), 13.9 (OCH_2CH_3). IR (hexane) ν(CO/cm^{-1}): 2071 (m), 2033 (s), 1982 (w), 1963 (w), 1951(m), 1942 (s), 1930 (w).

2.5.7 [W(CO)$_5${C(OEt)Rc] 7[76,88]

Yield = 28%. ^{1}H NMR (300 MHz, $CDCl_3$) δ 5.26 (s, 2H, RuCp'-$H_{\alpha,\alpha'}$), 5.02 (s, 2H, RuCp'-$H_{\beta,\beta'}$) , 4.82 (q, ^3J(HH) = 7.1 Hz, 2H, OCH_2CH_3), 4.56 (s, 5H, RuCp), 1.48 (t, ^3J = 7.0 Hz, 3H, OCH_2CH_3). $^{13}C\{^1H\}$ NMR (75 MHz, $CDCl_3$) δ 297.5 ($C_{carbene}$), 202.3 (CO_{trans}), 198.3 (CO_{cis}), 101.3 (RuCp'-C_{ipso}), 77.3 (OCH_2CH_3), 74.3 (RuCp'-$C_{\alpha,\alpha'}$), 73.3 (RuCp'-$C_{\beta,\beta'}$), 70.3 (RuCp), 15.0 (OCH_2CH_3). IR (hexane) ν(CO/cm^{-1}): 2063 (w), 1972 (w), 1940 (m), 1933 (s).

2.5.8 [W(CO)$_5${C(OEt)Fc] 8[57–59]

Yield = 15%. ^{1}H NMR (300 MHz, $CDCl_3$) δ 5.01 – 4.97 (m, 2H, FeCp'-$\underline{H_{\alpha,\alpha'}}$), 4.88 (q, ^3J(HH)= 7.1 Hz, 2H, O$\underline{CH_2}CH_3$), 4.84 – 4.81 (m, 2H, FeCp'-$\underline{H_{\beta,\beta'}}$), 4.25 (s, 5H, FeCp), 1.60 (t, ^3J(HH)= 7.1 Hz, 3H, $OCH_2\underline{CH_3}$). ^{13}C{^{1}H} NMR (75 MHz, $CDCl_3$) δ 304.5 ($C_{carbene}$), 202.5 (CO_{trans}), 198.0 (CO_{cis}), 95.2 (FeCp'-C_{ipso}), 78.0 (O$\underline{CH_2}CH_3$), 74.9 (FeCp'-$\underline{C_{\alpha,\alpha'}}$), 73.3 (FeCp'-$\underline{C_{\beta,\beta'}}$), 70.8 (FeCp), 15.3 ($OCH_2\underline{CH_3}$). IR (hexane) ν(CO/cm^{-1}): 2066 (w), 1976 (w), 1948 (m), 1936 (s).

2.5.9 [Rh(cod){C(OEt)(Cp'Re(CO)$_3$)}Cl] 9b

A mixture of [W(CO)$_5${C(OEt)(Cp'Re(CO)$_3$)}] **6** (0.534 g, 0.75 mmol) and [Rh(cod)Cl]$_2$ (0.184 g, 0.37 mmol) in deoxygenated CH_2Cl_2 (10 mL) was stirred for 5 days at room temperature. The resulting reddish-brown solution was reduced *in vacuo* and added to an alumina chromatography column. Elution with CH_2Cl_2 gave a red band, which was collected and evaporated to dryness, resulting in a red powder. Yield = 77%. ^{1}H NMR (300 MHz, C_6D_6) δ 6.16 (s, 1H, ReCp'), 5.82 – 5.74 (m, 2H, cod-$\underline{CH}$(overlap with O$\underline{CH_2}CH_3$), 5.51 – 5.49 (m, 1H, cod-$\underline{CH}$), 5.22 (dd, ^3J(HH) = 3.0 Hz, ^{4}J(HH) = 1.5 Hz, 1H, ReCp'), 5.13 (dq, ^2J(HH) = 10.2 Hz, ^3J(HH) = 7.1 Hz, 1H, O$\underline{CH_2}CH_3$), 4.38 – 4.36 (m, 1H, ReCp'), 4.33 – 4.30 (m, 1H, ReCp'), 3.23 (s, br, 2H, cod-$\underline{CH}$), 2.27 – 1.60 (m, 8H, cod-$\underline{CH_2}$), 1.28 (t, ^3J(HH) = 7.1 Hz, 3H, $OCH_2\underline{CH_3}$). ^{13}C{^{1}H} NMR (75 MHz, C_6D_6) δ 300.6 (d, ^2J(RhC) = 45.4 Hz, $C_{carbene}$), 192.3 (Re{CO}$_3$), 109.4 (cod-$\underline{CH}$), 103.6 (d, ^3J(RhC) = 2.7 Hz, (ReCp'-C_{ipso}), 95.5 (ReCp'), 88.8 (ReCp'), 84.0 (ReCp'), 79.3 (O$\underline{CH_2}CH_3$), 75.3 (d, ^2J(RhC) = 14.0 Hz, cod-$\underline{CH}$), 69.3 (d, ^2J(RhC) = 14.2 Hz, cod-$\underline{CH}$), 33.9 (cod-$\underline{CH_2}$), 32.0 (cod-$\underline{CH_2}$), 29.1 (cod-$\underline{CH_2}$), 27.3 (cod-$\underline{CH_2}$), 15.0 ($OCH_2\underline{CH_3}$).

2.5.10 [Rh(cod){C(OEt)*p*-DMA}Cl] 10

In like-manner, a mixture of [W(CO)$_5${C(OEt)*p*-DMA}] **3** (0.500 g, 1.0 mmol) and [Rh(cod)Cl]$_2$ (0.247 g, 0.50 mmol) in deoxygenated CH_2Cl_2 (10 mL) was stirred for 3 days at room temperature. The resulting brown solution was reduced *in vacuo* and added to an alumina chromatography column. Elution with CH_2Cl_2 gave a yellow band, which was collected and evaporated to dryness, resulting in a yellow powder. Yield = 0.165 g, 78%. Mp: 156 – 157 °C. ^{1}H NMR (500 MHz, CD_2Cl_2) δ 8.40 (d, br, ^3J(HH) = 8.6 Hz, 2H, DMA-$\underline{H_{\alpha,\alpha'}}$), 6.68 (d, ^3J(HH) = 8.8 Hz, 2H, DMA-$\underline{H_{\beta,\beta'}}$), 5.90 (dq, ^2J(HH) = 14.1 Hz, ^3J(HH) = 7.4 Hz, 1H, O$\underline{CH_2}CH_3$), 5.66 (dq, ^2J(HH) = 13.9, ^3J(HH)= 7.5 Hz Hz, 1H, O$\underline{CH_2}CH_3$), 5.27 – 5.24 (m, 1H, cod-$\underline{CH}$), 5.15 – 5.10 (m, 1H, cod-$\underline{CH}$), 3.27 – 3.23 (m, 2H, cod-$\underline{CH}$), 3.10 (s, 6H, N($\underline{CH_3}$)$_2$), 2.56 – 2.29 (m, 4H, cod-$\underline{CH_2}$), 2.14 – 1.97 (m, 4H, cod-$\underline{CH_2}$), 1.65 (t, ^3J(HH)= 7.2 Hz, 3H, $OCH_2\underline{CH_3}$). ^{13}C{^{1}H} NMR (126 MHz, CD_2Cl_2) δ 297.9 (d, ^1J(RhC) = 43.0 Hz, $C_{carbene}$), 155.1 (C_q) , 132.9 (d, ^2J(RhC) = 2.2 Hz, C_{ipso}), n.o. (DMA-$\underline{C_{\alpha,\alpha'}}$), 110.7 (DMA-$\underline{C_{\beta,\beta'}}$) , 106.3 (d, ^1J(RhC) = 4.9 Hz, cod-$\underline{CH}$), 105.9 (d, ^1J(RhC) = 4.6 Hz, cod-$\underline{CH}$), 77.2 (O$\underline{CH_2}CH_3$) , 73.0 (d, ^1J(RhC) = 15.0 Hz, cod-$\underline{CH}$), 67.9 (d, ^1J(RhC) = 14.8 Hz, cod-$\underline{CH}$), 40.5 (N($\underline{CH_3}$)$_2$), 33.5

(cod-$\underline{CH_2}$), 32.9 (cod-$\underline{CH_2}$), 29.0 (cod-$\underline{CH_2}$), 28.5, (cod-$\underline{CH_2}$), 15.6 ($OCH_2\underline{CH_3}$). Anal. Calcd for $C_{19}H_{27}ONClRh$: C 53.85, H 6.42, N 3.31. Found: C 53.89, H 6.40, N 3.24. ESI-MS (15 V, positive mode, *m/z*): calcd for $[M - Cl]^+$ 388.1148; found 388.1146.

2.5.11 [Rh(cod){C(OEt)Rc}Cl] 11

This complex was prepared similarly from $[W(CO)_5\{C(OEt)Rc\}]$ **7** (0.250 g, 0.41 mmol) and $[Rh(cod)Cl]_2$ (0.101 g, 0.21 mmol). The reaction was stirred for 8 days to allow for complete conversion of the starting materials. The product was isolated as an orange powder. Yield = 0.185 g, 84%. Mp: 119 – 120 °C. ^{1}H NMR (300 MHz, $CDCl_3$) δ 5.81 (dq, ^2J(HH) = 10.2 Hz, ^3J(HH) = 7.1 Hz, 1H, $O\underline{CH_2}CH_3$), 5.49 (dq,^2J(HH) = 10.4 Hz, ^3J(HH) = 7.1 Hz, 1H, $O\underline{CH_2}CH_3$), 5.43 – 5.42 (m, 1H, RuCp'), 5.33 – 5.27 (m, 1H, cod-$\underline{CH}$), 5.27 (s, 1H, RuCp'), 5.18 – 5.11 (m, 1H, cod-$\underline{CH}$), 4.93 – 4.91 (m, 1H, RuCp'), 4.89 – 4.87 (m, 1H, RuCp'), 4.64 (s, 5H, RuCp), 3.60 – 3.55 (m, 1H, cod-$\underline{CH}$), 3.31 – 3.26 (m, 1H, cod-$\underline{CH}$), 2.58 – 1.90 (m, 8H, cod-$\underline{CH_2}$), 1.54 (t, ^3J(HH) = 7.1 Hz, 3H, $OCH_2\underline{CH_3}$). $^{13}C\{^1H\}$ NMR (75 MHz, $CDCl_3$) δ 304.7 (d, ^2J(RhC) = 43.3 Hz, $C_{carbene}$), 106.9 (d, ^2J(RhC) = 4.5 Hz, cod-$\underline{CH}$), 106.6 (d,^2J(RhC) = 4.4 Hz, cod-$\underline{CH}$), 91.5 (d, ^3J(RhC) = 1.8 Hz, RuCp'-C_{ipso}), 77.9 ($O\underline{CH_2}CH_3$), 75.3 (RuCp'-$\underline{C_{\alpha,\alpha'}}$), 74.9 (RuCp'-$\underline{C_{\beta,\beta'}}$), 74.5 (d, ^2J(RhC) = 14.7 Hz, cod-$\underline{CH}$), 72.3 (RuCp), 67.9 (d, ^2J(RhC) = 14.9 Hz, cod-$\underline{CH}$), 33.8 (cod-$\underline{CH_2}$), 32.1 (cod-$\underline{CH_2}$), 28.9 (cod-$\underline{CH_2}$), 27.6 (cod-$\underline{CH_2}$), 15.3 ($OCH_2\underline{CH_3}$). Anal. Calcd for $C_{21}H_{26}OClRuRh$: C 47.25, H 4.91. Found: C 47.15, H 4.90. ESI-MS (15 V, positive mode, *m/z*): calcd for $[M - Cl]^+$ 449.0082; found 449.0085.

2.5.12 [Rh(CO)$_2${C(OEt)*p*-DMA}Cl] 12

Carbon monoxide gas was bubbled for 5 minutes through a stirred solution of **10** (0.050 g, 0.11 mmol) in CH_2Cl_2 (10 mL) in the absence of light and at room temperature. An immediate colour change from orange to pale-yellow was observed. The flow of CO was stopped, and golden crystals were grown by slow diffusion of *n*-hexane (2 mL) into the concentrated CH_2Cl_2 reaction mixture at -30 °C. Yield = 0.035 g, 86%. Mp: 116 – 118 °C. ^{1}H NMR (400 MHz, CD_2Cl_2) δ 8.32 (s, 2H, DMA-$\underline{H_{\alpha,\alpha'}}$), 6.70 (d, ^3J(HH)= 9.7 Hz, 2H, DMA-$\underline{H_{\beta,\beta'}}$), 5.41 – 5.35 (m, 2H, $O\underline{CH_2}CH_3$), 3.17 (s, 6H, $N(\underline{CH_3})_2$), 1.61 (t, ^3J(HH) = 7.1 Hz, 3H, $OCH_2\underline{CH_3}$). $^{13}C\{^1H\}$ NMR (101 MHz, CD_2Cl_2) δ 277.1 (d, ^1J(RhC) = 36.9 Hz, $C_{carbene}$), 187.7 (d, ^1J(RhC) = 50.0 Hz, CO_{trans}), 183.9 (d, ^1J(RhC) = 77.7 Hz, CO_{cis}), 157.1 (C_q), 131.9 (d, ^2J(RhC) = 2.3 Hz, C_{ipso}), n.o. (DMA-$\underline{C_{\alpha,\alpha'}}$), 111.2 (DMA-$\underline{C_{\beta,\beta'}}$), 79.5 (d, ^3J(RhC) = 1.7 Hz, $O\underline{CH_2}CH_3$), 40.7 ($N(\underline{CH_3})_2$), 15.1 ($OCH_2\underline{CH_3}$). IR (CH_2Cl_2, ν(CO), cm^{-1}): 1995 (s), 2078 (s). Anal. Calcd for $C_{13}H_{15}O_3NClRh$: C 42.02, H 4.07, N 3.77. Found: C 42.08, H 4.09, N 3.69. ESI-MS (15 V, positive mode, *m/z*): calcd for $[M - Cl - CO]^+$ 308.0158; found 308.0155.

2.5.13 [Rh(CO)$_2${C(OEt)Rc}Cl] 13

Similarly, this complex was synthesized from **11** (0.050 g, 0.09 mmol). The product was isolated as yellow fine crystals. Yield = 0.038 g 88%. Mp: 98 – 101 °C. ^{1}H NMR (400 MHz, C_6D_6) δ 5.31 (s, br, 1H, RuCp'-$\underline{H_{\alpha/\alpha'}}$), 5.21 (s, br, 1H, RuCp'-$\underline{H_{\alpha/\alpha'}}$), 5.13 (dq, ^2J(HH) = 14.3 Hz, ^{3}J(HH) = 7.3 Hz, 1H, O$\underline{CH_2}CH_3$), 4.92 (dq, ^2J(HH) = 14.0 Hz, ^3J(HH) = 7.4 Hz, 1H, O$\underline{CH_2}CH_3$), 4.56 – 4.55 (m, 2H, RuCp'-$\underline{H_{\beta,\beta'}}$), 4.54 (s, 5H, RuCp), 1.04 (t, ^3J(HH) = 7.1 Hz, 3H, OCH$_2\underline{CH_3}$). ^{13}C{^{1}H} NMR (101 MHz, C_6D_6) δ 283.5 (d, ^1J(RhC) = 38.6 Hz, $C_{carbene}$), 187.8 (d, ^1J(RhC) = 49.9 Hz, CO_{trans}), 184.2 (d, ^1J(RhC) = 75.8 Hz, CO_{cis}), 92.0 (d, ^2J(RhC) = 2.8 Hz, C_{ipso}), 80.6 (d, ^3J(RhC) = 1.8 Hz, O$\underline{CH_2}CH_3$), 77.3 (RuCp'-$\underline{C_{\alpha,\alpha'}}$), 76.9 (RuCp'-$\underline{C_{\beta,\beta'}}$), 73.9 (RuCp), 14.3 (OCH$_2\underline{CH_3}$). IR (CH_2Cl_2, ν(CO), cm^{-1}): 2001 (s), 2084 (s). Anal. Calcd for $C_{15}H_{14}O_3ClRuRh$: C 37.40, H 2.93. Found: C 36.95, H 3.01. ESI-MS (15 V, positive mode, *m/z*): calcd for [M – Cl – CO]$^+$ 418.9041; found 418.9021.

2.5.14 [Rh(CO)$_2${C(NH^{n}Pr)Fc$^+$}Cl][PF$_6^-$] 17$^+$

A mixture of [Rh(CO)$_2${C(NH^{n}Pr)Fc}Cl] **17** (0.020 g, 0.04 mmol) and [FcOAc][PF$_6$] (0.021 g, 0.06 mmol) was dissolved in deoxygenated CH_2Cl_2 (5 mL) at room temperature and stirred for 24 hours. The resulting brown solution was evaporated to dryness *in vacuo*, then washed with diethyl ether, and extracted with CH_2Cl_2 *via* cannula filtration. Slow concentration of the CH_2Cl_2 solution under reduced pressure gave a brown powder. Yield = 0.019 g, 73%. Mp: 142 – 143 °C. ^{19}F{^{1}H} NMR (376 MHz, CD_2Cl_2) δ -82.6 (d, ^1J(PF) = 712.9 Hz, P$\underline{F_6}$). IR (CH_2Cl_2, ν(CO) and ν(NH), cm^{-1}): 2018 (s), 2089 (s), 3306 (w).

2.6 References

1 K. H. Dötz and J. Stendel, *Chem. Rev.*, 2009, **109**, 3227–3274.

2 M. A. Sierra, *Chem. Rev.*, 2000, **100**, 3591–3638.

3 K. H. Dötz, *Angew. Chem. Int. Ed. Engl.* 1984, **23**, 587–608.

4 W. D. Wulff and D. C. Yang, *J. Am. Chem. Soc.*, 1983, **105**, 6726–6727.

5 K. H. Dötz, *Angew. Chem. Int. Ed. Engl.* 1975, **14**, 644–645.

6 K. H. Dötz and W. Kuhn, *Angew. Chem. Int. Ed. Engl.* 1983, **22**, 732.

7 M. M. Gleichmann, K. H. Dötz and B. a. Hess, *J. Am. Chem. Soc.*, 1996, **118**, 10551–10560.

8 J. Barluenga, S. Martínez, A. L. Suárez-Sobrino and M. Tomás, *J. Am. Chem. Soc.*, 2002, **124**, 5948–5949.

9 J. Barluenga, P. Barrio, L. A. López, M. Tomás, S. García-Granda and C. Alvarez-Rúa, *Angew. Chem. Int. Ed.*, 2003, **42**, 3008–3011.

10 J. Barluenga, P. Barrio, L. Riesgo, L. A. López and M. Tomás, *J. Am. Chem. Soc.*, 2007, **129**, 14422–14426.

11 J. Barluenga, R. Vicente, L. A. López and M. Tomás, *J. Organomet. Chem.*, 2006, **691**, 5654–5659.

12 J. Barluenga, R. Vicente, L. A. López, E. Rubio, M. Tomás and C. Álvarez-Rúa, *J. Am. Chem. Soc.*, 2004, **126**, 470–471.

13 J. Barluenga, R. Vicente, L. A. López and M. Tomás, *J. Am. Chem. Soc.*, 2006, **128**, 7050–7054.

14 J. Barluenga, P. Barrio, R. Vicente, L. A. López and M. Tomás, *J. Organomet. Chem.*, 2004, **689**, 3793–3799.

15 M. Fañanás-Mastral and F. Aznar, *Organometallics*, 2009, **28**, 666–668.

16 M. A. Sierra, M. J. Mancheño, E. Sáez and J. C. del Amo, *J. Am. Chem. Soc.*, 1998, **120**, 6812–6813.

17 J. C. Del Amo, M. J. Mancheño, M. Gómez-Gallego and M. A. Sierra, *Organometallics*, 2004, **23**, 5021–5029.

18 M. Gómez-Gallego, M. J. Mancheño and M. A. Sierra, *Acc. Chem. Res.*, 2005, **38**, 44–53.

19 I. Fernández, F. P. Cossío and M. A. Sierra, *Acc. Chem. Res.*, 2011, **44**, 479–490.

20 N. Faux, F. Robin-Le Guen, P. Le Poul, B. Caro, N. Le Poul, Y. Le Mest, S. J. Green, S. Le Roux, S. Kahlal and J. Y. Saillard, *Tetrahedron*, 2007, **63**, 7142–7153.

21 J. Barluenga, R. Vicente, P. Barrio, L. A. López and M. Tomás, *J. Am. Chem. Soc.*, 2004, **126**, 5974–5975.

22 J. Barluenga, P. Barrio, L. Riesgo, L. A. López and M. Tomás, *Tetrahedron*, 2006, **62**, 7547–7551.

23 K. Kamikawa, Y. Shimizu, S. Takemoto and H. Matsuzaka, *Org. Lett.*, 2006, **8**, 4011–4014.

24 M. L. Lage, D. Curiel, I. Fernández, M. J. Mancheño, M. Gómez-Gallego, P. Molina and M. A. Sierra, *Organometallics*, 2011, **30**, 1794–1803.

25 G. M. Chu, I. Fernández and M. A. Sierra, *J. Org. Chem.*, 2013, **78**, 865–871.

26 J. Barluenga, R. Vicente, L. A. López and M. Tomás, *Tetrahedron*, 2010, **66**, 6335–6339.

27 J. Barluenga, R. Vicente, L. A. López and M. Tomás, *Tetrahedron*, 2005, **61**, 11327–11332.

28 A. T. Nielsen and W. J. Houlihan, in *Organic Reactions*, American Cancer Society, 2011, pp. 1–438.

29 A. Michael, *J. Prakt. Chem.* 1887, **35**, 349–356.

30 W. D. Wulff and S. R. Gilbertson, *J. Am. Chem. Soc.*, 1985, **107**, 503–505.

31 B. A. Anderson, W. D. Wulff and A. Rahm, *J. Am. Chem. Soc.*, 1993, **115**, 4602–4611.

32 E. O. Fischer and H.-J. Beck, *Angew. Chem. Int. Ed. Engl.* 1970, **9**, 72–73.

33 J. Barluenga, L. A. López, O. Löber, M. Tomás, S. García-Granda, C. Alvarez-Rúa and J. Borge, *Angew. Chem. Int. Ed.*, 2001, **40**, 3392–3394.

34 I. Meana, A. Toledo, A. C. Albéniz and P. Espinet, *Chem. –Eur. J.*, 2012, **18**, 7658–7661.

35 A. C. Albéniz, P. Espinet, R. Manrique and A. Pérez-Mateo, *Angew. Chem. Int. Ed.*, 2002, **41**, 2363–2366.

36 M. P. López-Alberca, M. J. Mancheño, I. Fernández, M. Gómez-Gallego, M. A. Sierra and R. Torres, *Chem. –Eur. J.*, 2009, **15**, 3595–3603.

37 I. Göttker-Schnetmann, R. Aumann and K. Bergander, *Organometallics*, 2001, **20**, 3574–3581.

38 I. Göttker-Schnetmann and R. Aumann, *Organometallics*, 2001, **20**, 346–354.

39 G. K. Ramollo, M. J. López-Gómez, D. C. Liles, L. C. Matsinha, G. S. Smith and D. I. Bezuidenhout, *Organometallics*, 2015, **34**, 5745–5753.

40 V. Lavallo, J. Mafhouz, Y. Canac, B. Donnadieu, W. W. Schoeller and G. Bertrand, *J. Am. Chem. Soc.*, 2004, **126**, 8670–8671.

41 S. Takano, T. Kochi and F. Kakiuchi, *Organometallics*, 2016, **35**, 4112–4125.

42 M. Talavera, R. Pereira-Cameselle and S. Bolaño, *Dalton Trans.*, 2018, **47**, 9064–9071.

43 J. A. Connor and E. M. Jones, *J. Chem. Soc. A Inorg. Phys. Theor.*, 1971, 1974.

44 A. J. van Rensburg, M. Landman, E. Erasmus, D. van der Westhuizen, H. Ferreira, M. M. Conradie and J. Conradie, *Electrochim. Acta*, 2016, **219**, 204–213.

45 M. Landman, B. E. Buitendach, M. M. Conradie, R. Fraser, P. H. van Rooyen and J. Conradie, *J. Electroanal. Chem.*, 2015, **739**, 202–210.

46 D. I. Bezuidenhout, B. van der Westhuizen, P. J. Swarts, T. Chatturgoon, O. Q. Munro, I. Fernández and J. C. Swarts, *Chem. –Eur. J.*, 2014, **20**, 4974–4985.

47 D. I. Bezuidenhout, S. Lotz, D. C. Liles and B. van der Westhuizen, *Coord. Chem. Rev.*, 2012, **256**, 479–524.

48 S. Klenk, S. Rupf, L. Suntrup, M. van der Meer and B. Sarkar, *Organometallics*, 2017, **36**, 2026–2035.

49 B. van der Westhuizen, P. J. Swarts, L. M. van Jaarsveld, D. C. Liles, U. Siegert, J. C. Swarts, I. Fernández and D. I. Bezuidenhout, *Inorg. Chem.*, 2013, **52**, 6674–6684.

50 E. O. Fischer, *Pure Appl. Chem.*, 1970, **24**, 407–424.

51 M. A. Sierra, J. C. del Amo, M. J. Mancheño, M. Gómez-Gallego and M. Gomez-Gallego, *J. Am. Chem. Soc.*, 2001, **123**, 851–861.

52 G. K. Ramollo, *Synthesis and application of rhodium(I) Fischer carbene complexes*, 2016, University of Pretoria.

53 M. Landman, R. Pretorius, B. E. Buitendach, P. H. van Rooyen and J. Conradie, *Organometallics*, 2013, **32**, 5491–5503.

54 C. Crause, H. Görls and S. Lotz, *Dalton Trans.*, 2005, 1649–1657.

55 M. Schwarz, M. Vollmann, R. Wartchow and H. Butenschön, *J. Organomet. Chem.*, 2005, **690**, 2263–2271.

56 R. Fraser, P. H. van Rooyen and M. Landman, *J. Mol. Struct.*, 2016, **1105**, 178–185.

57 E. O. Fischer, F. J. Gammel, J. O. Besenhard, A. Frank and D. Neugebauer, *J. Organomet. Chem.*, 1980, **191**, 261–282.

58 D. I. Bezuidenhout, W. Barnard, B. van der Westhuizen, E. van der Watt and D. C. Liles, *Dalton Trans.*, 2011, **40**, 6711–6721.

59 J. G. López-Cortés, L. F. Contreras De La Cruz, M. C. Ortega-Alfaro, R. A. Toscano, C. Alvarez-Toledano and H. Rudler, *J. Organomet. Chem.*, 2005, **690**, 2240–2248.

60 M. L. Lage, I. Fernández, M. J. Mancheño, M. Gómez-Gallego and M. A. Sierra, *Chem. –Eur. J.*, 2010, **16**, 6616–6624.

61 N. Weststrate, *Structural and electronic features of tungsten(0) and platinum(II) complexes with Fischer carbene ligands*, 2017, University of Pretoria.

62 S. Lotz, M. van den Berg and J. L. M. Dillen, *Transit. Met. Chem.*, 1988, **13**, 170–175.

63 B. van der Westhuizen, P. J. Swarts, I. Strydom, D. C. Liles, I. Fernández, J. C. Swarts and D. I. Bezuidenhout, *Dalton Trans.*, 2013, **42**, 5367–5378.

64 R. J. Abrahams, J. Fischer and P. Loftus, *Introduction to NMR Spectroscopy*, John Wiley and Sons, Somerset, New Jersey, 1st edn., 1989.

65 D. M. Adams, *Metal-Ligand and Relative Vibrations: A Critical Survey of the Infrared and Raman Spectra of Metallic and Organometallic Compounds*, Edinburg University Press, London, 1967.

66 T. Dröge and F. Glorius, *Angew. Chem. Int. Ed.*, 2010, **49**, 6940–6952.

67 E. C. Keske, O. V Zenkina, R. Wang and C. M. Crudden, *Organometallics*, 2012, **31**, 456–461.

68 C. A. Tolman, *J. Am. Chem. Soc.*, 1969, **1**, 2953–2956.

69 C. A. Tolman, *Chem. Rev.*, 1977, **77**, 313–348.

70 A. R. Chianese, X. Li, M. C. Janzen, J. W. Faller and R. H. Crabtree, *Organometallics*, 2003, **22**, 1663–1667.

71 R. A. Kelly III, H. Clavier, S. Giudice, N. M. Scott, E. D. Stevens, J. Bordner, I. Samardjiev, C. D. Hoff, L. Cavallo and S. P. Nolan, *Organometallics*, 2008, **27**, 202–210.

72 S. Wolf and H. Plenio, *J. Organomet. Chem.*, 2009, **694**, 1487–1492.

73 T. L. Mashabane, G. K. Ramollo, G. Kleinhans, S. De Doncker, S. Siangwata, M. A. Fernandes, A. Lemmerer, G. S. Smith and D. I. Bezuidenhout, *J. Organomet. Chem.*, 2020, **920**, 121341.

74 A. R. Kenaree, T. J. Cuthbert, S. M. Barbon, P. D. Boyle, E. R. Gillies, P. J. Ragogna and J. B. Gilroy, *Organometallics*, 2015, **34**, 4272–4280.

75 N. G. Connelly and W. E. Geiger, *Chem. Rev.*, 1996, **96**, 877–910.

76 D. I. Bezuidenhout, I. Fernández, B. Van Der Westhuizen, P. J. Swarts and J. C. Swarts, *Organometallics*, 2013, **32**, 7334–7344.

77 D. Aucamp, T. Witteler, F. Dielmann, S. Siangwata, D. C. Liles, G. S. Smith and D. I. Bezuidenhout, *Eur. J. Inorg. Chem.*, 2017, **2017**, 1227–1236.

78 S. A. Laneman and G. G. Stanley, in *Homogeneous Transition Metal Catalyzed Reactions*, American Chemical Society, 1992, vol. 230, pp. 24–349.

79 M. E. Broussard, B. Juma, S. G. Train, W.-J. Peng, S. A. Laneman and G. G. Stanley, *Science* 1993, **260**, 1784 – 1788.

80 D. G. H. Hetterscheid, S. H. Chikkali, B. de Bruin and J. N. H. Reek, *ChemCatChem*, 2013, **5**, 2785–2793.

81 A. Kämper, P. Kucmierczyk, T. Seidensticker, A. J. Vorholt, R. Franke and A. Behr, *Catal. Sci. Technol.*, 2016, **6**, 8072–8079.

82 L. Wu, I. Fleischer, R. Jackstell, I. Profir, R. Franke and M. Beller, *J. Am. Chem. Soc.*, 2013, **135**, 14306–14312.

83 L. Alvila, T. A. Pakkanen and O. Krause, *J. Mol. Catal.*, 1993, **84**, 145–156.

84 W. Gil, A. M. Trzeciak and J. J. Ziółkowski, *Organometallics*, 2008, **27**, 4131–4138.

85 M. Bortenschlager, J. Schütz, D. von Preysing, O. Nuyken, W. A. Herrmann and R. Weberskirch, *J. Organomet. Chem.*, 2005, **690**, 6233–6237.

86 B. Van Der Westhuizen, J. M. Speck, M. Korb, J. Friedrich, D. I. Bezuidenhout and H. Lang, *Inorg. Chem.*, 2013, **52**, 14253–14263.

87 B. van der Westhuizen, J. Matthäus Speck, M. Korb, D. I. Bezuidenhout and H. Lang, *J. Organomet. Chem.*, 2014, **772**–**773**, 18–26.

88 E. O. Fischer, F. J. Gammel, J. O. Besenhard, A. Frank and D. Neugebauer, *J. Organomet. Chem.*, 1980, **191**, 261–282.

Chapter 3: Synthesis and application of iridium(I) Fischer carbene complexes in transfer hydrogenation reactions

3.1 Literature review

Literature reports of mono-heteroatom stabilized iridium Fischer carbene complexes (FCCs) are rare. Complicated or serendipitous synthetic strategies mainly involving the iridium-initiated double C-H activation of alkyl- ethers and amines, resulting in alkoxy- and aminocarbene complexes, respectively, can be attributed to the dearth of such reports. In addition, the vast majority of reported iridium FCCs feature cyclic carbene ligands, which aid in the stabilization and isolability of the resultant FCCs.

3.1.1 Synthetic strategies towards Fischer-type carbene complexes of iridium

The first isolated iridium FCC was reported by Stone and coworkers in 1974, whereby oxidative substitution of the iridate complex $[Ir(CO)_3PPh_3)]^-$ by the oxidant *N*-methyl-2-chloro-pyridinium tetrafluoroborate salt resulted in a monocationic Ir^I cyclic-aminocarbene complex.[1] Reports of iridium-supported FCCs reemerged in 1990, wherein Rheingold and coworkers reported the α,α-dehydrogenation of 3-butyn-1-ol by an iridacyclic compound, resulting in the monocationic Ir^{III} cyclic-carbene complex depicted in Figure 3.1 (a).[2] The isolated complex was structurally characterized and showed a Ir-$C_{carbene}$ bond order of 2. Later reports of α,α-dehydrogenation of *O*- or *N*-atom bound methylene moieties of selected ethers or amines, respectively, resulted in a range of Ir^{III} FCCs depicted in Figure 3.1 below. The thermolysis of an iridium(I) bis(ethylene) precursor in THF proceeds through an isolable Ir^{III} hydride-vinyl complex, which in turn promotes the C-H activation of THF, resulting in the Ir^{III} cyclic(alkoxy)carbene complex (b), as reported by Carmona and coworkers in 1992.[3] Analogously, Luecke and coworkers later reported the thermal substitution of a neutral Ir^{III} precursor by THF resulting in the monocationic Ir^{III} cyclic FCC (c).[4] These reaction conditions were later adapted for similar Ir^{III} cyclic(alkoxy) FCCs, and the isolated complexes were thermodynamically stable enough for structural characterization.[5,6] For access to a classic (aryl-substituted) acyclic (alkoxy) complex, the alkylation of an existing Ir^{III} benzolyl complex reportedly proceeds to the monocationic Ir^{III} FCC salt (d), which could in turn be converted to its neutral analogue or to a phenylcarbyne complex, by reaction with trimethylsilyl triflate or various lithium salts, respectively.

Additionally, Ir^{III} aminocarbene complexes (e) and (f) could also be isolated *via* the above-mentioned double C-H activation of the relevant amines. The α,α-dehydrogenation of 2-dimethylaminopyridine by the Ir^{III} precursor $[Ir(OCMe_2)_2(PPh_3)_2H_2][BF_4]$ resulted in the Ir^{III} *N*-atom chelated iridacyclic(amino)carbene complex (e), as reported by Crabtree and coworkers.[7] The acyclic aminocarbene complex (f) was reported by Whited and Grubbs in 2008, as accessed *via* the (double C-H activation) reaction of an iridium(III) pincer(PNP) compound and *N,N,N',N'*-tetramethylethylenediamine (TMEDA).[8] Not long after, the authors also reported the acyclic *tert*-butoxycarbene complex (g) *via* reaction of the same Ir^{III}(PNP) precursor and methyl *tert*-butylether (MTBE) instead of TMEDA.[9] While the MTBE reaction proceeds through a Ir^{III} dihydrido complex analogous to (f), formation of the Ir^{I} FCC (g) is favoured *via* dehydrogenation of the non-isolated Ir^{III} intermediate. Similarly, *n*- and *sec*-butoxycarbene complexes analogous to (g) were reported by the authors in 2009.[10] These C-H activation reactions towards iridium FCCs were thoroughly reviewed in 2005 and 2009, by the research groups of Carmona and Grubbs, respectively,[11,12] and are succinctly summarized in a 2014 review article by Raubenheimer.[13]

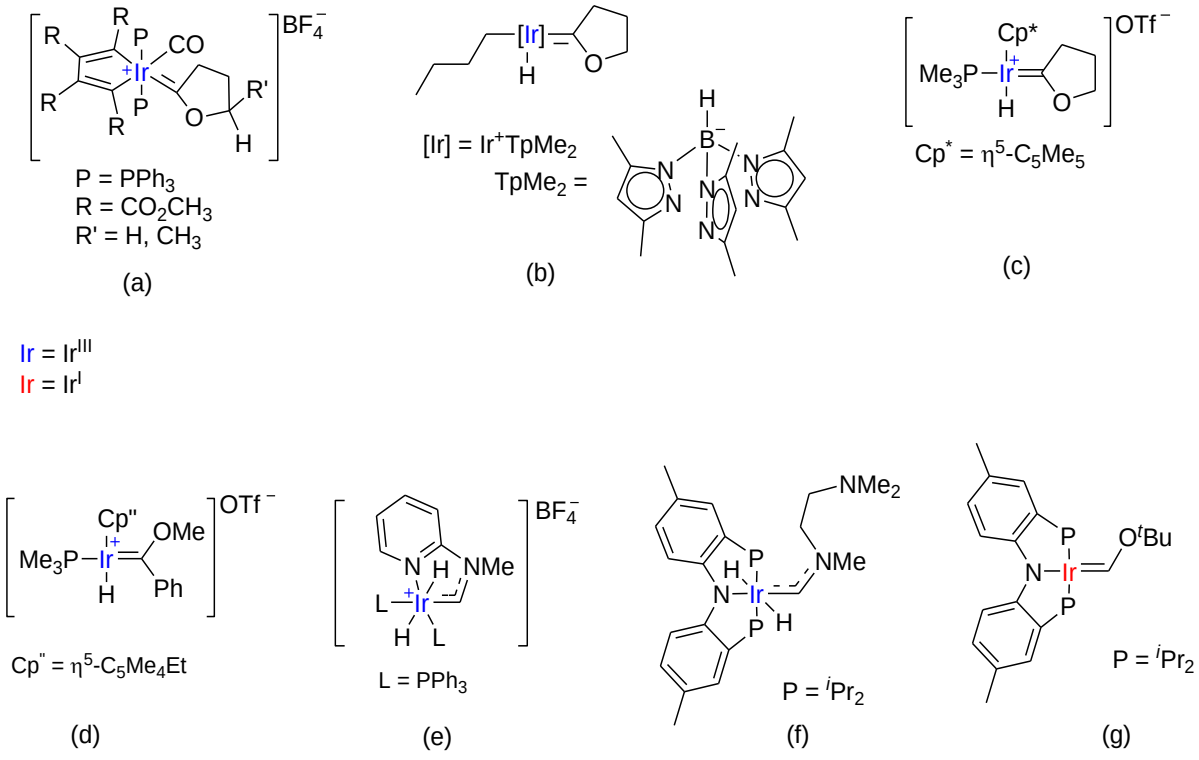

Figure 3.1 Selected examples of reported iridium Fischer carbene complexes.

Other than these examples, the only other mono-heteroatom stabilized iridium FCC was accessed *via* the stoichiometric reaction of an existing 7-membered cyclic(imino)(ferrocenyl) ligand salt and the iridium precursor $[Ir(cod)Cl]_2$, wherein the inclusion of a copper iodide additive and a strong base such as lithium hexamethyldisilazide proved necessary for low to moderate yields of the resultant Ir^{I} cyclic(amino)(ferrocenyl)carbene complex, as reported by Yoshida and coworkers in 2017.[14] The authors later reported a similar Ir^{I} FCC featuring a pentamethylcyclopentadienyl group (instead of a simple cyclopentadienyl entity) at the ferrocenyl (Fc) site, resulting in a comparatively more electron rich cyclic(amino)carbene complex which was subsequently employed in the transfer hydrogenation of cyclic *N*-sulfonylimine.[15] In our case, such stringent synthetic strategies are avoided, and the facile transmetallation route will instead be employed for access to classic acyclic mono-heteroatom stabilized aryl-carbene complexes for catalytic application towards the transfer hydrogenation (TH) of ketones.

3.1.2 Special considerations for the transfer hydrogenation reactions

The TH process has rapidly become a more attractive alternative to the direct hydrogenation method, mainly due to the potential hazards associated with gaseous hydrogen required for the latter process.[16] Other advantages of employing the TH process include the requirement of varied easy-to-handle and affordable H-donor chemicals (such as *iso*-propanol, water, glycerol, etc), as well as the possible formation of useful side-products during the catalytic cycle.[17]

Mechanistic studies of metal-catalyzed TH reactions specify either inner-sphere or outer-sphere pathways, the former of which involves the direct binding of the substrate into the metal coordination sphere during the catalytic cycle, while the latter pathway excludes the metal-substrate coordination step usually associated with homogenous catalysis (and instead involves the direct transfer of a proton and hydride from the catalyst system to the unsaturated substrate, usually in a concerted manner).[18] While outer-sphere mechanisms have been occasionally reported, the vast majority of metal-catalyzed TH reactions are said to proceed through inner-sphere mechanisms, which can be further classified as monohydridic, dihydridic, or *Meerwein-Ponndorf-Verley* (MPV) type as per the respective formation of metal- monohydride, dihydride, or solvent-M-substrate active species during the catalytic cycle.[19–21] For the base-assisted TH of ketones relevant to this chapter, iridium NHC (pre)catalysts are generally accepted as proceeding through the monohydridic inner-sphere mechanism depicted in Scheme 3.1.[22] The base-initiated deprotonation of a weakly coordinated *iso*-propanol solvent molecule of the Ir-NHC complex **I** results in the Ir-2-propoxide complex **II**. Subsequent β-hydride elimination and expulsion of an acetone molecule results in the Ir-NHC

monohydride species **III**. The ketone substrate (acetophenone) is then coordinated to the Ir-metal atom resulting in **IV**, which in turn undergoes intramolecular Ir-hydride transfer to the carbonyl carbon atom resulting in complex **V** with a coordinated 1-phenyl-ethoxide ligand. A second *iso*-propanol molecule is then deprotonated and coordinated to the Ir-metal site regenerating the 2-propoxide complex **II** with release of the targeted alcohol product (phenylethanol).

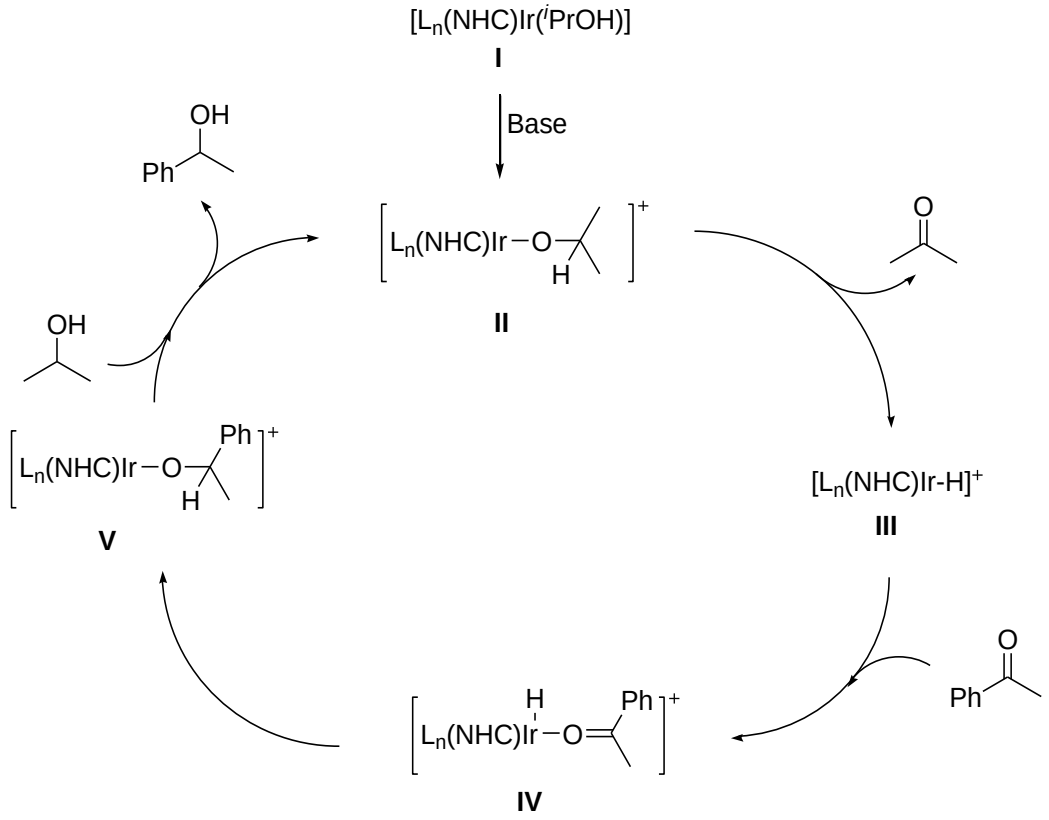

Scheme 3.1 Generally accepted mechanism for Ir^{I} NHC-catalyzed utilized TH of ketones

This reaction mechanism is usually reported for Ir^{I} and Ir^{III} NHC complexes in literature, with superior catalytic activity and selectivity usually reported for the latter class. Furthermore, the use of iridacyclic NHC precatalysts of the form $[IrL_n(NHC\text{-}X)]$ featuring a chelating amine, phosphine, or NHC entity (X) effects the best catalytic activity towards the TH of ketones, with the Ir^{III} complexes again indicating enhanced activity compared to the Ir^{I} analogues.[19,23] As such, literature reports of Ir^{III}-NHC catalyzed TH frequently employ mild catalytic conditions with a low precatalysts/base/substrate ratio of 1/5/1000 (i.e 0.1 mol% Ir complex and 0.5 mol% base amounts with respect to the substrate). These optimized conditions were employed for the successful TH of acetophenone utilizing Ir^{III} NHC precatalysts with excellent catalytic activity,[24,25] wherein unprecedented catalytic activity at ambient temperatures was also observed for some chelated Ir^{III} NHC systems.[26] Similarly, Ir^{I} NHC precatalysts

(such as the ones depicted in Figure 3.2 below) also reportedly exhibit excellent catalytic activities under these conditions. Iridium(I) NHC complex (a) indicates the efficient TH of ketones with turnover frequencies (TOFs) up to 4622 hr^{-1} due in part to the hemilabile effect of the pendant *O*-heteroatom during the catalytic cycle, as reported by Jiménez and coworkers.[27] The authors also therein reported the relatively poor catalytic activity of a chelated monocationic Ir^{I} NHC complex with TOFs less than 250 hr^{-1}. This chelation effect in Ir^{I} NHC precatalysts is further illustrated by normal- and abnormal NHC complexes (b) and (c), wherein the stronger electron-donating ligand of (b) effects poor catalytic activity in contrast to the excellent activity of (c) effected by the weaker electron donating nature of the accompanying abnormal NHC ligand.[28] Carbene ligands with hemilabile entities are thus touted as effecting the best Ir^{I} carbene precatalysts for the TH of ketones. No literature reports of iridium-catalyzed TH utilizing acyclic Fischer-type carbene complexes were available prior to this study.

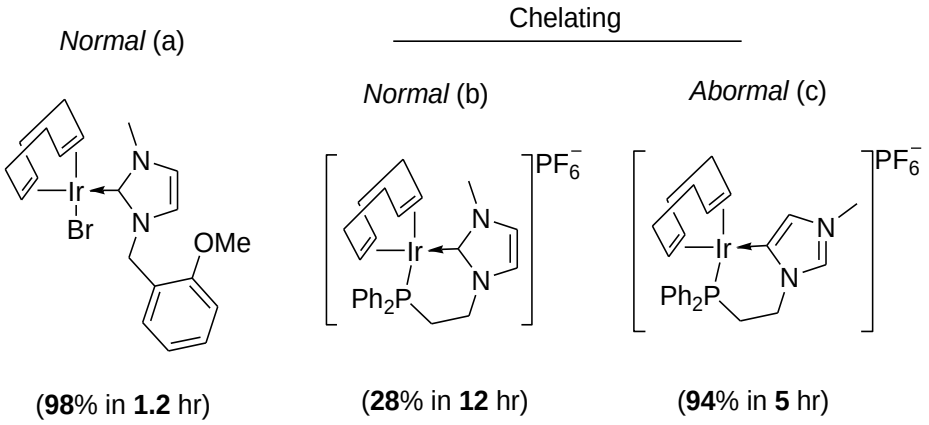

Figure 3.2 Selected examples of Ir^{I} NHC complexes employed as precatalysts towards the TH of ketones.

3.2 Aim

The main aim of this chapter is the synthesis and characterization of new iridium(I) FCCs for catalytic application in the TH of ketones. As discussed in Chapter 2, the calculated electron donating strength of Fc-carbene ligands :C(OEt)Fc and :C($NH^{n}Pr$)Fc, in terms of calculated TEPs 2054 cm^{-1} and 2049 cm^{-1},[29] respectively, were found to be comparable to some commonly reported NHC, CAAC (cyclic(alkyl)(amino)carbene), and acyclic diaminocarbene ligands in literature.[30,31] The excellent catalytic activity of the isolated rhodium(I) FCCs towards the hydroformylation of 1-octene (*vide supra*)

prompted us to envisage the viability of similarly synthesizing iridium(I) analogues, and their potential catalytic application in the TH of ketones for comparison with iridium-NHC precatalysts. The objectives of this chapter are thus (i) to investigate the facile carbene ligand transfer method employed for rhodium(I) FCCs in Chapter 2, towards iridium(I) analogues, (ii) to study the electronic effects of the carbene ligand substituents (by variation of the strongly electron- donating or withdrawing carbene substituents ferrocenyl (Fc), piano stool cyclopentadienylrheniumtricarbonyl ($Cp^{'}Re(CO)_3$), or *para-N,N*-dimethylaniline (*p*-DMA), (iii) to determine the effect of *O*- vs *N*-heteroatom stabilization by variation of ethoxy- and aminocarbene substituents, as well as (iv) the effect of co-ligand substitution reactions tailored towards finetuning the iridium(I)-metal atom coordination sphere. The final objective (v) is to investigate the possibility of including a carbene ligand with a hemilabile *N*-donor pendant moiety by including aminolysis of ethoxycarbene complexes with a diamine, to pave the way towards cooperative carbene ligand behaviour in the mechanism underlying TH. These substituent/ co-ligand modifications will be monitored by spectroscopic (NMR, FT-IR), mass spectrometric, and single-crystal X-ray diffraction methods, as the main techniques towards characterization of the envisioned novel Ir^{I} FCCs.

3.3 Results and Discussion

3.3.1 Synthetic strategy

The synthesis of new iridium(I) FCCs was achieved by transmetallation[32] between the iridium precursor and relevant tungsten(0) carbene complex as depicted in Scheme 3.2 below. The carbene transfer reaction route was for the first time employed towards iridium FCC synthesis to give complexes **18** – **20** in high yields. Initially, preparation of the targeted complexes at room temperature proved unsuccessful, with multiple futile attempts resulting in the unreacted tungsten(0) carbene complex and unidentified decomposition products of the $[Ir(cod)Cl]_2$ precursor. All transmetallation reactions were thus done at -78 °C henceforth, as is sometimes required for iridium carbene complexes.[14] For the transmetallation reaction, the iridium dimer precursor and relevant tungsten carbene complex mixture was vacuum-dried at room temperature for 1 hour before dissolution in deoxygenated CH_2Cl_2 at -78 °C under an inert argon gas atmosphere. The reaction was allowed to warm up to room temperature with vigorous stirring overnight, wherein product formation was detected by thin layer chromatography. The iridium carbene complex was then isolated *via* flash column chromatography using oven-dried alumina (120 °C) and CH_2Cl_2 as eluent.

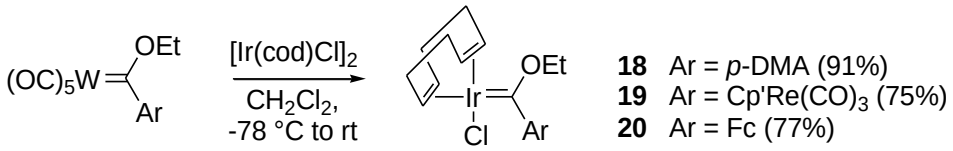

Scheme 3.2 Synthesis of Ir^{I} FCCs **18** – **20** *via* transmetallation from W^{0} precursors **3, 6** and **8** respectively.

Iridium(I) carbene complexes **18** and **20** were subsequently used as precursors for the synthesis of complexes **21** – **25** as depicted in Scheme 3.3 (a) and (b), respectively. The direct transfer of aminocarbene ligands from W^{0} to Ir^{I} was unsuccessful (due to difficulties in separating the Ir^{I} aminocarbene complex from unreacted starting material and unidentified side-products). This synthetic method was thus discontinued, and the targeted Ir^{I} aminocarbene complexes were instead accessed *via* post-transmetallation carbene modification reactions. Aminolysis of complex **18** (*p*-DMA) to form **21** proceeded at room temperature whilst similar reactions with Fc-carbene complex **19** only occurred at higher temperatures. As such, aminocarbene complex **21** was synthesized at room temperature, and the Fc-aminocarbene complexes **22** and **23** were prepared at 60 °C as depicted in Scheme 3.3 below.

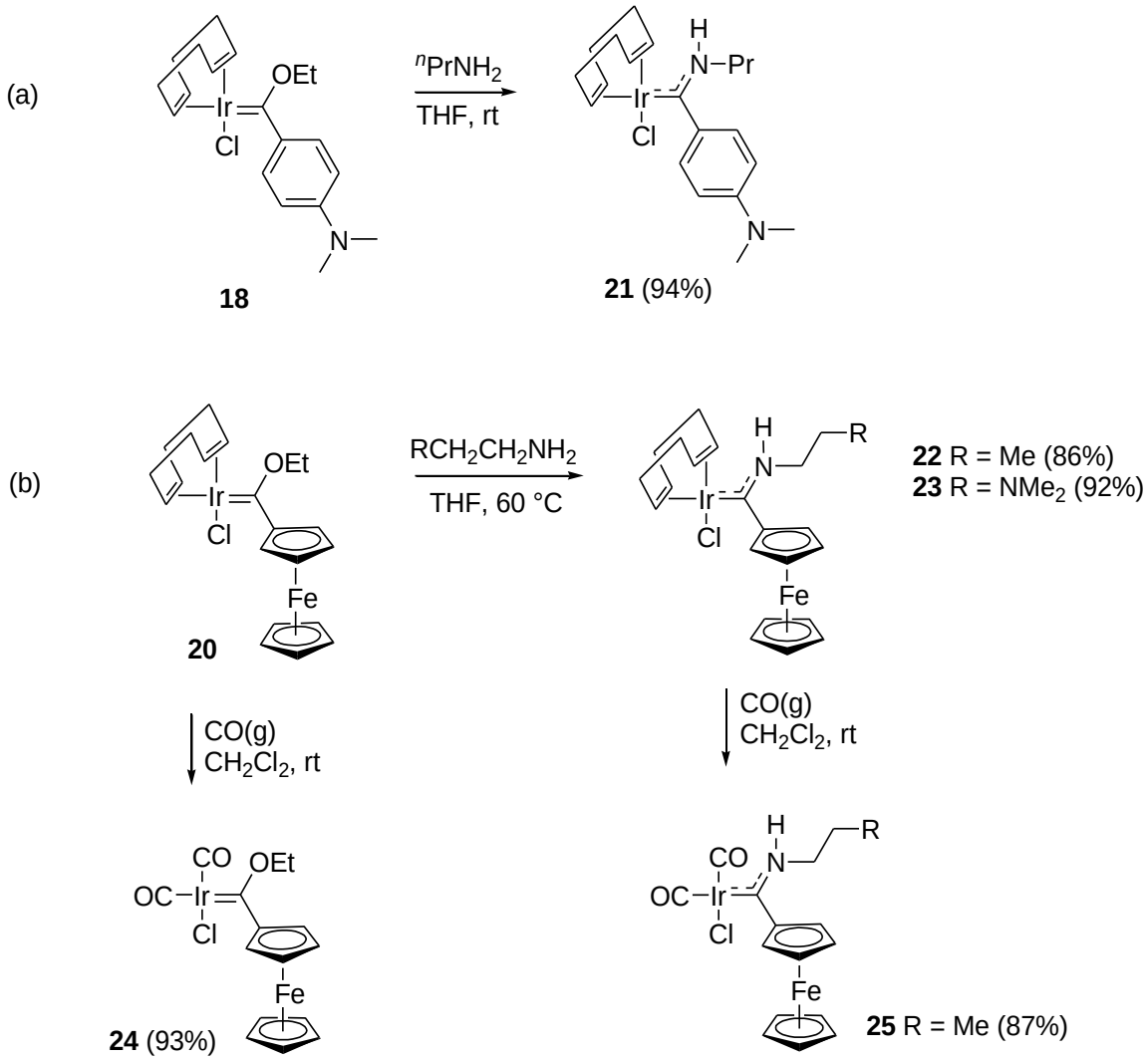

Scheme 3.3 Synthesis of carbene complexes **21** (a) and **22** – **25** (b) *via* ligand modification or substitution reactions of complexes **18** and **20**, respectively.

3.3.2 Synthesis and Characterization of iridium(I) Fischer carbene complexes

Iridium(I) ethoxycarbene complexes **18** – **20** were isolated *via* carbene transfer (W^0-Ir^I transmetallation) with carbene ligand dissociation from W^0 metal as the key step.

3.3.2.1 1,5-cyclooctadienechlorido{*p*-(*N*,*N*-dimethylaniline)ethoxycarbene}iridium(I) complex 18

As outlined in Scheme 3.1 (*vide supra*), complex **18** was synthesized from tungsten(0) ethoxycarbene complex **3** and $[Ir(cod)Cl]_2$ precursor with 91% yield. The ^1H NMR spectrum of **18** (Figure 3.3) was consistent with Rh^I(cod)-complexes discussed in Chapter 2 and reported in literature,[29] with the asymmetrical Ir(cod)-moiety evident in the chemical environment of **18**.

The integrated ^{1}H NMR spectrum of **18** indicates two sets of doublet of quartets, one for each of the two ethoxy-CH_2 protons, which is in agreement with restricted rotation of the $C_{carbene}$-*O* bond (OEt-CH_2 chemical shifts 5.67 ppm, dq, ^{2}J(HH) = 10.4 Hz, ^{3}J(HH) = 7.2 Hz; 5.39 ppm, dq, ^{2}J(HH) = 10.4 Hz, ^{3}J(HH) = 7.1 Hz). This is in contrast to what is observed for the W^0 precursor complex [$W(CO)_5${C(OEt)*p*-DMA}] (**3**). However, only one triplet signal is observed for the ethoxy-CH_3 group in **18**, integrating to the expected 3 H-atoms. The *p*-DMA carbene substituent remains unaffected by the Ir(cod)Cl-moiety as both α-protons are chemically equivalent, as is the case with both β-protons and all *p*-DMA methyl-protons (8.36 ppm, 2H, $H_{\alpha,\alpha'}$; 6.65 ppm, 2H, $H_{\beta,\beta'}$; 3.07 ppm, 6H, -NMe_2). The $^{13}C\{^{1}H\}$ NMR spectrum of **18** (Figure 3.4) indicated a 22 ppm upfield shift of the carbene carbon signal (276.7 ppm) from the precursor complex **3** (299.7 ppm), due to the lesser electron-withdrawing effect of the Ir(cod)Cl-moiety in **18** as compared to the more electron withdrawing $W(CO)_5$-moiety in **3**. This drastic upfield-shift of the carbene carbon resonance was the first spectroscopic evidence of successful W^0-Ir^{I} transmetallation in the synthesis of **18**, and is within the range of reported Ir^{I} and Ir^{III} FCCs in literature (216 – 275 ppm).[4,5,10] Additionally, both the ^{1}H and $^{13}C\{^{1}H\}$ NMR spectra of **18** indicate that the *p*-DMA substituent remains symmetrical in solution for the Ir^{I} FCC, as was the case for the Rh^{I} analogues (Chapter 2).

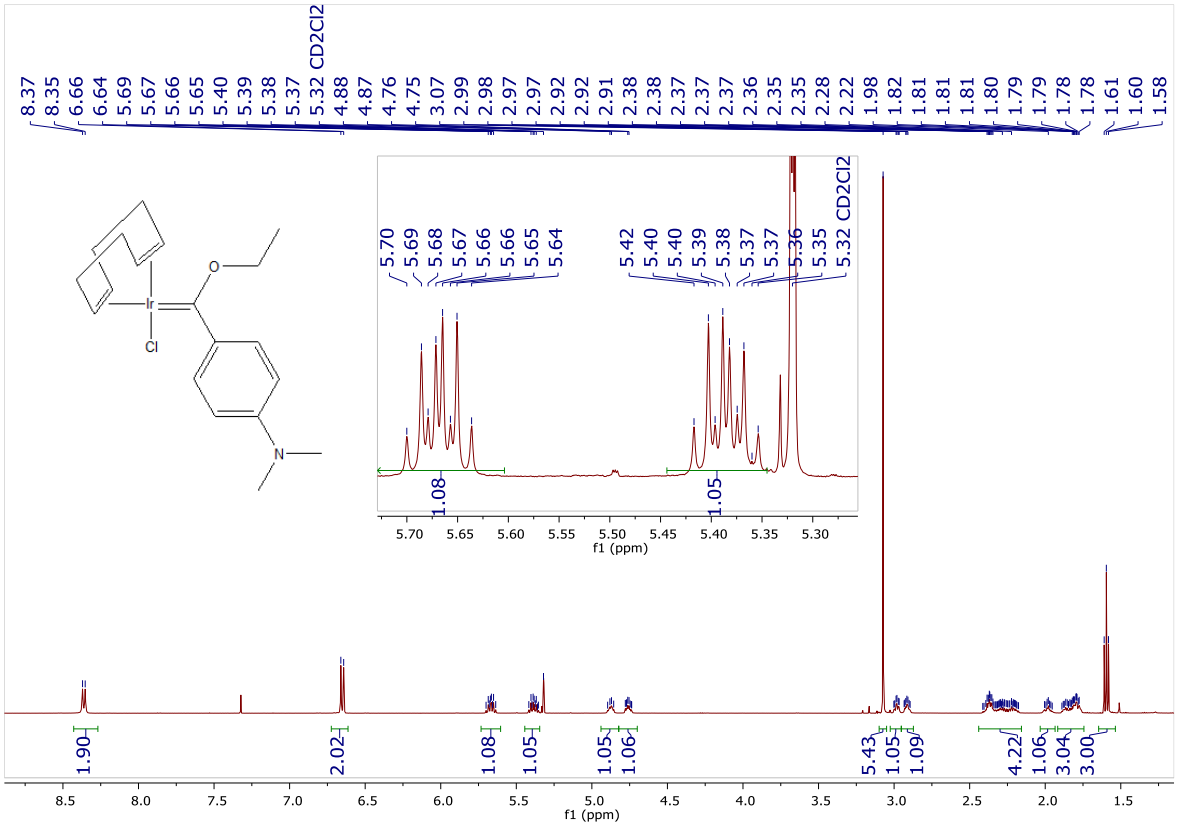

Figure 3.3 ^{1}H NMR spectrum of **18** in CD_2Cl_2

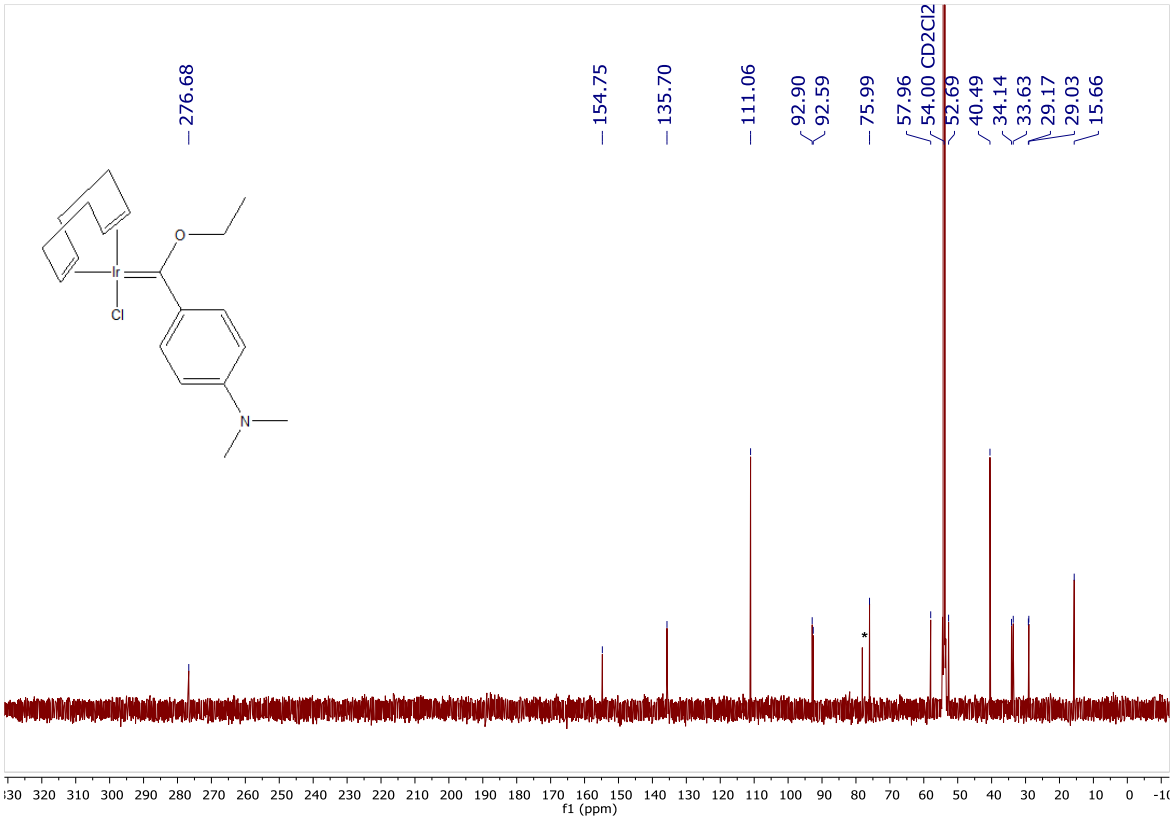

Figure 3.4 $^{13}C\{^{1}H\}$ NMR spectrum of **18** in CD_2Cl_2. *Residual $CHCl_3$

3.3.2.2 1,5-cyclooctadienechlorido{(cyclopentadienylrheniumtricarbonyl)ethoxycarbene}iridium(I) complex 19

For comparison with a strictly electron withdrawing carbene substituent, the $Cp'Re(CO)_3$ carbene substituent with strong π-accepting carbonyl ligands was employed for the synthesis of complex **19** (77% yield), from W^0 carbene complex **6** and the Ir^I precursor $[Ir(cod)Cl]_2$. ^{1}H and $^{13}C\{^{1}H\}$ NMR spectra of Ir^I FCC **19** (Figure 3.5 and 3.6 respectively) indicate the above-mentioned lack of symmetry as a result of the bulky Ir(cod)Cl-moiety, again resulting in restricted rotation of the $C_{carbene}$-C_{ipso} bond. Evidence of this includes duplication of the ethoxy-CH_2 proton signals, as well as partial duplication of the $Cp'Re(CO)_3$ substituent $H_{\alpha,\alpha}/H_{\beta,\beta'}$ signals. In addition, a 21 ppm upfield-shift of the $C_{carbene}$ carbon resonance of **19** in comparison to the W^0 precursor **6** was evident, suggesting successful carbene ligand transfer in the synthesis of complex **19**. FT-IR spectroscopy of **19** showed two carbonyl vibration bands at 2031 cm^{-1} (sharp) and 1937 cm^{-1} (broad) for the $Re(CO)_3$-moiety as is customary for $[M(CO)_3(\pi\text{-arene})]$ complexes in literature.[33]

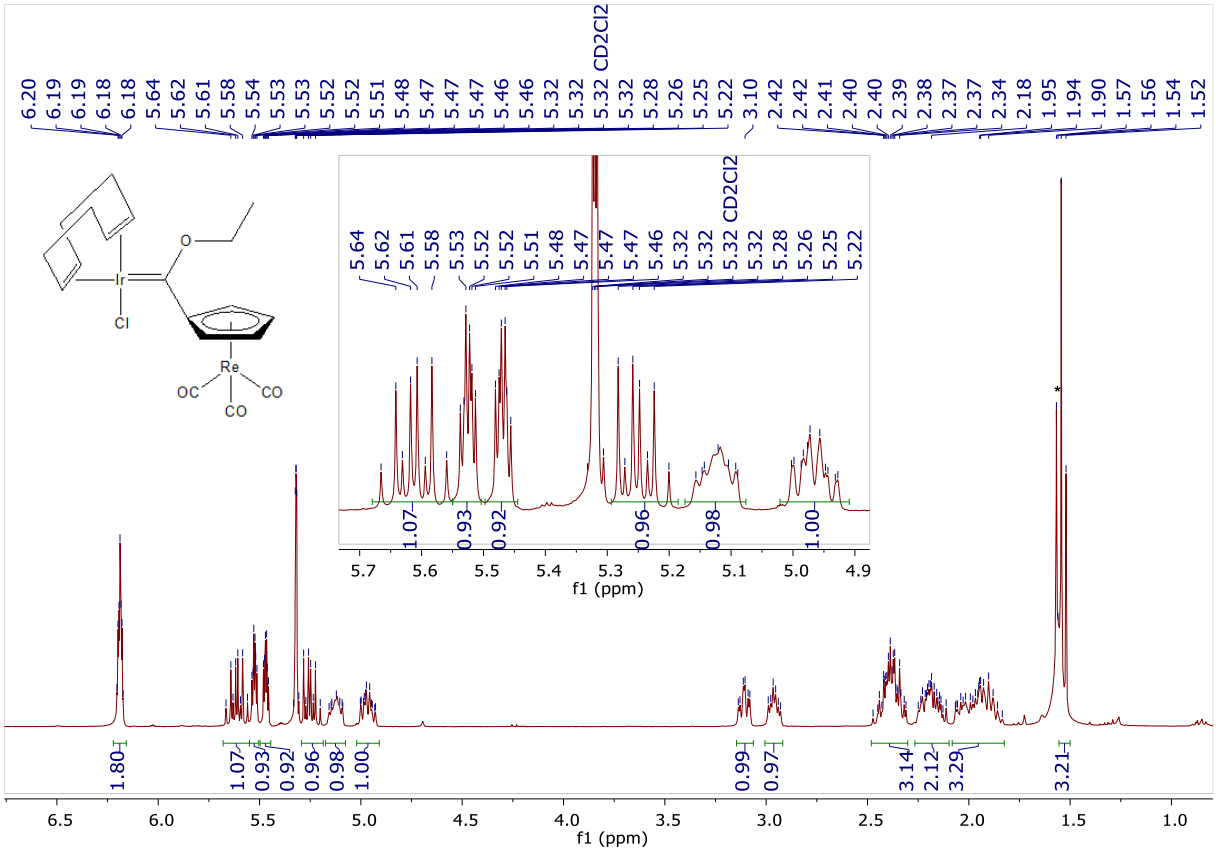

Figure 3.5 ^{1}H NMR spectrum of **19** in CD_2Cl_2. *Residual H_2O contaminant

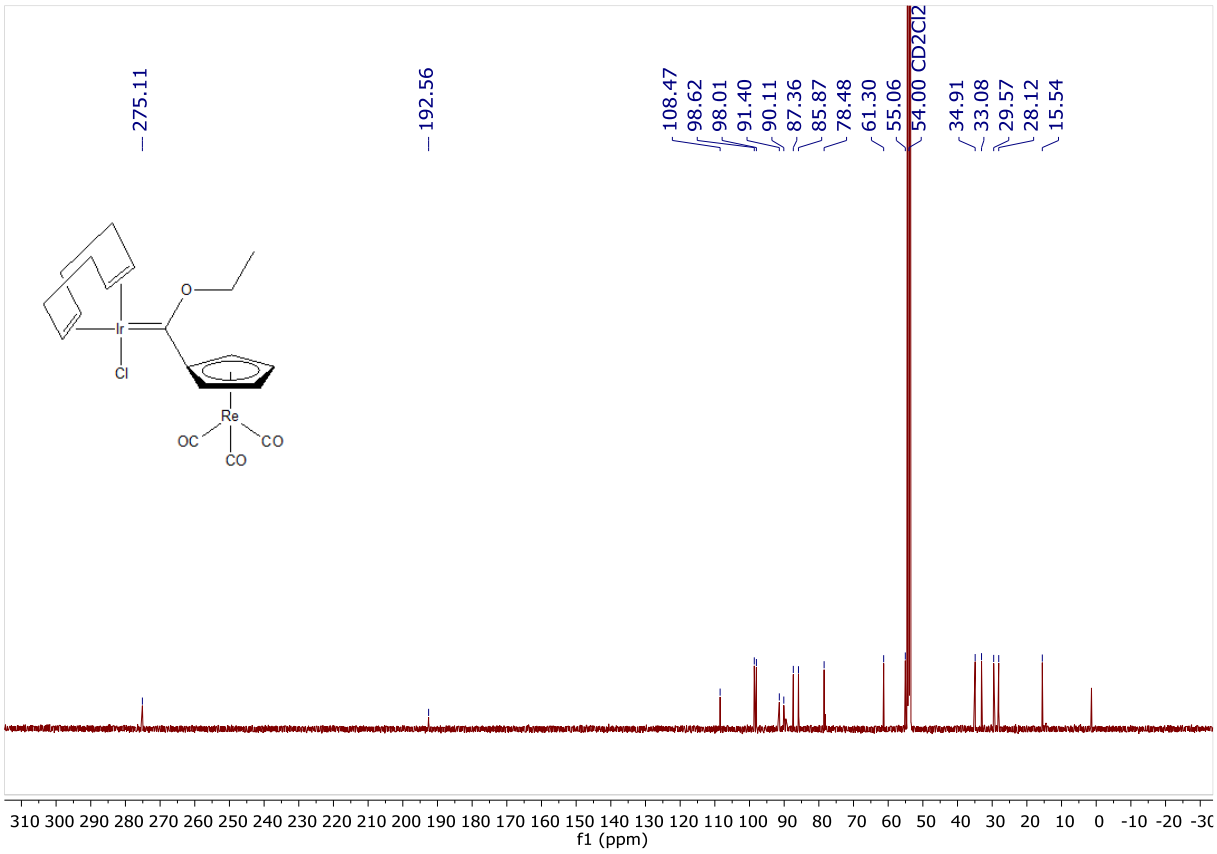

Figure 3.6 $^{13}C\{^{1}H\}$ NMR spectrum of **19** in CD_2Cl_2

3.3.2.3 1,5-cyclooctadienechlorido{(ferrocenyl)ethoxycarbene}iridium(I) complex 20

For comparison with an electron donating carbene substituent, Ir^{I} Fc-carbene complex **20** was also similarly synthesized from its tungsten analogue **8** and the $[Ir(cod)Cl]_2$ dimer with 75% yield.

The ^{1}H NMR spectrum of **20** (Figure 3.7) showed duplication of the ethoxy-CH_2 protons, as well as complete loss of symmetry of the Fc carbene substituent as opposed to the partial symmetry of complex **19**, a result of the above mentioned bulky Ir(cod)Cl-moiety again restricting $C_{carbene}$-C_{ipso} bond rotation. As such, each of the four Fc substituent $Cp^{'}$ protons are not chemically equivalent as evidenced by distinct chemical environments (5.32, 4.86, 4.76 and 4.64 ppm). This complete loss of symmetry is also evident in the $^{13}C\{^{1}H\}$ NMR spectrum of **19** (Figure 3.8) (75.4, 74.8, n.o. (or overlaps with cod-CH as per ^{1}H NMR spectrum), and 73.7 ppm). Additionally, a 18 ppm upfield shift of the carbene carbon atom resonance in **20** as compared to the W^{0} precursor **8** was observed, and was the first spectroscopic evidence of successful W^{0}-Ir^{I} transmetallation.

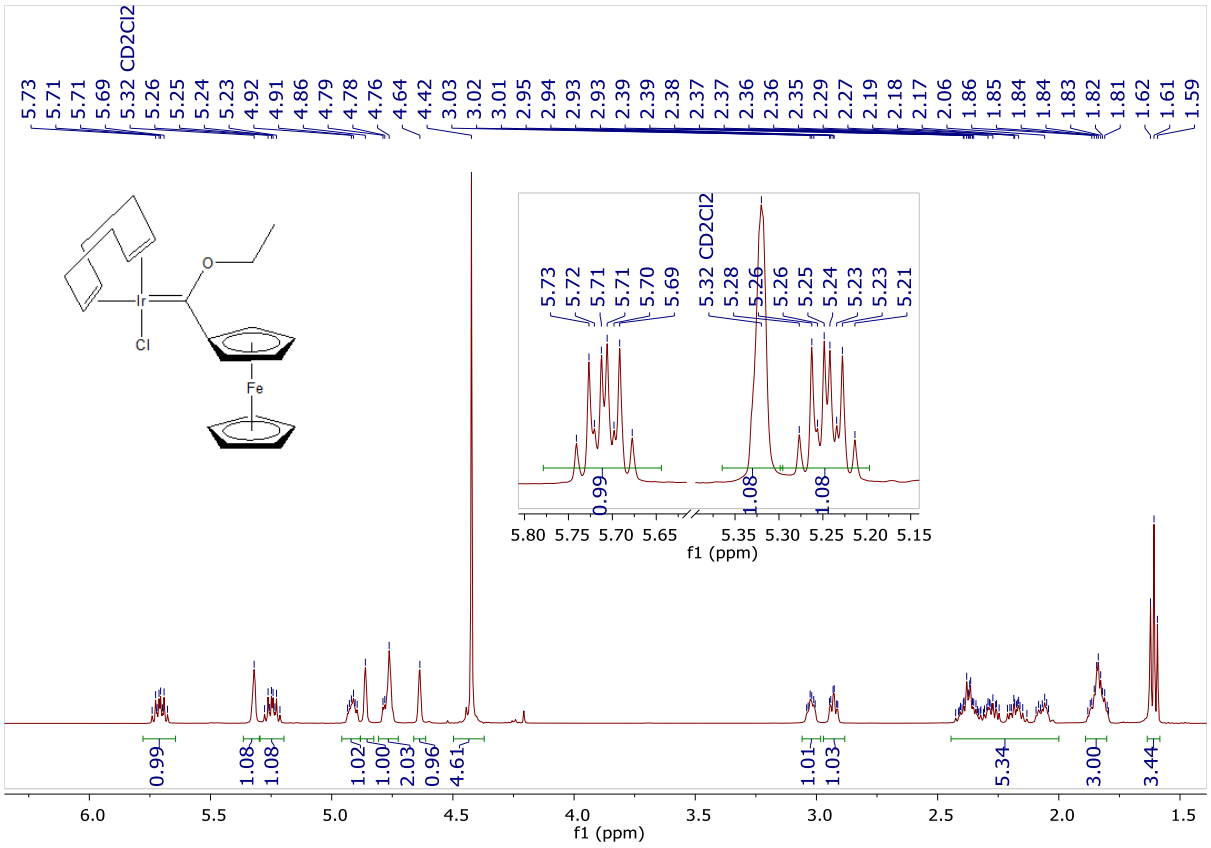

Figure 3.7 ^{1}H NMR spectrum of **20** in CD_2Cl_2

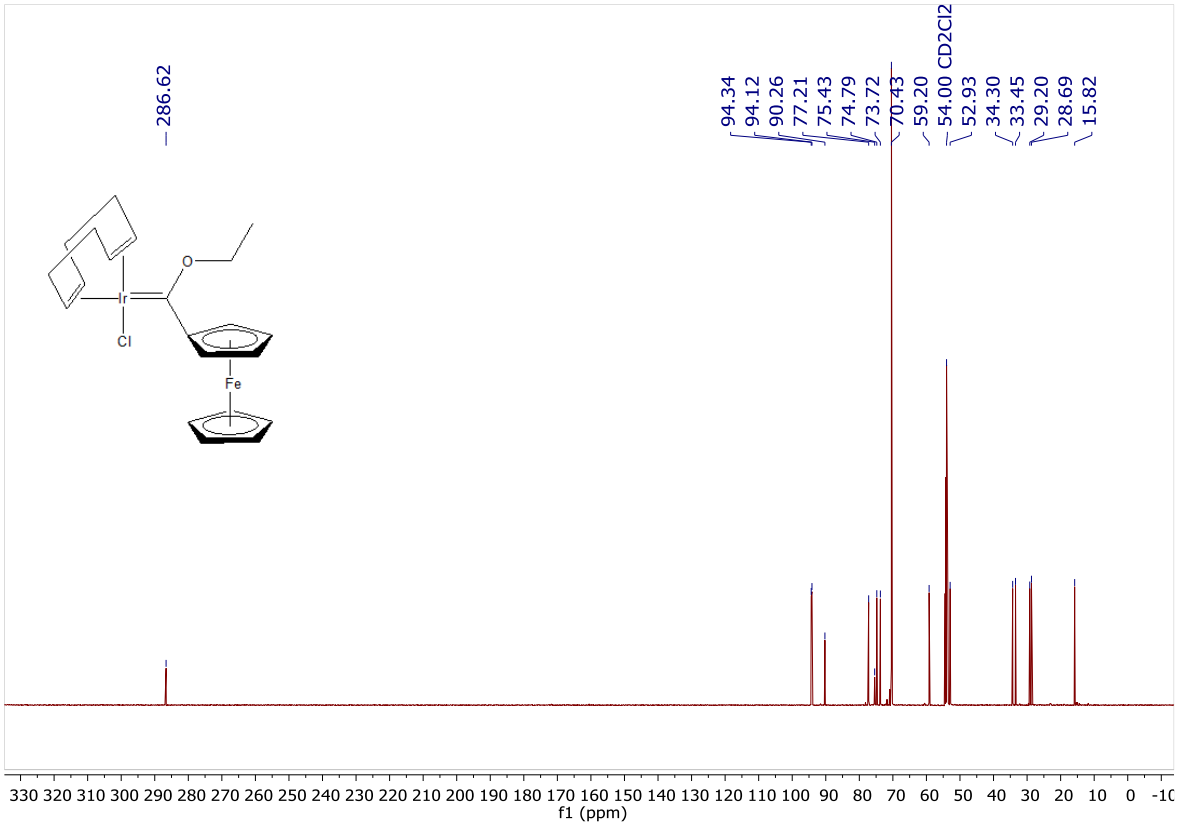

Figure 3.8 $^{13}C\{^{1}H\}$ NMR spectrum of **20** in CD_2Cl_2

3.3.2.4 1,5-cyclooctadienechlorido{*p*-(*N*,*N*-dimethylaniline)-*n*-propylaminocarbene}iridium(I) complex 21

Direct aminolysis of complex **18** was achieved by reaction with *n*-propylamine in THF at room temperature to afford aminocarbene complex **21**. Although aminolysis reactions usually result in both *syn*- and *anti*-conformers in literature (Figure 3.9), exclusive formation of the *anti*-isomer was observed for the synthesis of complex **21** (and for all aminolysis reactions reported in this thesis), presumably as a result of the steric bulk of the aryl carbene substituents in the square planar coordination sphere surrounding the iridium(I) metal center.

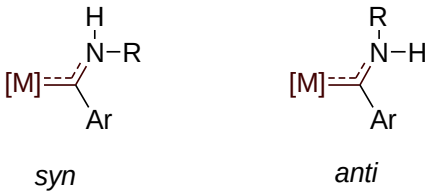

syn *anti*

Figure 3.9 Schematic representation of *syn*- and *anti*-isomers formed from aminolysis of alkoxycarbene complexes in literature.[34]

The synthesis of aminocarbene complex **21** was undertaken to afford a less electrophilic carbene complex with a less electronegative/better donating stabilizing-heteroatom than in the ethoxycarbene analogue **18** (nitrogen *vs* oxygen atom respectively). ^{1}H NMR spectrum of complex **21** (Figure 3.10) indicated successful replacement of the ethoxy- by aminopropyl-carbene substituent with acidic amino-proton (NH) resonance at 8.51 ppm, and displayed the same symmetry pattern observed for the ethoxy-analogue **18**. The ^{13}C{^{1}H} NMR spectrum of **21** (Figure 3.11) with a carbene carbon resonance of 240.3 ppm is indicative of a less electrophilic carbene carbon atom evidenced by the significant 36 ppm upfield-shift from analogous ethoxycarbene complex **18** (276.7 ppm).

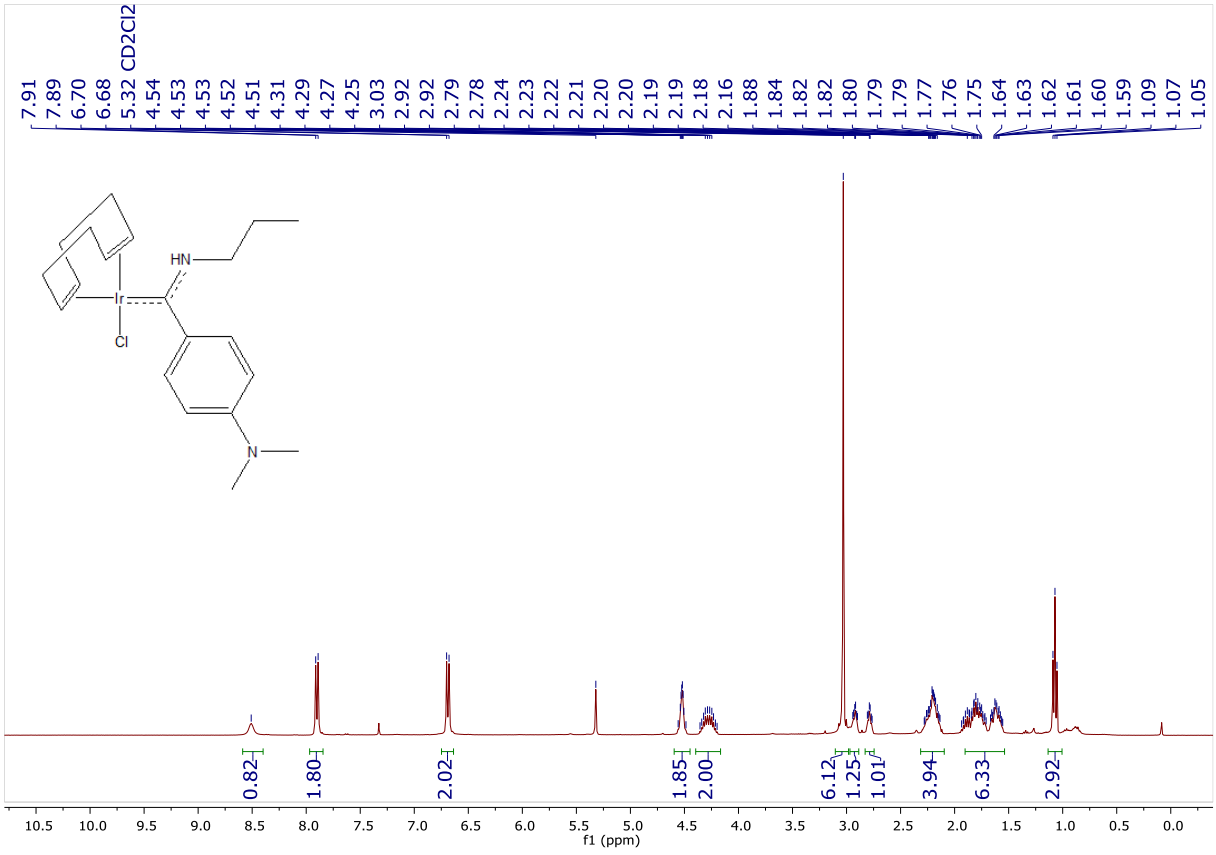

Figure 3.10 ^{1}H NMR spectrum of **21** in CD_2Cl_2

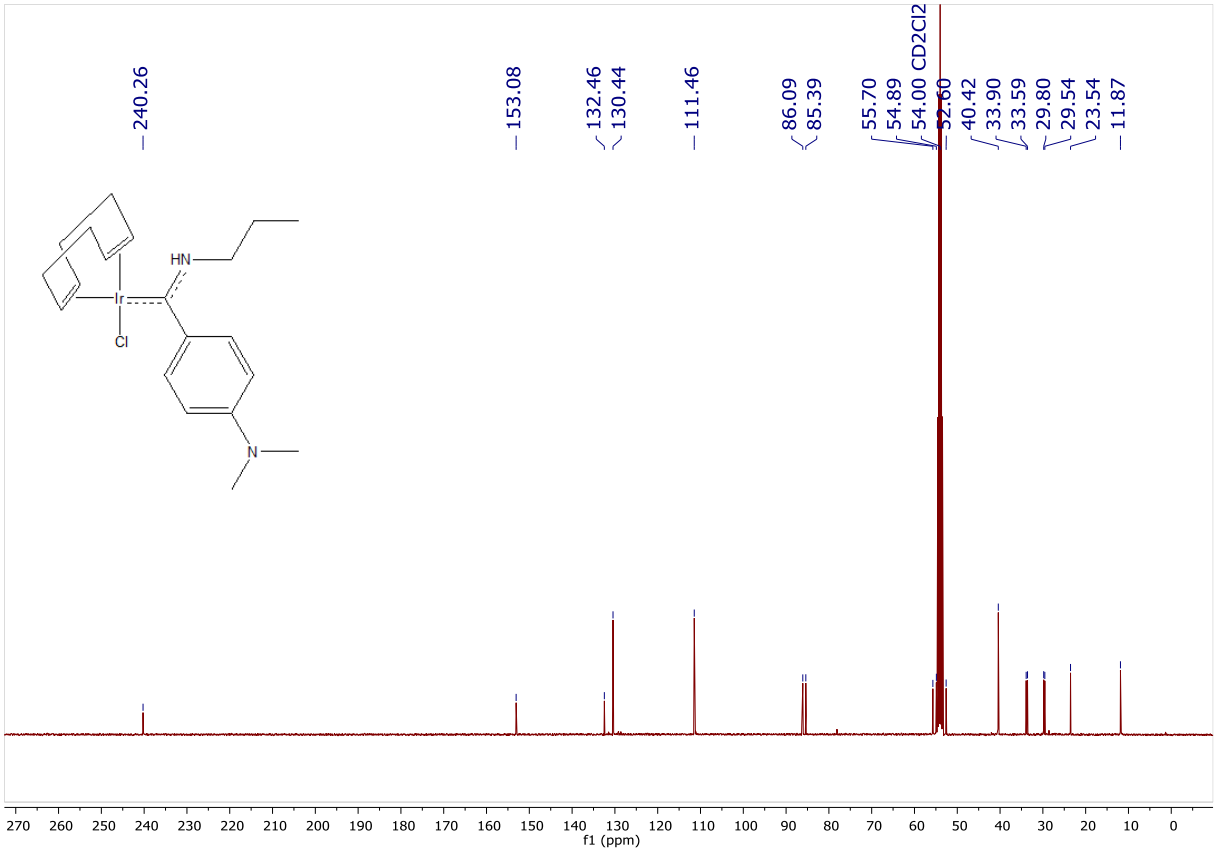

Figure 3.11 $^{13}C\{^{1}H\}$ NMR spectrum of **21** in CD_2Cl_2

3.3.2.5 1,5-cyclooctadienechlorido{(ferrocenyl)-*n*-propylaminocarbene}iridium(I) complex 22

This complex was synthesized similarly to complex **21** from the reaction of ethoxycarbene complex **20** with *n*-propylamine in THF under reflux conditions, with 86% yield. ^{1}H and $^{13}C\{^{1}H\}$ NMR spectra of Ir^{I} Fc-propylaminocarbene complex **22** (Figure 3.12 and 3.13 respectively) clearly indicate complete conversion of alkoxycarbene complex **20** to aminocarbene **22**, attested by the acidic amino-proton resonance of 8.36 ppm (Figure 3.12). Additionally, a 41 ppm upfield-shift of the $C_{carbene}$ signal of **22** (Figure 3.13, 245.4 ppm) from the alkoxy-analogue **20** is also evident. Thus another less electrophilic carbene complex, with a more electron donating carbene-substituent was successfully synthesized.

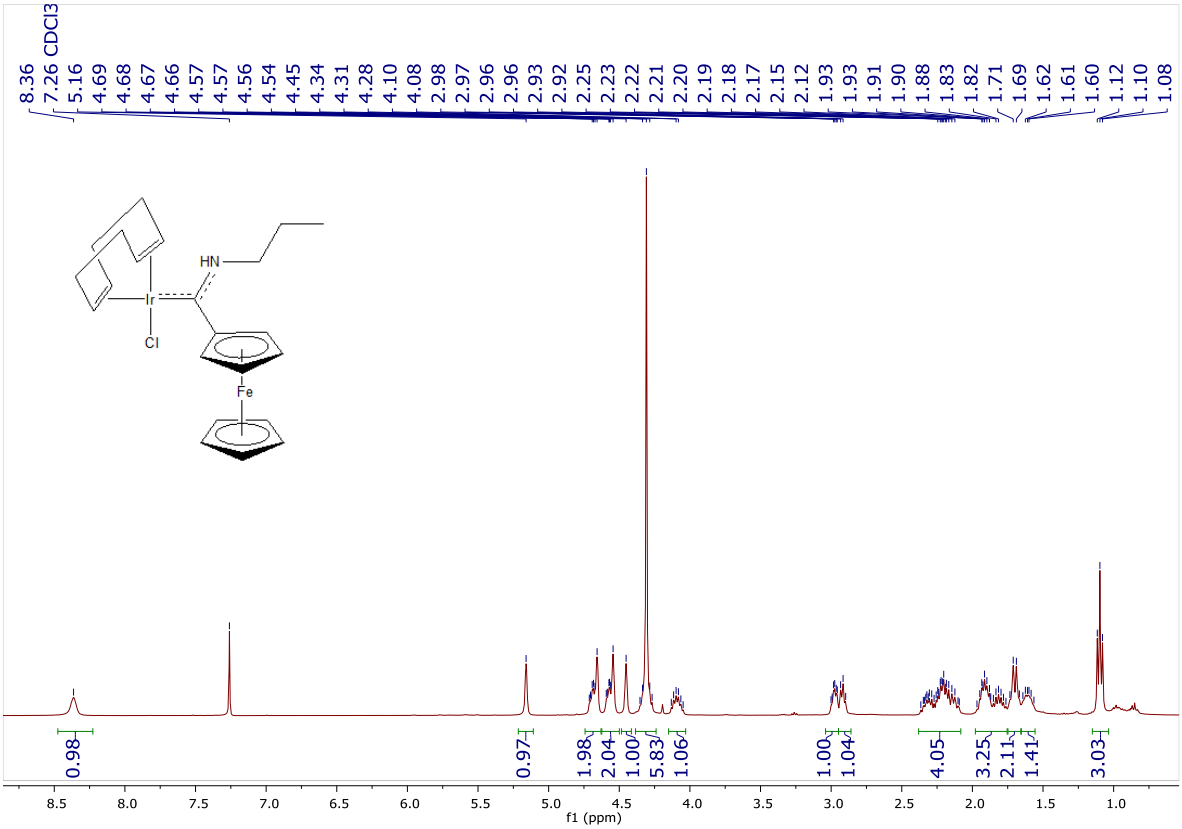

Figure 3.12 ^{1}H NMR spectrum of **22** in $CDCl_3$

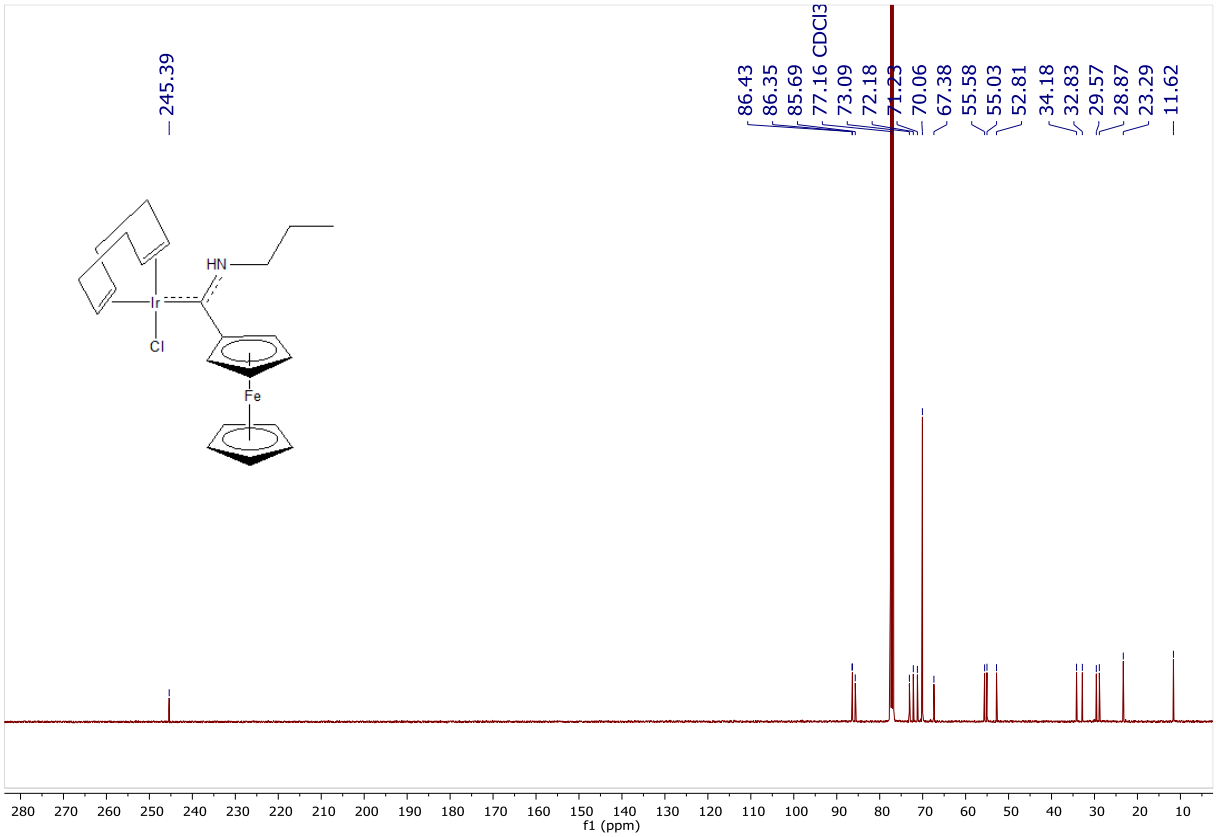

Figure 3.13 $^{13}C\{^{1}H\}$ NMR spectrum of **22** in $CDCl_3$

3.3.2.6 1,5-cyclooctadienechlorido{(ferrocenyl)(*N,N*-dimethylethylenediamino)carbene}iridium(I) complex 23

This complex was synthesized similarly to complex **22** by reaction of alkoxy- **20** with *N,N*-dimethyl-1,2-diaminoethane resulting in amino-carbene complex **23**, with 92% yield. The diamino-carbene substituent was utilized for comparison with propylaminocarbene complex **22**, and the role of the pendant tertiary amino group (-NMe_2) towards catalytic activity of **23** will become evident (*vide infra*). ^{1}H and $^{13}C\{^{1}H\}$ NMR spectra of aminocarbene complex **23** (Figure 3.14 and 3.15 respectively) indicate another less electrophilic Fc-carbene complex with an NH signal of 9.13 ppm and $C_{carbene}$ resonance of 245.5 ppm. No spectroscopic evidence for the coordination of the pendant NMe_2 moiety was observed.

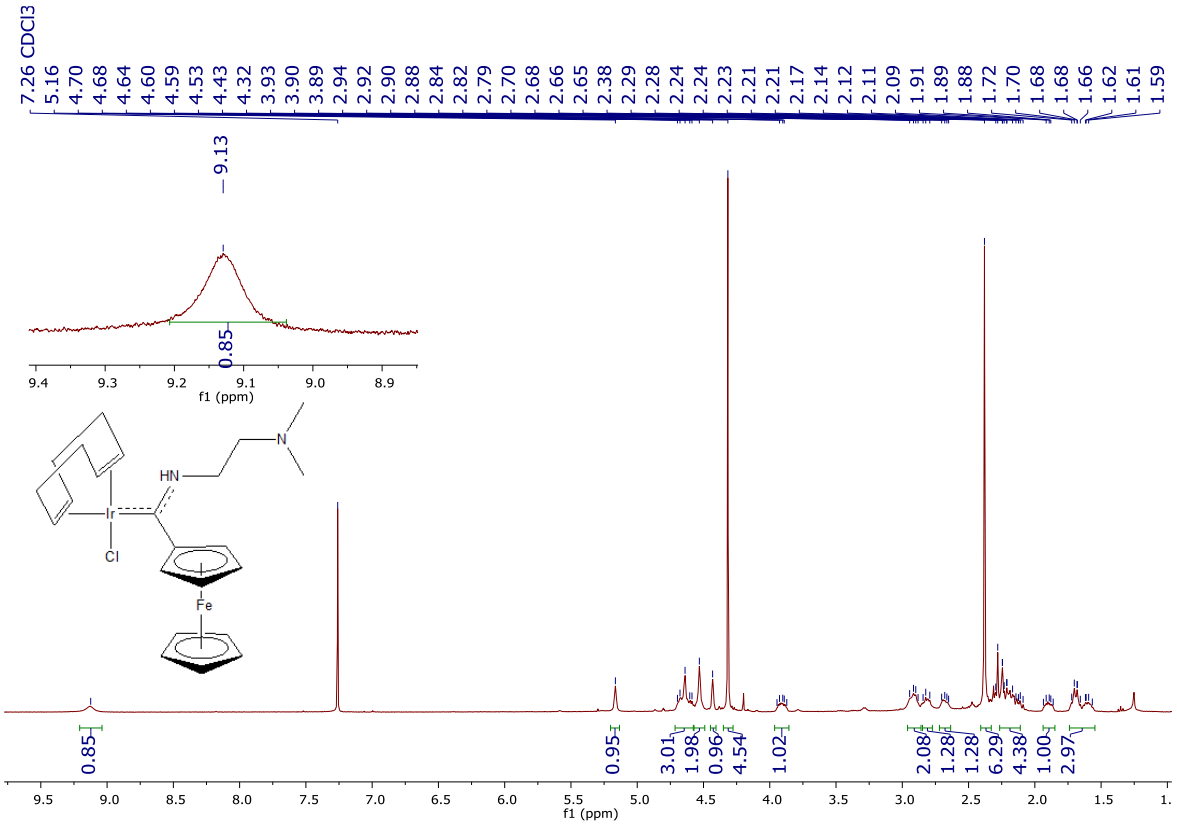

Figure 3.14 ^{1}H NMR spectrum of **23** in $CDCl_3$

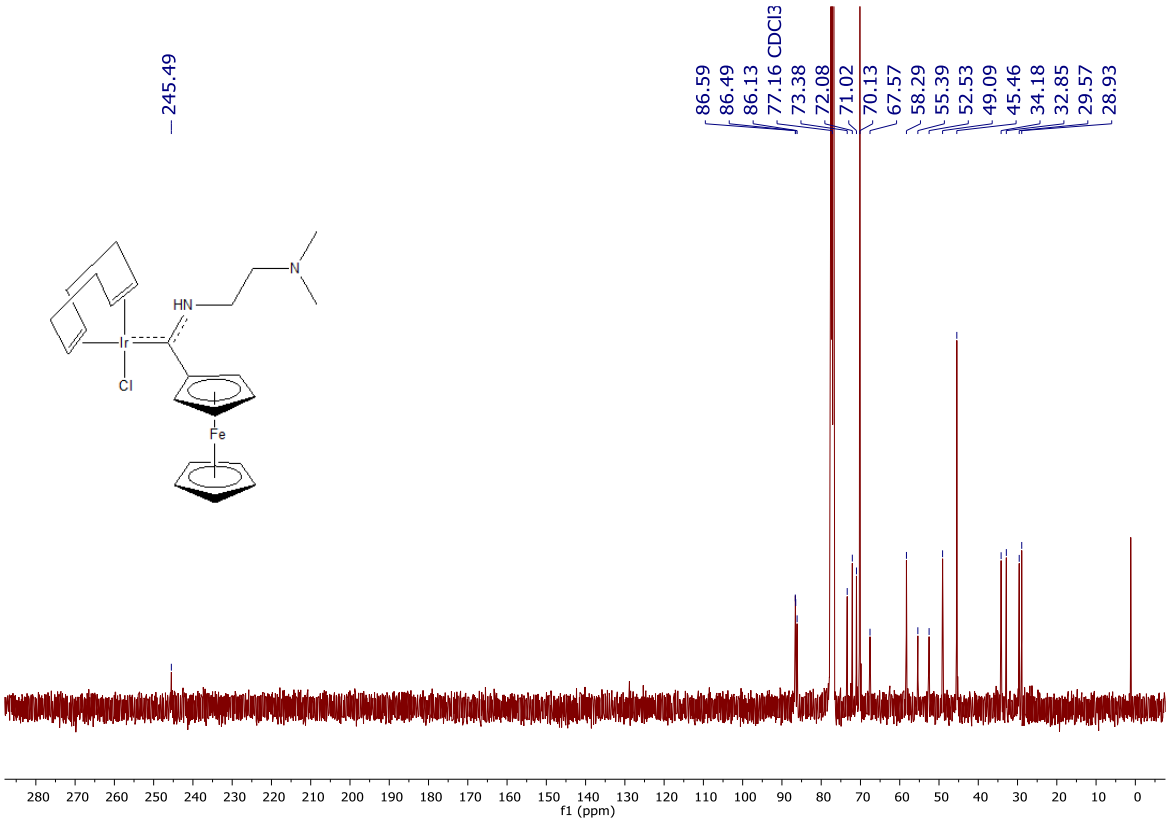

Figure 3.15 $^{13}C\{^{1}H\}$ NMR spectrum of **23** in$CDCl_3$

3.3.2.7 *cis*-(dicarbonyl)chlorido{(ferrocenyl)ethoxycarbene}iridium(I) complex 24

The ligand substitution reaction of Ir^{I} cod Fc-ethoxycarbene complex **20**, whereby gaseous carbon monoxide was bubbled through a solution of **20** in dichloromethane, resulted in the immediate substitution of the cod ligand with two carbonyl ligands. Ir^{I} dicarbonyl-carbene complex **24** was prepared in high yield (93%). The introduction of strong π-acceptor carbonyl ligands into the Ir^{I} coordination sphere would eventually enable comparison of complex **20** to **24**, with the effect of π-acidic (carbonyl) ligands on catalytic activity towards the TH of ketones as the main point of interest in a structure-activity catalytic investigation.

Spectroscopic characterization of **24** indicated the disappearance of all cod signals in both ^{1}H and $^{13}C\{^{1}H\}$ NMR spectra of **24** (Figure 3.16 and Figure 3.17 respectively) in comparison to **20** (Figure 3.7 and 3.8). Consequently, a completely symmetrical chemical environment is evident in both the ^{1}H and $^{13}C\{^{1}H\}$ NMR spectra. This is evidenced by both ethoxy-CH_2 protons resonating as one multiplet signal, as well as chemical equivalence of the Cp' ring H/$C_{\alpha,\alpha',\beta,\beta'}$ signals, as observed for the W^0 analogue **8**. Additionally, $^{13}C\{^{1}H\}$ NMR spectrum of **24** also indicated the presence of two signals in the M-carbonyl region (184.1 and 170.1 ppm), with a $C_{carbene}$ signal resonance at 277.4 ppm. Furthermore, an FT-IR

spectrum of **24** confirmed the presence of two carbonyl ligands coordinated to the central Ir^{I} metal atom, with carbonyl vibration bands observed at 2069 and 1989 cm^{-1}, respectively.

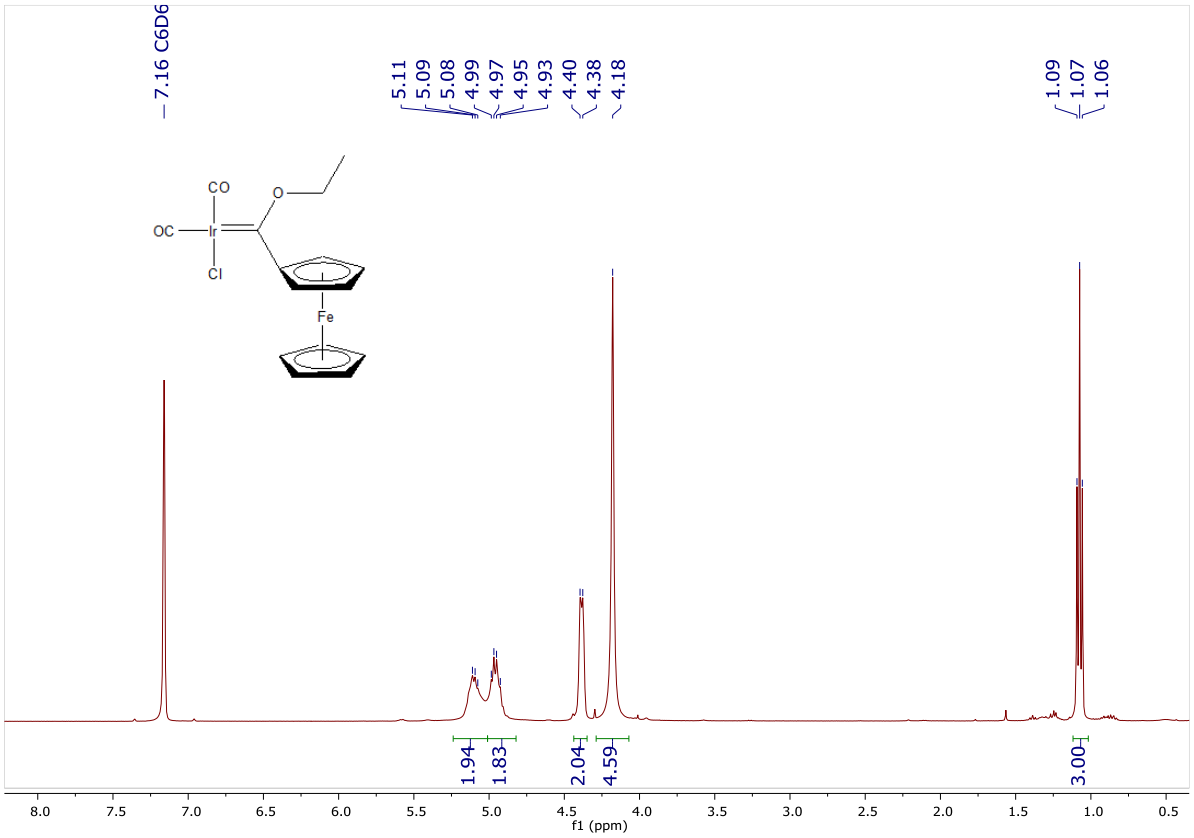

Figure 3.16 ^{1}H NMR spectrum of **24** in C_6D_6

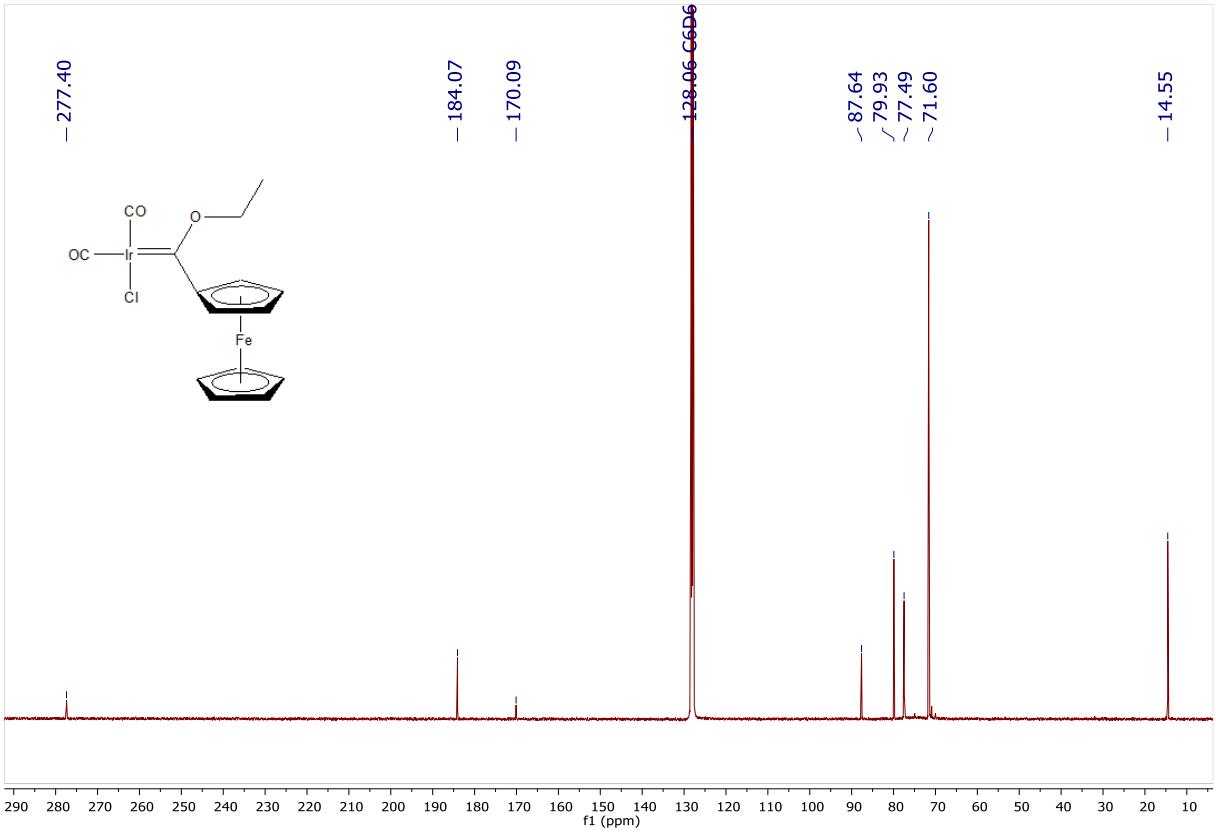

Figure 3.17 $^{13}C\{^{1}H\}$ NMR spectrum of **24** in C_6D_6

3.3.2.8 *cis*-(dicarbonyl)chlorido{(ferrocenyl)-*n*-propylaminocarbene}iridium(I) complex 25

This complex was synthesized in like manner to **24** whereby carbon monoxide gas was bubbled through a solution of **22** in dichloromethane, resulting in Ir^{I} dicarbonyl Fc-aminocarbene complex **25** (87% yield). Similarly to **24**, the ^{1}H and $^{13}C\{^{1}H\}$ NMR spectra of **25** (Figure 3.18 and 3.19 respectively) indicated quantitative replacement of the cod ligand by two carbonyl ligands, with carbonyl-carbon resonances at 182.7 and 169.6 ppm, respectively, and a $C_{carbene}$ signal at 232.6 ppm. In this case, substitution of the chelating cod ligand did not result in regaining of the symmetrical chemical environment around the iridium-carbene center as seen for **24**. Due to the steric bulk of both the propylamino- the Fc carbene substituents, different chemical shifts are observed for the propylamino-NCH_2 protons and the Fc-$H_{\alpha,\alpha'}$ protons (Figure 3.18), with extensive broadening of these signals. The FT-IR spectrum of **25** also displayed the presence of the carbonyl ligands with vibration bands at 2063 and 1980 cm^{-1}, respectively.

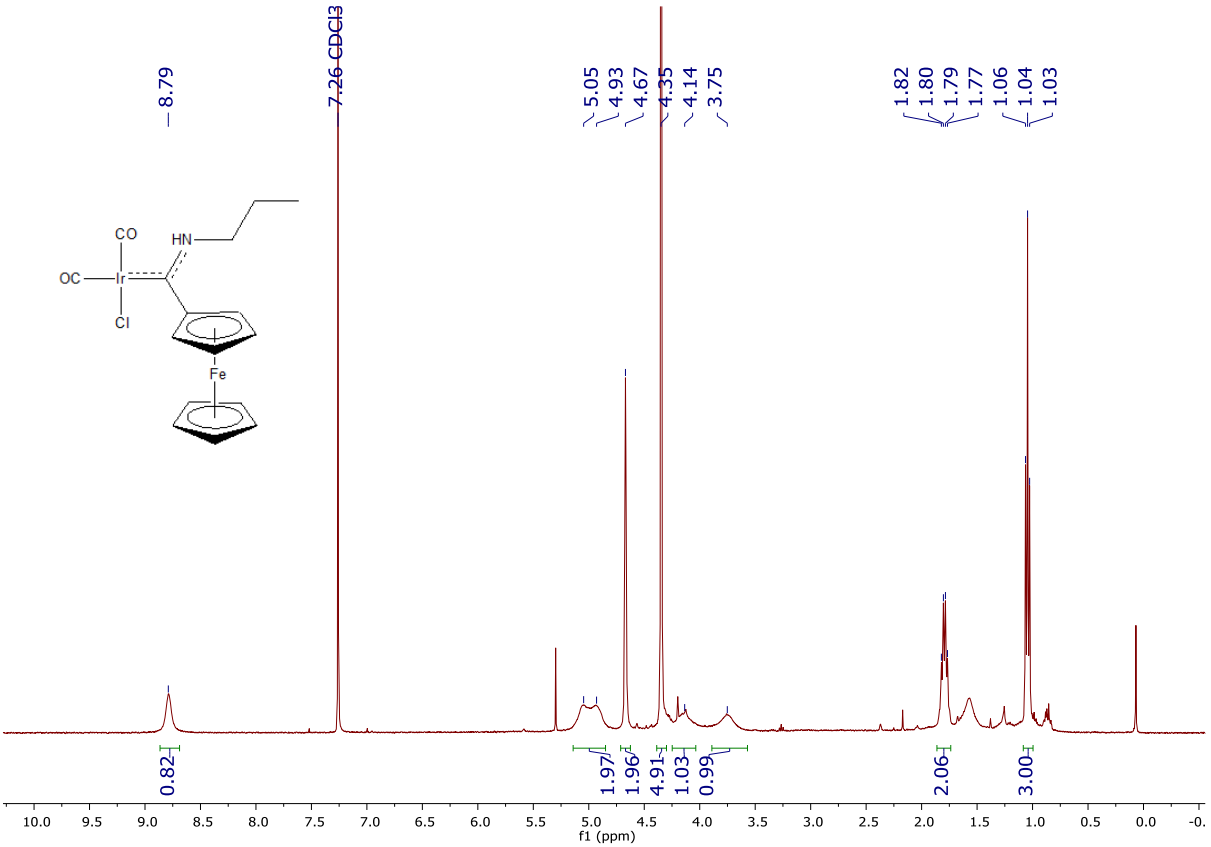

Figure 3.18 ^{1}H NMR spectrum of **25** in $CDCl_3$

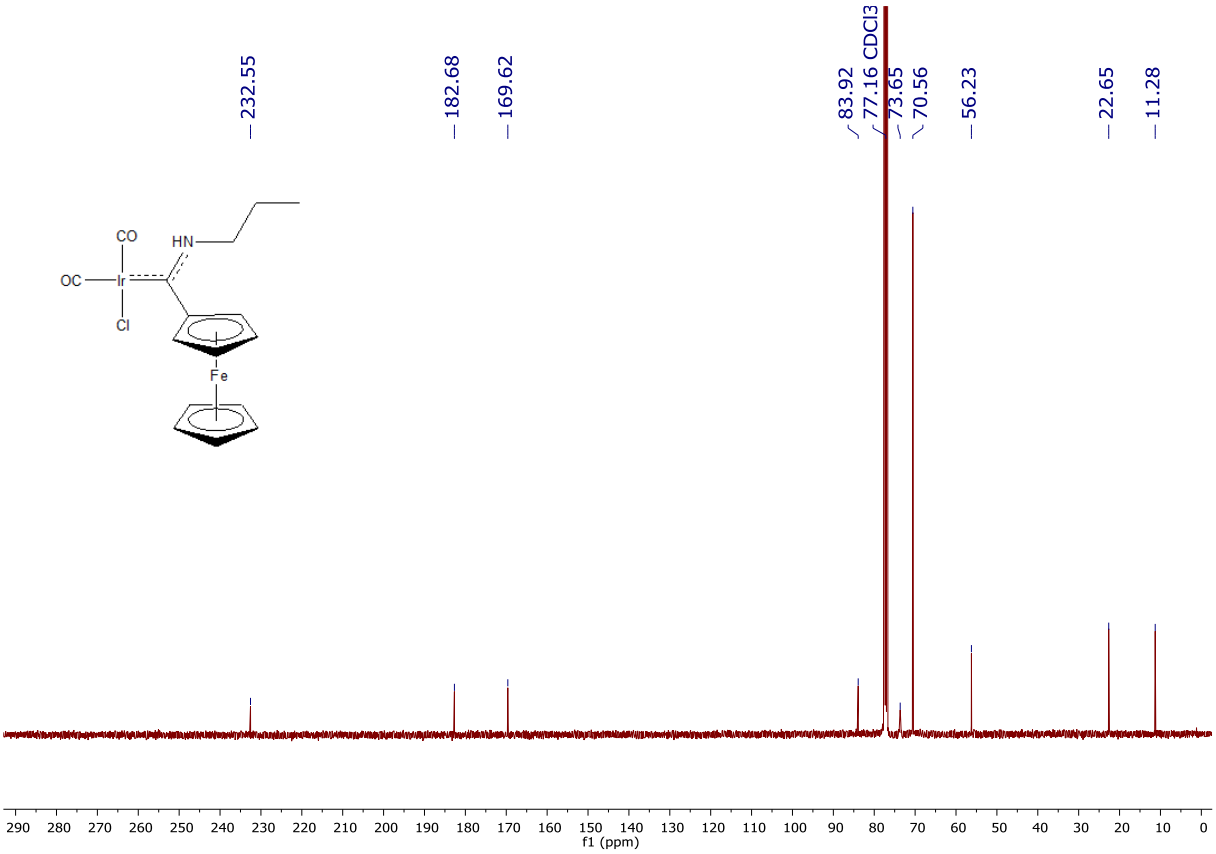

Figure 3.19 $^{13}C\{^{1}H\}$ NMR spectrum of **25** in $CDCl_3$

3.3.3 A comparative view

In this section, selected spectroscopic, X-ray crystallographic, and mass spectrometric characterization data of the novel Ir^{I} FCCs **18** – **25** are discussed.

3.3.3.1 NMR and FT-IR spectroscopic trends of iridium(I) Fischer carbene complexes

The isolated iridium dicarbonyl carbene complexes **24** and **25** afforded the opportunity to determine the Tolman electronic parameter (TEP), and thus the electron-donating strength of the accompanying FC ligands can be quantified employing the linear regression formula $TEP_{Ir} = 0.8475\nu_{av}(CO)Ir + 336.2$ cm^{-1} (*vide supra*, Chapter 2).[35,36] However, in order to directly compare the electron-donating ability of the different carbene ligands of Ir^{I} FCCs reported herein, the TEPs of all of the FC ligands were determined by measurement of the FT-IR spectra of *in situ*-generated dicarbonyl analogues of the Ir-cod complexes. Iridium-$(CO)_2$ complexes of **18, 19, 21**, and **23** were synthesized similarly to Fc-substituted **24** and **25** (Table 3.1, *vide infra*), and the resultant Ir^{I} $(CO)_2$ complexes $\mathbf{18_{CO}}$, $\mathbf{19_{CO}}$, $\mathbf{21_{CO}}$, and $\mathbf{23_{CO}}$ were not purified and isolated (see Scheme 3.4 below). For the synthesis of these non-isolated complexes, carbon monoxide gas was bubbled for 10 – 20 minutes through solutions of the respective Ir-cod complexes in dichloromethane at room temperature. FT-IR spectra of the resultant crude solution mixtures were subsequently recorded (see Figure 3.20 below) and are clearly indicative of successful replacement of the cod- by $(CO)_2$-ligands, and the two Ir^{I} carbonyl stretching frequencies were utilized for TEP calculations to quantify the relative electron-donor strengths of the specific carbene ligand towards central Ir^{I} metal atom in complexes **18**, **19**, **21**, and **23**.

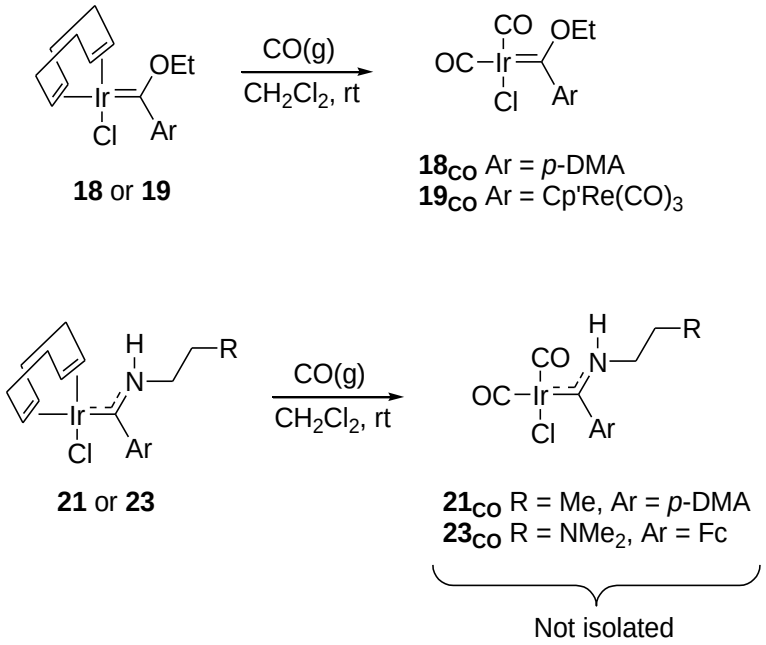

Scheme 3.4 Synthesis of non-isolated carbene complexes $\mathbf{18_{CO}}$, $\mathbf{19_{CO}}$, $\mathbf{21_{CO}}$, and $\mathbf{23_{CO}}$.

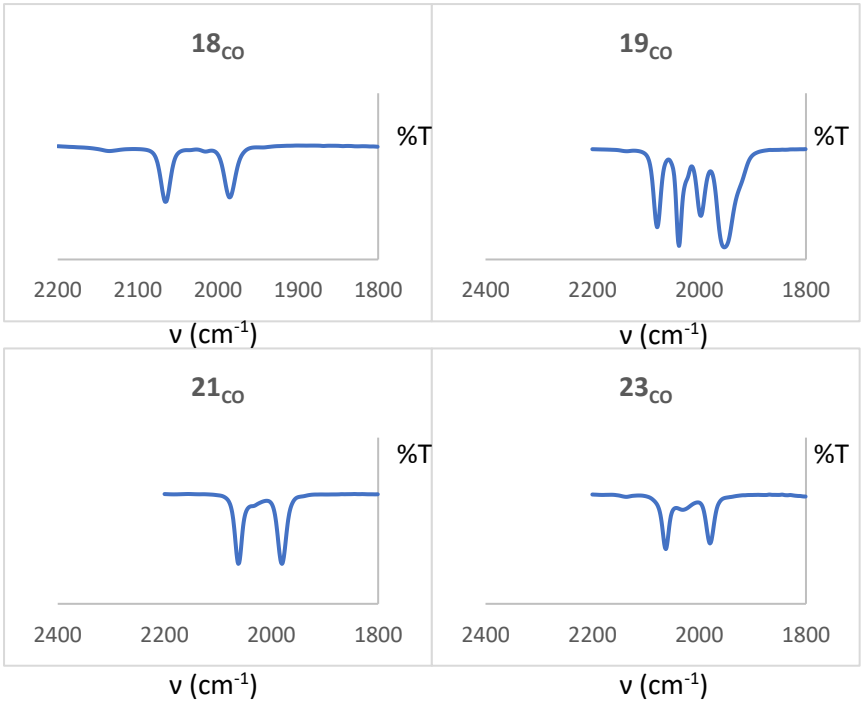

Figure 3.20 FT-IR spectra of the carbonyl-substituted complexes **18**$_{CO}$, **19**$_{CO}$, **21**$_{CO}$ and **23**$_{CO}$

Table 3.1 Selected $^{13}C\{^1H\}$ NMR and FT-IR spectroscopic data for complexes **18** – **25**.

Complex	$^{13}C\{^1H\}$ δ($C_{carbene}$) [a,b,c]	$^{13}C\{^1H\}$ δ(CO)	IR[f] ν(CO) (cm^{-1})	TEP[g] (cm^{-1})
18	276.7[a]			2052[h]
19	275.1[a]			2063[h]
20	286.6[a]			2055[i]
21	240.3[a]			2049[h]
22	245.4[b]			2050[i]
23	245.3[b]			2043[h]
24	277.4[c]	184.1[d], 170.1[e]	1987[e], 2069[d]	2055
25	233.1[b]	183.6[d], 170.3[e]	1980[e], 2063[d]	2050

[a]Recorded in CD_2Cl_2. [b]Recorded in $CDCl_3$. [c]Recorded in C_6D_6. [d]CO ligand *trans* to carbene. [e]CO ligand *trans* to Cl. [f]Recorded in CH_2Cl_2. [g]Calculated using the linear regression model TEP = 0.8475ν_{av}(CO)Ir + 336.2 cm^{-1}.[35,36] [h]Calculated for the non-isolated dicarbonyl complexes **18**$_{CO}$, **19**$_{CO}$, **21**$_{CO}$ and **23**$_{CO}$. [i]Calculated for isolated carbonyl complexes **24** and **25**.

$^{13}C\{^1H\}$ NMR $C_{carbene}$ signals of Ir^{I}-cod ethoxycarbene complexes **18** – **20** all within ~10 ppm of one another (275 – 286 ppm), and are indicative of the electron rich nature of the Ir(cod)Cl-moiety

compared to the Rh(cod)Cl-analogue (Chapter 2). This is evidenced by ~20 ppm upfield shift of iridium complexes **18**, **19**, and **20** (δ $C_{carbene}$ 276, 275, and 286 ppm, respectively) as compared to the respective rhodium-analogues **10**, **9b**, and **14** (δ $C_{carbene}$ 298 ppm, 298 ppm, and 310 ppm, respectively), and is further reinforced by isolation of the $Cp'Re(CO)_3$-substituted Ir^I complex **19** whereas the analogous Rh^I **9b** resulted in decomposition (dimerization) products and could not be purified and isolated (vide supra, Chapter 2). Aminocarbene complexes **21** and **22** with $C_{carbene}$ resonances of 240 and 245 ppm respectively attest to the decreased electrophilicity of the carbene carbon atom in **21** and **22** effected by a less electronegative *N*-atom in comparison to the *O*-atom in analogous **18** and **20** ($C_{carbene}$ 276 and 286 ppm respectively), and are in line with literature observations.[34] Additionally, equal $C_{carbene}$ resonances of Fc-aminocarbene complexes **22** and **23** (245 ppm) and the near-exact nature of respective $^{13}C\{^1H\}$ NMR spectra (Figure 3.13 and 3.15) confirm that the pendant tertiary amino NMe_2 group in **23** remains untethered. The calculated TEPs show that organic *p*-DMA-containing ligands ({:C(OEt)*p*-DMA}, **18**, 2052 cm^{-1}; {:C(NH^{n}Pr)*p*-DMA}, **21**, 2049 cm^{-1}) are consistently more electron-donating than analogous Fc-carbene ligands in **19** (2055 cm^{-1}) and **22** (2050 cm^{-1}), respectively), with the $Cp'Re(CO)_3$-substituted ligand in **20** as expectedly the least donating (2063 cm^{-1}). Additionally, the respective TEPs calculated for aminocarbene complexes **22** and **23** (2050 and 2043 cm^{-1}) clearly indicate the increased electron-donating strength of the aminocarbene ligand in **23** as effected by the pendant NMe_2 moiety in comparison to terminal CH_3 in propylaminocarbene **22**. Finally, while the determined TEPs of the :C(OEt)*p*-DMA (**18**) and :C(NH^{n}Pr)Fc (**22**) ligands of iridium FCCs differ slightly from the rhodium analogues **10** and **16** (1 – 3 cm^{-1} frequency-difference), the overall electron-donating ability of :C(OEt)*p*-DMA is consistently stronger than that of :C(OEt)Fc and rivals :C(NH^{n}Pr)Fc for both the Rh^I and Ir^I FCCs. As such, the investigated FC ligands of Ir-(cod) complexes **18** – **23** can be arranged in order of decreasing electron-donating strength as :C(NH$(CH_2)_2NMe_2$)Fc (**23**) > :C(NH^{n}Pr)*p*-DMA (**21**) > :C(NH^{n}Pr)Fc (**22**) > :C(OEt)*p*-DMA (**18**) > :C(OEt)Fc (**20**) >> :C(OEt)($Cp'Re(CO)_3$) (**19**).

3.3.3.2 Single-crystal XRD crystallography

Molecular structures of complexes **18** – **22**, and **24** were determined by X-ray diffraction of suitable crystals, which were obtained *via* slow-diffusion of *n*-hexane into concentrated CH_2Cl_2 solutions of the complexes, and are displayed as Figure 3.21 (a) – (e), respectively. These complexes display *pseudo*-square planar (for Ir(cod)- **18** – **22**) or square planar (for $Ir(CO)_2$- **24**) geometries around the central Ir^I metal, and the structures are comparable to Rh^I analogues discussed in Chapter 2.

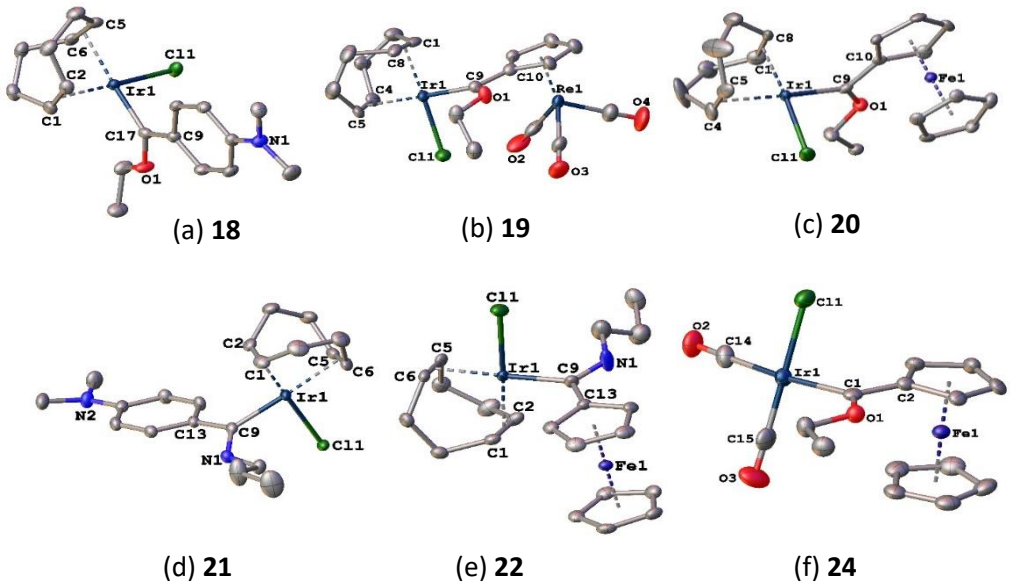

(a) **18** (b) **19** (c) **20**

(d) **21** (e) **22** (f) **24**

Figure 3.21 Partially labelled crystal structures of new Ir^{I} FCCs **18** – **22**, and **24** ((a) – (f)). Hydrogen atoms and solvent molecules are omitted for clarity.

Table 3.2 Selected bond lengths (Å) and angles (°) for complexes **18** – **22**, and **24**

	18	**19**	**20**	**21**	**22**	**24**
			Bond lengths			
Ir-C$_{carbene}$	1.972(2)	1.954(7)	1.963(9)	2.0145(17)	2.029(3)	2.065(9)
C$_{carbene}$-O/N	1.349(2)	1.319(10)	1.317(11)	1.315(2)	1.305(5)	1.311(10)
C$_{carbene}$-C$_{ipso}$	1.443(3)	1.449(12)	1.458(13)	1.475(2)	1.458(5)	1.430(12)
Ir-Cl	2.3653(6)	2.357(2)	2.361(2)	2.3684(4)	2.3770(9)	2.350(2)
Ir-Y^{a-e} or Ir-CO$_{trans}$	2.092(2)^{a}	2.113(8)^{c}	2.132(10)^{b}	2.088(18)^{d}	2.076(4)^{e}	1.914(10)
Ir-Y^{f-j} or Ir-CO$_{cis}$	1.983(2)^{f}	1.998(9)^{h}	1.991(8)^{g}	1.979(17)^{i}	1.981(3)^{j}	1.832(12)
			Bond angles			
C$_{carbene}$-Ir-Cl	89.40(6)	90.8(2)	93.10(3)	89.13(5)	88.08(11)	86.0(2)
O/N-C$_{carbene}$-C$_{ipso}$	110.37(17)	107.9(6)	110.2(8)	115.08(15)	114.7(3)	111.8(7)
			Torsion angles			
C$_{\alpha}$-C$_{ipso}$-C$_{carbene}$-O/N	8.4(3)	2.7(12)	3.1(13)	27.4(2)	2.4(6)	9.7(12)

^{a}Y = midpoint of C(5)-C(6). ^{b}Y = midpoint of C(4)-C(5). ^{c}Y = midpoint of C(4)-C(5). ^{d}Y = midpoint of C(5)-C(6). ^{e}Y = midpoint of C(1)-C(2). ^{f}Y = midpoint of C(1)-C(2). ^{g}Y = midpoint of C(1)-C(8). ^{h}Y = midpoint of C(1)-C(8). ^{i}Y = midpoint of C(1)-C(2). ^{j}Y = midpoint of C(5)-C(8).

The Ir-$C_{carbene}$ bond distances for complexes **18** – **22** and **24** are comparable with literature findings of both alkoxy- and aminocarbene complexes (1.930(8) and 1.970(3) Å).[4,8] The decreasing Ir-$C_{carbene}$ lengths in the order **18**, **20**, and **19** (1.972(2), 1.962(9), and 1.954(7) Å, respectively) indicates the respective increasing π-backbonding from the Ir-metal to the electrophilic carbene carbon atom (**18** < **20** < **19**) as required to stabilize the resultant Ir-$C_{carbene}$ bond, and is consistent with TEP trend (Table 3.1). Additionally, the increased carbene bond length of the *p*-DMA-substituted aminocarbene complex **21** (2.0145(17) Å) as compared to analogous ethoxycarbene **18** (1.972(2) Å) with accompanying acute decrease in the $C_{carbene}$-*N* distance (**21**, 1.315(2) Å) compared to $C_{carbene}$-*O* distance (**18**, 1.349(2) Å), is a consequence of strong electron donation towards the carbene carbon atom from *N*-atom (lone electron-pair) in **21** *vs O*-atom in **18**. As electron donation from carbene substituents increases (such from **18** and **20** to **21** and **22**, respectively), less Ir-$C_{carbene}$ π-backbonding is required to stabilize the resulting Ir-carbene bond, resulting in longer Ir-carbene distances as observed for aminocarbene complexes **21** and **22** (2.0145(17) Å and 2.029(3) Å) compared to their ethoxycarbene analogues **18** and **20** respectively (1.972(2) Å and 1.963(9) Å). Consequently, $C_{carbene}$-C_{ipso}-X bond angles (X = *O*/*N*) are shorter for ethoxycarbene complexes **18** and **20** (110.37(17)° and 110.2(8)°) compared to respective aminocarbene analogues **21** and **22** (115.08(15)° and 114.7(3)°). In addition, the Ir-$C_{carbene}$ distance in the dicarbonyl complex **24** (2.065(9) Å) is longer than for analogous -cod complex **20** (1.972(2) Å) due to the presence of π-acceptor co-ligands in the former, with Ir-mediated π-backbonding predominantly towards the π-acidic carbonyl carbon atoms (**24**) as opposed to strong π-backbonding towards electrophilic carbene carbon atom evident in **20**. Finally, significantly smaller C_{α}-C_{ipso}-$C_{carbene}$-X (X = *O*/*N*) torsion angles are observed for the bimetallic Ir-cod complexes ($Cp^{'}Re(CO)_3$-**19**, 2.7(12)°; Fc-**20**, 3.1(13)°; **22**, 2.4(6)°) compared to the monometallic *p*-DMA-substituted analogues (**18**, 8.4(3)°; **21**, 29.4(2)°). In Fc-substituted complexes, a shorter C_{α}-C_{ipso}-$C_{carbene}$-*O* torsion angle is observed for the Ir-(cod) complex **20** (3.1(13)°) compared to the Ir-$(CO)_2$ analogue **24** (9.7(12)°). Therefore the organic *p*-DMA substituent is more electron-donating than the bimetallic ($Cp^{'}Re(CO)_3$ and Fc) counterparts based on XRD data of complexes **18** – **25**, which is in agreement with the calculated TEPs discussed above.

3.3.3.3 Mass spectrometry of iridium(I) Fischer carbene complexes

Mass spectral analyses were performed to confirm identity of the isolated complexes. The common mass fragment ion (*m/z*) $[M - Cl]^+$ is observed for Ir- cod and $(CO)_2$ complexes **18** – **25**, with an additional $[M - Cl - CO]^+$ ion evident in –$(CO)_2$ complexes **24** and **25**. The observed *m/z* $[M - Cl]^+$ ion is common for Rh-cod complexes while the *m/z* $[M - Cl - CO]^+$ ion is reminiscent of Rh-$(CO)_2$ analogues,

as discussed in Chapter 2. The observed ions were thus assigned as specified in the experimental section (*vide infra*). The absence of any tungsten carbonyl *m/z* fragments was indication of successful W^0-Ir^I transmetallation.

3.3.4 Catalytic application of iridium(I) carbene complexes in the transfer hydrogenation of acetophenone

Iridium(I) carbene complexes **18** – **25** were tested as precatalysts in the TH of acetophenone by *iso*-propanol as depicted in Scheme 3.5 below.

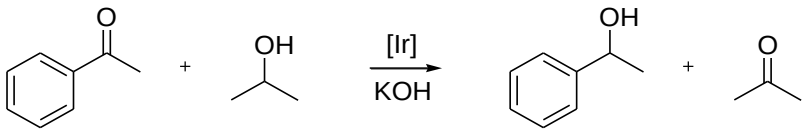

Scheme 3.5 Iridium catalysed carbonyl reduction of acetophenone by *iso*-propanol.

Table 3.3 Optimization of the TH reaction mediated by Ir^I FCC **20**.

Entry	Ir Comp.	Loading (mol%)	KOH (mol%)	Time (h)	Yield (%)	TOF[a]
1	**20**	0.5	0.5	24	79	07
2	**20**	0.5	0.25	24	31	03
3	**20**	0.1	0.5	24	67	28
4[b]	**20**	0.1	0.5	16	65(1.6)	41
5	**20**	0.05	0.25	16	27	34
6	**20**	0.1	0.5	8	18	23
7	**20**	0.1	0.5	4	11	29
8[b]	**-**	-	0.5	24	3(0.6)	
9[b]	**-**	-	10	24	8(2.2)	
10[b]	**-**	-	20	24	23(4.7)	
11[b]	**-**	-	100	24	47(8.4)	

All reactions were done in condenser-fitted round-bottomed flasks at 82 °C under argon gas atmosphere. [a]Average turnover frequency ((mol of product)/((mmol of catalyst) h)) determined at the specified reaction time. [b]These reactions were done as triplicates with standard deviations indicated in parentheses.

For the transfer hydrogenation (TH) reactions, Ir-cod complex **20** was utilized as the model precatalyst under various reaction conditions as specified in Table 3.3 above. Entries 1 – 3 indicate that an excess amount of base is required to achieve optimum conversion of the substrate at different Ir/KOH ratios. The optimum TOF of 41 hr^{-1} (65% conversion in 16 hours) was achieved under mild catalytic conditions of 0.1 mol% Ir^{I} complex and 0.5 mol% KOH with respect to substrate acetophenone (entry 4). This is comparatively milder than is sometimes reported for Ir^{I} NHCs in literature, wherein 0.5 – 1.0 mol% precatalyst and excessive amounts of KOH (up to 100 mol%) prove necessary for catalytic activity.[37–39] KOH-catalyzed reactions were also carried out and are indicative of the necessity of **20** to achieve a higher percentage conversion of acetophenone to phenylethanol (entries 8 – 11), with equimolar KOH and acetophenone in the absence of Ir^{I} complex **20** resulting in 47% conversion after 24 hours at 82 °C. All further catalytic reactions were thus carried out under optimum conditions (entry 4), with results summarized in Table 3.4 below.

Table 3.4 Reduction of acetophenone using complexes **18** – **25** under optimum catalytic conditions[a,b]

Entry	Ir Comp.	Time (h)	Yield (%)	TOF[c] (hr^{-1})
1	**18**	16	22(2.4)	14
2	**19**	16	13(1.7)	8
3	**20**	16	71(2.4)	45
4	**21**	16	87(1.7)	55
5	**22**	16	73(7.8)	45
6	**23**	16	97(1.0)	61
7	**24**	16	23(2.8)	14
8	**25**	16	51(5.4)	32
9	**21**	2	55(6.2)	273
10	**23**	2	89(4.3)	445
11	**23 + Hg**	16	98(0.0)	61

All reactions were done in thick glass reaction tubes fitted with a greaseless high-vacuum stopcock under an argon atmosphere. [a]Reaction conditions: catalyst/base/substrate 1/5/1000 in *iso*-propanol at 82 °C. [b]Reactions were monitored by GC using *n*-decane as internal standard. [c]Average turnover frequency ((mol of product)/((mmol of catalyst) h)) determined at the reaction time.

The most electrophilic ethoxycarbene complex **19** showed poor catalytic activity in the TH of acetophenone as depicted in Table 3.4 (entry 3), and is comparable with electrophilic ethoxycarbene complexes **18** and **24** (entries 1 and 7). The exceptional catalytic activity of ethoxycarbene complex **20** is ascribed to presumed catalytic activity at Fe^{II} centre as additional active site, based on literature reports of excellent Fe^{II} precatalysts.[40,41] As heuristically expected, the best precatalysts in the reported Ir^{I} series are the less electrophilic aminocarbene **21** and **23** (entries 4 and 6), with excellent respective TOFs of 273 and 445 achieved within 2 hours. These results are comparable with state-of-the-art Ir^{I} NHCs in literature (TOF 14 – 4622 hr^{-1}).[27,28] Aminocarbene complex **23** yields the best catalytic result. From this preliminary catalytic investigation, an explanation for the improved catalytic performance of **23** could include the role of the potentially hemilabile nature of the pendant tertiary amino NMe_2 carbene substituent. This would stabilize the dechlorinated catalytic species *via* dative bonding of the *N*-atom to the Ir^{I} vacant site, resulting in a more robust Ir^{I} analogue of **23** with improved catalytic activity. Additionally, increasing the electrophilicity of the carbene carbon atom from Ir-cod complexes **20** and **22** by incorporating π-acceptor carbonyl ligands into the Ir^{I} coordination sphere results in decreased catalytic activity of the resultant **24** and **25** (entries 3 *vs* 7 and 5 *vs* 8). The mercury-test reaction with no change in percentage conversion (entry 6 *vs* 11) is indicative of a homogeneous mode of action in these TH reactions, although a heterogeneous mechanism cannot be conclusively excluded without mechanistic studies.[42]

Finally, the reaction of **23** with excess KOH at 82 °C for 16 hours was carried out to determine stability of the FC ligand during the catalytic cycle, with substrate and internal standard excluded for clarity. As such, a mixture of the Ir^{I} complex **23** and KOH was dissolved in *iso*-propanol under an argon atmosphere and magnetically stirred for 16 hours at 82 °C. The *iso*-propanol solvent was subsequently removed under vacuum, and the resulting brown paste was dissolved in $CDCl_3$ for NMR spectroscopy. ^{1}H and $^{13}C\{^{1}H\}$ NMR spectra recorded (Figure 3.22 and 3.23 respectively) provide evidence that supports the stability of the Ir-carbene bond with an amino-proton resonance at 9.22 ppm and a $C_{carbene}$ resonance of 249.5 ppm, and thus indicates that the carbene ligand stays intact during the catalytic cycle.

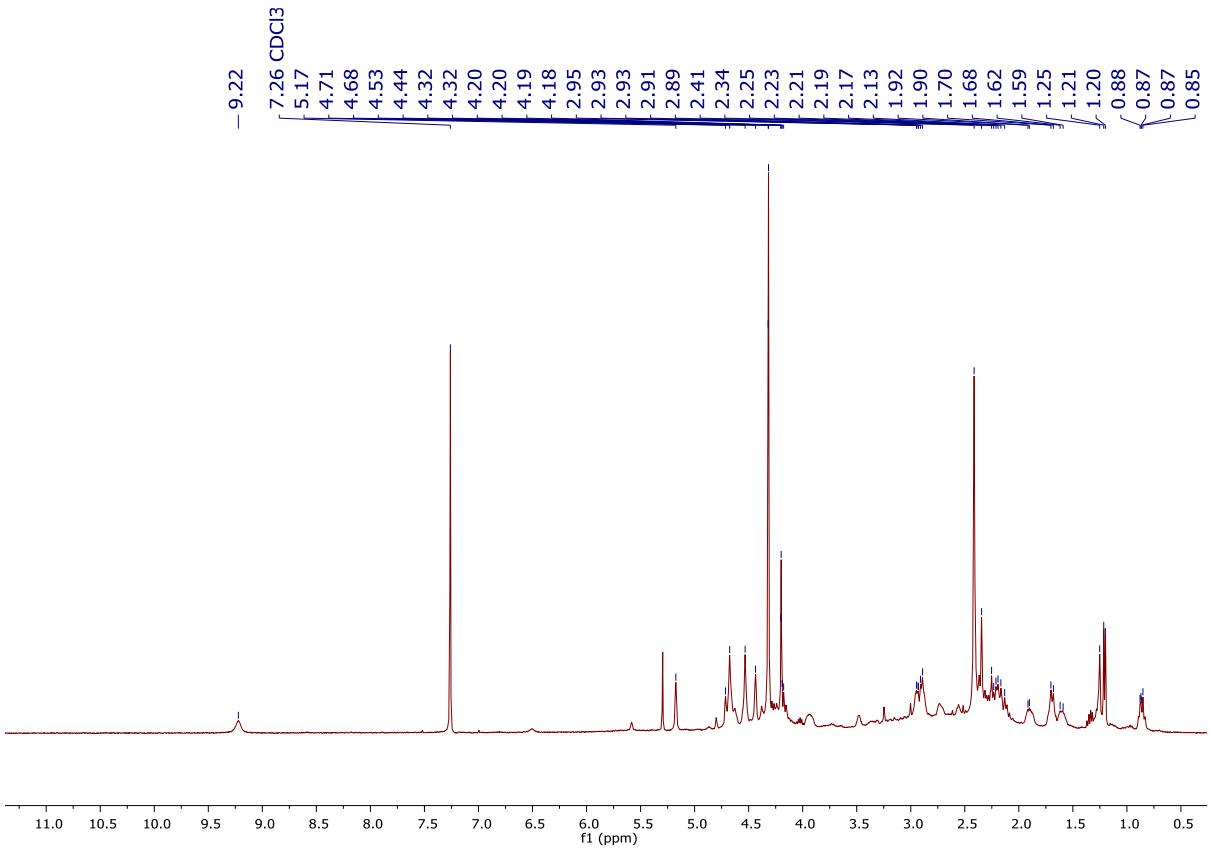

Figure 3.22 ^{1}H NMR spectrum in $CDCl_3$ of the stability test reaction mixture for catalyst **23**

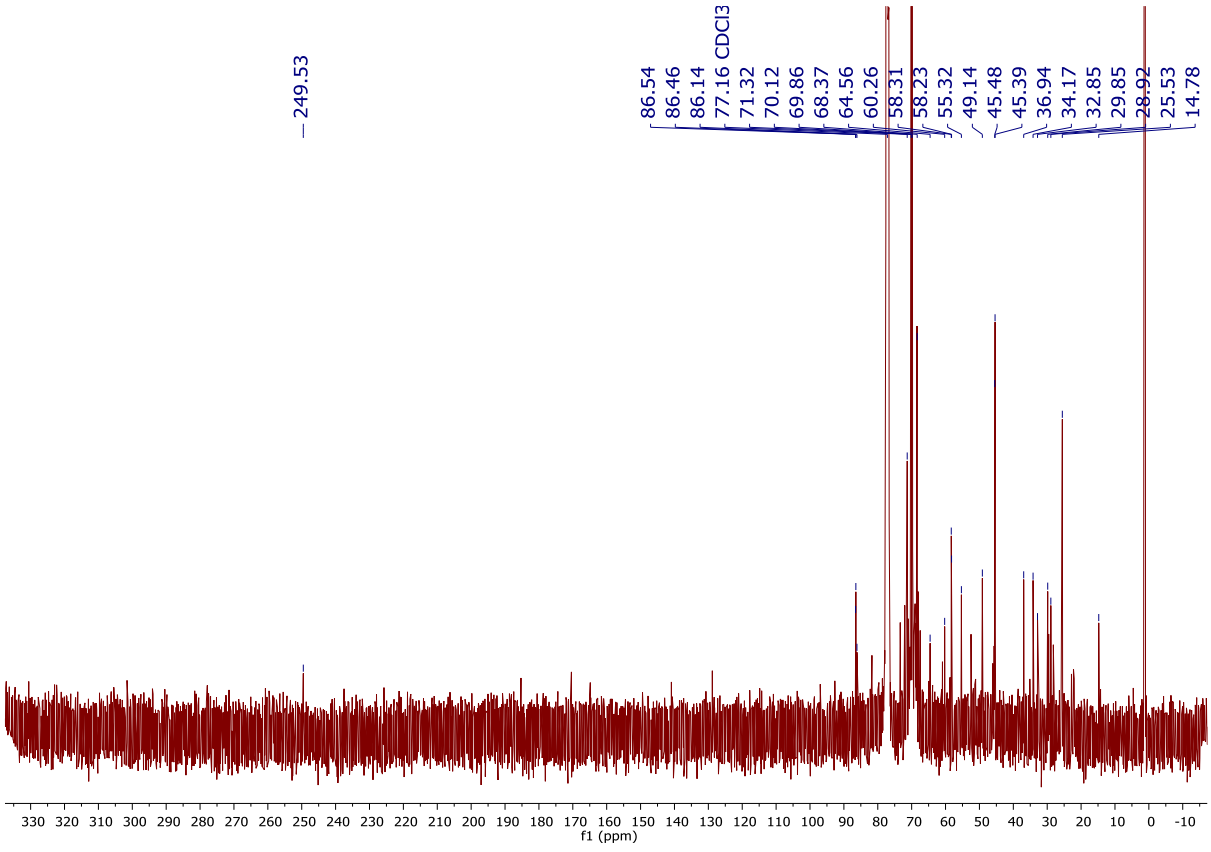

Figure 3.23 $^{13}C\{^{1}H\}$ NMR spectrum of the stability test reaction mixture of **23** in $CDCl_3$

3.4 Conclusion

In summary, novel Ir^{I} FCCs featuring *p*-DMA (**18**), $Cp'Re(CO)_3$ (**19**), and Fc (**20**) carbene substituents were synthesized *via* simple transmetallation from W^0 analogues, as a first in the synthetic methodology available to prepare Ir^{I} carbene complexes. Complexes **18** and **20** were subsequently modified by varying the stabilizing heteroatom and co-ligand environment to afford Ir^{I} **21** – **25**. Characterization of these complexes indicates that the *p*-DMA carbene substituent is more electron-donating than the $Cp'Re(CO)_3$ and Fc counterparts, in agreement with observations made for Rh^{I}-analogues in Chapter 2. However unlike with the Rh^{I}-analogues, no evidence for carbene dissociation or dimerization resulting in decomposition organic olefins was observed, even at higher temperatures. Thus the strongly electron-withdrawing moiety $Cp'Re(CO)_3$ could be employed to yield a stable electrophilic Ir^{I} FCC, which was not possible with the Rh^{I} analogue. TEPs of the reported complexes were established, and the featured FC ligands exhibit a decrease in electron-donating strength from Fc- to piano stool-substituted ligands in the order :C(NH$(CH_2)_2$$NMe_2$)Fc (**23**) > :C(NH^{n}Pr)*p*-DMA (**21**) > :C(NH^{n}Pr)Fc (**22**) > :C(OEt)*p*-DMA (**18**) > :C(OEt)Fc (**20**) >> :C(OEt)($Cp'Re(CO)_3$) (**19**).

In addition, this report details the first account of the use of acyclic FCCs of iridium(I) as precatalysts in the TH of acetophenone. Catalytic activity employing the Ir^{I} FCCs **18** – **25** was achieved under mild conditions (Ir-FCC/base/substrate 1/5/1000) and generally increases with reduced electrophilicity of the precatalyst. Thus *N*-atom stabilized aminocarbene complexes were found to show improved catalytic activity in comparison to the *O*-atom stabilized counterparts, as was the case with the superior catalytic behaviour of Ir-cod complexes in comparison to their -$(CO)_2$ analogues. The best catalytic performance (89% conversion of acetophenone in 2 hours) was achieved using the Fc-substituted aminocarbene complex **23** featuring a pendant *tert*-amino (-NMe_2) moiety, presumably due to potential chelation-effect of the NMe_2 entity as well as potential catalytic activity at the additional (Fe) metal-site, in line with (multinuclear) cooperative catalytic mechanisms in literature. Moreover, the catalytic performance of these new compounds is comparable with prevalent Ir^{I}-NHCs in literature.

3.5 Experimental

3.5.1 [Ir(cod){C(OEt)*p*-DMA}Cl] 18.

A mixture of [$W(CO)_5${C(OEt)*p*-DMA}] **3** (0.200 g, 0.40 mmol) and $[Ir(cod)Cl]_2$ (0.120 g, 0.20 mmol) in deoxygenated CH_2Cl_2 was stirred for 24 hours at -78 °C while slowly warming to room temperature

(18 °C). The resulting dark-brown solution was reduced *in vacuo* and added to an alumina chromatography column. Elution with CH_2Cl_2 gave an orange band, which was collected and reduced under vacuum. Slow diffusion of *n*-hexane (3 mL) into the concentrated CH_2Cl_2 solution (2 mL) resulted in orange crystals. Yield = 0.186 g, 91%. Mp (dec): 149 – 151 °C. ^{1}H NMR (500 MHz, CD_2Cl_2) δ 8.36 (d, ^3J(HH) = 8.8 Hz, 2H, DMA-$H_{\alpha,\alpha'}$), 6.65 (d, ^3J(HH) = 9.4 Hz, 2H, DMA-$H_{\beta,\beta'}$), 5.67 (dq, ^2J(HH) = 10.4 Hz, ^3J(HH) = 7.2 Hz, 1H, OCH_2CH$_3$), 5.39 (dq, ^2J(HH) = 10.4 Hz, ^3J(HH) = 7.1 Hz, 1H, OCH_2CH$_3$), 4.90 – 4.86 (m, 1H, cod-CH), 4.78 – 4.74 (m, 1H, cod-CH), 3.07 (s, 6H, N$(CH_3)_2$), 2.99 – 2.97 (m, 1H, cod-CH), 2.92 – 2.91 (m, 1H, cod-CH), 2.41 – 2.18 (m, 4H, cod-CH_2), 2.00 – 1.78 (m, 4H, cod-CH_2), 1.60 (t, ^3J(HH) = 7.1 Hz, 3H, OCH$_2$CH$_3$). ^{13}C{^{1}H} NMR (126 MHz, CD_2Cl_2) δ 276.7 ($C_{carbene}$), 154.8 (C_q) , 135.7 (C_{ipso}), n.o. (DMA-$C_{\alpha,\alpha'}$), 111.1 (DMA-$C_{\beta,\beta'}$) , 92.9 (cod-CH), 92.6 (cod-CH), 76.0 (OCH_2CH$_3$), 58.0 (cod-CH), 52.7 (cod-CH), 40.5 (N$(CH_3)_2$), 34.1 (cod-CH_2), 33.6 (cod-CH_2), 29.2 (cod-CH_2), 29.0 (cod-CH_2), 15.7 (OCH$_2$CH$_3$). Anal. Calcd for $C_{19}H_{27}ONClIr$: C 44.48, H 5.30, N 2.73. Found: C 44.64, H 5.20, N 2.75. ESI-MS (15 V, positive mode, *m/z*): calcd for $[M - Cl]^+$ 478.1722; found 478.1588.

3.5.2 [Ir(cod){C(OEt)(Cp'Re(CO)$_3$)}Cl] 19

In like manner, complex **19** was synthesized from [W(CO)$_5${C(OEt) (Cp'Re(CO)$_3$)}] **6** (0.200 g, 0.28 mmol) and $[Ir(cod)Cl]_2$ (0.084 g, 0.14 mmol). The resulting orange oil was dissolved in CH_2Cl_2 (1 mL) and treated with n-hexane (3 mL) to precipitate an orange crystalline solid. Yield = 0.152 g, 75%. Mp: 112 – 114 °C. ^{1}H NMR (300 MHz, CD_2Cl_2) δ 6.20 – 6.17 (m, 2H, ReCp'-$H_{\alpha,\alpha'}$), 5.61 (dq, ^2J(HH) = 10.4 Hz, ^3J(HH) = 7.2 Hz, 1H, OCH_2CH$_3$), 5.53 (dt, ^3J(HH) = 2.8 Hz, ^4J(HH) = 1.8 Hz, 1H, ReCp'-$H_{\beta/\beta'}$), 5.47 (dt, ^3J(HH) = 2.8 Hz, ^4J(HH) = 1.8 Hz, 1H, ReCp'-$H_{\beta/\beta'}$), 5.25 (dq,^2J(HH) = 10.4 Hz, ^3J(HH) = 7.1 Hz, 1H, OCH_2CH$_3$), 5.16 – 5.09 (m, 1H, cod-CH), 5.00 – 4.93 (m, 1H, cod-CH), 3.14 – 3.08 (m, 1H, cod-CH), 2.99 – 2.93 (m, 1H, cod-CH), 2.47 – 1.83 (m, 8H, cod-CH_2), 1.54 (t, ^3J(HH) = 7.1 Hz, 3H, OCH$_2$CH$_3$). ^{13}C{^{1}H} NMR (126 MHz, CD_2Cl_2) δ 275.1 ($C_{carbene}$), 192.6 (Re$(CO)_3$), 108.5 (ReCp'-C_{ipso}), 98.6 (cod-CH), 98.0 (cod-CH), 91.4 (ReCp'), 90.1 (ReCp'), 87.4 (ReCp'), 85.9 (ReCp'), 78.1 (OCH_2CH$_3$), 61.3 (cod-CH), 55.1 (cod-CH), 34.1 (cod-CH_2), 33.1 (cod-CH_2), 29.6 (cod-CH_2), 28.1 (cod-CH_2), 15.5 (OCH$_2$CH$_3$). IR (CH_2Cl_2, ν(CO), cm^{-1}): 1937 (w), 2031 (s). Anal. Calcd for $C_{19}H_{21}O_4ClReIr$: C 31.38, H 2.91. Found: C 31.87, H 2.76. ESI-MS (15 V, positive mode, *m/z*): calcd for $[M - Cl]^+$ 693.0627; found 693.0616.

3.5.3 [Ir(cod){C(OEt)Fc}Cl] 20

This complex was similarly prepared from [W(CO)$_5${C(OEt)Fc}] **8** (0.566 g, 1.00 mmol) and $[Ir(cod)Cl]_2$ (0.300 g, 0.50 mmol). The resulting red oil was dissolved in CH_2Cl_2 (2 mL) and treated with *n*-hexane (5 mL) at -30 °C to precipitate a red crystalline solid. Yield = 0.445 g, 77%. Mp: 115 – 117 °C. ^{1}H NMR (500 MHz, CD_2Cl_2) δ 5.71 (dq, ^2J(HH) = 10.4 Hz, ^3J(HH) = 7.2 Hz, 1H, OCH_2CH$_3$), 5.32 (s, br, 1H, FeCp'), 5.25 (dq,^2J(HH) = 10.4 Hz, ^3J(HH) = 7.1 Hz, 1H, OCH_2CH$_3$), 4.93 – 4.89 (m, 1H, cod-CH), 4.86 (s, br, 1H,

FeCp$^{'}$), 4.79 – 4.76 (m, 2H, cod-CH, FeCp$^{'}$), 4.64 (s, br, 1H, FeCp$^{'}$), 4.42 (s, 5H, FeCp), 3.04 – 3.01 (m, 1H, cod-CH), 2.95 – 2.91 (m, 1H, cod-CH), 2.43 – 2.04 (m, 5H, cod-CH_2), 1.88 – 1.80 (m, 3H, cod-CH_2), 1.61 (t, ^3J(HH) = 7.2 Hz, 3H, OCH_2CH_3). $^{13}C\{^1H\}$ NMR (75 MHz, CD_2Cl_2) δ 286.6 ($C_{carbene}$), 94.3 (cod-CH), 94.1 (cod-CH), 90.3 (FeCp$^{'}$-C_{ipso}), 77.2 (OCH_2CH_3), 75.4 (FeCp$^{'}$), 74.8 (FeCp$^{'}$), 73.7 (FeCp$^{'}$), n.o. (FeCp$^{'}$), 70.4 (FeCp), 59.2 (cod-CH), 52.9 (cod-CH), 34.3 (cod-CH_2), 33.5 (cod-CH_2), 29.2 (cod-CH_2), 28.7 (cod-CH_2), 15.8 (OCH_2CH_3). Anal. Calcd for $C_{21}H_{26}OClFeIr$: C 43.64, H 4.53. Found: C 44.00, H 4.46. ESI-MS (15 V, positive mode, *m/z*): calcd for $[M - Cl]^+$ 543.0962; found 543.0967.

3.5.4 [Ir(cod){C(NH^{n}Pr)*p*-DMA}Cl] 21

^{n}PrNH$_2$ was slowly added to a brown-orange solution of **18** (0.100 g, 0.20 mmol) in THF at room temperature and the colour immediately changed to yellow. The THF solvent was removed *in vacuo*. The resulting yellow paste was washed with *n*-hexane (2 x 5 mL) and cannula-extracted with CH_2Cl_2 to give a yellow-lime powder after drying. Yellow crystals were obtained by slow diffusion of *n*-hexane (2 mL) into a concentrated CH_2Cl_2 solution of the powder. Yield = 0.099 g, 94%. Mp (dec): 150 – 153 °C. ^{1}H NMR (400 MHz, CD_2Cl_2) δ 8.51 (s, br, 1H, $NHCH_2CH_2CH_3$), 7.90 (d, ^3J(HH) = 9.0 Hz, 2H, DMA-$H_{\alpha,\alpha'}$), 6.69 (d, ^3J(HH) = 9.0 Hz, 2H, DMA-$H_{\beta,\beta'}$), 4.56 – 4.49 (m, 2H, cod-CH), 4.36 – 4.20 (m, 2H, $NHCH_2CH_2CH_3$), 3.03 (s, 6H, $N(CH_3)_2$), 2.94 – 2.90 (m, 1H, cod-CH), 2.81 – 2.76 (m, 1H, cod-CH), 2.28 – 2.14 (m, 4H, cod-CH_2), 1.92 – 1.55 (m, 6H, cod-CH_2, $NHCH_2CH_2CH_3$), 1.07 (t, ^3J(HH)= 7.2 Hz, 3H, $NHCH_2CH_2CH_3$). $^{13}C\{^1H\}$ NMR (101 MHz, CD_2Cl_2) δ 240.3 ($C_{carbene}$), 153.1 (C_q), 132.5 (C_{ipso}), 130.4 (DMA-$C_{\alpha,\alpha'}$), 111.5 (DMA-$C_{\beta,\beta'}$), 86.1 (cod-CH), 85.4 (cod-CH), 55.7 (cod-CH), 54.9 ($NHCH_2CH_2CH_3$), 52.6 (cod-CH), 40.4 ($N(CH_3)_2$), 33.9 (cod-CH_2), 33.6 (cod-CH_2), 29.8 (cod-CH_2), 29.5 (cod-CH_2), 23.5 ($NHCH_2CH_2CH_3$), 11.9 ($NHCH_2CH_2CH_3$). IR (CH_2Cl_2, ν(NH), cm^{-1}): 3332. Anal. Calcd for $C_{20}H_{30}N_2ClIr$: C 45.66, H 5.75, N 5.32. Found: C 45.72, H 5.53, N 6.24. ESI-MS (15 V, positive mode, *m/z*): calcd for $[M - Cl]^+$ 491.2038; found 491.1966.

The aminocarbene complexes; [Ir(cod){C(NH^{n}Pr)Fc}Cl] **22** and [Ir(cod){C(NH(CH_2CH_2)NMe$_2$)Fc}Cl] **23** were also prepared.

3.5.5 [Ir(cod){C(NH^{n}Pr)Fc}Cl] 22

Excess ^{n}PrNH$_2$ was added to a dark red solution of **20** (0.090 g, 0.16 mmol) in THF and stirred at 60 °C for 5 hours. The THF solvent was then evaporated to dryness, resulting in a red-orange paste. Washing with *n*-hexane (3 x 5 mL) and subsequent CH_2Cl_2 cannula-extraction resulted in a red-orange powder after the CH_2Cl_2 solvent was removed in *vacuo*. Yield = 0.082 g, 86%. Mp (dec): 171 – 173 °C. ^{1}H NMR (400 MHz, $CDCl_3$) δ 8.36 (s, br, 1H, $NHCH_2CH_2CH_3$), 5.16 (s, br, 1H, FeCp$^{'}$), 4.71 – 4.67 (m, 1H, cod-CH), 4.66 (s, br, 1H, FeCp$^{'}$), 4.59 – 4.56 (m, 1H, cod-CH), 4.54 (s, br, 1H, FeCp$^{'}$), 4.45 (s, br, 1H, FeCp$^{'}$), 4.35 – 4.27 (m, 1H, $NHCH_2CH_2CH_3$), 4.31 (s, 5H, FeCp), 4.13 – 4.05 (m, 1H, $NHCH_2CH_2CH_3$), 3.00 – 2.96 (m,

1H, cod-CH), 2.93 – 2.90 (m, 1H, cod-CH), 2.37 – 2.09 (m, 4H, cod-CH_2) 1.97 – 1.56 (m, 6H, cod-CH_2, $NHCH_2CH_2CH_3$), 1.10 (t, ^3J(HH) = 7.4 Hz, 3H, $NHCH_2CH_2CH_3$). $^{13}C\{^1H\}$ NMR (101 MHz, $CDCl_3$) δ 245.4 ($C_{carbene}$), 86.4 (cod-CH), 86.4 (cod-CH), 85.7 (FeCp'-C_{ipso}), 73.1 (FeCp'), 72.2 (FeCp'), 71.3 (FeCp'), 70.1 (FeCp), 67.3 (FeCp'), 55.6 (cod-CH), 55.0 (cod-CH), 52.8 ($NHCH_2CH_2CH_3$), 34.2 (cod-CH_2), 32.8 (cod-CH_2), 28.6 (cod-CH_2), 28.9 (cod-CH_2), 23.3 ($NHCH_2CH_2CH_3$), 11.6 ($NHCH_2CH_2CH_3$). IR (CH_2Cl_2, ν(NH), cm^{-1}): 3332. Anal. Calcd for $C_{22}H_{29}NClFeIr$: C 44.71, H 4.95, N 2.37. Found: C 44.82, H 4.92, N 2.46. ESI-MS (15 V, positive mode, *m/z*): calcd for $[M - Cl]^+$ 556.1279; found 556.1201.

3.5.6 [Ir(cod){C(NH(CH_2CH_2)NMe_2)Fc}Cl] 23

This complex was prepared similarly to **22** using excess $NH_2(CH_2CH_2)NMe_2$ and **20** (0.100 g, 0.17 mmol) resulting in a yellow-orange powder. Yield = 0.082 g, 86%. Mp : 109 – 110 °C. ^1H NMR (400 MHz, $CDCl_3$) δ 9.13 (s, br, 1H, $NHCH_2CH_2(CH_3)_2$), 5.16 (s, br, 1H, FeCp'), 4.68 – 4.59 (m, 2H, cod-CH, $NHCH_2CH_2(CH_3)_2$), 4.64 (s, br, 1H, FeCp'), 4.53 (s, br, 2H, cod-CH, FeCp'), 4.43 (s, br, 1H, FeCp'), 4.32 (s, 5H, FeCp), 3.93 – 3.89 (m, 1H, $NHCH_2CH_2(CH_3)_2$), 2.94 – 2.88 (m, 2H, $NHCH_2CH_2(CH_3)_2$), 2.84 – 2.79 (m, 1H, cod-CH), 2.70 – 2.65 (m, 1H, cod-CH), 2.38 (s, 6H, $NHCH_2CH_2(CH_3)_2$), 2.29 – 2.09 (m, 4H, cod-CH_2), 1.91 – 1.88 (m, 1H, cod-CH_2), 1.72 – 1.59 (m, 3H, cod-CH_2). $^{13}C\{^1H\}$ NMR (101 MHz, $CDCl_3$) δ 245.5 ($C_{carbene}$), 86.6 (cod-CH), 86.5 (cod-CH), 86.1 (FeCp'-C_{ipso}), 73.4 (FeCp'), 72.1 (FeCp'), 71.0 (FeCp'), 70.1 (FeCp), 67.6 (FeCp'), 58.3 ($NHCH_2CH_2(CH_3)_2$), 55.4 (cod-CH), 52.5 (cod-CH), 49.1 ($NHCH_2CH_2N(CH_3)_2$), 45.5 ($NHCH_2CH_2N(CH_3)_2$), 34.2 (cod-CH_2), 32.9 (cod-CH_2), 29.6 (cod-CH_2), 28.9 (cod-CH_2). IR (CH_2Cl_2, ν(NH), cm^{-1}): 3288. Anal. Calcd for $C_{23}H_{32}N_2ClFeIr$: C 44.55, H 5.20, N 4.52. Found: C 44.01, H 5.30, N 4.56. ESI-MS (15 V, positive mode, *m/z*): calcd for $[M - Cl]^+$ 585.1544; found 585.1405.

3.5.7 [Ir(CO)$_2${C(OEt)Fc}Cl] 24

Carbon monoxide gas was bubbled for 5 minutes through a stirred solution of **20** (0.100 g, 0.17 mmol) in CH_2Cl_2 (10 mL) at room temperature. An immediate colour change from dark-red to dark-purple was observed. The flow of CO was stopped, and black crystals were grown by slow diffusion of *n*-hexane (2 mL) into the concentrated CH_2Cl_2 reaction mixture at -30 °C. Yield = 0.085 g 93%. Mp: 103 – 104 °C. ^1H NMR (400 MHz, C_6D_6) δ 5.11 – 5.08 (m, br, 2H, FeCp'-$H_{\alpha,\alpha'}$), 4.96 (q, br, ^3J(HH) = 8.4 Hz, 2H, OCH_2CH_3), 4.39 (d, br, ^3J(HH) = 7.2 Hz, 2H, FeCp'-$H_{\beta,\beta'}$), 4.18 (s, 5H, FeCp), 1.07 (t, ^3J(HH) = 7.1 Hz, 3H, OCH_2CH_3). $^{13}C\{^1H\}$ NMR (101 MHz, C_6D_6) δ 277.4 ($C_{carbene}$), 184.1 (CO_{trans}), 170.1 (CO_{cis}), 87.6 (C_{ipso}), 79.9 (OCH_2CH_3, FeCp'-$C_{\alpha,\alpha'}$), 77.5 (FeCp'-$C_{\beta,\beta'}$), 71.6 (FeCp), 14.6 (OCH_2CH_3). IR (CH_2Cl_2, ν(CO), cm^{-1}): 1989, 2069. Anal. Calcd for $C_{15}H_{14}O_3ClFeIr$: C 34.27, H 2.68. Found: C 34.10, H 2.66. ESI-MS (15 V, positive mode, *m/z*): calcd for $[M - Cl]^+$ 490.9922, $[M - Cl - CO]^+$ 462.9973; found [M – Cl] 490.9924, $[M - Cl - CO]^+$ 462.9975.

3.3.8 $[Ir(CO)_2\{C(NH^nPr)Fc\}Cl]$ 25

Carbon monoxide gas was bubbled for 10 minutes through a stirred solution of **22** (0.100 g, 0.17 mmol) in CH_2Cl_2 (15 mL) at room temperature. The flow of CO was stopped, and the CH_2Cl_2 solvent was removed under vacuum. The resulting orange-red paste was washed with *n*-hexane (3 x 10 mL) and cannula-extracted with CH_2Cl_2. Dark-red crystals were grown by slow diffusion of *n*-hexane (2 mL) into the concentrated CH_2Cl_2 solution at -30 °C. Yield = 0.085 g, 93%. Mp (dec): 173 – 175 °C. ^{1}H NMR (400 MHz, $CDCl_3$) δ 8.79 (s, br, 1H, $\underline{NH}CH_2CH_2CH_3$), 5.05 (s, br, 1H, FeCp'-$\underline{H_{\alpha/\alpha'}}$), 4.93 (s, br, 1H, FeCp'-$\underline{H_{\alpha/\alpha'}}$), 4.67 (s, 2H, FeCp'-$\underline{H_{\beta,\beta'}}$), 4.35 (s, 5H, FeCp), 4.14 (s, br, 1H, $NH\underline{CH_2}CH_2CH_3$), 3.75 (s, br, 1H, $NH\underline{CH_2}CH_2CH_3$), 1.79 (q, br, ^3J(HH) = 7.4 Hz, 2H, $NHCH_2\underline{CH_2}CH_3$), 1.04 (t, ^3J(HH) = 7.3 Hz, 3H, $NHCH_2CH_2\underline{CH_3}$). $^{13}C\{^1H\}$ NMR (101 MHz, $CDCl_3$) δ 232.6 ($C_{carbene}$), 182.7 (CO_{trans}), 169.6 (CO_{cis}), 83.9 (C_{ipso}), n.o (FeCp'-$\underline{C_{\alpha,\alpha'}}$), 73.7 (FeCp'-$\underline{C_{\beta,\beta'}}$), 70.6 (FeCp), 56.2 ($NH\underline{CH_2}CH_2CH_3$), 22.7 ($NHCH_2\underline{CH_2}CH_3$), 11.3 $NHCH_2CH_2\underline{CH_3}$). IR ($CH_2Cl_2$, ν(CO) and ν(NH), cm^{-1}): 1980, 2063, 3323. Anal. Calcd for $C_{16}H_{17}O_2NClFeIr$: C 35.67, H 3.18, N 2.60. Found: C 36.62, H 3.01, N 3.73. ESI-MS (15 V, positive mode, *m/z*): calcd for $[M - Cl]^+$ 504.0238, $[M - Cl - CO]^+$ 476.0289; found [M – Cl] 504.0235, $[M - Cl - CO]^+$ 476.0235.

3.6 References

1 P. J. Fraser, W. R. Roper and F. G. A. Stone, *J. Chem. Soc. Dalton Trans.*, 1974, 760–764.

2 J. M. O'Connor, L. Pu and A. L. Rheingold, *J. Am. Chem. Soc.*, 1990, **112**, 6232–6247.

3 O. Boutry, E. Gutierrez, A. Monge, M. C. Nicasio, P. J. Perez and E. Carmona, *J. Am. Chem. Soc.*, 1992, **114**, 7288–7290.

4 H. F. Luecke, B. A. Arndtsen, P. Burger and R. G. Bergman, *J. Am. Chem. Soc.*, 1996, **118**, 2517–2518.

5 C. Slugovc, K. Mereiter, S. Trofimenko and E. Carmona, *Angew. Chem. Int. Ed.*, 2000, **39**, 2158–2160.

6 J. Meiners, A. Friedrich, E. Herdtweck and S. Schneider, *Organometallics*, 2009, **28**, 6331–6338.

7 D.-H. Lee, J. Chen, J. W. Faller and R. H. Crabtree, *Chem. Commun.*, 2001, 213–214.

8 M. T. Whited and R. H. Grubbs, *Organometallics*, 2008, **27**, 5737–5740.

9 M. T. Whited and R. H. Grubbs, *J. Am. Chem. Soc.*, 2008, **130**, 5874–5875.

10 M. T. Whited, Y. Zhu, S. D. Timpa, C.-H. Chen, B. M. Foxman, O. V. Ozerov and R. H. Grubbs, *Organometallics*, 2009, **28**, 4560–4570.

11 E. Carmona, M. Paneque, L. L. Santos and V. Salazar, *Coord. Chem. Rev.*, 2005, **249**, 1729–1735.

12 M. T. Whited and R. H. Grubbs, *Acc. Chem. Res.*, 2009, **42**, 1607–1616.

13 H. G. Raubenheimer, *Dalton Trans.*, 2014, **43**, 16959–16973.

14 Y. Shikata, R. Yasue and K. Yoshida, *Chem. -Eur. J.*, 2017, **23**, 16806–16812.

15 R. Yasue and K. Yoshida, *Organometallics*, 2019, **38**, 2211–2217.

16 F. Rigas and S. Sklavounos, *Int. J. Hydrog. Energy*, 2005, **30**, 1501–1510.

17 B. Štefane and F. Požgan, *Top. Curr. Chem.*, 2016, **374**, 18.

18 O. Eisenstein and R. H. Crabtree, *New J. Chem.*, 2013, **37**, 21–27.

19 R. Malacea, R. Poli and E. Manoury, *Coord. Chem. Rev.*, 2010, **254**, 729–752.

20 D. Wang and D. Astruc, *Chem. Rev.*, 2015, **115**, 6621–6686.

21 S. E. Clapham, A. Hadzovic and R. H. Morris, *Coord. Chem. Rev.*, 2004, **248**, 2201–2237.

22 S. Kaufhold, L. Petermann, R. Staehle and S. Rau, *Coord. Chem. Rev.*, 2015, **304**–**305**, 73–87.

23 E. Peris and R. H. Crabtree, *Coord. Chem. Rev.*, 2004, **248**, 2239–2246.

24 M. Albrecht, J. R. Miecznikowski, A. Samuel, J. W. Faller and R. H. Crabtree, *Organometallics*, 2002, **21**, 3596–3604.

25 N. García, E. A. Jaseer, J. Munarriz, P. J. Sanz Miguel, V. Polo, M. Iglesias and L. A. Oro, *Eur. J. Inorg. Chem.*, 2015, **2015**, 4388–4395.

26 L. Yang, A. Krüger, A. Neels and M. Albrecht, *Organometallics*, 2008, **27**, 3161–3171.

27 M. V. Jiménez, J. Fernández-Tornos, J. J. Pérez-Torrente, F. J. Modrego, S. Winterle, C. Cunchillos, F. J. Lahoz and L. A. Oro, *Organometallics*, 2011, **30**, 5493–5508.

28 X. Gong, H. Zhang and X. Li, *Tetrahedron Lett.*, 2011, **52**, 5596–5600.

29 G. K. Ramollo, M. J. López-Gómez, D. C. Liles, L. C. Matsinha, G. S. Smith and D. I. Bezuidenhout, *Organometallics*, 2015, **34**, 5745–5753.

30 T. Dröge and F. Glorius, *Angew. Chem. Int. Ed.*, 2010, **49**, 6940–6952.

31 D. Munz, *Organometallics*, 2018, **37**, 275–289.

32 J. Barluenga, R. Vicente, L. A. López and M. Tomás, *J. Organomet. Chem.*, 2006, **691**, 5654–5659.

33 D. M. Adams, *Metal-Ligand and Relative Vibrations: A Critical Survey of the Infrared and Raman Spectra of Metallic and Organometallic Compounds*, Edinburg University Press, London, 1967.

34 B. van der Westhuizen, P. J. Swarts, I. Strydom, D. C. Liles, I. Fernández, J. C. Swarts and D. I. Bezuidenhout, *Dalton Trans.*, 2013, **42**, 5367–5378.

35 A. R. Chianese, X. Li, M. C. Janzen, J. W. Faller and R. H. Crabtree, *Organometallics*, 2003, **22**, 1663–1667.

36 R. A. Kelly III, H. Clavier, S. Giudice, N. M. Scott, E. D. Stevens, J. Bordner, I. Samardjiev, C. D. Hoff, L. Cavallo and S. P. Nolan, *Organometallics*, 2008, **27**, 202–210.

37 F. E. Hahn, C. Holtgrewe, T. Pape, M. Martin, E. Sola and L. A. Oro, *Organometallics*, 2005, **24**, 2203–2209.

38 S. Gülcemal, A. G. Gökçe and B. Çetinkaya, *Dalton Trans.*, 2013, **42**, 7305–7311.

39 D. Gnanamgari, A. Moores, E. Rajaseelan and R. H. Crabtree, *Organometallics*, 2007, **26**, 1226–1230.

40 A. Naik, T. Maji and O. Reiser, *Chem. Commun.*, 2010, **46**, 4475–4477.

41 J. P. Hopewell, J. E. D. Martins, T. C. Johnson, J. Godfrey and M. Wills, *Org. Biomol. Chem.*, 2012, **10**, 134–145.

42 R. H. Crabtree, *Chem. Rev.*, 2012, **112**, 1536–1554.

Chapter 4: Synthesis of gold(I) Fischer carbene complexes for application in redox-switchable catalysis

4.1 Literature review

Molecular gold complexes have been widely applied in π-acidic catalysis since the carbophilic properties of gold were highlighted over two decades ago.[1–3] A wide array of gold complexes have consequently been utilized as (pre)catalysts in multiple C-C and C-X (X = *O*- or *N*-atom) bond activation reactions and have been extensively reviewed.[4–8] Theoretical (computational) studies of gold complexes have also similarly exponentiated, where the aurophilicity phenomenon, defined as inter- or intramolecular Au-Au attractions governed by relativistic effects (resulting in Au-Au bond distances ranging from 2.50 to 3.50 Å), is also important in the research community's efforts in rationalizing the chemical behavior of gold(I) complexes.[9,10] The general consensus is that both experimental and corresponding theoretical studies are valuable in characterizing the exact nature of the gold-metal (pre)catalysts in the gas-, liquid-, and solid- states. Thus ideally, the synthesis and computational molecular orbital/bonding studies of gold complexes should be integrated.[11–13]

4.1.1 Gold(I) Fischer carbene complexes

Gold(I) complexes possessing either alkyl, alkenyl or (hetero)aryl- acyclic Fischer carbene (FC) ligands have been reported over the past four decades.[14–23] However, catalytic application[23] and computational studies[18,23] of these complexes are limited. All reported gold(I) FCCs to date were synthesized *via* the facile transmetallation reaction of chromium(0), molybdenum(0), or tungsten(0) FCC precursors and the relevant gold precursor compound, resulting in the desired gold(I) FCCs depicted in Figure 4.1 below. Gold(III) precursors were initially utilized for these transmetallations in the early 1980s, with instantaneous reductive elimination implicated as the terminal step towards formation of the isolated gold(I) FCCs. Later reports, however, specify gold(I) precursors bearing labile ligands (such as SMe_2), or utilize dehalogenating additives (such as $AgBF_4$) to aid in the transmetallation process. Regardless of the gold metal oxidation state, these reactions reportedly proceed smoothly within a few hours, and the gold(I) FCCs were isolated in moderate to high yields as detailed below (62 – 95%).

Fischer and co-workers reported in 1981 the simple transmetallation reaction of W^0 phenyl methoxy- and -aminocarbene complexes with auric acid to afford Au^I chloro phenyl-carbene complexes (a).[14] Au^I bromo- and iodo-analogues of Au^I chloro FCCs (a) were subsequently reported in 1983.[17] The dinuclear Au^I biscarbene complex (b) was similarly transmetallated from a W^0-analogue to auric acid in 1984.[16] Inclusion of heteroaryl carbene substituents was later reported by Raubenheimer and co-workers in 2010 (c), and by our research group in 2014 (d), where the gold(I) chloro FCCs resulted from the facile transmetallation of W^0 FCCs and [Au(tht)Cl] (tht = tetrahydrothiophene) in both cases. Complimentary, an ethoxycarbene analogue of methoxycarbene complex (d) was recently reported, where reaction of a W^0 ferrocenyl (Fc) ethoxycarbene complex and [Au(SMe_2)Cl] yielded the desired neutral Au^I FCC [Au{(OEt)Fc}Cl].[23] Additionally, cationic [L-Au^I-FC] complexes stabilized by the electron-donating effect of the *trans*-ligand (L) have also been reported (e – h).[20–22,24,25] In these cases, existing Au^I complexes bearing basic phosphine or NHC ligands readily reacted with Cr^0 or W^0 FCCs aided by the selected silver metal salt. The resulting Au^I FCC salts exhibit electron donation-acceptance synergy from L to the FC ligand respectively, which aids in stabilizing said FCC.

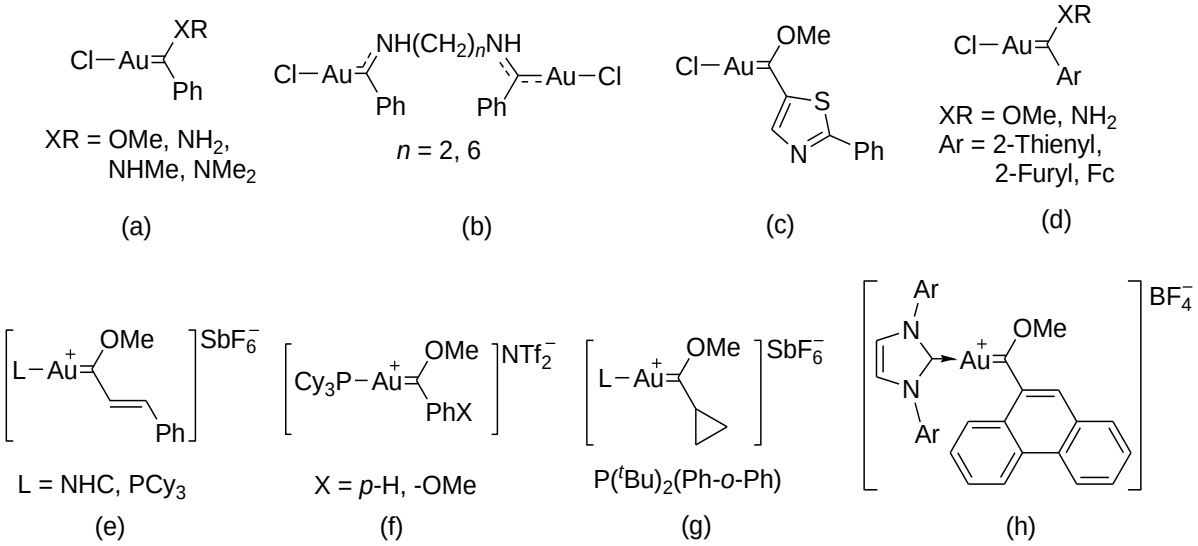

Figure 4.1 Selected examples of neutral (top) and cationic (bottom) Au^I FCCs in literature.

4.1.2 Gold carbene complexes as precatalysts

Since the pioneering work on the gold-NHC catalyzed hydration of 3-hexyne reported by Schneider and co-workers in 2003,[26] these complexes have gained attention as efficient (pre)catalysts, notably in the activation of alkyne- and *iso*cyano-bonds. Gold(I) NHCs have been utilized in the catalytic hydroamination of terminal alkenes and alkynes, wherein the required use of halide-scavenger additives such as silver metal salts was reported.[27,28] These Au^I-NHC catalyzed hydroaminations are

typically conducted at elevated temperatures, however, the hydroamination of 1-hexyne was reportedly achieved at room temperature by inclusion of a cyclic(alkyl)(amino) carbene (CAAC) ligand instead of NHCs.[29] Additionally, Au^{I} NHCs have also been employed in the catalytic synthesis of oxazolines. In 2013, the research group of Albrecht reported the cycloaddition of methyl *iso*cyanoacetate and a variety of activated aldehydes at 40 °C, catalyzed by Au^{I} chloro NHC complexes in the presence of a silver-metal salt and tertiary amine as additives, and the oxazoline resulted in high yields within an hour.[30] The reported Au^{I} NHC proved catalytically active in the absence of any additive (even at ambient temperatures), with the silver-metal salt and *tert*-amine additives effecting a slight increase in catalytic activity and regioselectivity, as indicated in Scheme 4.1 below.

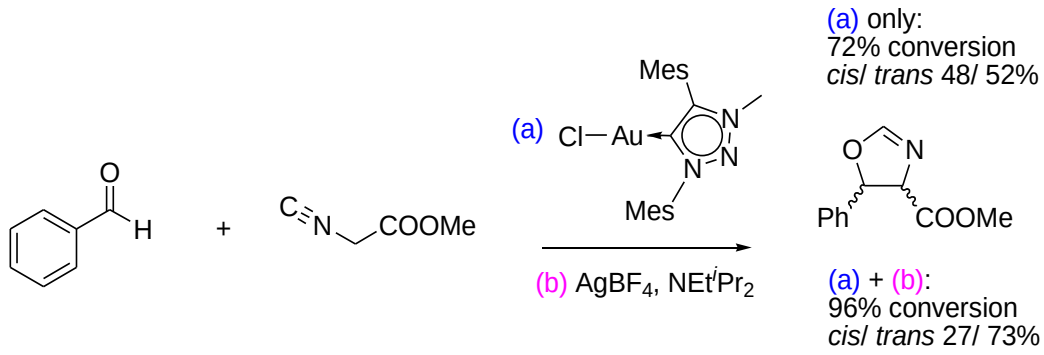

Scheme 4.1 Selected example of Au^{I}-NHC catalyzed intermolecular oxazoline synthesis

More recent reports of Au^{I}-NHC catalyzed oxazoline synthesis lean towards the intramolecular cyclization of *N*(2-propyn-1-yl)- aryl- or alkyl-amides, presumably due to the apparent ease with which the targeted oxazoline is formed at room temperature. Consequently, these reactions usually proceed after several hours,[31,32] and even longer optimum catalytic periods of up to 2 days have also been reported.[33] Additionally, non-halogen-scavenger additives such as acetyl ferrocenium salts reportedly activate Au^{I} NHCs, wherein the accompanying non-redox-innocent NHC ligand is oxidized by the ferrocenium salt and the precatalyst is consequently "switched on". In this case, the presence of an oxidizable carbene substituent (such as a remote Fc unit) is essential, and the catalytic cycle can be interrupted by addition of a suitable reductant in a "switching off" of the active Au-NHC species. For example, the redox-switchable catalytic activity of a gold(I) chloro NHC precatalyst in intramolecular oxazoline synthesis reactions was achieved by consecutive addition of an oxidant and a reductant, in the respective activation and deactivation of the aforementioned Au^{I}-NHC species.[34,35]

The recent surge in Au^{I}-NHC catalyzed oxazoline synthesis prompted us to envisage utilization of classical Au^{I} FCCs as precatalysts instead, literature reports of which were thitherto unavailable. However, this study coincided with the report by the research group of Heinze of the redox switchable intramolecular oxazoline synthesis,[23] utilizing a gold(I) chloro- Fc-ethoxycarbene complex in 2019,

details of which are summarized below. At the same time, we were using the same complex and a range of related Au^{I} (heteroaryl) FCCs (*vide supra*) in silver-metal assisted Au^{I}-FCC catalyzed intermolecular oxazoline synthesis studies wherein a variety of Au^{I} FCCs bearing (hetero)aryl carbene substituents were evaluated as precatalysts. Results of the intermolecular oxazoline synthesis are tabulated in Chapter 6 (Table 6.4). Due to the overlap in research interest, we did not pursue the independent line of research but instead joined a collaborative investigation with the Heinze research group, which is the topic of this thesis chapter.

4.2 Aim

As reported by the Heinze group, intramolecular cyclization of *N*(2-propyn-1-yl)-benzamide catalyzed by the [Au{C(OEt)Fc}Cl] FCC results in the targeted oxazoline *via* redox-switching at the ferrocenyl (Fc) site (Scheme 4.2).[23] The catalytically inactive neutral gold(I)-FCC (a) was chemically oxidized *in situ*, whereby $[N(p\text{-}C_6H_4Br)_3][SbCl_6]$ (Magic Blue) was employed as a suitable oxidant resulting in the active species (b). Similarly to gold(I) Fc-NHC precatalysts in literature, one-electron oxidation at the Fc Fe^{II} site switches on catalytic activity, and proved reversible as one-electron reduction promptly turns off catalytic activity. The resultant $Au^{I}Fe^{III}$ FCC is said to convert to the $Au^{II}Fe^{II}$ analogue *via* intramolecular reduction and oxidation of the Fe^{III} and Au^{I} metal centers, respectively, thus the $Au^{II}Fe^{II}$ electromer was postulated as the catalytically active species. Density Functional Theory (DFT) calculations and Electron Paramagnetic Resonance (EPR) spectroscopy were in agreement with the suggested $Au^{II}Fe^{II}$ FCC active species. Although the exact nature of the active Au^{II}-FCC is unknown (as this cationic species proved non-isolable), calculated electron spin densities of a $[Au\{C(OEt)Fc\}Cl]^{+}$ model indicated that electron density is initially located at the iron metal, then slowly transfers to the gold metal site. Subsequently, the initially linear geometry of the Fe^{III} Cl-Au^{I}-FC species (Cl-Au-$C_{carbene}$ bond angle = 177 °) also changes to a four-coordinate geometry upon formation of the $Au^{II}Fe^{II}$ complex (Cl-Au-$C_{carbene}$ bond angle = 93 °), and the *N*(2-propyn-1-yl)-benzamide substrate could thus weakly coordinate to the Au^{II} metal vacant site as a crucial first step towards the successful formation of 2-phenyl-5-vinylidene-2-oxazoline. Additionally, EPR spectroscopy of an equimolar solution of the precatalyst ([Au{C(OEt)Fc}Cl]) and oxidant Magic Blue indicated a paramagnetic resonance converging to a rhombic *g* tensor of 2 as per literature reports of Au^{II} molecules. Apparently, observation of the paramagnetic resonance at room temperature excludes the existence of Fe^{III} species in the analyzed solution, thus the $Au^{II}Fe^{II}$ electromer was shown to be the active catalytic species.

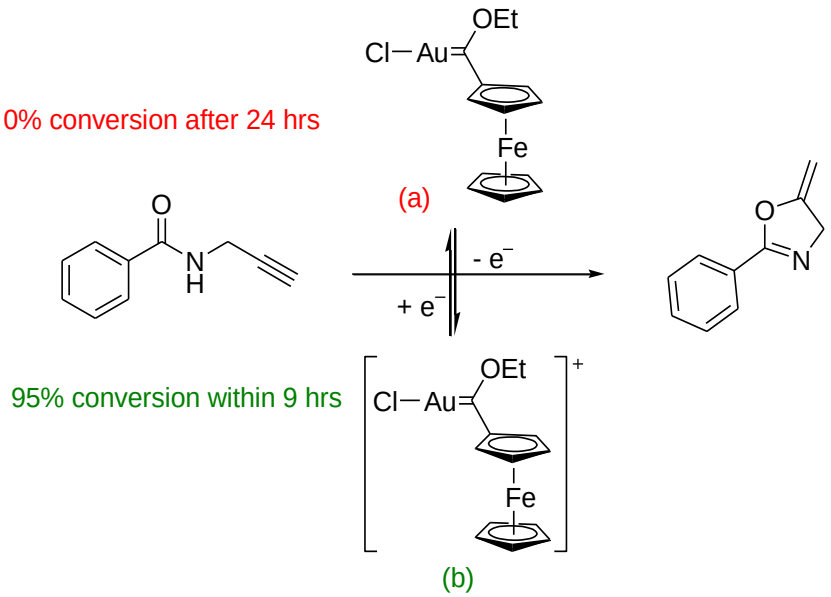

Scheme 4.2 Intramolecular cyclization of *N*(2-propyn-1-yl)-benzamide assisted by catalytically-on Au^{II}-FCC (b) *via* one-electron oxidation of catalytically-off Au^{I}-FCC (a).

The possibility of varying the carbene carbon atom substituents in fine-tuning the catalytic behavior of Au^{I} FCCs towards the reported redox-switchable intramolecular cyclization, is thus envisaged as the main aim of this chapter. Moreover, the requirement of the redox-active, ancillary metal-containing Fc group as oxidizable carbene substituent is investigated. In a collaborative effort with the Heinze group, we embarked on experimental and theoretical studies of gold-catalyzed oxazoline synthesis, objectives of which include investigation of (i) the effect of employing a more electron-donating Fc-aminocarbene ligand as opposed to the less electron-donating Fc-ethoxycarbene analogue, for a more detailed profiling of the catalytically active $Au^{II}Fe^{II}$ species, (ii) the possibility of employing Au^{I} precatalysts bearing organic aryl carbene substituents such as 2-thienyl (Th), 2-furyl (Fu), or *para-N,N*-dimethylaniline (*p*-DMA) in variation of the Fc unit towards redox switchable oxazoline synthesis. The final objective is (iii) to investigate the viability of including carbene ligands with hemilabile *N*-donor pendant moieties to potentially stabilize the catalytically active Au^{II} species.

To this effect, the facile transmetallation route discussed in Chapters 2 and 3 will again be employed for synthesis of gold(I) ethoxycarbene complexes. Due to the increased ease of oxidation of aminocarbene complexes as compared to alkoxy-analogues,[36] and to the known ability of amines to induce the oxidative-addition in metal-complexes,[37,38] aminocarbene complexes bearing Fc, Th, Fu, and *p*-DMA carbene substituents are hence targeted as precatalysts for the redox-switchable cyclization of *N*(2-propyn-1-yl)-benzamide. All envisaged gold(I) aminocarbene precatalysts will be

accessed *via* aminolysis of their ethoxy-analogues, synthesized prior by transmetallation methods from their tungsten(0) analogues. Complete characterization (NMR, FT-IR, XRD, MS, EA) of all new gold(I) FCCs will be done prior to the redox-switchable catalytic studies.

4.3 Results and discussion

4.3.1 Synthetic strategy

In this section, the synthesis and characterization of a series of gold(I) ethoxy- and *sec*-aminocarbene complexes bearing Th, Fu, *p*-DMA, and Fc carbene substituents will be discussed. As gold(I) methoxy- and *n*-aminocarbene analogues of all but the *p*-DMA complex have been previously reported by our research group,[18] the synthesis and characterization of all gold(I) FCCs reported herein will be discussed in brief. Where details differ from the literature reports of methoxy- and *n*-amino-analogues, the differences will be highlighted and elaborated upon.

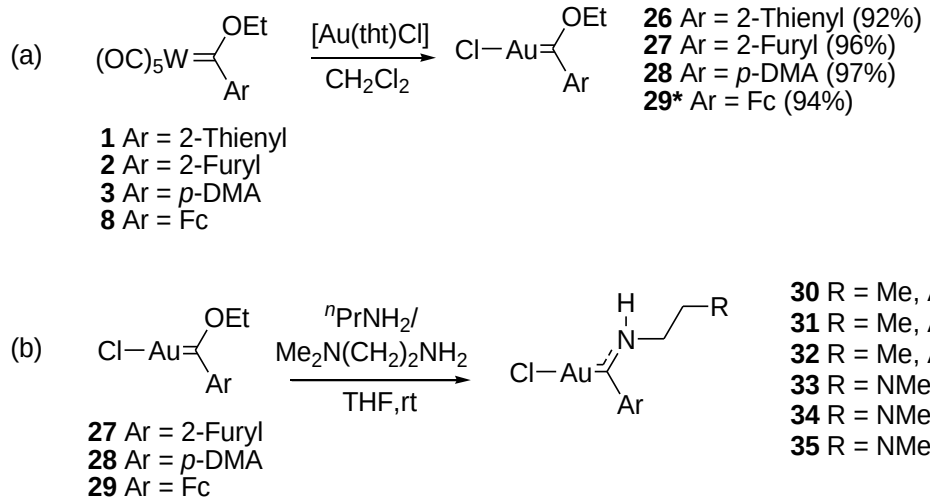

Scheme 4.3 Synthesis of Au^{I} FCCs **26** – **35** *via* transmetallation (a) and subsequent carbene ligand modification (b). *This complex has been recently reported.[23]

New examples of gold(I) (hetero)aryl-ethoxycarbene FCCs **26** – **28**, and **29**, were synthesized as outlined in Scheme 4.3, following adapted literature procedures reported for methoxycarbene-analogues (a) and aminolysis of alkoxycarbene complexes (b).[18,36] The previously reported Fc-ethoxycarbene complex **29** is included herein for comparison with (hetero)aryl analogues **26** – **28**, and for application as a precursor to aminocarbene complexes. The facile transmetallation reaction of tungsten(0) ethoxycarbene complexes **1** – **3** and **8** with the gold(I) precursor [Au(tht)Cl] was achieved

via reaction of equimolar amounts of the aforementioned tungsten(0) FCCs and gold(I) precursor in dichloromethane (CH_2Cl_2) at room temperature (Scheme 4.3 (a)). The reactions were monitored by thin layer chromatography (TLC) wherein complete disappearance of the starting W^0 FCCs was observed after several hours. The CH_2Cl_2 solvent was removed *in vacuo* and the reaction mixtures were washed with *n*-hexane and subsequently extracted with CH_2Cl_2 *via* cannula-filtration methods. The CH_2Cl_2 solvent was then removed under vacuum to afford the desired Au^I-FCCs **26** – **29** in near-quantitative yields (92 – 97%). All synthesized ethoxycarbene complexes were subsequently utilized as precursors for access to their less electrophilic *sec*-aminocarbene-analogues *via* reaction with selected primary amines, as indicated in Scheme 4.3 (b) above. The reaction of *n*-propylamine ($^nPrNH_2$) and Au^I ethoxycarbene complexes **27** – **29** in tetrahydrofuran (THF) proceeded smoothly to the formation of new aminocarbene-analogues **30** – **32**. Immediate colour-changes from olive-green (Fu, **27**), yellow (*p*-DMA, **28**), and purple (Fc, **29**) to colourless (Fu, **30**), lime-green (*p*-DMA, **31**), and red (Fc, **32**), respectively, were observed upon addition of $^nPrNH_2$ to the Au^I ethoxycarbene complex solutions. The synthesized gold(I) (hetero)aryl-*n*-propylaminocarbene complexes **30** – **32** were purified by cannula filtration methods as described above, and the complexes were isolated in high yields (90 – 93%). Analogously, reaction of Au^I FCCs **27** – **29** with *N,N*-dimethylethylenediamine (DMEN) in THF at room temperature resulted in modified aminocarbene complexes (**33** – **35**) bearing a pendant tertiary amino (-NMe_2) moiety. The complexes were purified and isolated similarly to the propylaminocarbene analogues. Unfortunately, reaction of the selected amines with the Th-substituted Au^I FCC **26** resulted consistently in reaction mixtures, wherein the targeted aminocarbene complexes could not be separated from unidentified side-products.

All successfully isolated Au^I ethoxy- and amino-carbene complexes (**26** – **29**, and **30** – **35** respectively) were characterized *via* NMR and FT-IR spectroscopic methods in addition to XRD crystallographic, elemental analysis, and mass spectrometry methods (see Section 4.5). Brief analyses of the NMR spectra of all isolated Au^I FCCs **26** – **35** are summarized as follows:

4.3.1.1 Chlorido{(2-thienyl)ethoxycarbene}gold(I) complex 26

The ^1H and $^{13}C\{^1H\}$ NMR spectra of **26** (Figures 4.2 and 4.3 respectively) indicated a chemical environment similar to its methoxy-analogue in literature. A general downfield-shift of all thienyl-ring signals was observed in both the ^1H and $^{13}C\{^1H\}$ NMR spectra (as compared to the W^0-analogue **1**). In addition, a 45 ppm upfield shift of the $C_{carbene}$ signal is evident in Au^I complex **26** in comparison to the

W^0 precursor **1**. This upfield-shift of the carbene carbon atom is consistent with literature reports of W^0-Au^I transmetallation, wherein the isolated Au^I FCCs exhibit $C_{carbene}$ chemical shifts ~50 ppm upfield of their W^0-analogues.[15,18]

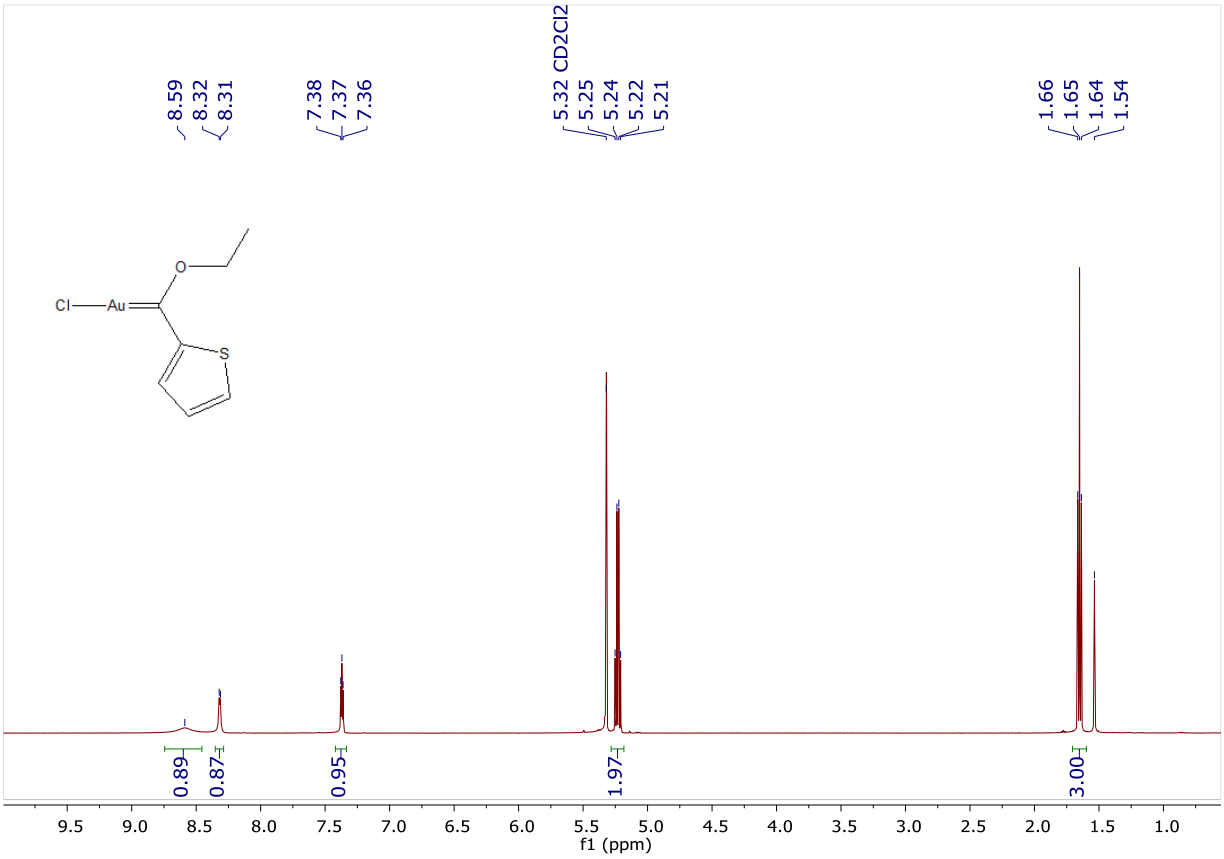

Figure 4.2 ^{1}H NMR spectrum of **26** in CD_2Cl_2

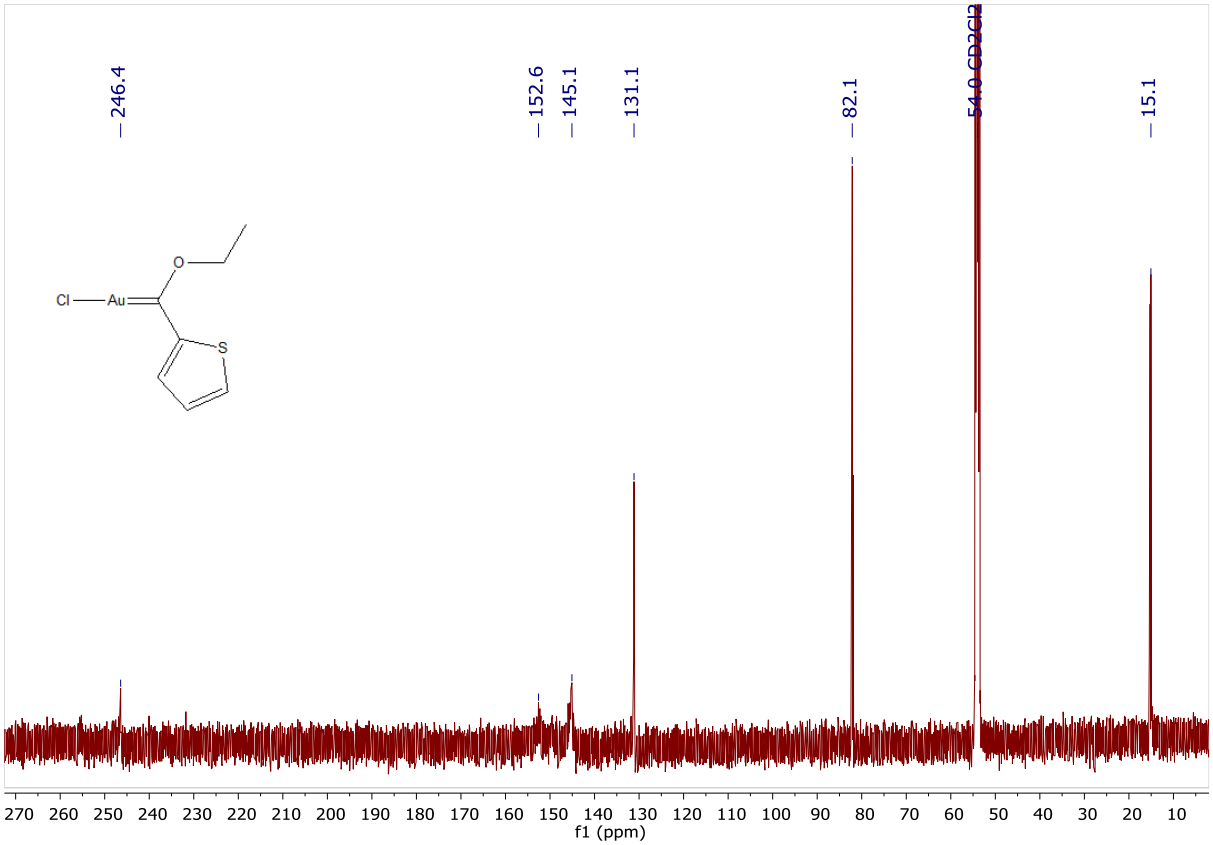

Figure 4.3 $^{13}C\{^{1}H\}$ NMR spectrum of **26** in CD_2Cl_2

4.3.1.2 Chlorido{(2-furyl)ethoxycarbene}gold(I) complex 27

Similarly to the Th-substituted complex **26**, ^{1}H and $^{13}C\{^{1}H\}$ NMR spectra of the Fu-analogue **27** (Figures 4.4 and 4.5 respectively) also indicated a chemical environment comparable its methoxy-analogue in literature.[18] Additionally, a general downfield-shift of all Fu-ring ^{1}H and $^{13}C\{^{1}H\}$ NMR signals, and a 50 ppm upfield sift of the $C_{carbene}$ signal (in comparison to the W^0-analogue **2**) was also observed.

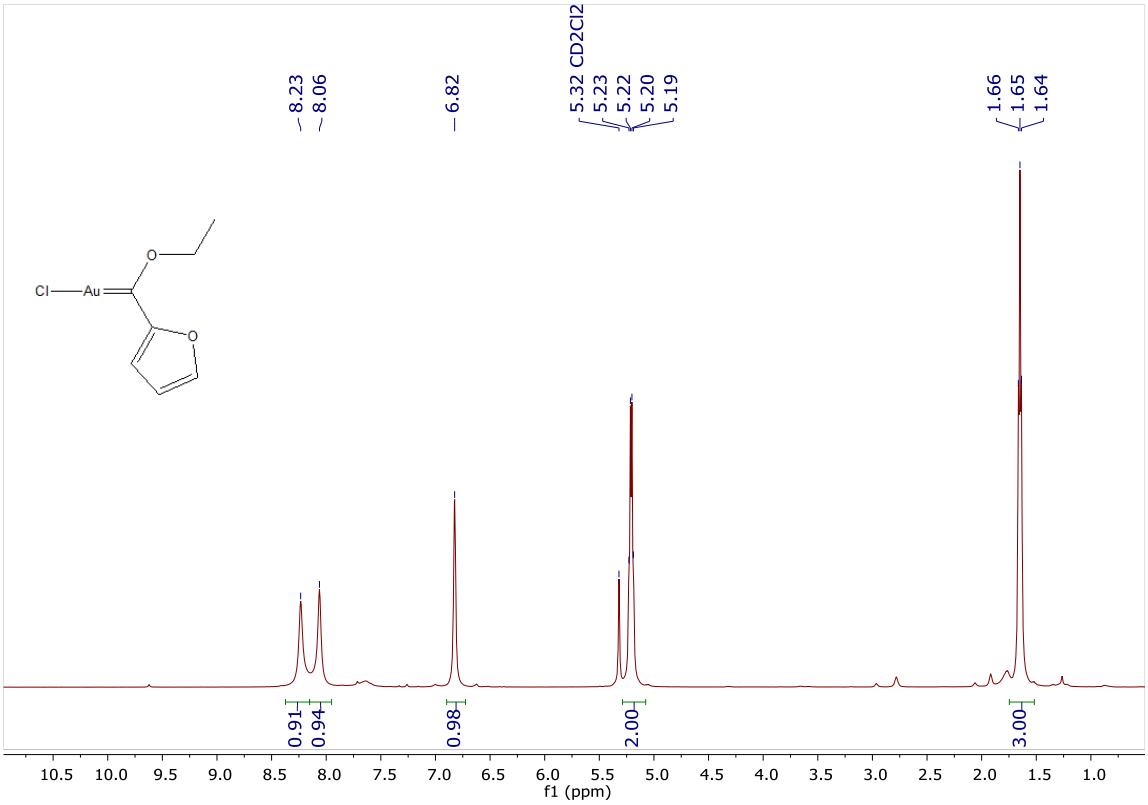

Figure 4.4 ^{1}H NMR spectrum of **27** in CD_2Cl_2

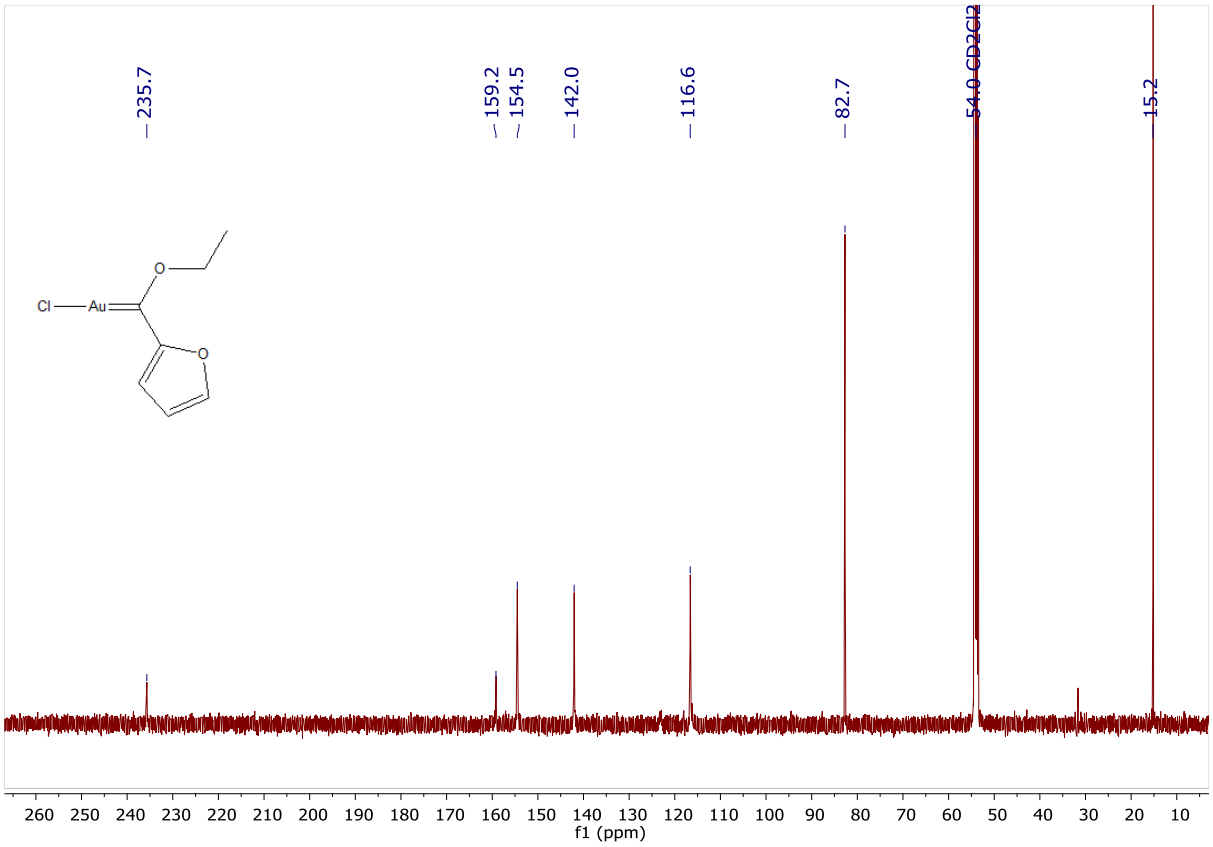

Figure 4.5 $^{13}C\{^{1}H\}$ NMR spectrum of **27** in CD_2Cl_2

4.3.1.3 Chlorido{*p*-(*N*,*N*-dimethylaniline)ethoxycarbene}gold(I) complex 28

^{1}H and $^{13}C\{^{1}H\}$ NMR spectra of complex **28** (see Figure 4.6 and 4.7 below) indicated a completely symmetrical chemical environment for the FC ligand comparable to the W^{0}-analogue **3**, and all *p*-DMA-ring ^{1}H and $^{13}C\{^{1}H\}$ signals resonate at slightly higher-field chemical shifts in the former. This down-field shift is indicative of greater ring-involvement in the stabilization of Au^{I} FCCs in comparison to W^{0}-analogues in literature.[18] In addition, a 53 ppm upfield-shift of the $C_{carbene}$ resonance in **28** (Figure 4.7, 246.2 ppm) as compared to the W^{0} precursor carbene complex **3** (299.7 ppm) was observed, and is in line with NMR spectral features of the Th- and Fu-analogues **26** and **27** discussed above.

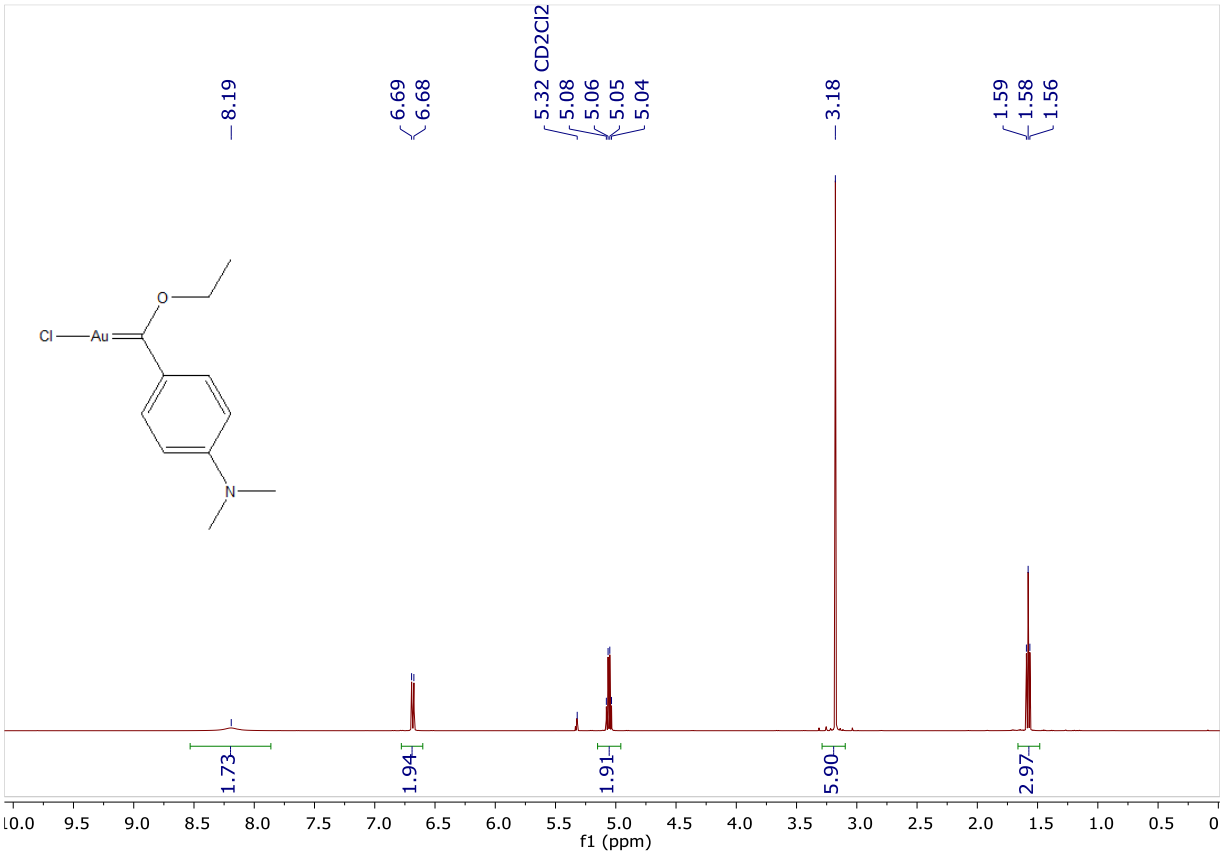

Figure 4.6 ^{1}H NMR spectrum of **28** in CD_2Cl_2

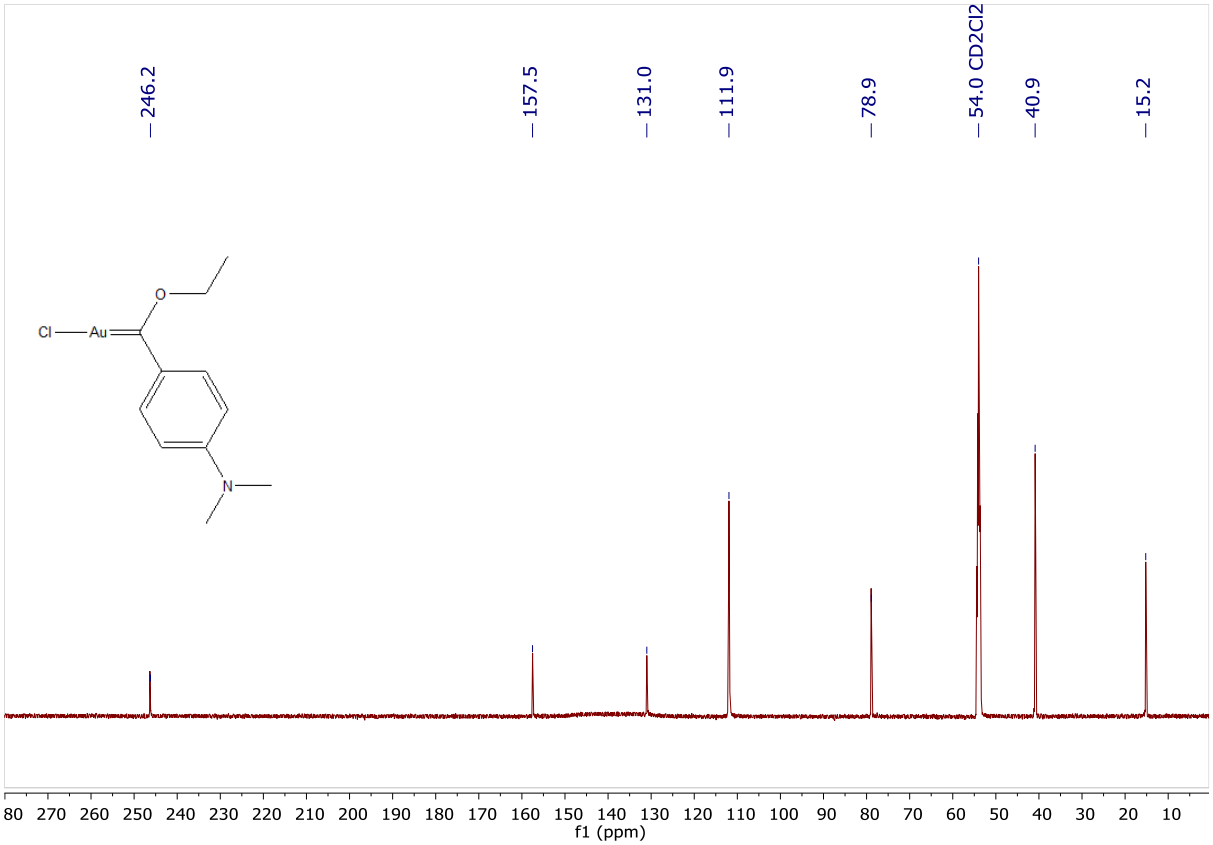

Figure 4.7 $^{13}C\{^{1}H\}$ NMR spectrum of **28** in CD_2Cl_2

4.3.1.4 Chlorido{(ferrocenyl)ethoxycarbene}gold(I) complex 29

This complex has been recently reported in its exact form and thoroughly characterized (*via* NMR and IR spectroscopic methods) by the group of Heinze.[23] ^{1}H, and $^{13}C\{^{1}H\}$ NMR spectra of complex **29** (Figures 4.8 and 4.9, respectively) are hence included only for ease of comparison to the new Fc-aminocarbene complexes **30** and **33** discussed below. A 53 ppm upfield-shift of the $C_{carbene}$ signal in the Au^{I} complex **29** as compared to its W^{0}-analogue **8** was the first indication of successful W^{0}-Au^{I} transmetallation in the synthesis **29**.

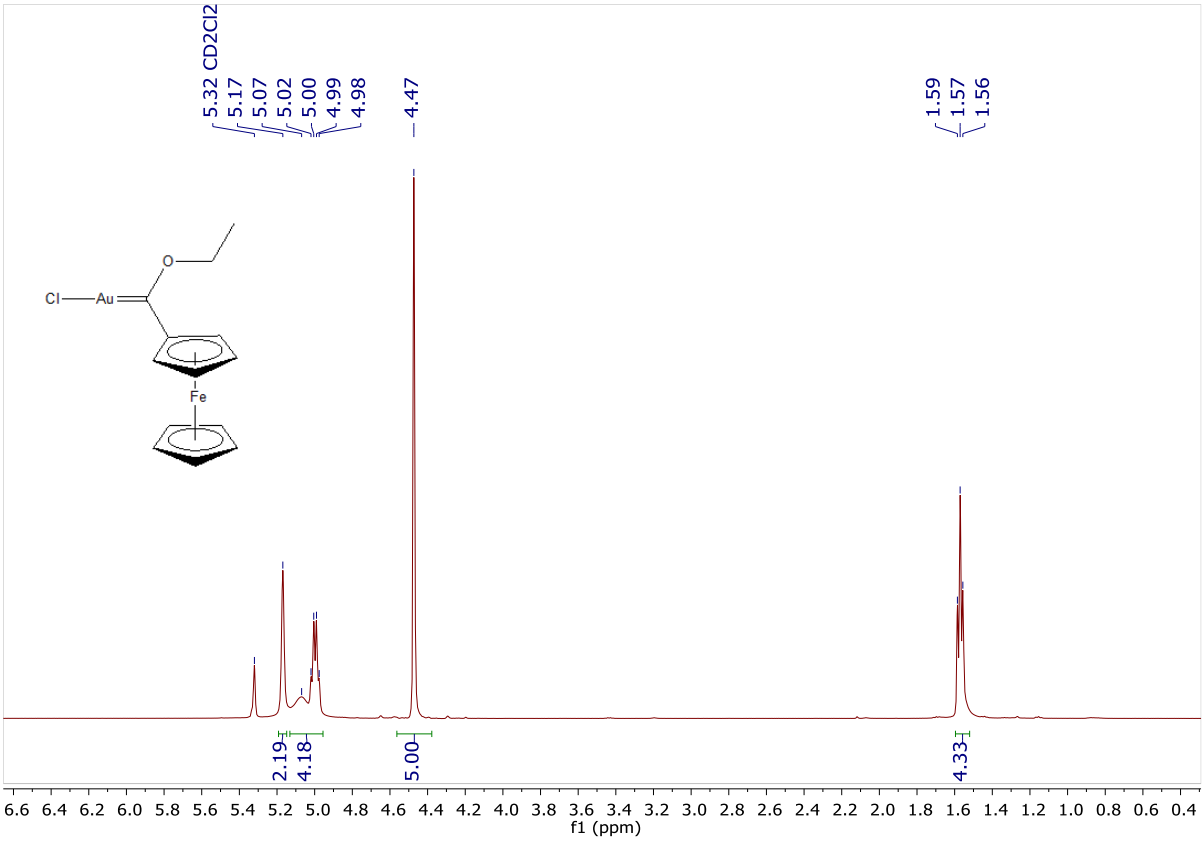

Figure 4.8 ^{1}H NMR spectrum of **29** in CD_2Cl_2

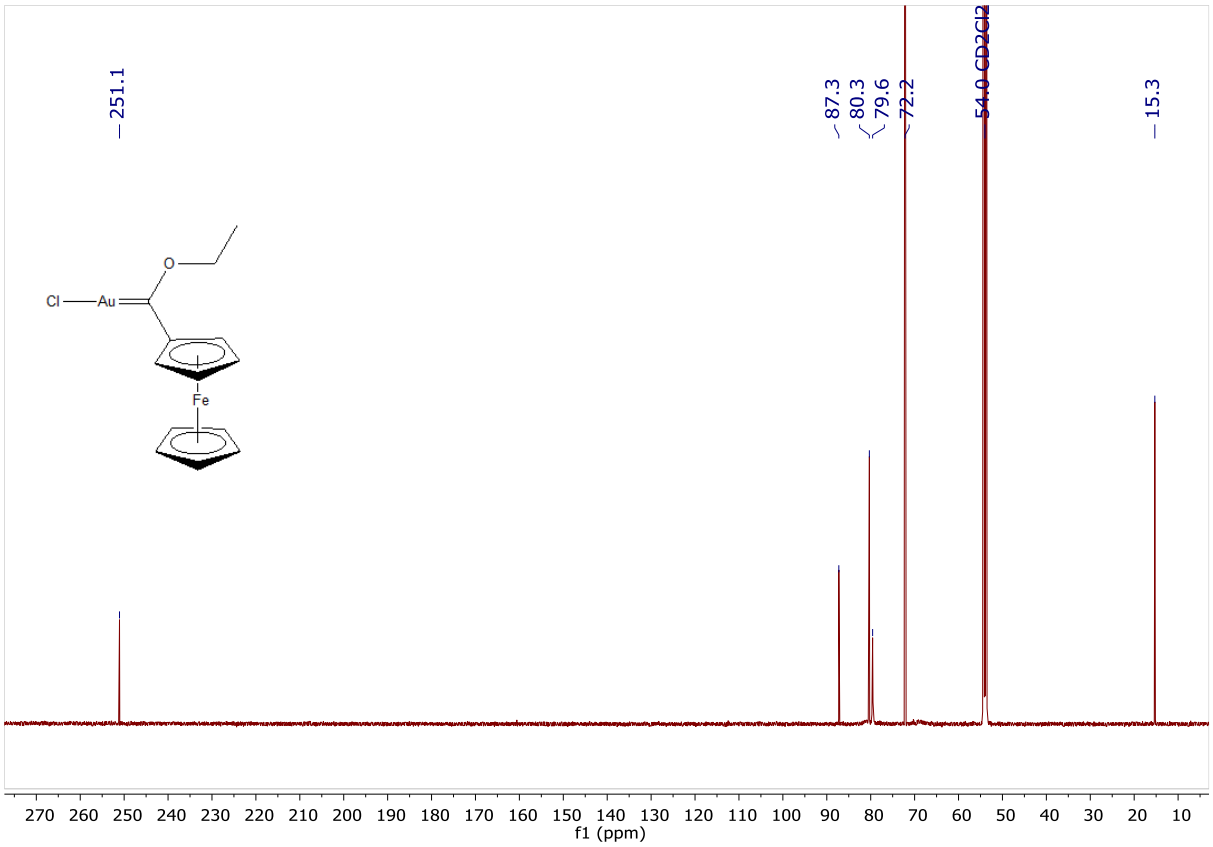

Figure 4.9 $^{13}C\{^{1}H\}$ NMR spectrum of **29** in CD_2Cl_2

4.3.1.5 Chlorido{(2-furyl)-*n*-propylaminocarbene}gold(I) complex 30

^{1}H and ^{13}C{^{1}H} NMR spectra of **30** (Figure 4.10 and 4.11 respectively) indicated a broad signal at 9.21 ppm for the amino-NH proton, and a general upfield-shift of the Fu-ring proton and carbon signals in comparison to its ethoxy-analogue **26**. This notable shielding of the Fu-ring protons and carbons in the *sec*-aminocarbene complex **30** was comparable to its *n*-amino analogue in literature,[18] and is a consequence of strong electron donation from the stabilizing *N*-atom to the carbene carbon atom, resulting in a predominantly more heteroatom-stabilized gold-carbene bond (**30** *vs* **26**). Consequently, the Fu-ring involvement in stabilizing the gold-carbene bond is reduced in the less electrophilic aminocarbene complex **30** as compared to the more electrophilic ethoxy-analogue **26**, and is evidenced by the above-mentioned general upfield-shift of ^{1}H/^{13}C{^{1}H} signals. Additionally, a 39 ppm upfield-shift of the $C_{carbene}$ signal from ethoxycarbene complex **26** to amino-analogue **30** is similarly effected, and is indicative of successful aminolysis in the synthesis complex **30**.

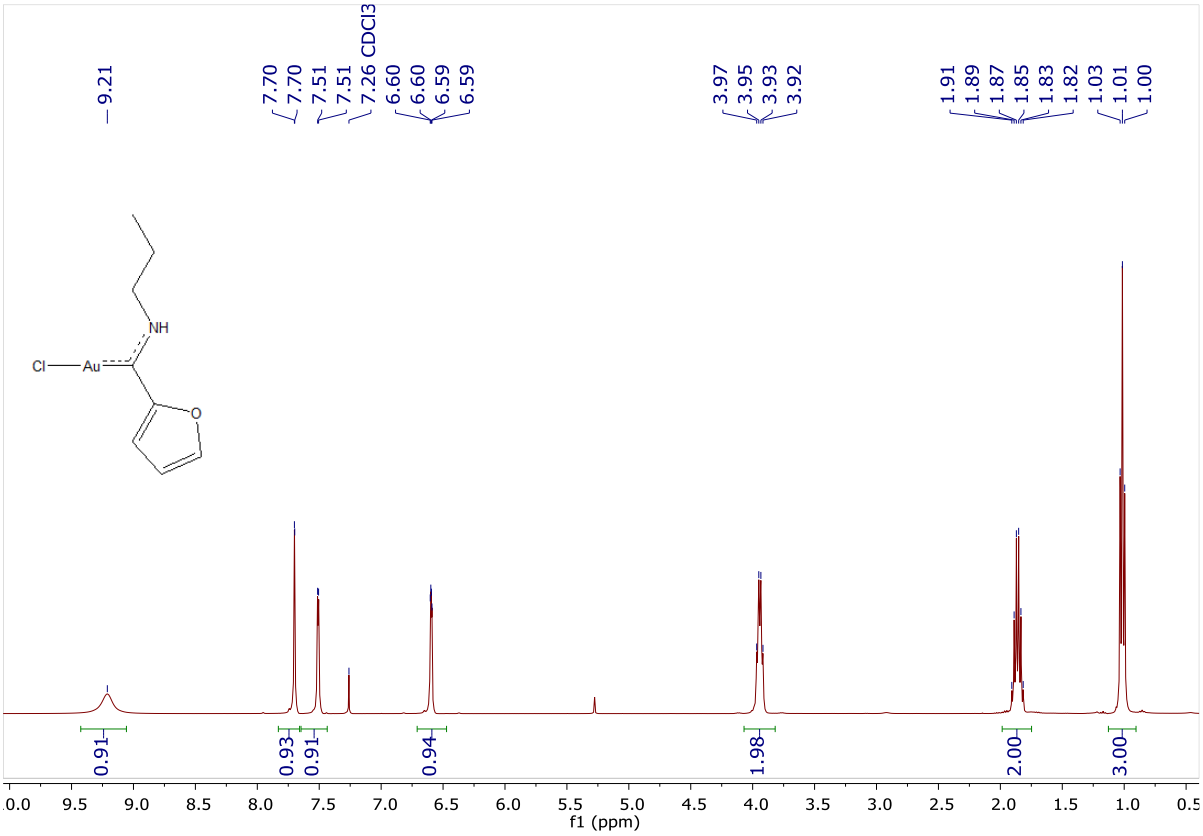

Figure 4.10 ^{1}H NMR spectrum of **30** in $CDCl_3$

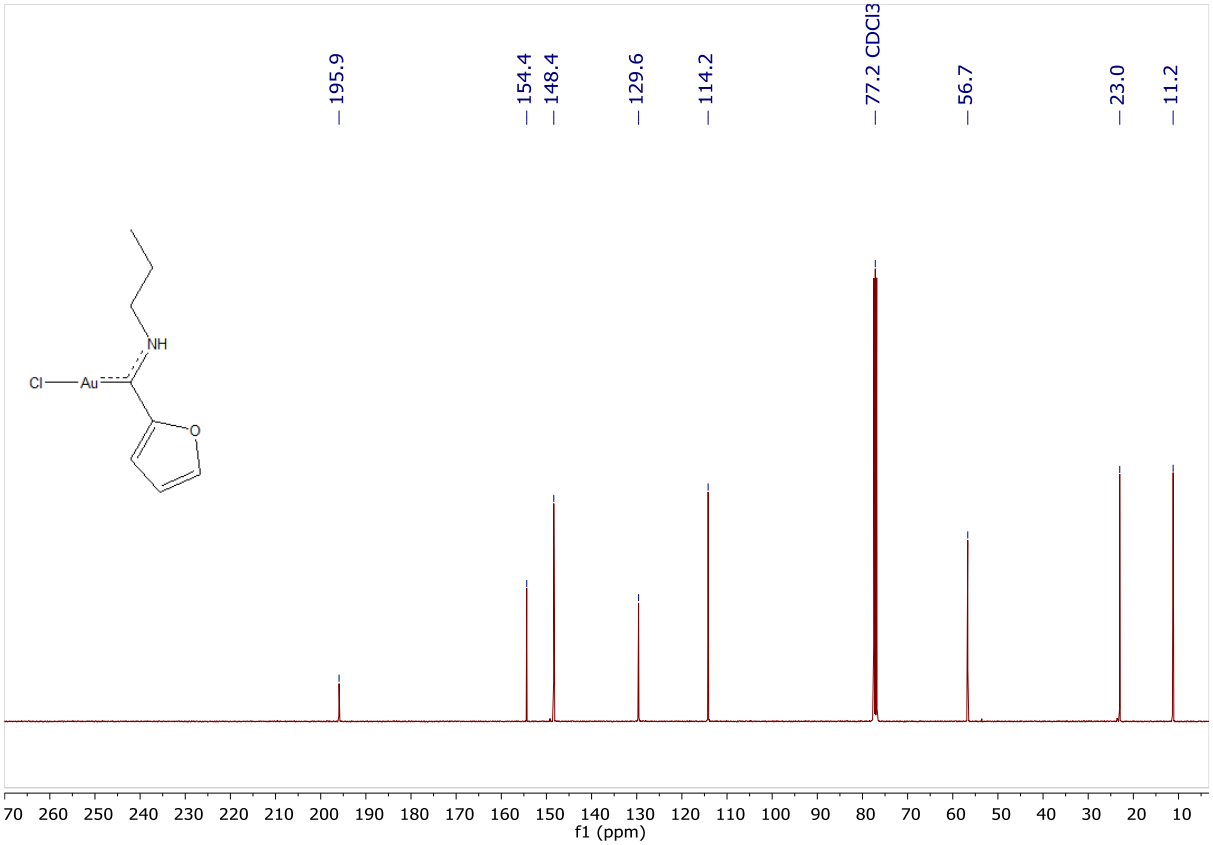

Figure 4.11 $^{13}C\{^{1}H\}$ NMR spectrum of **30** in $CDCl_3$

4.3.1.6 Chlorido{*p*-(*N*,*N*-dimethylaniline)-*n*-propylaminocarbene}gold(I) complex 31

Similarly to the Fu-analogue **30** discussed above, the ^{1}H NMR spectrum of the *p*-DMA complex **31** also indicated a broad signal for the most-downfield chemical shift assigned to the amino-NH proton (8.86 ppm, see Figure 4.12 below). Additionally, the $^{13}C\{^{1}H\}$ NMR spectrum of **31** (Figure 4.13) indicated a 32 ppm upfield-shift of the $C_{carbene}$ signal in comparison to the ethoxy-analogue **28**, and was thus indicative of significant *N*-heteroatom stabilization in **31** as compared to *O*-heteroatom effects in the latter complex.

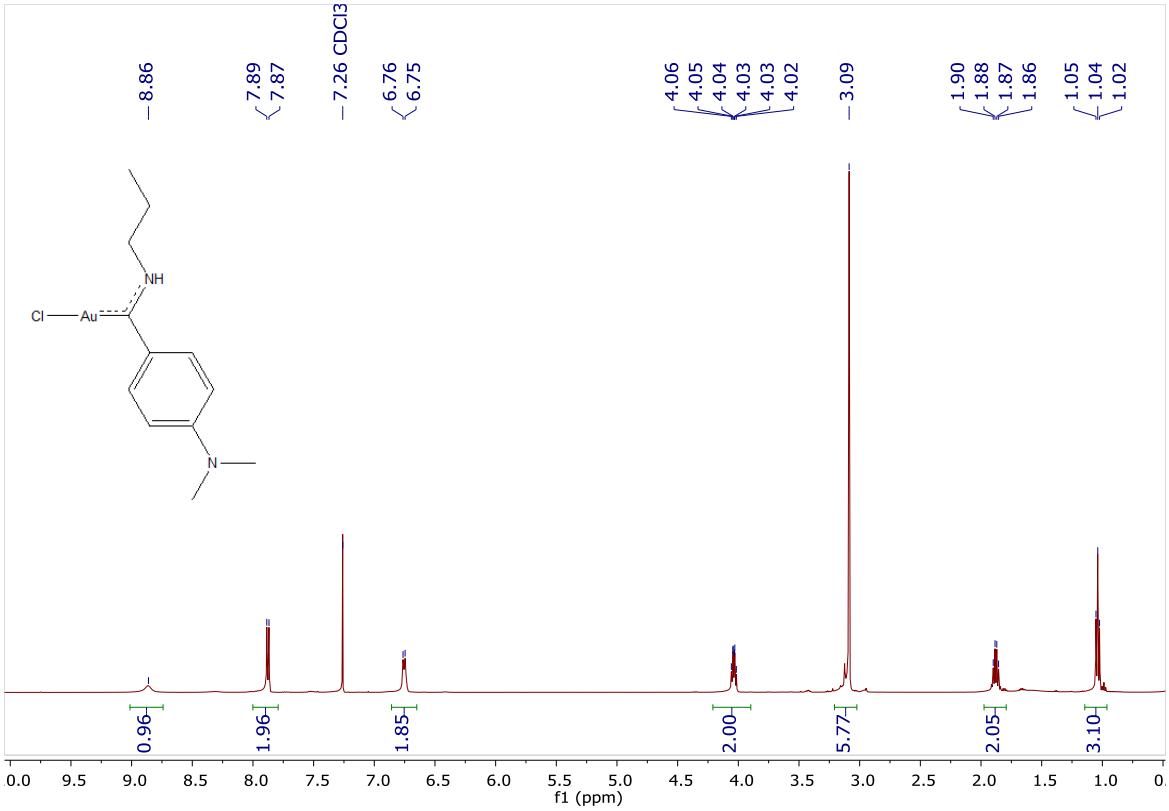

Figure 4.12 ^{1}H NMR spectrum of **31** in $CDCl_3$

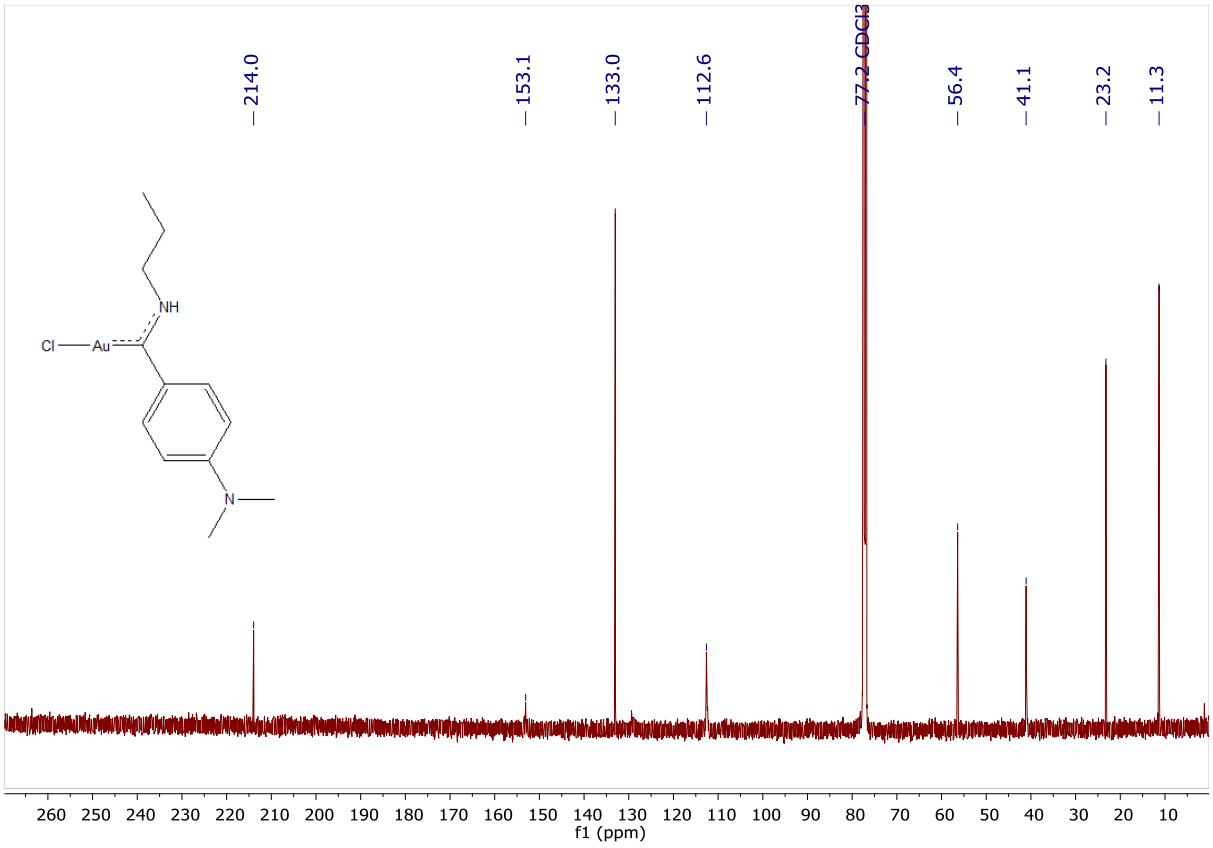

Figure 4.13 $^{13}C\{^{1}H\}$ NMR spectrum of **31** in $CDCl_3$

4.3.1.7 Chlorido{(ferrocenyl)-*n*-propylaminocarbene}gold(I) complex 32

In accordance with respective Fu- and *p*-DMA-substituted aminocarbene complexes **30** and **31** discussed above, ^{1}H NMR spectrum of the Fc-analogue **32** also indicated the amino-NH proton signal at the most-downfield chemical shift (8.29 ppm, see Figure 4.14 below). A 35 ppm upfield-shift of the $C_{carbene}$ signal is also observed in the $^{13}C\{^{1}H\}$ NMR spectrum of aminocarbene complex **32** (Figure 4.15) as compared to its ethoxy-analogue **29**, and is again indication of stronger gold-$C_{carbene}$ bond stabilization by the *N*-atom in complex **32** as compared to the *O*-atom in **29**.

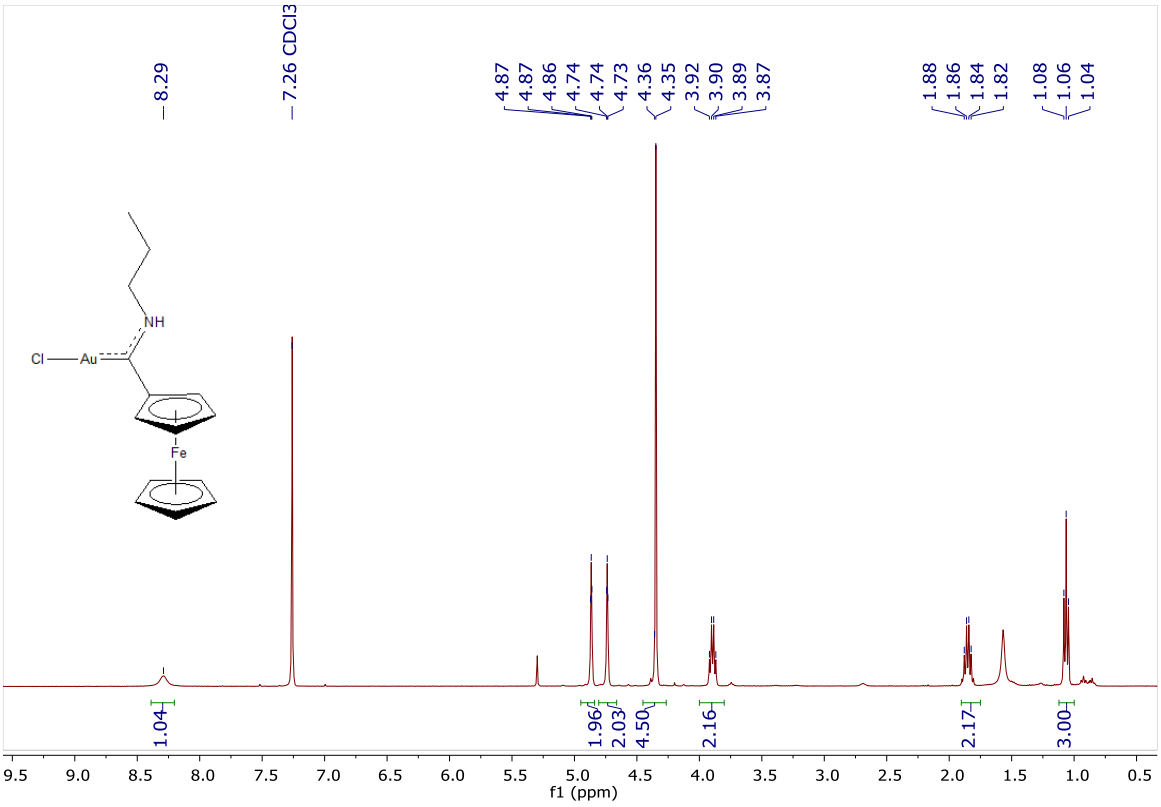

Figure 4.14 ^{1}H NMR spectrum of **32** in $CDCl_3$

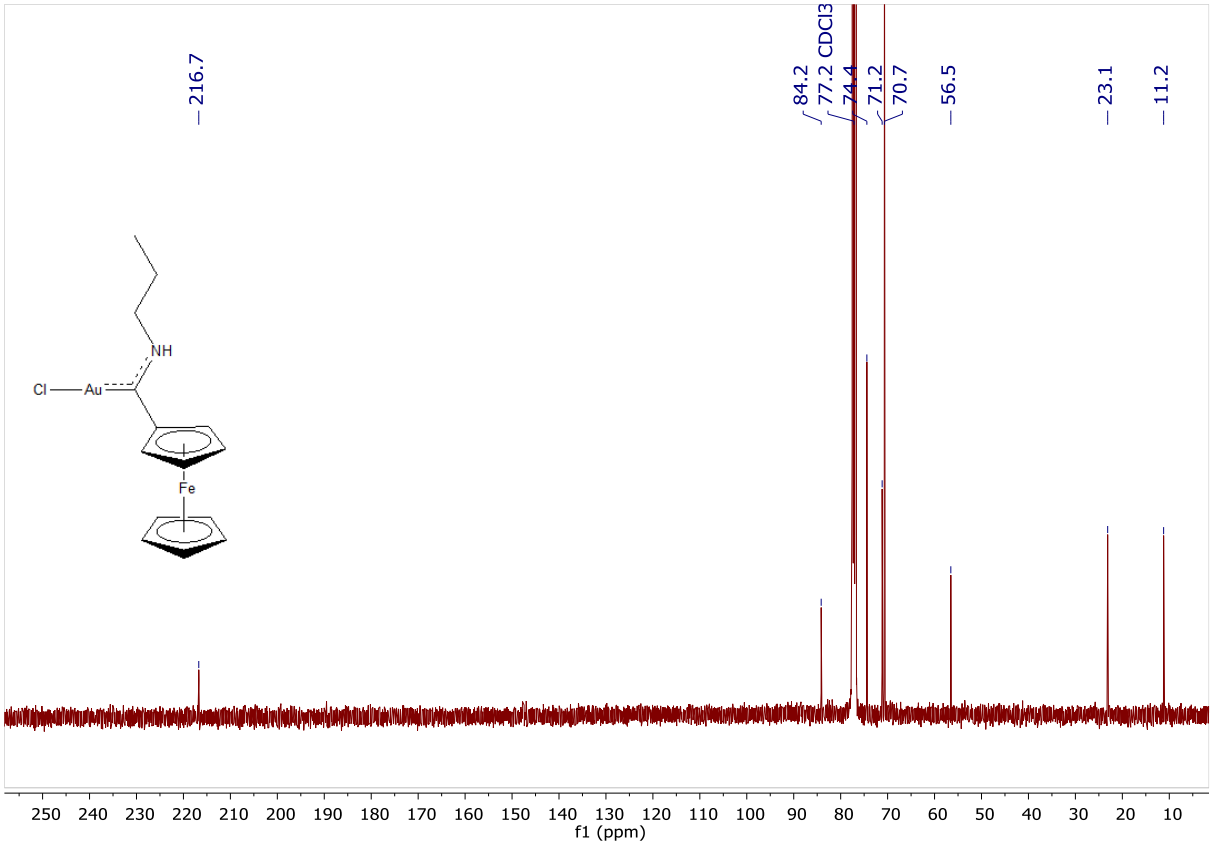

Figure 4.15 $^{13}C\{^{1}H\}$ NMR spectrum of **32** in $CDCl_3$

4.3.1.8 Chlorido{(2-furyl)(*N,N*-dimethylethylenediamino)carbene}gold(I) complex 33

The ^{1}H and $^{13}C\{^{1}H\}$ NMR spectra of diamino complex **33** (Figures 4.16 and 4.17, respectively) indicated a similar chemical environment to the *n*-propylamino analogue **30**. Transformation of the pendant -CH_3 group in complex **30** to a -NMe_2 moiety in **33** does not affect the chemical shift resonances of the proton- or carbon NMR signals in either complex. The $C_{carbene}$ NMR signal remains unchanged in both aminocarbene complexes **30** and **33** (196 ppm in Figure 4.11 and 4.17 respectively) as evidence that the pendant NMe_2 moiety in **33** remains untethered. Therefore, Au^{I} FCC **33** was successfully synthesized.

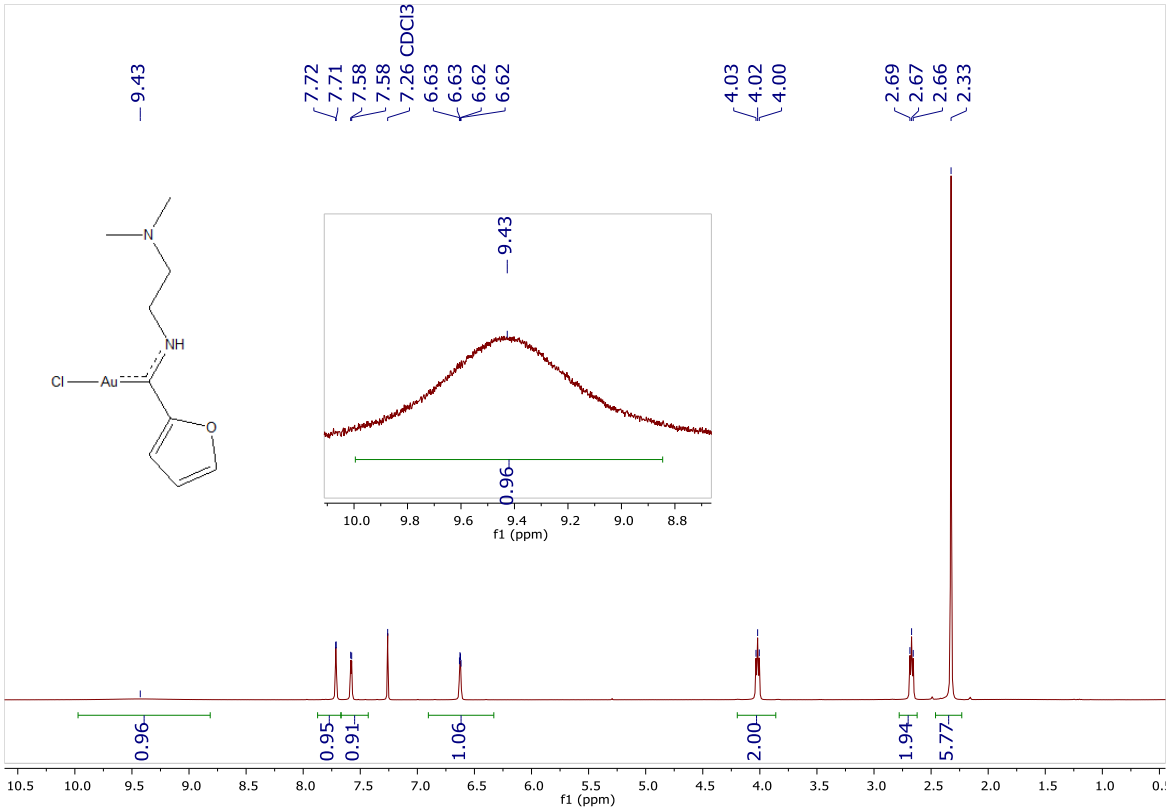

Figure 4.16 ^{1}H NMR spectrum of **33** in $CDCl_3$

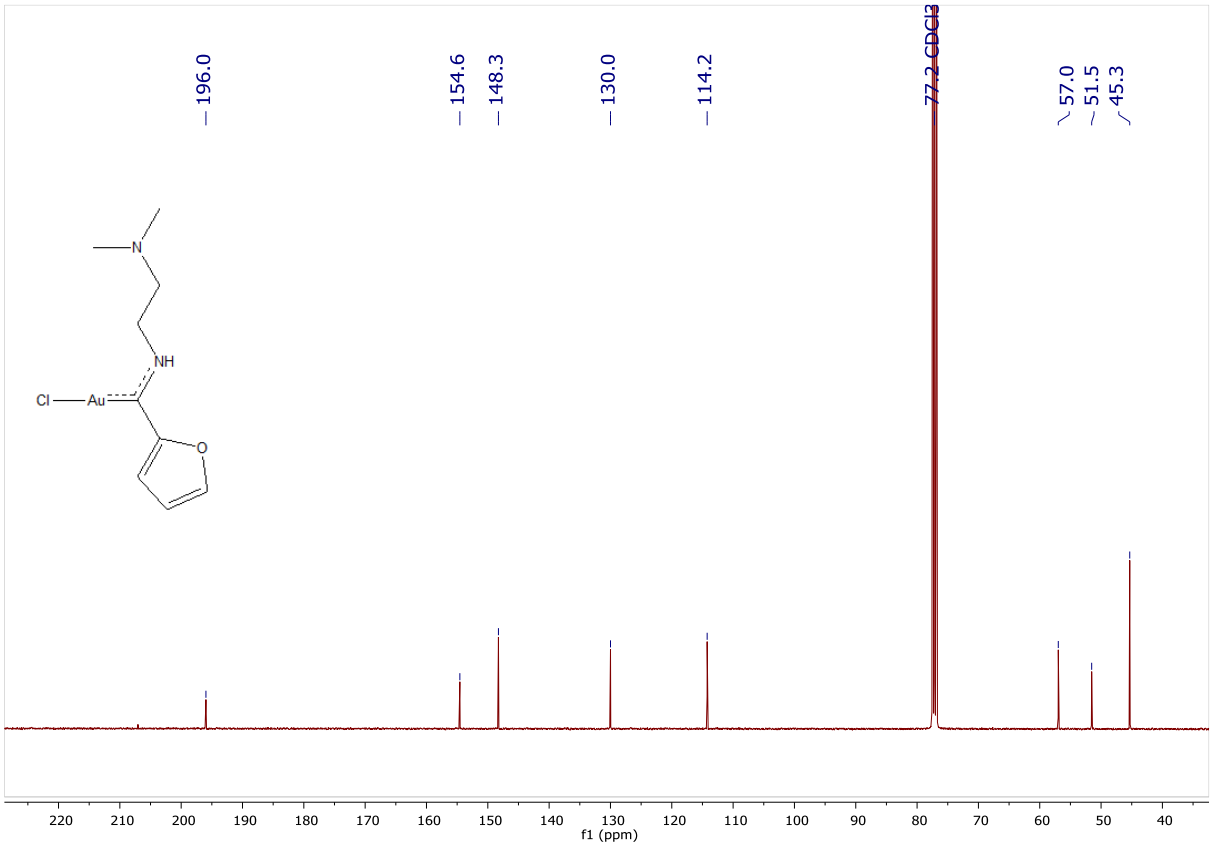

Figure 4.17 $^{13}C\{^{1}H\}$ NMR spectrum of **33** in $CDCl_3$

4.3.1.9 Chlorido{*p*-(*N*,*N*-dimethylaniline)(*N*,*N*-dimethylethylenediamino)carbene}gold(I) complex **34**

Similarly, the ^{1}H and $^{13}C\{^{1}H\}$ NMR spectra of complex **34** (Figures 4.18 and 4.19 respectively) also indicated negligible to no change in ^{1}H or $^{13}C\{^{1}H\}$ NMR signals as compared to the propylamino-analogue **31**. Additionally, only a 1 ppm difference is evident in the $C_{carbene}$ chemical shift for complex **34** as compared to **31**, and is reminiscent of -NMe_2 and -CH_3 effects (in **31** vs **28** respectively) discussed above. Thus, the targeted complex **34** was successfully synthesized, and the pendant -NMe_2 moiety remains untethered.

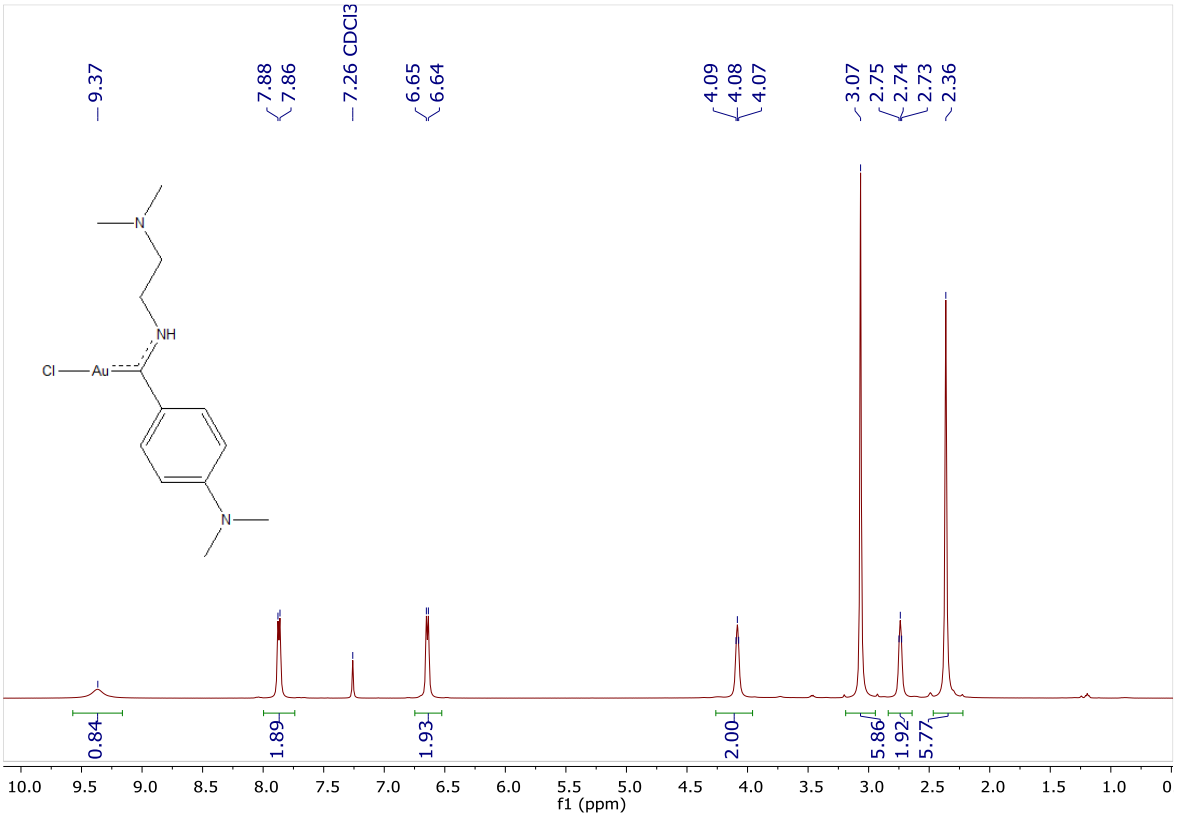

Figure 4.18 ^{1}H NMR spectrum of **34** in $CDCl_3$

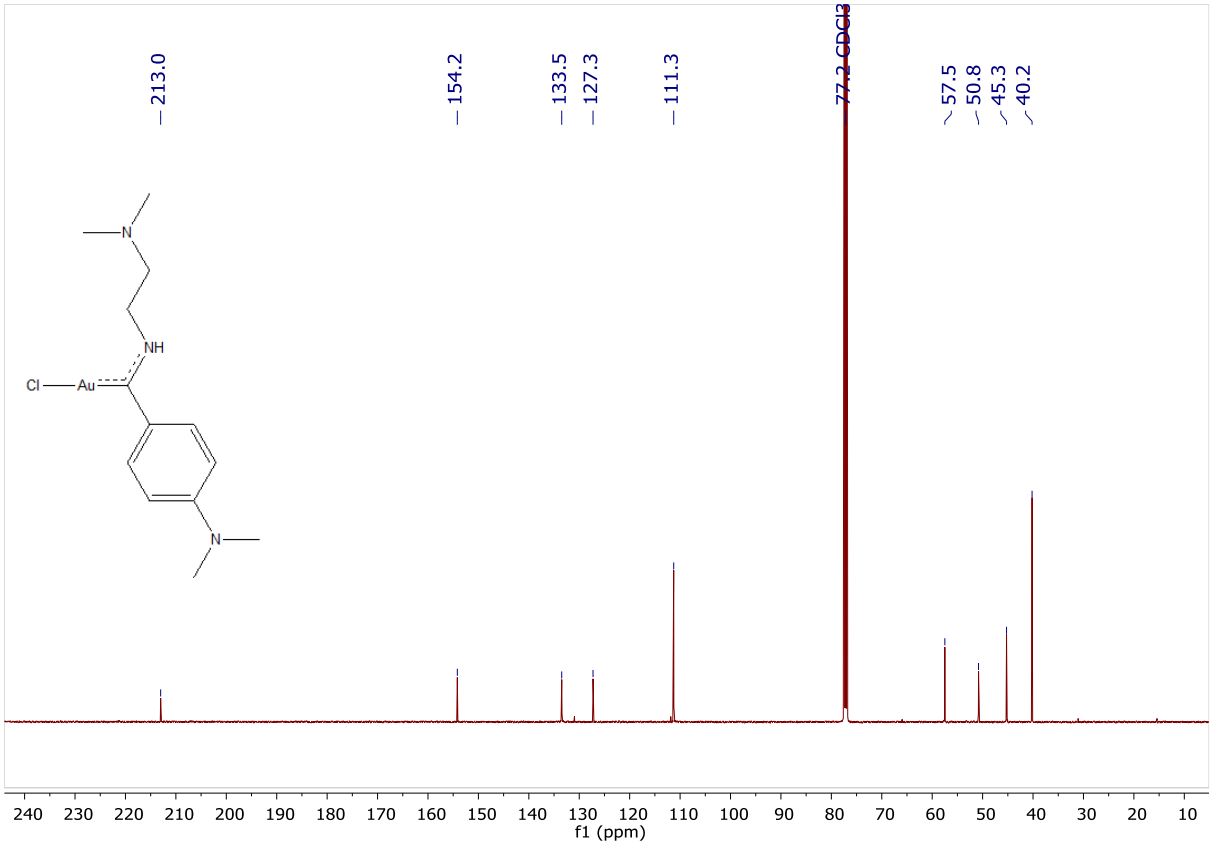

Figure 4.19 $^{13}C\{^{1}H\}$ NMR spectrum of **34** in $CDCl_3$

4.3.1.10 Chlorido{(ferrocenyl)(*N,N*-dimethylethylenediamino)carbene}gold(I) complex 35

In like manner to the Fu- and *p*-DMA analogues **33** and **34**, the ^{1}H and $^{13}C\{^{1}H\}$ NMR spectra of Fc-carbene complex **35** (Figures 4.20 and 4.21) also indicated a similar chemical environment to its propylamino-analogue **32**. A constant chemical shift of 216 ppm is observed for the $C_{carbene}$ signal in both Fc-aminocarbene complexes **32** and **35**, as indication that the -NMe_2 moiety in **35** remains untethered.

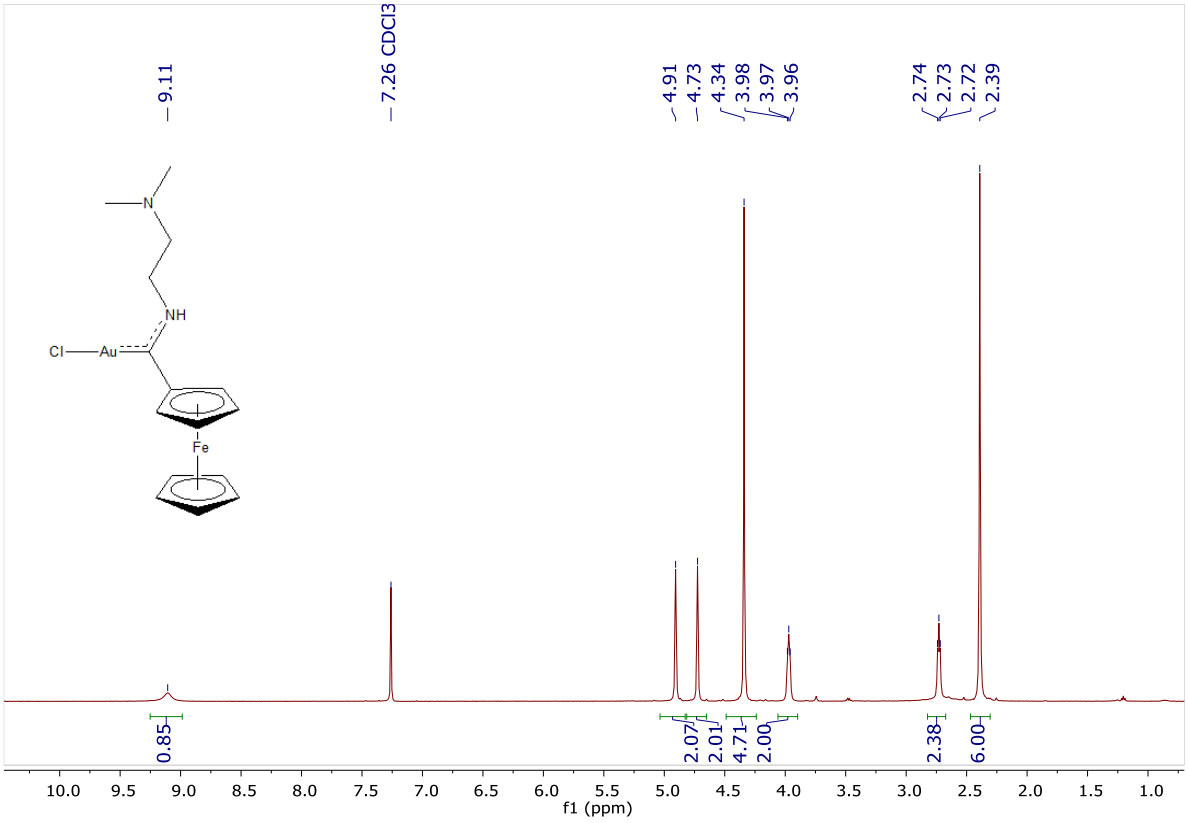

Figure 4.20 ^{1}H NMR spectrum of **35** in $CDCl_3$

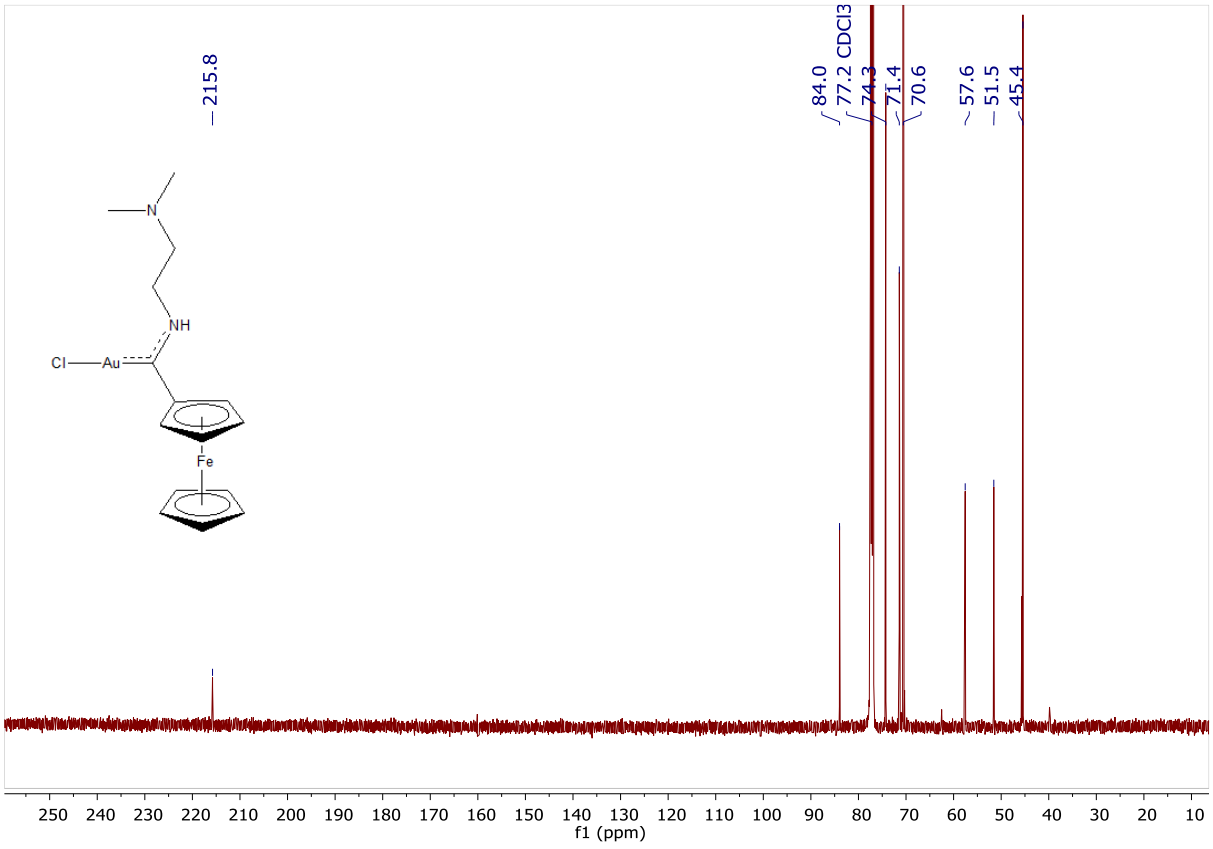

Figure 4.21 $^{13}C\{^{1}H\}$ NMR spectrum of **35** in $CDCl_3$

4.3.2 A comparative view

A more detailed comparison of the different alkoxy-, amino- and (hetero)aryl carbene substituents NMR spectroscopic effects is discussed in this section. All isolated gold(I) FCCs **26** – **35** were also characterized by single crystal X-ray diffraction and mass spectrometry, and the results are briefly discussed in this section. The redox behaviour of aminocarbene complexes **30** – **35** was also investigated *via* electrochemical analysis and computational calculations, and the results are also discussed herein.

4.3.2.1 NMR spectroscopic trends of gold(I) Fischer carbene complexes

Comparison of the $^{13}C\{^{1}H\}$ NMR spectra of gold(I) complexes discussed above is hence reported to highlight the different electron-donating ability of the Th, Fu, *p*-DMA, and Fc carbene substituents. The NMR $C_{carbene}$ resonances of Au^{I} ethoxycarbene complexes increase in magnitude from the Fu-substituted **27** (235.7 ppm) through the Th- and *p*-DMA-substituted **26** and **28** (246.4 and 246.2 ppm respectively), with the Fc-substituted analogue **29** (251.1 ppm) showing the highest chemical shift in the series. This suggests that the Fu carbene substituent is more electron donating than the *p*-DMA, Th, and Fc substituents. A similar trend is observed in the $C_{carbene}$ NMR resonances of aminocarbene complexes **30** – **35**. The lowest $C_{carbene}$ chemical shifts are consistently observed for Fu-substituted complexes (**30**, -NH^{n}Pr, 195.9 ppm; **33**, -NH$(CH_2)_2NMe_2$, 196.0 ppm) as compared to the *p*-DMA- (**31**, -NH^{n}Pr, 214.0 ppm; **34**, -NH$(CH_2)_2NMe_2$, 213.0 ppm) and Fc-substituted analogues (**33**, NH^{n}Pr, 216.7 ppm; **35**, -NH$(CH_2)_2NMe_2$, 215.8 ppm). This electron-donation trend is however inverted, in terms of the TEPs of FC ligands discussed in Chapters 2 and 3. Specifically, *p*-DMA-substituted ethoxy- and aminocarbene ligands were shown to be consistently more electron-donating than their Fc-analogues. In addition, the previously reported instability of Fu- and Th-substituted Rh^{I}-cod complexes resulting in carbene-dimerization decomposition whereas the *p*-DMA and Fc analogues were stable and could be characterized, suggests a much weaker electron-donating strength of Fu and Th carbene substituents within the reported series. Therefore, $^{13}C\{^{1}H\}$ NMR spectroscopy of Au^{I} FCCs **26** – **35** is an unreliable tool to determine the electron-donating ability of the different aryl carbene substituents.

4.3.2.2 Single-crystal XRD crystallography

XRD crystallography was employed to confirm the solid-state structures of complexes **26** – **32**, **34**, and **35**. Single-crystals suitable for X-ray diffraction were grown by slow diffusion of *n*-hexanes into concentrated CH_2Cl_2 solutions of the Au^{I} FCCs, and the crystal structures of complexes **26** – **32**, **34**, and **35** were determined (see Figure 4.22 (a) – (i) below). Selected bond lengths and angles of the

complexes are subsequently summarized in Table 4.1. Crystal structures of aminocarbene complexes **34** (h) and **35** (i) indicate that the pendant -NMe_2 moiety remains untethered in the solid state.

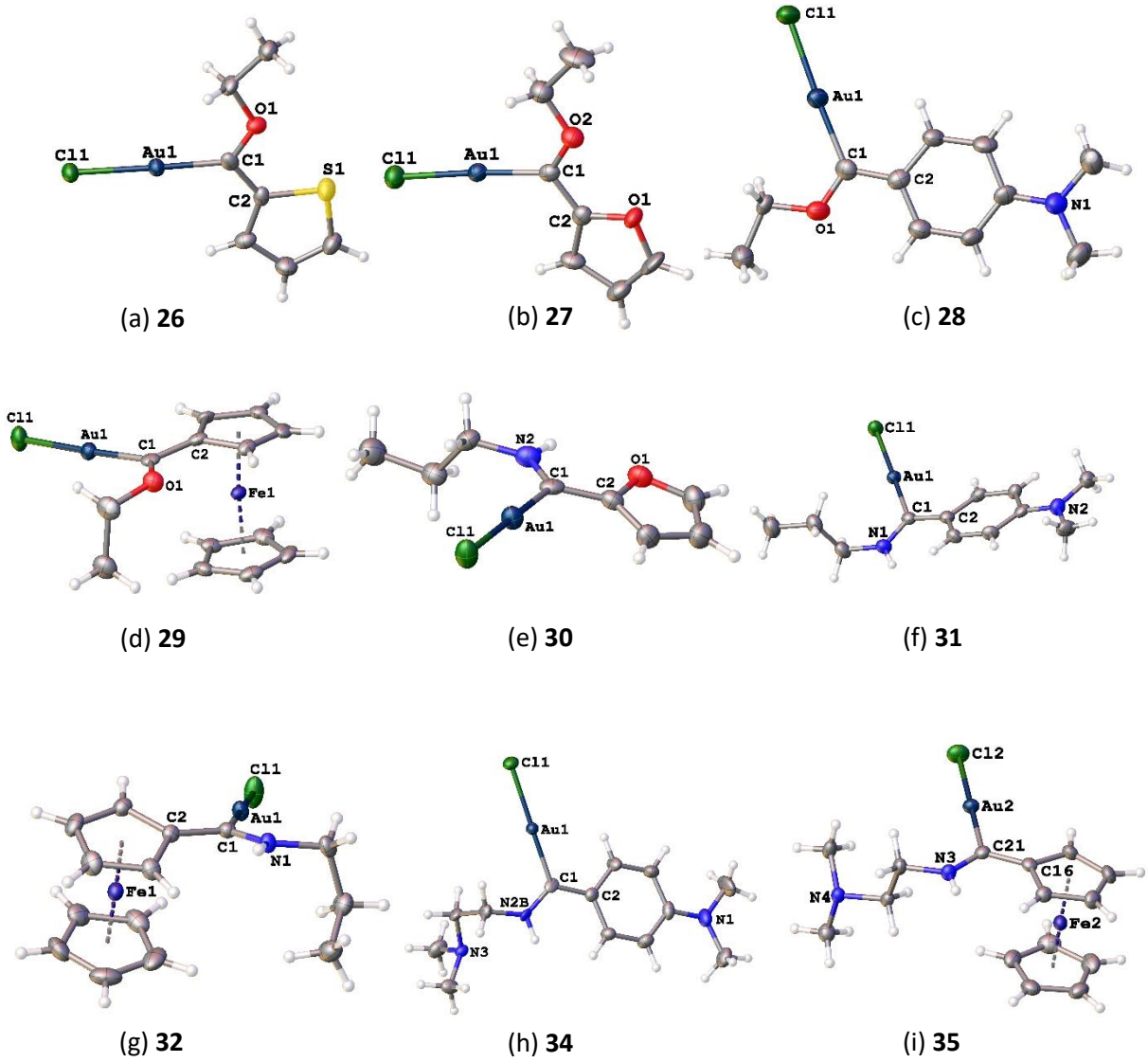

Figure 4.22 Crystal structures of Au^{I} FCCs **26** – **32**, **34**, and **35**.

Table 4.1 Selected bond lengths (Å) and angles (°) of Au^{I} FCCs **26** – **32**, **34**, and **35**.

	26	**27**	**28**	**29**	**30**	**31**	**32**	**34**	**35**
					Bond lengths				
Au-$C_{carbene}$	1.954(6)	1.956(7)	2.001(15)	1.972(5)	1.991(5)	1.992(5)	1.982(4)	2.011(12)	2.000(3)
$C_{carbene}$-O/N	1.311(6)	1.299(8)	1.314(17)	1.309(6)	1.294(6)	1.306(6)	1.310(5)	1.338(15)	1.300(4)
$C_{carbene}$-C_{ipso}	1.434(8)	1.411(10)	1.410(2)	1.424(7)	1.450(7)	1.468(6)	1.447(5)	1.457(16)	1.454(5)
Au-Cl	2.292(14)	2.279(19)	2.301(4)	2.285(13)	2.294(12)	2.308(11)	2.292(11)	2.299(3)	2.311(9)
					Bond angles				
$C_{carbene}$-Au-Cl	175.4(15)	176.4(2)	177.4(4)	177.4(15)	179.8(14)	177.5(12)	177.4(11)	179.2(4)	178.6(9)
O/N-$C_{carbene}$-C_{ipso}	111.1(5)	113.2(7)	114.6(13)	112.2(4)	116.6(4)	117.4(4)	116.0(3)	120.8(10)	117.0(3)
					Torsion angles				
C_{α}-C_{ipso}-$C_{carbene}$-O/N	1.8(6)	0.0(2)	0.0(2)	10.6(6)	4.3(6)	18.6(6)	28.2(6)	10.0(18)	3.7(5)

A linear geometry around the central Au^{I} metal is evident in the crystal structures of carbene complexes **26** – **32**, **34**, and **35**, with Cl-Au-$C_{carbene}$ bond angles ranging between 175.4(15)° and 179.2(4)°. Shorter C_{ipso}-$C_{carbene}$-X (X = *O*, *N*) bond angles are consistently observed for ethoxycarbene complexes **27** – **29** in comparison their respective amino-analogues **30** (Fu), **31**/**34** (*p*-DMA), and **32**/**35** (Fc), and are ascribed to stronger electron donation from the stabilizing *N*-heteroatom in aminocarbene complexes as compared to the ethoxy-analogues (*O*-heteroatom). In general, short Au-$C_{carbene}$ bond distances in the range 1.954(6) – 2.001(15) Å were observed for ethoxycarbene complexes, as compared to the longer Au-$C_{carbene}$ bond lengths (1.982(4) – 2.011(12) Å) evident in aminocarbene complexes. However, acute and ambiguous changes in these bond-lengths are observed when comparing ethoxy- complexes bearing Fu, *p*-DMA, and Fc FC ligand substituents to their amino-analogues. As expected, shorter Au-$C_{carbene}$ bond lengths are evident for Fu- and Fc-ethoxycarbene complexes **27** and **29** (1.956(7) Å and 1.972(5) Å respectively) in comparison to their respective amino-analogues **30** and **32**/**35** (1.991(5) Å and 1.982(4)/ 2.000(3) Å respectively).

Comparison of the *p*-DMA-ethoxycarbene complex **28** to its propylamino-analogue **31** inexplicably deviates from the expected effect of *O*- and *N*-heteroatoms, whereby the Au-$C_{carbene}$ bond length is longer in complex **28** (*O*-, 2.001(15) Å) and shorter in **31** (*N*-, 1.992(5) Å). However, the accompanying high standard deviation in the Au-$C_{carbene}$ bond length of **28**, indicating a high level of uncertainty in the measured distance, suggests that these bond lengths are similar in the ethoxycarbene complex **28** and amino-analogue **31**. In addition, a slightly longer $C_{carbene}$-*O* bond length is observed in the Fu-substituted ethoxycarbene complex **27** (1.299(8) Å) as compared to the $C_{carbene}$-*N* distance in aminocarbene-analogue **30** (1.294(6) Å), due to lesser *O*-heteroatom stabilization in the former as compared to greater *N*-heteroatom stabilization in the latter. A similar trend is observed for the *p*-DMA-substituted complexes **28** and **31** (a slightly longer $C_{carbene}$-X bond length is observed for ethoxy-**28** (*O*-, 1.314(17) Å) compared to mono-amino **31** (*N*-, 1.306(6) Å)). The opposite trend is however evident in the di-amino *p*-DMA-carbene complex **34**, where a notably higher $C_{carbene}$-*N* bond length of 1.338(15) is evident (as compared to the 1.314(17) Å $C_{carbene}$-*O* distance in **28**). The high standard deviations of $C_{carbene}$-X (X = *O*, *N*) bond lengths of **28** and **34** again suggest that the observed trends may be inaccurate. Comparison of the Fc-substituted complexes indicates equivalent $C_{carbene}$-X (X = *O*,*N*) bond lengths, whereby an insignificantly shorter $C_{carbene}$-X (X = *O*, *N*) bond length is observed for Fc-diaminocarbene complex **35** (*N*-, 1.300(4) Å) compared to its mono-amino analogue **32** (*N*-, 1.310(5) Å) and to the ethoxy-counterpart **29** (*O*-, 1.309(6) Å). The evident, albeit minor elongation of Au-$C_{carbene}$ and $C_{carbene}$-X bond distances (and wider X-$C_{carbene}$-C_{ipso} (X = *O*, *N*) angles) in aminocarbene complexes when compared to their ethoxy-analogues, is brought about by stronger electron donation from the stabilizing *N*-atom to the carbene carbon atom as compared to weaker electron donation from *O*-atom, respectively. These heteroatom-effects are in agreement with similar comparisons of Au^{I} alkoxy- and amino-FCCs in literature,[18] as well as analogous effects in group 6 and 9 FCCs.[39–42] Finally, the observed C_{α}-C_{ipso}-$C_{carbene}$-X (X = *O*, *N*) torsion angles mostly indicate an almost-planar FC ligand in complexes **26** – **30**, **34**, and **35** (0.0(2) – 10.6(6)°), except in the case of the propylamino-substituted *p*-DMA complex **31** and Fc analogue **32** where torsion angles increase to 18.6(6)° and 28.2(6)°, respectively.

Crystal structures of gold(I) complexes occasionally exhibit close inter- and intramolecular Au···Au interactions, wherein unusually strong closed-shell interactions ($d^{10}\cdots d^{10}$) governed by relativistic contraction of gold orbitals, are evident as reported in literature.[43,44] These closed-shell interactions are observed in the solid-state of gold(I) complexes and clusters, and have also been reported for the neighbor-metals silver, copper, platinum, and mercury.[9] In Au^{I} complexes, aurophilic interactions are said to be genuine if the ensuing Au-Au bond distances range from 2.50 Å to 3.50 Å.[45] Additionally,

aurophilic interactions are classified as semi- or fully-supported depending on the presence of one or two multi-atomic bridging moieties, respectively. In the absence of any bridging molecules, the rare unsupported aurophilic interactions are occasionally reported. Strong electron-donor ligands are said to promote aurophilicity when coordinated to Au^{I} metal centers, while more steric bulk in the ligand environment destabilizes the ensuing Au···Au interaction.[43] Inter- and intramolecular Au···Au interactions have been sparingly reported for Au^{I}-NHCs in literature, and are generally associated with the luminescent behavior of these complexes in both the solution and solid-state.[46] For Au^{I} FCCs in literature, a Au^{I}-Au^{I} bond distance of 3.3866(3) Å was first observed for Raubenheimer's thiazolyl-substituted Au^{I}-FCC.[15] Additionally, our research group reported Au···Au interactions of (hetero)aryl- and ferrocenophane-substituted mono- and biscarbene complexes respectively (Au-Au bond distances ranging between 3.0354(10) Å and 3.3073(2) Å).[18] The reported methoxy- and *n*-aminocarbene complexes bearing Th, Fu, and Fc, carbene substituents indicated unsupported Au···Au interactions, while a semi-supported aurophilicity was reported for a ferrocenophane-bridged dinuclear biscarbene complex. DFT calculations (at the Atoms In Molecule (AIM) and Natural Bond Orbital (NBO) levels of theory) reportedly characterized the Au···Au interactions as donation of electron density from a doubly-occupied d-orbital of one Au^{I}-metal atom to an empty p-orbital of the other (interacting) Au^{I} metal atom.

Of the nine Au^{I}-FCC crystal structures reported herein, genuine aurophlilic interactions (depicted in Figure 4.23 below) were only observed in the crystal structures of Th- and Fu-ethoxycarbene complexes **26** ((a), (d)) and **27** ((b), (e)), respectively and in the Fc-aminocarbene complex **35** ((c), (f)). Infinite Au···Au interactions are evident in the Fu-substituted complex **27**, wherein every Au^{I} metal center interacts with two other Au^{I} centers in continuous Au-Au chains (Au-Au = 3.3641(2) Å). However, finite aurophilic interactions are observed in Th- and Fc-substituted complexes **26** and **35**, respectively ((d) and (f), Au-Au = 3.2557 (3) and 3.0783(2) Å, respectively). The shortest Au-Au bond distance is observed for the Fc-carbene complex **35**. During the crystallization process, *in situ* protonation of the pendant -NMe_2 moiety yields a monocationic -NMe_2H analogue stabilized by a chloride counterion ([**35**H]$^{+}$$Cl^{-}$) and by strong aurophilic interaction with the neutral isolated complex **35** (see Figure 4.23 (c)). The observed Au-Au distances all fall within range of unsupported Au···Au interactions for Au^{I}- FCCs (3.0925(2) – 3.3866(3) Å)[15,18] and -NHCs (3.2042(2) Å)[47] in literature.

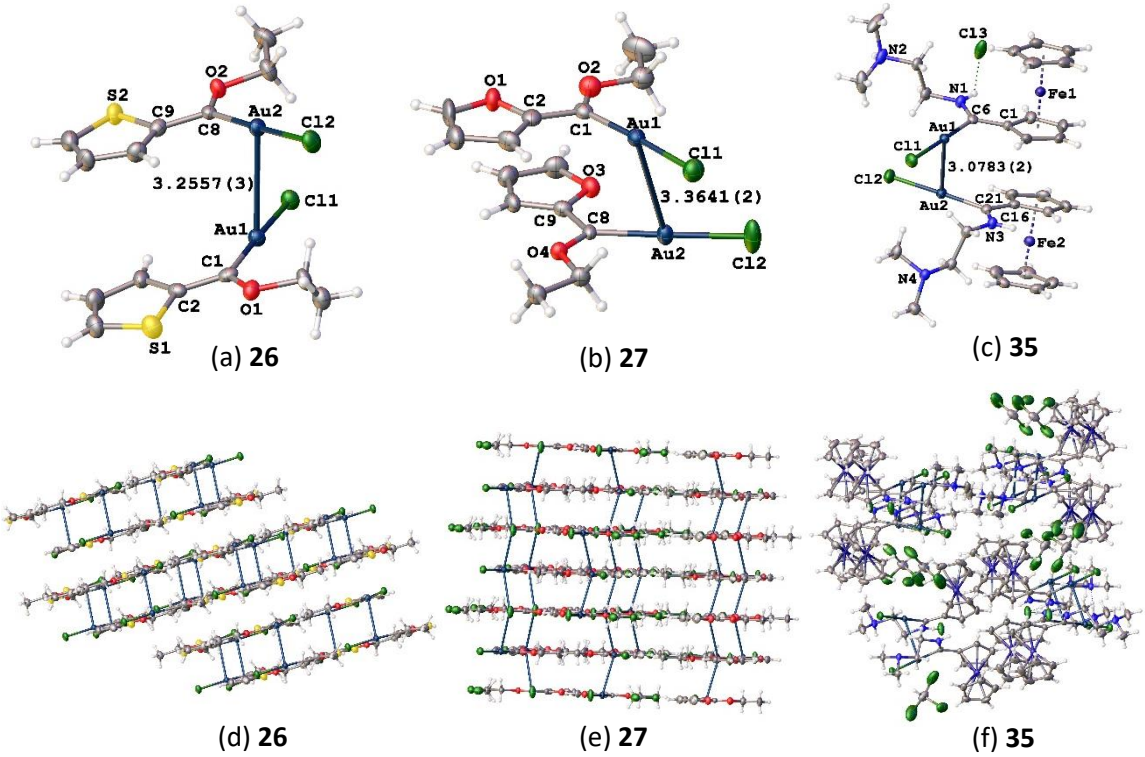

(a) **26** (b) **27** (c) **35**

(d) **26** (e) **27** (f) **35**

Figure 4.23 Genuine aurophilic interactions observed in the crystal structures of **26** ((a), (d)), **27** ((b), (e)), and **35** ((c), (f)). Solvent molecules were omitted from (b) and (c) for clarity.

4.3.2.3 Mass spectrometry of gold(I) Fischer carbene complexes

Mass spectral analysis indicated a $[M - Cl]^+$ common mass fragment ion for all gold(I) FCCs **26** – **35** (as assigned in Section 4.5 below). This $[M - Cl]^+$ fragmentation was in agreement with literature reports of Au^I methoxy- and aminocarbene complexes bearing heteroaryl and Fc carbene ligands.[18]

4.3.2.4 Electrochemical analysis of gold(I) aminocarbene complexes

Electrochemical analysis of the isolated aminocarbene complexes was carried out. A series of cyclic voltammetry experiments were done on complexes **30** – **35** in MeCN with 0.1 M $[N^nBu]_4[PF_6]$ as a supporting electrolyte at a continuous scan rate of 100 mV/s, and the resulting cyclic voltammograms (CVs, recorded on a BioLogic SP-50 voltammetric analyser using platinum wires as counter and working electrodes) are depicted in Figure 4.24 below. For all analyzed Au^I aminocarbene complexes **30** – **35**, reduction of the gold-carbene bond at negative potentials was not observed in the solvent window employed. However, the first oxidation waves (1st run of 4 for complexes **30** – **35**, Figure 4.24 (a) – (f)) were observed in the range 0.26 – 0.98 V (*vs* Ag/Ag^+, referenced to the ferrocene/ferrocenium couple

at 0 V as internal standard). The observed 1st oxidation waves proved irreversible in the Fu- and *p*-DMA-substituted complexes, for both the -NH^{n}Pr and -NH(CH$_2$)$_2$NMe$_2$ carbene substituents (Figure 4.24, (a) *vs* (b) for Fu- **31** and **33**; (c) *vs* (d) for *p*-DMA- **31** and **34**). Reversible redox waves were however observed for the Fc-substituted complexes **32** and **35** (Figure 4.24 (e) *vs* (f), $E_{1/2}$ 0.31 V and 0.35 V, respectively). Lower oxidation potentials are observed for the -NH(CH$_2$)$_2$NMe$_2$ substituted Fu- (**33**) and *p*-DMA- (**34**) carbene complexes as compared to the -NH^{n}Pr analogues **30** and **31**, respectively. The opposite effect is evident for the Fc-substituted analogues, whereby a higher-positive potential redox wave is evident in the -NH(CH$_2$)$_2$NMe$_2$ complex **35** as compared to the -NH^{n}Pr analogue **32**. Comparison of the effect of -NH^{n}Pr and -NH(CH$_2$)$_2$NMe$_2$ substituents on the redox-behaviour of the (hetero)aryl amino-carbene complexes is thus ambiguous. However, comparison of aryl-carbene substituents of either -NH^{n}Pr (**30** – **32**) or -NH(CH$_2$)$_2$NMe$_2$ (**33** – **35**) amino-carbene complexes, consistently showed less positive oxidation potentials for Fc-substituted complexes (**32**/**35**) in comparison to the *p*-DMA- (**31**/**34**) and Fu-substituted (**30**/**33**) analogues (-NH^{n}Pr; Fu, **30**, 0.98 V. *p*-DMA-, **31**, 0.71 V. Fc, **32**, 0.35 V. And -NH(CH$_2$)$_2$NMe$_2$; Fu, **33**, 0.66 V. *p*-DMA, **34**, 0.44 V. Fc, **35**, 0.39 V). The Fu-propylaminocarbene complex **30** indicated additional redox waves on the 2nd – 4th runs of the CV due to electrochemical decomposition of the complexes, resulting in deposition of the decomposition products onto the working electrode (see Figure 4.24 (a)). Amines and furans are known to precipitate onto electrodes and undergo further redox processes during electrochemical analysis,[48–52] thus it is important to record the first oxidation wave in a series of CV measurements of compounds featuring these electroplating moieties. In line with the electroplating effect of amines, CVs of the Fc-substituted aminocarbene complexes **32** and **35** also indicated further irreversible oxidation waves (throughout the 1st – 4th runs) which could not be conclusively extrapolated, and are hence not discussed. The obtained CVs are depicted in Chapter 6, Figure 6.2.

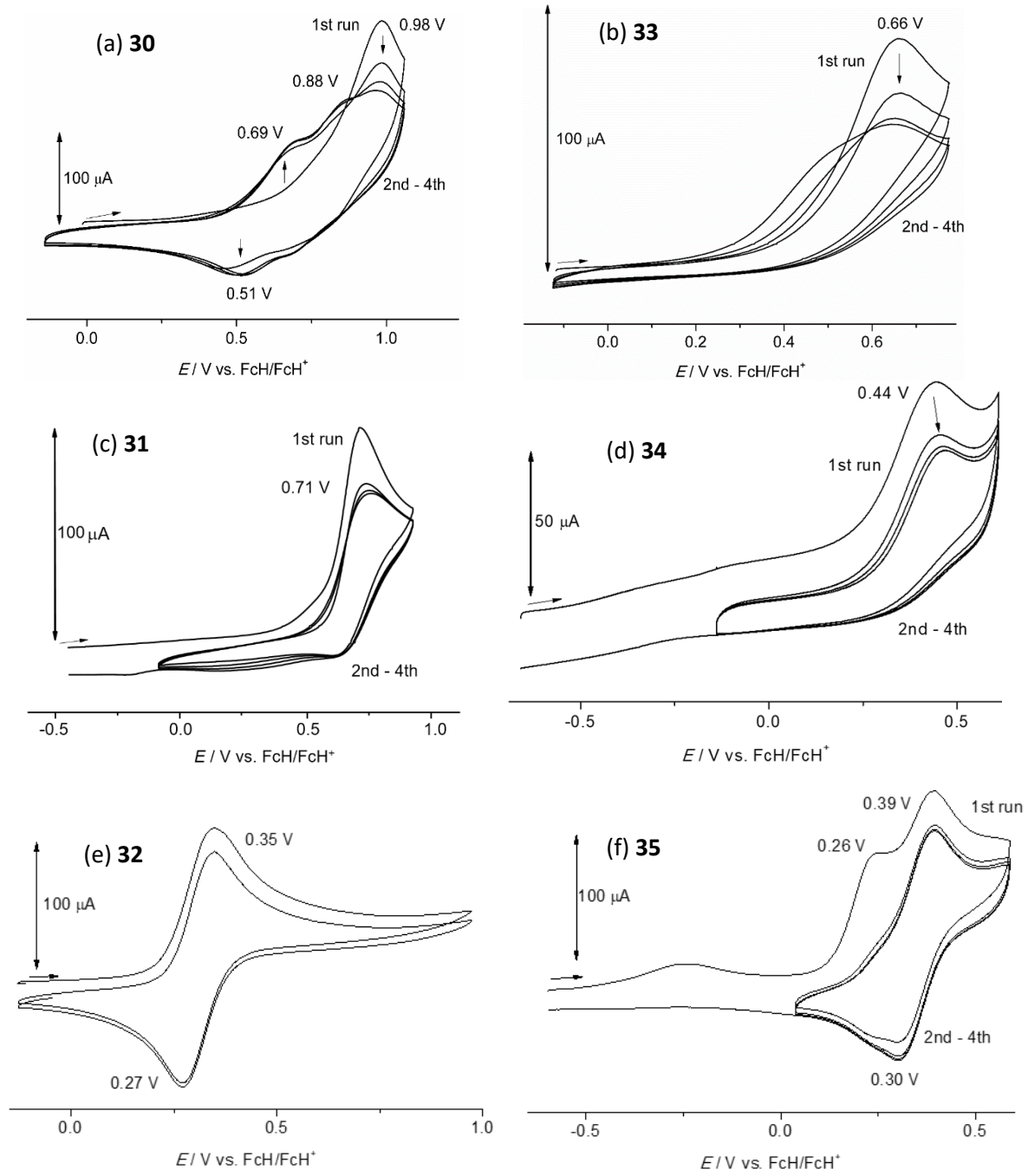

Figure 4.24 Cyclic voltammograms of examined gold(I) aminocarbene complexes **30** – **35** ((a) – (f)) in MeCN at a scan rate of 100 mV/s with 0.1 M [N^nBu_4][PF_6] as a supporting electrolyte.

4.3.2.5 Molecular orbital calculations

Density Function Theory (DFT) was employed for a more detailed analysis of the redox behaviour of the aminocarbene complexes discussed above. For the -NH^nPr complexes **30** – **32**, the calculated electron spin densities are located at the carbene *p*-DMA-ring and at the Fc substituent Fe-metal atom, in the cations $\mathbf{31}^+$ and $\mathbf{32}^+$, respectively, while spin density is shared between the Fu-ring substituent

and the Au-metal atom in **30**$^{+}$ (see Figure 4.25 below). For the -NH$(CH_2)_2NMe_2$ complexes **33** – **35**, the lowest-lying energy cation indicates that electron density is shared between the Au-metal atom and pendant nitrogen atom (N_2) in Fu- and *p*-DMA complexes **33**$^{+}$ and **34**$^{+}$ respectively, while electron density is located at the Fe-metal atom in **35**$^{+}$ (see Figure 4.26). Additionally, geometry optimization for these diamino-complexes indicated intramolecular hydrogen-bonding when the N_2-atom is oriented away from the central Au-metal atom. N-H bonds between the N_1-bound H-atom and N_2 are evident in complexes **34** (*p*-DMA, 2.19 Å) and **35** (Fc, 2.22 Å), while an O-H bond between the Fu-O- and N_1H- atoms is evident in complex **33** (2.20 A). Furthermore, geometry optimization for **35**$^{+}$ converge to Au^{I}-Fe^{III} or Au^{II}-Fe^{II} electromers, when N_2 is oriented away from or towards the gold metal atom, respectively, with the former electromer more favored than the latter. Thus the reversible oxidation waves of Fc-substituted complexes **32**$^{+}$ and **35**$^{+}$ are assigned to the $Fe^{II/III}$ couple, and are depicted as [**32**-Fe]$^{+}$ and [**35**-Fe]$^{+}$, respectively, while the irreversible oxidation wave observed for **31**$^{+}$ is annotated as [**31**-anilinyl]$^{+}$. For the complexes indicating a distribution of electron-spin density between the Au-metal atom and other moieties within the specified complex, the possibility of direct one-electron oxidation at the Au-metal atom cannot be ruled out. In these cases, the presumptive Au^{II} species is stabilized by coordination of the pendant-amino -NMe_2 N_2 atom in Fu and *p*-DMA cations **33**$^{+}$ and **34**$^{+}$, respectively, or by π-resonance effect through the Fu-ring substituent in **30**$^{+}$. The 1st oxidation waves are thus denoted as [**33**-Au-N_2]$^{+}$, [**34**-Au-N_2]$^{+}$, and [**30**-Au-Furyl]$^{+}$ based on DFT results.

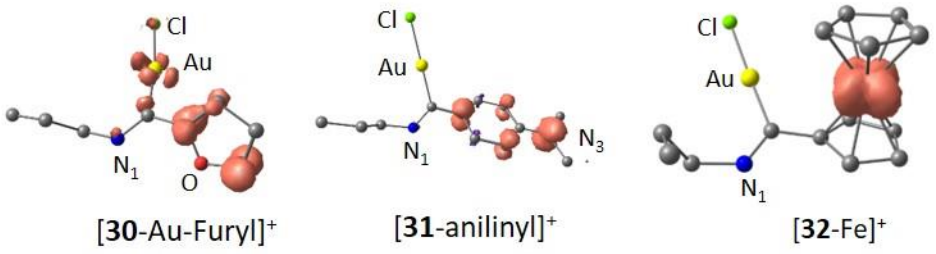

Figure 4.25 Calculated spin densities, for complexes **30**$^{+}$, **31**$^{+}$, and **32**$^{+}$ (CPMC(CH_2Cl_2)-RIJCOSX-B3LYP-D3BJ-ZORA-DEF2-TZVP). Distances given in Å. All hydrogen atoms are omitted, contour value at 0.01 a.u.

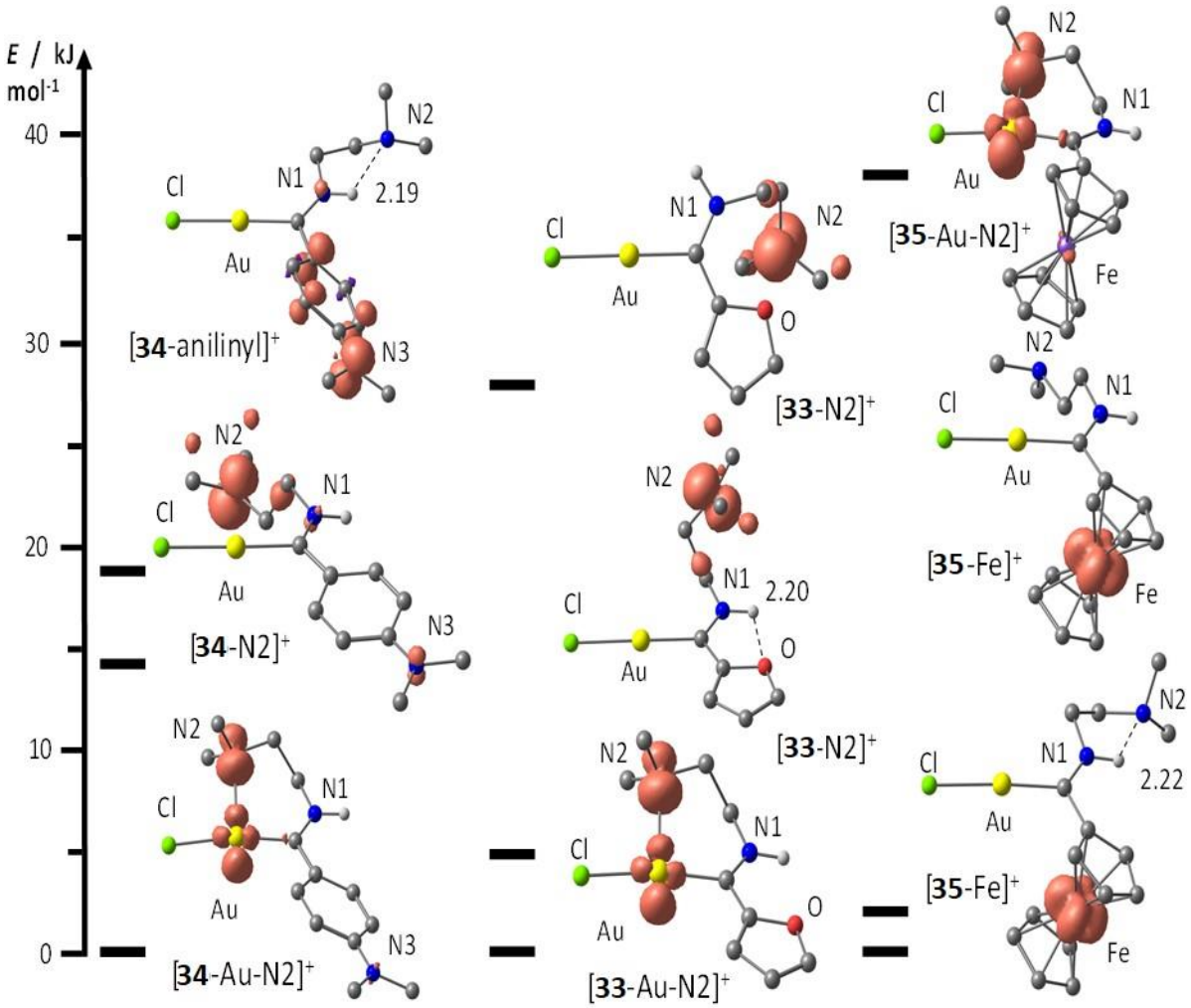

Figure 4.26 Calculated spin densities, for complexes **33**$^{+}$, **34**$^{+}$, and **35**$^{+}$ (CPMC(CH_2Cl_2)-RIJCOSX-B3LYP-D3BJ-ZORA-DEF2-TZVP). Distances given in Å. All C-bound hydrogen atoms are omitted, contour value at 0.01 a.u.

4.3.3 Evaluation of the catalytic behaviour of gold(I) FCCs in redox-switchable oxazoline synthesis reactions

The isolated aminocarbene complexes **30** – **35** were employed as precatalysts in the gold-mediated cyclization of *N*(2-propyn-1-yl)benzamide depicted in Scheme 4.4 below. The catalytic reactions were mediated by the addition of Magic Blue to generate the active Au^{II} species *in situ*,[23] and the results are summarized in Table 4.2. Data for the previously reported Fc-ethoxycarbene complex **29** was included for comparison.

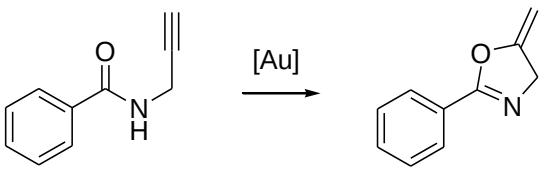

Scheme 4.4 Gold-catalyzed Intramolecular oxazoline synthesis investigated herein.

Table 4.2 Gold-catalyzed cyclization of *N*(2-propyn-1-yl)benzamide employing Au^{I} FCCs **29** – **35** as precatalysts.[a]

Entry	Gold complex	Magic Blue (Y/N)	[b]Conversion (%)	[c]Yield (%)
1	**29**	Y	98(1.0)	59(9.9)
2	**29**	N	0	0
3	**30**	Y	98(1.0)	42(2.2)
4	**30**	N	0	0
5	**31**	Y	99(2.2)	40(6.3)
6	**31**	N	0	0
7	**32**	Y	99(1.4)	59(8.6)
8	**32**	N	0	0
9	**33**	Y	100	71(1.0)
10	**33**	N	1 (1.0)	1(1.0)
11	**34**	Y	100	71
12	**34**	N	3(1.0)	0
13	**35**	Y	100	88(6.4)
14	**35**	N	1(1.0)	0
15	*DMEN	Y	1(1.4)	0
16	**35** + Hg	Y	100	83

[a]Catalytic conditions: *N*(2-propyn-1-yl)benzamide was dissolved in CD_2Cl_2 in a high-pressure NMR tube fitted with a J. Young valve. The specified Au^{I} complex, tris(4-bromophenyl)ammoniumyl hexachloroantimonate (Magic Blue) and 1,4-di-*tert*-butylbenzene as internal standard were added to the NMR tube. All reactions were done in duplicate, and the average percentages are reported with standard deviations indicated in brackets. [b]Calculated as ((mmol of substrate after 24 hrs)/ (initial mmol of substrate at 0 hrs)). [c]Calculated as ((mmol of oxazoline after 24 hrs)/ (initial mmol of substrate at 0 hrs)) *The uncoordinated ligand DMEN (*N,N*-dimethylethylenediamine) was employed instead of a gold complex.

As was the case with the previously reported Fc-ethoxycarbene complex **29** (see Table 4.2, entries 1 and 2), addition of the oxidant Magic Blue (MB) was necessary for catalytic activation of the herein utilized Au^{I} FCCs **30** – **35**. Quantitative conversions of the substrate were observed for all Au^{I} precatalysts (98 – 100%), and are comparable with the previously employed Fc-ethoxycarbene precatalyst in literature.[23] Insignificant changes are observed in the catalytic activity of Fc-substituted complexes **29** and **32**, when comparing ethoxy- and propylamino-carbene substituents, respectively (compare entries 1 and 7). Comparison of the percentage yield of the targeted oxazoline, showed enhanced catalytic activity of -$NH(CH_2)_2NMe_2$ substituted complexes as compared to the -NH^nPr substituted analogues (*ca*. 30% difference) across the board. For the -NH^nPr complexes, the observed percentage yield of the targeted oxazoline increases from Fu- (**30**, 42%) and *p*-DMA- (**31**, 40%) to Fc- (**32**, 59%) precatalysts. Similarly for the -$NH(CH_2)_2NMe_2$ complexes, an increase in oxazoline percentage yield from precatalysts **33** (Fu, 71%) and **34** (*p*-DMA, 71%) to **35** (Fc, 88%) is observed. The formation of Au^0 nanoparticles was also evident during the catalytic application of Fu- (**30**, **33**) and *p*-DMA- (**31**, **34**) substituted complexes, while no Au^0 mirror was evident in Fc-substituted analogues **32** and **35**. The inclusion of mercury in the catalytic application of **35**, resulting in excellent oxazoline yield (83%), is indicative of the absence of Au^0 nanoparticles in Fc-substituted precatalysts.[53] The uncoordinated DMEN diamino-substituent was also tested (under the same catalytic conditions as precatalysts **30** – **35**), and showed no activity both with and without the MB additive.

Time-dependent catalytic studies were also carried out for the -$NH(CH_2)_2NMe_2$-substituted complexes **33** (Fu), **34** (*p*-DMA), and **35** (Fc), and the resulting conversion *vs* time plots are displayed as indicated in Figure 4.27 below. Analysis of the Fu-substituted complex **33** in the presence of MB (**33/MB**) indicated 32% conversion after 30 minutes, and 90% conversion after 1 hour, with complete conversion (>99%) observed after 6 hours. In the case of the Fc-substituted complex, catalytic activity of **35/MB** indicated 64% conversion after 30 minutes and complete conversion was observed after 2 hours. A slower activity rate is however evident in the *p*-DMA-substituted complex (**34/MB**), whereby 4% conversion was observed after 30 minutes, with a steady increase of ~5% per hour, reaching 85% only after 20 hours. In addition, reaction of the reductant decamethylferrocene ($FeCp^*_2$) with **33/MB** or **34/MB** resulted exclusively in decomposition mixtures, wherein organic amides C(O){$NH(CH_2)_2NMe_2$)}Fu and C(O){$NH(CH_2)_2NMe_2$)}*p*-DMA could be identified as oxidized carbene ligands of **33** and **34**, respectively. The catalytic activity and redox behaviour of the Fu-substituted complex **33**, suggests the formation of an active (albeit unstable) Au^{II} intermediate during the catalytic cycle, which is supported by DFT calculations discussed above (Au^{II} lowest-lying energy cation [**33**-Au-N_2]$^+$). In the case of the *p*-DMA complex **34**, comparison of the slow catalytic conversion rate to the

Au^{II} lowest-lying energy cation (*vide supra*) provides paradoxical results. However, regeneration of the Fc-substituted complex (**35**) proved possible by reaction of **35/MB** with $FeCp^*_2$, in accordance with the regeneration of Fc-ethoxycarbene **29** reported previously.[23]

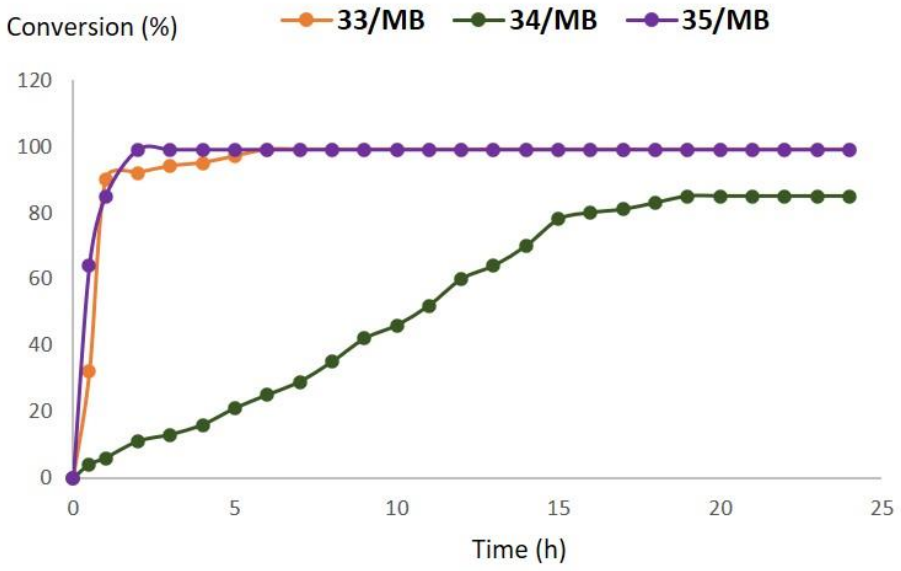

Figure 4.27 Time-dependent Magic Blue (MB)-assisted catalytic studies of complexes **33** – **35**.

Chemical oxidation of the utilized Au^{I} precatalysts **30** – **35** by the oxidant MB was undertaken (MB = $[N(p\text{-}C_6H_4Br)_3][SbCl_6]$, with a potential of 0.67 V in MeCN vs FcH/FcH^+),[54] to determine the paramagnetic behaviour of potential Au^{II} intermediates formed during the oxidation reactions, using X-band electron paramagnetic resonance (EPR) spectroscopy[55] in time dependent studies. No EPR-activity was observed for the Fu- (**30**,**33**) or *p*-DMA-substituted (**31**,**34**) precatalysts during the MB-induced chemical oxidation reactions. This was unexpected, especially for the **30/MB**, **33/MB**, and **34/MB** mixtures, due to the formation of Au^{II} intermediates observed upon electrochemical oxidation (supported by DFT results, *vide supra*). Gratifyingly, broad resonances with rhombic *g* tensor (*g*) values of ~2 evident at room temperature, are observed for the Fc-containing mixtures **32/MB** and **35/MB** (see Figure 4.28 below). The observed *g* resonances are in agreement with the previously reported Au^{I} ethoxycarbene complex (**29**) upon oxidation,[23] and are thus assigned to the monocations $\mathbf{32}^+$ and $\mathbf{35}^+$. However, these resonances cannot be assigned to the $Au^{I}Fe^{III}$ electromer suggested by DFT results of $\mathbf{32}^+$ and $\mathbf{35}^+$, due to the known EPR-inactivity of the corresponding Fc^+ entity at room temperature.[56] Gold(II) species that exhibit *g* tensors with small *g* anisotropy and hyperfine coupling to the nucleus (^{197}Au: $I = {}^3/_2$), have been reported in literature.[57–59] As hyperfine couplings were not observed for the $\mathbf{32}^+$ and $\mathbf{35}^+$ oxidation products, only the g_{iso} values are provided (2.0003 and 2.0001, respectively),

and fall within range of reported values for Au^{II} complexes in literature.[57–60] The EPR resonances were quantified by double integration *vs* a calibration curve over time (see Section 6.2.8 in Chapter 6).

The observed resonance rises slowly in **32**$^+$ and reaches a maximum point after 6 hours, while the faster-rising resonance of **35**$^+$ reaches its maximum point after 1 hour (Figure 2.28 (a) and (b), respectively). Plots of the doubly integrated intensities of the EPR resonances *vs* time are displayed in Figure 4.28 (c) and (d), for **32**$^+$ and **35**$^+$, respectively. The integral accounts for 62±17% of the paramagnetic species in **32**$^+$ (as observed after 6 hours). For the cation **35**$^+$, 89±16% of the paramagnetic species is accounted for, after 1 hour. Addition of diphenylacetylene to the reaction mixtures **32/MB** and **35/MB**, was done to mimic the benzamide substrate employed in the redox switchable catalysis discussed above, and the observed EPR resonances again appeared to be slow-rising in **32**$^+$ and faster-rising in **35**$^+$. The doubly integrated intensity of the EPR resonance *vs* time plot for **32**$^+$ (Figure 4.28 (e)), indicated that 94±17% of the paramagnetic species was accounted for after 6 hours. The integral of **35**$^+$ (Figure 4.28 (f)) accounts for 52±18% of the paramagnetic species after 30 minutes, and reaches a maximum concentration accounting for 81±18% of the paramagnetic species after 4 hours.

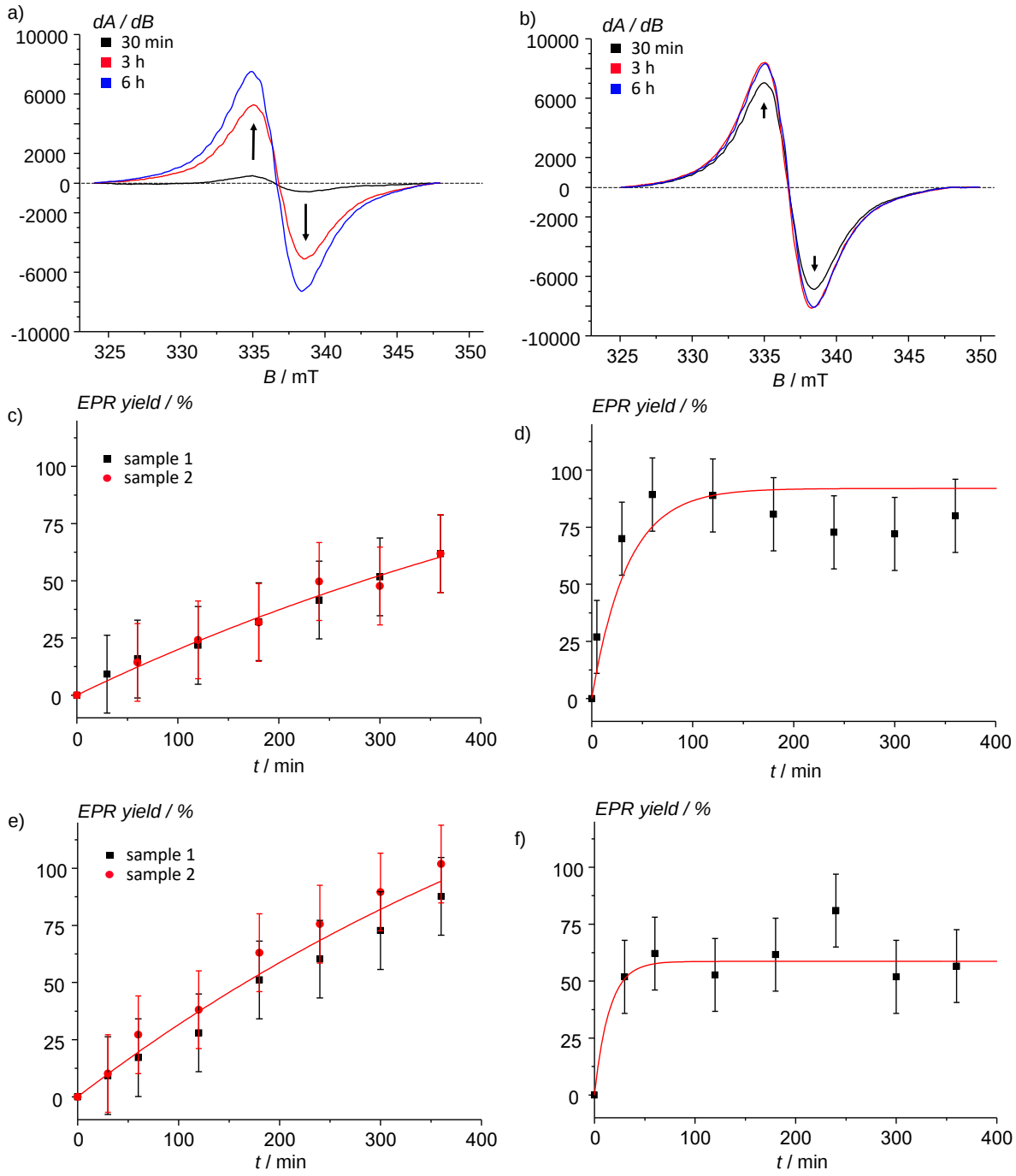

Figure 4.28 EPR spectra of **32/MB** and **35/MB** in THF over time at 295 K, a) **32**, b) **35**; doubly integrated intensity of the EPR resonance versus time plot c) **32**, d) **35**; doubly integrated intensity of the EPR resonance versus time plot with addition of diphenylacetylene e) **32**, f) **35**. The data were fit by an exponential growth model and the fit is essentially intended as a guide to the eye.

The EPR measurements of **32**$^+$ and **35**$^+$ clearly indicate the existence of Au^{II} species in these Fc-substituted Au-FCC monocations. However, this is in contradiction with DFT results, which specified the formation of $Au^{I}Fe^{III}$ intermediates after electrochemical oxidation of the precatalysts **32** and **35**, respectively. Additionally, geometry optimization of the diamino (-$NH(CH_2)_2NMe_2$ substituted) complex **35**, indicated the targeted $Au^{II}Fe^{II}$ intermediate as the least favoured of 3 possible structures (Figure 4.26, *vide supra*). To address the contradiction in DFT and EPR studies, further reaction pathways leading to the EPR-active Au^{II} species of **32**$^+$ and **35**$^+$, are hence proposed to proceed *in situ* during the chemical oxidation with MB, as depicted in Scheme 4.5 below. The proposed reaction entails the initial expected oxidation at the Fe^{II} metal atom, resulting in the $Au^{I}Fe^{III}$ intermediates (**32**$^+$ and **35**$^+$). Subsequent deprotonation of the Fc cyclopentadienyl (Cp) ring (that is not coordinated to the carbene carbon atom) results in the depicted Fc-radicals **36** and **37**, respectively. In this case, the amino-function of a second molecule- or the triarylamine of the oxidant (MB) could act as base, which subsequently deprotonates the Cp ring.[61] Intramolecular cyclization of the intermediate radicals (**36** and **37**) occurs as the terminal step, resulting in the ferrocenophane- (Fc') substituted Au^{II} compounds **36**$^+$ and **37**$^+$.

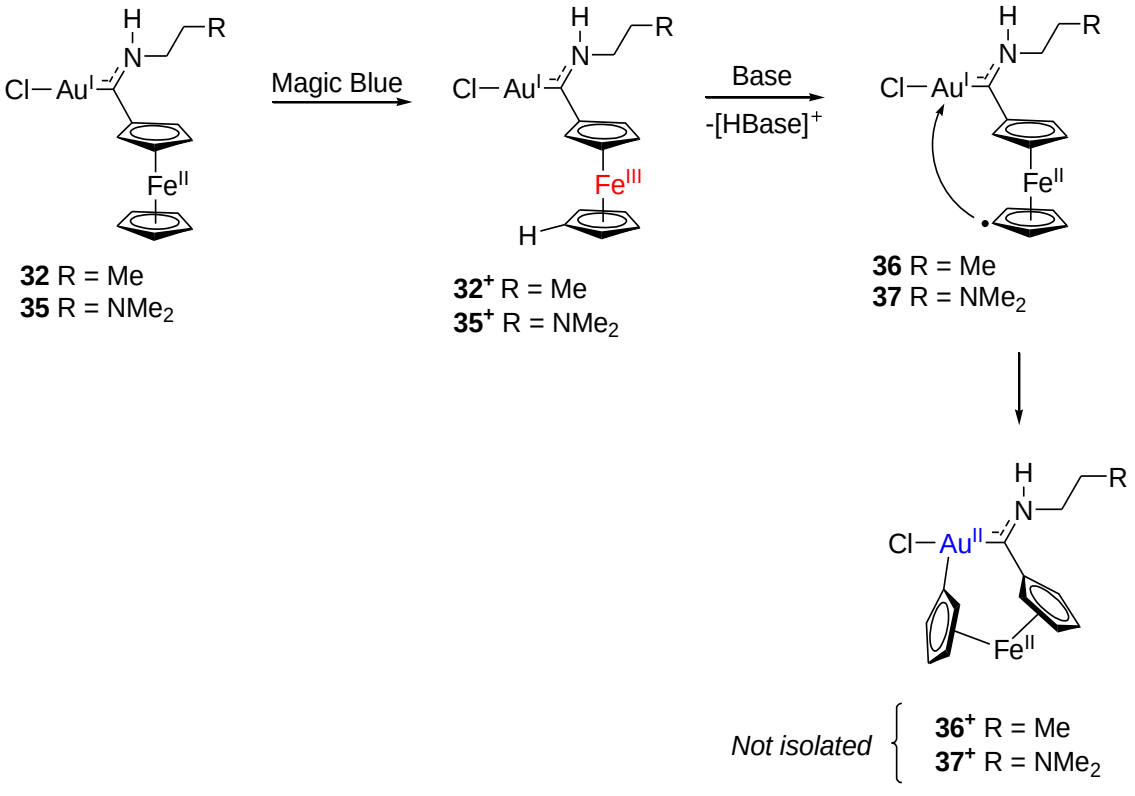

Scheme 4.5 Proposed reaction mechanism of the chemical oxidation of **32** and **35** by MB, leading to possible gold(II) intermediates **36**$^+$ and **37**$^+$, respectively.

Finally, geometries of these Fc˙ Au^{II} intermediates **36**$^{+}$ and **37**$^{+}$ were investigated, and the results are depicted in Figure 4.29. DFT calculations for the NH^{n}Pr-substituted entity **36**$^{+}$, showed that the spin density is shared between the Au-metal atom and the coordinated Fc˙-C atom, as specified by the [**36**-Au-Cp]$^{+}$ notation. In the case of the -NH(CH$_2$)$_2$NMe$_2$ ananlogue **37**$^{+}$, 2 possible isomers with a Au-Cp spin distribution ([**37**-Au-Cp]$^{+}$) are observed when the pendant-amino N$_2$ atom is oriented away from the Au-metal atom. The most-favoured isomer indicates that the spin density is shared between the Au-metal and C$_{carbene}$ atoms ([**37**-Au-C$_{carbene}$]$^{+}$), with coordination of the N$_2$ atom to the central Au-metal atom. Thus the Au^{II} intermediates **36**$^{+}$ and **37**$^{+}$, likely formed from the **32/MB** and **35/MB** mixtures, respectively, are feasible as supported by DFT results, rationalizing the EPR-activity of the mixtures.

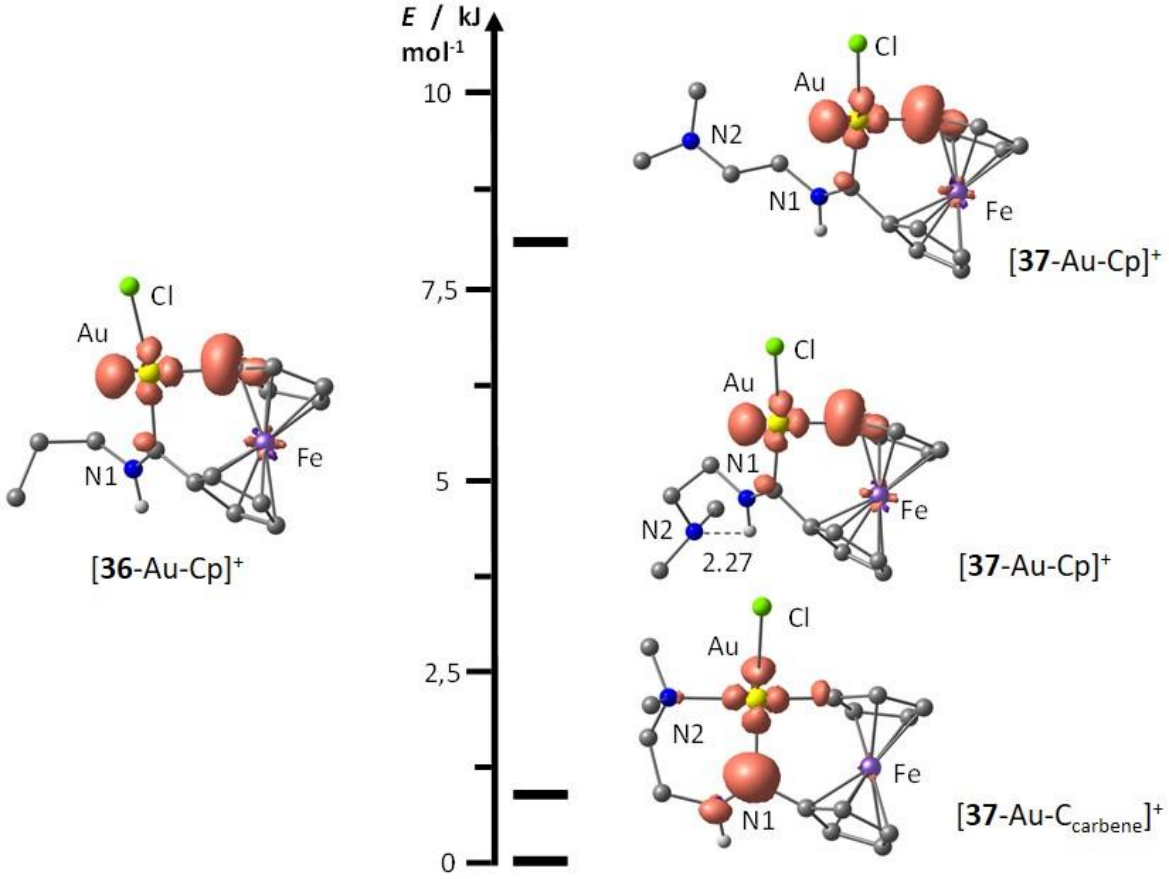

Figure 4.29 Calculated spin densities, for complexes **36**$^{+}$ (left) and **37**$^{+}$ (right) (CPMC(CH$_2$Cl$_2$)-RIJCOSX-B3LYP-D3BJ-ZORA-DEF2-TZVP). Distances given in Å. All C-bound hydrogen atoms are omitted, contour value at 0.01 a.u.

4.4 Conclusion

In summary, the synthesis of new Au^{I} ethoxycarbene complexes featuring organic (hetero)aryl carbene substituents (**26** – **28**), and of a known Fc-substituted analogue (**29**), as achieved *via* W^{0}-Au^{I} transmetallation. Subsequent aminolysis of the Au^{I} -OEt complexes by reaction with selected primary amines, was undertaken for access to less electrophilic aminocarbene complexes featuring -$NH^{n}Pr$ (**30** – **32**) or -$NH(CH_2)_2NMe_2$ (**33** – **35**) carbene substituents. Spectroscopic and structural characterization of all aminocarbene **30** – **35**, indicated that the pendant-amino -NMe_2 substituent in **33** – **35** remains untethered.

The isolated aminocarbene complexes were employed as precatalysts for redox-switchable intramolecular oxazoline synthesis reactions, wherein addition of the oxidant Magic Blue (MB) was prerequisite for catalytic activity. Complexes featuring the redox-non-innocent Fc substituent showed the best catalytic activity than those with organic (Fu, *p*-DMA) carbene substituents. In addition, -$NH(CH_2)_2NMe_2$ substituted complexes **33** – **35** showed much enhanced catalytic activity (~30%) as compared to the -$NH^{n}Pr$ analogues **30** – **32**, due to coordination of the pendant -NMe_2 moiety to the Au-metal atom during the catalytic cycle, as suggested by DFT calculations. Electrochemical analysis and DFT studies of the Fu- (**30**, **33**) and *p*-DMA-substituted (**31**, **34**) complexes, suggest the formation of catalytically active Au^{II} species during the MB-induced catalytic studies. The EPR-inactivity of **30/MB**, **31/MB**, **33/MB**, and **34/MB** mixtures, as well as the formation of Au^{0} mirrors observed during the respective catalytic applications, is an indication that the targeted Au^{II} intermediates are unstable. This was further supported by carbene ligand dissociation products observed during attempted chemical reduction reactions (to regenerate the Au^{I} complexes after oxidation with MB), wherein the amides C(O)(NR)(Ar) (R = ^{n}Pr, $(CH_2)_2NMe_2$; Ar = Fu, *p*-DMA) were identified as carbene ligand oxidation products. Regeneration of the Fc-substituted complexes **32** and **35** under analogous conditions proved possible. However, the EPR-activity of these complexes at room temperature contradicts the Fe^{III} species suggested by DFT calculations of the respective cations. A different reactivity pathway involving *in situ* deprotonation of the Fc-entity and subsequent intramolecular cyclization, was therefore proposed, and the postulated ferrocenophane (Fc') substituted Au^{II} intermediate was supported by DFT studies.

4.5 Experimental

4.5.1 [Au{C(OEt)(2-thienyl)}Cl] 26

A dried mixture of [Au(tht)Cl] (0.290 g, 0.90 mmol) and [$W(CO)_5${C(OEt)Th}] complex **1** (0.420 g, 0.90 mmol) was dissolved in CH_2Cl_2 (10 mL) and stirred for 16 hours at -78 °C. The resulting dark brown solution was warmed up to room temperature, at which point the CH_2Cl_2 solvent was completely removed *in vacuo*. The resulting brown paste was then washed with *n*-hexane (2 x 10 mL). The product was extracted with CH_2Cl_2 (10 mL) *via* cannula filtration methods and dried *in vacuo* to give a yellow powder. Yield = 0.309 g, 92%. Mp (dec): 122 – 124 °C. ^{1}H NMR (500 MHz, CD_2Cl_2) δ 8.59 (s, br, 1H, Th-H_α), 8.32 (d, br, ^3J(HH) = 4.9 Hz, 1H, Th-H_γ), 7.37 (dd, ^3J(HH) = 4.6 Hz, ^3J(HH) = 4.1 Hz, 1H, Th-H_β), 5.23 (q, ^3J(HH) = 7.2 Hz, 2H, O$\underline{CH_2}CH_3$), 1.65 (t, ^3J(HH) = 7.2 Hz, 3H, $OCH_2\underline{CH_3}$). ^{13}C{^{1}H} NMR (126 MHz, CD_2Cl_2) δ 246.4 ($C_{carbene}$), n.o. (Th-C_{ipso}), 152.6 (Th-C_α), 145.1 (Th-C_γ), 131.1 (Th-C_β), 82.1 (O$\underline{CH_2}CH_3$), 15.1 ($OCH_2\underline{CH_3}$). Anal. Calcd for $C_7H_8SOClAu$: C 22.56, H 2.16, S 8.61. Found: C 22.84, H 2.24, S 8.55. ESI-HRMS (15 V, positive mode, *m/z*): calcd for [M-Cl]$^+$ 336.9961, found 336.9702.

The analogues [Au{C(OEt)Ar}Cl] (Ar = 2-Furyl, *p*-DMA and Fc), **27** – **29** were prepared in like manner from W^0 precursors (**2**, **3**, and **8** respectively) as; an orange powder (Fu, **27**), a yellow powder (*p*-DMA, **28**) and a purple powder (Fc, **29**).

4.5.2 [Au{C(OEt)(2-furyl)}Cl] 27

Yield = 0.308 g, 96%. Mp (dec): 131 – 132 °C. ^{1}H NMR (500 MHz, CD_2Cl_2) δ 8.23 (s, br, 1H, Fu-H_γ), 8.06 (s, br, 1H, Fu-H_α), 6.82 (s, br, 1H, Fu-H_β), 5.21 (q, ^3J(HH) = 6.7 Hz, 2H, O$\underline{CH_2}CH_3$), 1.65 (t, ^3J(HH) = 7.2 Hz, 3H, $OCH_2\underline{CH_3}$). ^{13}C{^{1}H} NMR (126 MHz, CD_2Cl_2) δ 235.7 ($C_{carbene}$), 159.2 (Fu-C_{ipso}), 154.5 (Fu-C_γ), 142.1 (Fu-C_α), 116.6 (Fu-C_β), 82.7 (O$\underline{CH_2}CH_3$), 15.2 ($OCH_2\underline{CH_3}$). Anal. Calcd for $C_7H_8O_2ClAu$: C 23.58, H 2.26. Found: C 23.49, H 2.25. ESI-HRMS (15 V, positive mode, *m/z*): calcd for [M-Cl]$^+$ 321.0190, found 320.9951.

4.5.3 [Au{C(OEt)(*p*-DMA)}Cl] 28

Yield = 0.199 g, 97%. Mp (dec) 143 – 145 °C. ^{1}H NMR (500 MHz, CD_2Cl_2) δ 8.20 (s, br, 2H, DMA-$\underline{H_{\alpha,\alpha'}}$), 6.68 (d, ^3J(HH) = 9.5 Hz, 2H, DMA-$\underline{H_{\beta,\beta'}}$), 5.06 (q, ^3J(HH) = 7.1 Hz, 2H, O$\underline{CH_2}CH_3$), 3.18 (s, 6H, DMA-N($\underline{CH_3}$)$_2$), 1.58 (t, ^3J(HH) = 7.2 Hz, 3H, $OCH_2\underline{CH_3}$). ^{13}C{^{1}H} NMR (126 MHz, CD_2Cl_2) δ 246.2 ($C_{carbene}$), 157.3 (DMA-C_q), 131.0 (DMA-C_{ipso}), n.o. (DMA-$\underline{C_{\alpha,\alpha'}}$), 111.9 (DMA-$\underline{C_{\beta,\beta'}}$), 78.9 (O$\underline{CH_2}CH_3$), 40.9 (DMA-N($\underline{CH_3}$)$_2$), 15.2 ($OCH_2\underline{CH_3}$). Anal. Calcd for $C_{11}H_{15}NOClAu$: C 32.25, H 3.69, N 3.42. Found: C 32.80, H 3.63, N 3.42. ESI-HRMS (15 V, positive mode, *m/z*): calcd for [M-Cl]$^+$ 374.0819, found 374.0792.

4.5.4 [Au{C(OEt)Fc}Cl] 29[23]

This complex has been recently reported.[23] Yield = 0.400 g, 94%. Mp: 92 – 94 °C. ^{1}H NMR (500 MHz, CD_2Cl_2) δ 5.17 (s, 2H, FeCp'-$\underline{H_{\alpha,\alpha'}}$), 5.07 (s, br, 2H, FeCp'-$\underline{H_{\beta,\beta'}}$), 5.00 (q, ^{3}J(HH) = 7.2 Hz, 2H, O$\underline{CH_2}CH_3$), 4.47 (s, 5H, FeCp), 1.57 (t, ^{3}J(HH) = 7.2 Hz, 3H, $OCH_2\underline{CH_3}$). $^{13}C\{^{1}H\}$ NMR (126 MHz, CD_2Cl_2) δ 251.1 ($C_{carbene}$), 87.3 (FeCp'-C_{ipso}), n.o. (FeCp'-$\underline{C_{\alpha,\alpha'}}$), 80.3 (FeCp'-$\underline{C_{\beta,\beta'}}$), 79.6 (O$\underline{CH_2}CH_3$), 72.2 (FeCp), 15.3 ($OCH_2\underline{CH_3}$). Anal. Calcd for $C_{13}H_{14}OClFeAu$: C 32.91, H 2.97. Found: C 32.94, H 2.93. ESI-HRMS (15 V, positive mode, *m/z*): calcd for $[M\text{-}Cl]^+$ 439.0060, found 439.0018.

4.5.5 [Au{C(NH^{n}Pr)(2-furyl)}Cl] 30

$^{n}PrNH_2$ was slowly added to a brown-orange solution of **26** (0.100 g, 0.28 mmol) in THF at room temperature. The mixture was stirred for 1 hour and the THF subsequently removed *in vacou*. The resulting grey-black paste was washed with *n*-hexane (4 x 10 mL) and cannula-extracted with CH_2Cl_2 to give a very pale grey powder after drying. Yield = 0.093 g, 90%. Mp (dec): 135 – 137 °C. ^{1}H NMR (400 MHz, $CDCl_3$) δ 9.21 (s, br, 1H, $\underline{NH}CH_2CH_2CH_3$), 7.70 (d, br, ^{3}J(HH) = 1.7 Hz, 1H, Fu-H_γ), 7.51 (d, ^{3}J(HH) = 3.9 Hz, 1H, Fu-H_α), 6.60 (dd, ^{3}J(HH) = 3.7 Hz, ^{3}J(HH) = 1.8 Hz, 1H, Fu-H_β), 3.94 (q, ^{3}J(HH) = 6.8 Hz, 2H, NH$\underline{CH_2}CH_2CH_3$), 1.86 (h, ^{3}J(HH) = 7.4 Hz, 2H, $NHCH_2\underline{CH_2}CH_3$), 1.01 (t, ^{3}J(HH) = 7.4 Hz, 3H, $NHCH_2CH_2\underline{CH_3}$). $^{13}C\{^{1}H\}$ NMR (101 MHz, $CDCl_3$) δ 195.9 ($C_{carbene}$), 154.4 (Fu-C_{ipso}), 148.4 (Fu-C_γ), 129.6 (Fu-C_α), 114.2 (Fu-C_β), 56.7 (NH$\underline{CH_2}CH_2CH_3$), 23.0 ($NHCH_2\underline{CH_2}CH_3$), 11.2 ($NHCH_2CH_2\underline{CH_3}$). IR ($CH_2Cl_2$, ν(NH), cm^{-1}): 3318. Anal. Calcd for $C_7H_8NOClAu$: C 26.00, H 3.00, N 3.79. Found: C 26.48, H 3.06, N 3.84. ESI-HRMS (15 V, positive mode, *m/z*): calcd for $[M\text{-}Cl]^+$ 334.0506, found 334.0467.

The analogues [Au{C(NH^{n}Pr)(Ar)}Cl] (Ar = *p*-DMA (**31**), Fc (**32**)) and [Au{C(NH(CH_2CH_2)NMe_2)(Ar)}Cl] (Ar = 2-furyl, *p*-DMA, Fc), **33** – **35** were prepared similarly as; a lime-green powders (*p*-DMA, **31, 34**), red powders (Fc, **32, 35**), and a grey powder (Fu, **33**).

4.5.6 [Au{C(NH^{n}Pr)(*p*-DMA)}Cl] 31

Yield = 0.196 g, 93%. Mp: 96 – 98 °C. ^{1}H NMR (500 MHz, $CDCl_3$) δ 8.86 (s, br, 1H, $\underline{NH}CH_2CH_2CH_3$), 7.88 (d, ^{3}J(HH) = 9.1 Hz, 2H, DMA-$\underline{H_{\alpha,\alpha'}}$), 6.75 (d, ^{3}J(HH) = 8.5 Hz, 2H, DMA-$\underline{H_{\beta,\beta'}}$), 4.04 (dt, ^{3}J(HH) = 7.6 Hz, ^{3}J(HH) = 6.2 Hz, 2H, NH$\underline{CH_2}CH_2CH_3$), 3.09 (s, 6H, DMA-N($\underline{CH_3}$)$_2$), 1.88 (h, ^{3}J(HH) = 7.3 Hz, 2H, $NHCH_2\underline{CH_2}CH_3$), 1.04 (t, ^{3}J(HH) = 7.4 Hz, 3H, $NHCH_2CH_2\underline{CH_3}$). $^{13}C\{^{1}H\}$ NMR (126 MHz, $CDCl_3$) δ 214.0 ($C_{carbene}$), 153.1 (DMA-C_q), 133.0 (DMA-C_{ipso}), n.o. (DMA-$\underline{C_{\alpha,\alpha'}}$), 112.6 (DMA-$\underline{C_{\beta,\beta'}}$), 56.4 (NH$\underline{CH_2}CH_2CH_3$), 41.1 (DMA-N($\underline{CH_3}$)$_2$), 23.2 ($NHCH_2\underline{CH_2}CH_3$), 11.3 ($NHCH_2CH_2\underline{CH_3}$). IR ($CH_2Cl_2$, ν(NH), cm^{-1}): 3333. Anal. Calcd for $C_{21}H_{18}N_2ClAu$: C 34.10, H 4.29, N 6.63. Found: C 34.12, H 4.22, N 6.39. ESI-HRMS (15 V, positive mode, *m/z*): calcd for $[M\text{-}Cl]^+$ 387.1136, found 387.1103.

4.5.7 [Au{C(NH^{n}Pr)Fc}Cl] 32

Yield = 0.286 g, 93%. Mp: 119 – 120 °C. ^{1}H NMR (400 MHz, $CDCl_3$) δ 8.29 (s, br, 1H, NHCH$_2$CH$_2$CH$_3$), 4.87 (dd, ^3J(HH) = 1.7 Hz, ^3J(HH) = 1.9 Hz, 2H, FeCp'-H$_{α,α'}$), 4.74 (dd, ^3J(HH) = 1.5 Hz, ^3J(HH) = 1.8 Hz, 2H, FeCp'-H$_{β,β'}$), 4.35 (s, 5H, FeCp), 3.89 (q, ^3J(HH) = 6.8 Hz, 2H, NHCH$_2$CH$_2$CH$_3$), 1.85 (h, ^3J(HH) = 7.3 Hz, 2H, NHCH$_2$CH$_2$CH$_3$), 1.06 (t, ^3J(HH) = 7.4 Hz, 3H, NHCH$_2$CH$_2$CH$_3$). ^{13}C{^{1}H} NMR (101 MHz, $CDCl_3$) δ 216.7 ($C_{carbene}$), 84.2 (FeCp'-C_{ipso}), 74.4 (FeCp'-C$_{α,α'}$), 71.2 (FeCp'-C$_{β,β'}$), 70.7 (FeCp), 56.5 (NHCH$_2$CH$_2$CH$_3$), 23.1 (NHCH$_2$CH$_2$CH$_3$), 11.2 (NHCH$_2$CH$_2$CH$_3$). IR (CH_2Cl_2, ν(NH), cm^{-1}): 3330. Anal. Calcd for $C_{21}H_{18}N_2ClAu$: C 34.49, H 3.51, N 2.87. Found: C 34.59, H 3.56, N 2.15. ESI-HRMS (15 V, positive mode, *m/z*): calcd for [M-Cl]$^+$ 452.0376, found 452.0149.

4.5.8 [Au{C(NH(CH$_2$CH$_2$)NMe$_2$)(2-furyl)}Cl] 33

Yield = 0.300 g, 95%. Mp: 119 – 121 °C. ^{1}H NMR (400 MHz, $CDCl_3$) δ 9.43 (s, br, 1H, NHCH$_2$CH$_2$N(CH$_3$)$_2$), 7.71 (d, ^3J(HH) = 1.8 Hz, 1H, Fu-H$_γ$), 7.58 (d, ^3J(HH) = 3.6 Hz, 1H, Fu-H$_α$), 6.62 (dd, ^3J(HH) = 3.6 Hz, ^3J(HH) = 1.8 Hz, 1H, Fu-H$_β$), 4.02 (t, ^3J(HH) = 5.8 Hz, 2H, NHCH$_2$CH$_2$N(CH$_3$)$_2$), 2.67 (t, ^3J(HH) = 5.8 Hz, 2H, NHCH$_2$CH$_2$N(CH$_3$)$_2$), 2.33 (s, 6H, NHCH$_2$CH$_2$N(CH$_3$)$_2$). ^{13}C{^{1}H} NMR (101 MHz, $CDCl_3$) δ 196.0 ($C_{carbene}$), 154.6 (Fu-C_{ipso}), 148.3 (Fu-C$_γ$), 130.0 (Fu-C$_α$), 114.2 (Fu-C$_β$), 57.0 (NHCH$_2$CH$_2$N(CH$_3$)$_2$), 51.5 (NHCH$_2$CH$_2$N(CH$_3$)$_2$), 45.3 (NHCH$_2$CH$_2$N(CH$_3$)$_2$). IR (CH_2Cl_2, ν(NH), cm^{-1}): 3273. Anal. Calcd for $C_9H_{14}N_2OClAu$: C 27.12, H 3.54, N 7.03. Found: C 27.23, H 3.37, N 7.80. ESI-HRMS (15 V, positive mode, *m/z*): calcd for [M-Cl]$^+$ 363.0772, found 363.0756.

4.5.9 [Au{C(NH(CH$_2$CH$_2$)NMe$_2$)(*p*-DMA)}Cl] 34

Yield = 0.259 g, 96%. Mp: 91 – 93 °C. ^{1}H NMR (500 MHz, $CDCl_3$) δ 9.37 (s, br, 1H, NHCH$_2$CH$_2$N(CH$_3$)$_2$), 7.87 (d, ^3J(HH) = 8.4 Hz, 2H, DMA-H$_{α,α'}$), 6.64 (d, ^3J(HH) = 8.3 Hz, 2H, DMA-H$_{β,β'}$), 4.08 (t, ^3J(HH) = 5.4 Hz, 2H, NHCH$_2$CH$_2$N(CH$_3$)$_2$), 3.07 (s, 6H, DMA-N(CH$_3$)$_2$), 2.73 (t, ^3J(HH) = 5.4 Hz, 2H, NHCH$_2$CH$_2$N(CH$_3$)$_2$), 2.36 (s, 6H, NHCH$_2$CH$_2$N(CH$_3$)$_2$). ^{13}C{^{1}H} NMR (126 MHz, $CDCl_3$) δ 213.0 ($C_{carbene}$), 154.2 (DMA-C$_q$), 133.5 (DMA-C_{ipso}), 127.3 (DMA-C$_{α,α'}$), 111.3 (DMA-C$_{β,β'}$), 57.5 (NHCH$_2$CH$_2$N(CH$_3$)$_2$), 50.8 (NHCH$_2$CH$_2$N(CH$_3$)$_2$), 45.3 (NHCH$_2$CH$_2$N(CH$_3$)$_2$), 40.2 (DMA-N(CH$_3$)$_2$). IR (CH_2Cl_2, ν(NH), cm^{-1}): 3266. Anal. Calcd for $C_{13}H_{21}N_3ClAu$: C 34.56, H 4.69, N 9.30. Found: C 35.19, H 4.75, N 9.28. ESI-HRMS (15 V, positive mode, *m/z*): calcd for [M-Cl]$^+$ 416.1401, found 416.1386.

4.5.10 [Au{C(NH(CH$_2$CH$_2$)NMe$_2$)Fc}Cl] 35

Yield = 0.098 g, 90%. Mp: 117 – 119 °C. ^{1}H NMR (500 MHz, $CDCl_3$) δ 9.11 (s, br, 1H, NHCH$_2$CH$_2$N(CH$_3$)$_2$), 4.91 (s, 2H, FeCp'-H$_{α,α'}$), 4.73 (s, 2H, FeCp'-H$_{β,β'}$), 4.34 (s, 5H, FeCp), 3.97 (t, ^3J(HH) = 5.6 Hz, 2H, NHCH$_2$CH$_2$N(CH$_3$)$_2$), 2.73 (t, ^3J(HH) = 5.7 Hz, 2H, NHCH$_2$CH$_2$N(CH$_3$)$_2$), 2.39 (s, 3H, NHCH$_2$CH$_2$N(CH$_3$)$_2$). ^{13}C{^{1}H} NMR (126 MHz, $CDCl_3$) δ 215.8 ($C_{carbene}$), 84.0 (FeCp'-C_{ipso}), 74.3 (FeCp'-C$_{α,α'}$), 71.4 (FeCp'-C$_{β,β'}$), 70.6 (FeCp), 57.6

(NH<u>CH$_2$</u>CH$_2$N(CH$_3$)$_2$), 51.6 (NHCH$_2$<u>CH$_2$</u>N(CH$_3$)$_2$), 45.4 (NHCH$_2$CH$_2$N(<u>CH$_3$)$_2$</u>). IR (CH_2Cl_2, ν(NH), cm^{-1}): 3266. Anal. Calcd for $C_{15}H_{20}N_2ClAu$: C 34.88, H 3.90, N 5.42. Found: C 35.19, H 3.90, N 5.38. ESI-HRMS (15 V, positive mode, *m/z*): calcd for $[M\text{-}Cl]^+$ 481.0641, found 481.0628.

4.6 References

1 H. Schmidbaur, *Naturwiss. Rundsch.*, 1995, **48**, 443–451.

2 A. S. K. Hashmi, T. M. Frost and J. W. Bats, *J. Am. Chem. Soc.* 2000, **122**, 11553–11554.

3 A. S. K. Hashmi, L. Schwarz, J.-. H. Choi and T. M. Frost, *Angew. Chem. Int. Ed.* 2000, **39**, 2285–2288.

4 A. S. K. Hashmi and G. J. Hutchings, *Angew. Chem. Int. Ed.*, 2006, **45**, 7896–7936.

5 A. S. K. Hashmi, *Gold Bull.* 2004, **37**, 51–65.

6 A. Fürstner and P. W. Davies, *Angew. Chem. Int. Ed.*, 2007, **46**, 3410–3449.

7 A. Fürstner, *Chem. Soc. Rev.*, 2009, **38**, 3208–3221.

8 M. Joost, A. Amgoune and D. Bourissou, *Angew. Chem. Int. Ed.*, 2015, **54**, 15022–15045.

9 H. Schmidbaur, *Gold Bull.*, 2000, **33**, 3–10.

10 H. Schmidbaur and A. Schier, *Chem. Soc. Rev.*, 2012, **41**, 370–412.

11 D. J. Gorin and F. D. Toste, *Nature*, 2007, **446**, 395–403.

12 P. Pyykkö, *Chem. Soc. Rev.*, 2008, **37**, 1967–1997.

13 D. J. Gorin, B. D. Sherry and F. D. Toste, *Chem. Rev.*, 2008, **108**, 3351–3378.

14 R. Aumann and E. O. Fischer, *Chem. Ber.*, 1981, **114**, 1853–1857.

15 C. E. Strasser, S. Cronje and H. G. Raubenheimer, *New J. Chem.*, 2010, **34**, 458–469.

16 E. O. Fischer and M. Böck, *Monatsh. Chem.*, 1984, **115**, 1159–1164.

17 E. O. Fischer, M. Böck and R. Aumann, *Chem. Ber.*, 1983, **116**, 3618–3623.

18 D. I. Bezuidenhout, B. van der Westhuizen, A. J. Rosenthal, M. Wörle, D. C. Liles and I. Fernández, *Dalton Trans.*, 2014, **43**, 398–401.

19 M. Fañanás-Mastral and F. Aznar, *Organometallics*, 2009, **28**, 666–668.

20 G. Seidel, B. Gabor, R. Goddard, B. Heggen, W. Thiel and A. Fürstner, *Angew. Chem. Int. Ed.*, 2014, **53**, 879–882.

21 W. Debrouwer and A. Fürstner, *Chem. –Eur. J.*, 2017, **23**, 4271–4275.

22 R. E. M. Brooner and R. A. Widenhoefer, *Chem. Commun.*, 2014, **50**, 2420–2423.

23 P. Veit, C. Volkert, V. Förster, Christoph Ksenofontov, S. Schlicher, M. Bauer and K. Heinze, *Chem. Commun.*, 2019, **55**, 4615–4618.

24 M. Fañanás-Mastral and F. Aznar, *Organometallics*, 2009, **28**, 666–668.

25 G. Seidel and A. Fürstner, *Angew. Chem. Int. Ed.*, 2014, **53**, 4807–4811.

26 S. K. Schneider, W. A. Herrmann and E. Herdtweck, *Zeitschrift für Anorg. und Allg. Chemie*, 2003, **629**, 2363–2370.

27 S. Ibáñez, M. Poyatos and E. Peris, *Organometallics*, 2017, **36**, 1447–1451.

28 G. Kovács, A. Lledós and G. Ujaque, *Angew. Chemie*, 2011, **123**, 11343–11347.

29 M. J. López-Gómez, D. Martin and G. Bertrand, *Chem. Commun.*, 2013, **49**, 4483.

30 D. Canseco-Gonzalez, A. Petronilho, H. Mueller-Bunz, K. Ohmatsu, T. Ooi and M. Albrecht, *J. Am. Chem. Soc.*, 2013, **135**, 13193–13203.

31 P. Brüggemann, M. Wahl, S. Schwengers, H. Buhl and C. Ganter, *Organometallics*, 2018, **37**, 4276–4286.

32 L. Hettmanczyk, D. Schulze, L. Suntrup and B. Sarkar, *Organometallics*, 2016, **35**, 3828–3836.

33 A. Priante-Flores, V. Salazar-Pereda, A. L. Rheingold and D. Mendoza-Espinosa, *New J. Chem.*, 2018, **42**, 15533–15537.

34 L. Hettmanczyk, L. Suntrup, S. Klenk, C. Hoyer and B. Sarkar, *Chem. –Eur. J.*, 2017, **23**, 576–585.

35 S. Klenk, S. Rupf, L. Suntrup, M. Van Der Meer and B. Sarkar, *Organometallics*, 2017, **36**, 2026–2035.

36 B. van der Westhuizen, P. J. Swarts, L. M. van Jaarsveld, D. C. Liles, U. Siegert, J. C. Swarts, I. Fernández and D. I. Bezuidenhout, *Inorg. Chem.*, 2013, **52**, 6674–6684.

37 A. Zeineddine, L. Estévez, S. Mallet-Ladeira, K. Miqueu, A. Amgoune and D. Bourissou, *Nat. Commun.*, 2017, **8**, 565.

38 A. Nijamudheen and A. Datta, *Chem. –Eur. J.*, 2020, **26**, 1442–1487.

39 B. van der Westhuizen, P. J. Swarts, I. Strydom, D. C. Liles, I. Fernández, J. C. Swarts and D. I. Bezuidenhout, *Dalton Trans.*, 2013, **42**, 5367–5378.

40 J. G. López-Cortés, L. F. Contreras De La Cruz, M. C. Ortega-Alfaro, R. a. Toscano, C. Alvarez-Toledano and H. Rudler, *J. Organomet. Chem.*, 2005, **690**, 2240–2248.

41 G. K. Ramollo, M. J. López-Gómez, D. C. Liles, L. C. Matsinha, G. S. Smith and D. I. Bezuidenhout, *Organometallics*, 2015, **34**, 5745–5753.

42 G. K. Ramollo, I. Strydom, M. A. Fernandes, A. Lemmerer, S. O. Ojwach, J. L. van Wyk and D. I. Bezuidenhout, *Inorg. Chem.*, 2020, **59**, 4810–4815.

43 S.-G. Wang and W. H. E. Schwarz, *J. Am. Chem. Soc.*, 2004, **126**, 1266–1276.

44 V. W.-W. Yam and E. C.-C. Cheng, *Chem. Soc. Rev.*, 2008, **37**, 1806.

45 H. Schmidbaur and A. Schier, *Chem. Soc. Rev.*, 2012, **41**, 370–412.

46 I. J. B. Lin and C. S. Vasam, *Can. J. Chem.*, 2005, **83**, 812–825.

47 L. Ray, M. M. Shaikh and P. Ghosh, *Inorg. Chem.*, 2008, **47**, 230–240.

48 D. Bejan and A. Duca, *Croat. Chem. acta*, 1998, **71**, 745–756.

49 M. Can and S. Uzun, *Asian J. Chem.*, 2010, **22**, 867.

50 L. Li, W. Chen, N. Xu, Z. Xiao and G. Xue, *J. Mater. Sci.*, 2004, **39**, 2395–2398.

51 J. L. J. Hallal, A. M. S. Lucho and R. S. Gonçalves, *Mater. Res.* , 2005, 8, 23–29.

52 G. Zotti, G. Schiavon, N. Comisso, A. Berlin and G. Pagani, *Synth. Met.*, 1990, **36**, 337–351.

53 R. H. Crabtree, *Chem. Rev.*, 2012, **112**, 1536–1554.

54 N. G. Connelly and W. E. Geiger, *Chem. Rev.*, 1996, **96**, 877–910.

55 M. M. Roessler and E. Salvadori, *Chem. Soc. Rev.*, 2018, **47**, 2534–2553.

56 K. Hüttinger, C. Förster and K. Heinze, *Chem. Commun.*, 2014, **50**, 4285–4288.

57 M. Kampf, J. Griebel and R. Kirmse, *Z. Anorg. Allg. Chem.*, 2004, **630**, 2669–2676.

58 D. Huang, X. Zhang, E. J. L. McInnes, J. McMaster, A. J. Blake, E. S. Davies, J. Wolowska, C. Wilson and M. Schröder, *Inorg. Chem.*, 2008, **47**, 9919–9929.

59 S. Preiß, J. Melomedov, A. von Leupoldt and K. Heinze, *Chem. Sci.*, 2016, **7**, 596–610.

60 S. Preiß, C. Förster, S. Otto, M. Bauer, P. Müller, D. Hinderberger, H. Hashemi Haeri, L. Carella and K. Heinze, *Nat. Chem.*, 2017, **9**, 1249–1255.

61 A. Neidlinger, T. Kienz and K. Heinze, *Organometallics*, 2015, **34**, 5310–5320.

Chapter 5: Conclusion

5.1 Summary of the study and its contribution to the field of Fischer carbene chemistry

Classic acyclic mono-heteroatom stabilized Fischer carbene complexes (FCCs) have found use in numerous organic transformation reactions over the past few decades. The scarcity of FCCs in catalysis can be attributed to the inaccessibility *via* the classic Fischer route of catalytically relevant late transition metal FCCs (which would require the reaction of an organolithium entity with metal-carbonyls, ideally in the absence of any halogenated species). As such, literature reports entailing the catalytic application of FCCs prior to this study were limited to ferrocenyl (Fc) substituted rhodium(I) FCC catalyzed olefin hydroformylation,[1] and more recently, a gold(I) Fc-alkoxycarbene complex for application in redox-switchable oxazoline synthesis.[2] In each case, carbene ligand transfer (transmetallation) from group 6 metals to the late transition metal (rhodium or gold) atom was prerequisite to synthesize the Fc-substituted precatalysts.

Additionally, iridium(I) FCCs were hitherto underexplored, and their catalytic application was consequently nonexistent. *N*-heterocyclic carbene (NHCs) complexes of rhodium, iridium, and gold (among a range of reported catalytically relevant metal-atoms) have however been extensively studied, and their respective catalytic applications thus continually reported. The strong electron donating property of NHC ligands, an effect of multi-heteroatom stabilization of the carbene carbon atom, is the main advantage leading to the isolability of free NHCs and increased stability of associated metal-complexes, and consequently, to the ample catalytic application of metal-NHCs in literature. Complimentary, the limited catalytic application of mono-heteroatom stabilized FCCs is thus attributed to the reduced stability of late transition metal FCCs in comparison to NHC analogues, and to the consequent decomplexation of the FC ligand previously reported for Rh^{I}, Pd^{II}, and Cu^{I} FCCs, wherein olefinic carbene (self-dimerization) products are formed even at ambient temperatures. This problematic self-dimerization of late transition metal FCCs can however be prevented by using more electron donating carbene substituents (such as metallocenes), and paves the way for the preparation of catalytically-relevant and easily-tunable FCCs with virtually any transition metal to open up new possibilities in molecular catalysis.

In this study, previously reported (**1** – **5**, **7**, **8**) and slightly modified (**6**) W^{0} ethoxy-FCCs, featuring the (hetero)aryl carbene substituents 2-thienyl (Th, **1**), 2-furyl (Fu, **2**), *para*-*N*,*N*-dimethylaniline (*p*-DMA, **3**) $Cp^{'}Fe(CO)_2Me$ (**4**), $Cp^{'}Mn(CO)_3$ (**5**), $Cp^{'}Re(CO)_3$ (**6**), ruthenocenyl (Rc, **7**), and Fc (**8**), were synthesized *via* the Fischer route for application in transmetallation reactions with Rh^{I}, Ir^{I}, and Au^{I} metal centers.

Spectroscopic and structural characterization of the isolated W^0, Rh^I, Ir^I, and Au^I FCCs generally indicated an increase in electron-donating ability the aryl carbene substituents in the order Th ≈ Fu < $Cp'M(CO)_2L$ (M = Fe, Mn, Re. L = Me, CO) << Fc ≈ Rc < *p*-DMA. Notably, a direct comparison of the carbene ligand donicity could be achieved by calculating the Tolman electronic parameters (TEPs) from the carbonyl stretching vibrations recorded in the measured FT-IR spectra of the corresponding rhodium(I)/ iridium(I) dicarbonyl chloride carbene complexes.[3,4] In this way, the (sometimes subtle) role played by the (hetero)aryl or metal-containing carbene substituent could be highlighted in structure-activity relationships of the carbene complexes and their catalytic performance. This new methodology consequently also allows for direct and unambiguous comparison with the electronic properties of other commonly used organometallic ligands, e.g. phosphines and NHCs.

5.2 Preparative challenges and catalytic performance of Rh^I FCCs

Carbene ligand transfer reactions from W^0 FCCs **4** ($Cp'Fe(CO)_2Me$), **5** ($Cp'Mn(CO)_3$), and **6** ($Cp'Re(CO)_3$ to rhodium proved problematic due to decomposition of the targeted Rh^I FCC/ starting material, and the envisaged Rh^I FCCs could not be isolated. This decomposition of piano stool substituted Rh^I FCCs was in agreement with the self-dimerization decomposition observed for heteroaryl (Th-, Fu-) analogues, as reported in previous studies. New examples of Rh^I carbene complexes **10** – **13** were successfully synthesized, *via* transmetallation from W^0 analogues **3** (*p*-DMA) and **7** (Rc) and subsequent co-ligand modification, for catalytic application in the hydroformylation of 1-octene.

Results obtained from the hydroformylation reactions were compared to the previously reported Fc analogues **14** – **17**. The Rc-substituted carbene complexes **11** and **13** showed the best catalytic activity with turnover frequencies (TOFs) of 650 and 608 hr^{-1}, respectively, and also surpass the previously reported Fc-analogues (TOFs up to 418 hr^{-1}). Comparison of the catalytic behaviour of metallocenyl-substituted Rh^I ethoxycarbene complexes indicated insignificant changes in catalytic activity, chemoselectivity, or regioselectivity as an effect of variation of the -cod or -$(CO)_2$ co-ligand environments. In the case of the *p*-DMA-substituted complexes however, significant decrease in the catalytic activity and chemoselectivity, along with a notable increase in regioselectivity, were observed when comparing Rh- cod (**10**) and -$(CO)_2$ (**12**) complexes.

Additionally, selective chemical oxidation of our previously reported Rh^I-$(CO)_2$ Fc-aminocarbene complex (**17**) at the Fe^{II} site yielded the desired Rh^I ferroceniumyl (Fc^+) complex **17**$^+$. Conversion of the electron- donating Fc substituent into the -withdrawing Fc^+ analogue effectively increases the electrophilicity of the carbene carbon atom, as corroborated by an increase in the calculated TEP value

from 2049 (**17**) to 2063 cm^{-1} (**17**$^{+}$). Catalytic evaluation of the *in situ*-generated **17**$^{+}$ indicated a significantly improved regioselectivity while catalytic activity and chemoselectivity decreased. The trade-off between catalytic activity and selectivity remains an area that can be further optimized with the availability of new (acyclic)carbene complexes of rhodium(I) where both steric and electronic properties can be altered significantly by facile ligand modification. This yields a class of compounds to rival the performance of the ubiquitous (cyclic) NHC complexes in olefin hydroformylation.

5.3 A new class of Ir^{I} FCCs and demonstration of their activity in homogeneous catalysis

A series of novel Ir^{I}-cod ethoxy-FCCs (**18** – **20**) were for the first time synthesized by direct transmetallation from W^{0} analogues. Subsequent carbene and co-ligand modification yielded Ir- cod aminocarbene (**21** – **23**) and -$(CO)_2$ (**24**, **25**) complexes. The stability of the Cp'$Re(CO)_3$-substituted complex **19** (attested to by the isolation and complete characterization of said complex) is in stark contrast to the inaccessibility of the Rh^{I} analogue (**9b**) that proved unstable and resulted in carbene-dimerization decomposition at room temperature. This suggests that the Ir(cod)Cl- moiety exhibits stronger π-backbonding with the carbene carbon atom (**19**) than does the Rh(cod)Cl- moiety (**9b**). The relative electron-donating ability of the different carbene ligands towards the central iridium metal, was established by calculation of the corresponding TEP values. The FC ligands could thus be arranged in order of increasing electron donating strength as :C(OEt)Cp'$Re(CO)_3$ (**19**) < :C(OEt)Fc (**20**) < :C(OEt)*p*-DMA (**18**) < :C(NH^{n}Pr)Fc (**22**) < :C(NH^{n}Pr)*p*-DMA (**21**) < :C(NH$(CH_2)_2NMe_2$)Fc (**23**).

The isolated Ir^{I} complexes were utilized as precatalysts in the base-assisted transfer hydrogenation (TH) of acetophenone, a first for classic FCCs of iridium. Results of the catalytic application of Ir^{I} FCCs (**18** – **25**) in the TH of acetophenone showed increase in percentage conversions/ yields with decreasing electrophilicity of the carbene carbon atom (as the electron-donating strength of the carbene substituents increased). Excellent TOFs were achieved at a low iridium/base/substrate ratio of 1/5/1000, and were comparable to state-of-the-art NHCs in literature. The best catalytic activity resulted from use of Fc-carbene complex **23**, where inclusion of a hemilabile carbene carbon substituent bearing a pendant tertiary-amino -NMe_2 moiety, resulted in a high TOF of 445 hr^{-1}. NMR spectroscopic characterization of the Fc-propylamino (**22**) and Fc-diamino (**23**) carbene complexes, indicated that the pendant -NMe_2 moiety in the latter complex remains untethered. However, the potential chelation-effect of the pendant -NMe_2 (to stabilize intermediates in the catalytic cycle) as an explanation for the much enhanced catalytic activity of **23** is not excluded. In addition, possible synergic effects due to the presence of the additional Fe^{II} metal site, in accordance with cooperative catalysis in literature, can be another reason to account for the improved catalytic performance.

5.4 The role of carbene substituents in redox-switchable gold(I) FCC (pre)catalysts

Lastly, a series of gold(I) ethoxycarbene complexes (**26** – **29**) were synthesized *via* transmetallation from W^0 analogues. Post-transmetallation aminolysis of the Fu- (**27**), *p*-DMA- (**28**) and Fc-substituted (**29**) ethoxycarbene complexes was achieved, resulting in a series of *N*-atom stabilized complexes **30** – **35** for application in redox-switchable catalytic reactions. Regrettably, aminolysis of the Th-ethoxycarbene complex **26** proved problematic, and this reaction pathway was subsequently discontinued. Spectroscopic and structural characterization of the isolated mono- (NH^nPr, **30** – **32**) and di-amino ($NH(CH_2)_2NMe_2$, **32** – **35**) carbene complexes indicated that the pendant amino-NMe_2 moiety in the latter class (**32** – **35**) remains untethered, as seen for the iridium analogues. However, cyclic voltammetry measurements of **30** – **35**, as well as DFT calculations of the respective monocations **30**$^+$ – **35**$^+$, suggest Au-NMe_2 coordination upon one-electron oxidation of the diamino-carbene complexes **33** – **35**.

Evaluation of complexes **30** – **35** as precatalysts in intramolecular oxazoline synthesis reactions was undertaken, wherein addition of the external oxidant Magic Blue (MB) was required for catalytic activity. Complexes bearing Fc- and/or di-amino -$NH(CH_2)_2NMe_2$ carbene substituents indicated the best catalytic activity as compared to the organic (Fu-, *p*-DMA-) and/or mono-amino (-NH^nPr) analogues, respectively. Thus cooperative Au-Fc and Au-NMe_2 catalytic activity is inferred for Fc- and diamino-substituted complexes, respectively. Time-dependent catalytic and electron paramagnetic resonance (EPR) studies were done to ascertain the exact nature of the catalytically active species. For the organic (Fu-, *p*-DMA-) substituted complexes, where DFT calculations had indicated Au^{II} monocationic species, the investigated catalytic activity suggests that the active Au^{II} intermediates (of **30**$^+$, **31**$^+$, **33**$^+$, **34**$^+$) are unstable, with no EPR-activity observed for the **30/MB**, **31/MB**, **33/MB**, and **34/MB** mixtures. In the case of the Fc-substituted complexes, however, where DFT calculations (of the monocations **32**$^+$ and **35**$^+$) had shown most-favoured Au^IFe^{III} species, EPR signals corresponding to Au^{II} species were observed for the **32/MB** and **35/MB** mixtures. In addition, recovery of the Fc precatalysts **32** and **35** was possible (by addition of a suitable reductant to the **32/MB** and **35/MB** mixtures, respectively). Therefore, additional reactivity pathways were suggested for the Fc-substituted precatalysts to account for the EPR-activity. The corresponding ferrocenophane-substituted Au^{II} intermediates were postulated as the catalytically active species, and the results were supported by DFT calculations. The suggested Au^{II} active species of the Fc-substituted aminocarbene precatalysts **32** and **35**, with the Fc unit acting as a temporary parking position for a positive charge upon reaction with MB in both cases, were in agreement with the previously reported ethoxy-analogue **29**.

5.5 Future perspectives

For a more in-depth understanding of the catalytic behaviour of Rh^{I} FCCs discussed in Chapter 2, further fine-tuning of the organic carbene-substituent in **10** and **12** (*p*-DMA) is hence envisaged as future work. This will be undertaken *via* inclusion of more- or less electron-donating non-organometallic carbene substituents (for example, by varying phenyl ring substituents (and *p*-, *m*-, or *o*- positions thereof) from *p*-(NMe_2)Ph (*p*-DMA) to *p*-(NPh_2)Ph, *p*-(OMe)Ph, etc). If isolable, the resulting Rh^{I} complexes featuring purely organic FC ligands would exhibit structural properties to be deduced from spectroscopic, electrochemical, and crystallographic characterization techniques, along with varied catalytic behaviours, which can thence be compared and tentatively be used to rationalize currently ambiguous trends of *p*-DMA-substituted complexes **10** and **12**.

Additionally, the synthesis of a *p*-DMA-substituted Ir^{I} diaminocarbene complex analogous to the Fc-substituted complex **23**, is intended. The featured :C($NH(CH_2)_2NMe_2$)*p*-DMA FC ligand should be more electron-donating towards the central Ir^{I} metal atom than is the :C($NH(CH_2)_2NMe_2$)Fc ligand, in line with the established stronger electron-donating property of the *p*-DMA substituent as compared to the Fc entity. Consequently, evaluation of the catalytic activity of the targeted *p*-DMA diaminocarbene complex in the TH of acetophenone, should result in TOFs greater than reported herein, and the catalytically active species can potentially be analyzed in more detail.

Finally, the role of other redox-non-innocent (metallocenyl or piano stool) carbene substituents in Au^{II}-mediated oxazoline synthesis will be investigated. The targeted bimetallic Au^{I} precatalysts will be synthesized *via* carbene ligand transfer and subsequent FC ligand modification, prior to catalytic application in intramolecular oxazoline synthesis reactions, as described in Chapter 4. Kinetic studies of Fc-substituted precatalysts **32** and **35**, further detailing the proposed mechanism leading to ferrocenophane-substituted Au^{II} catalytically active species, are currently underway.

5.6 References

1 G. K. Ramollo, M. J. López-Gómez, D. C. Liles, L. C. Matsinha, G. S. Smith and D. I. Bezuidenhout, *Organometallics*, 2015, **34**, 5745–5753.

2 P. Veit, C. Volkert, V. Förster, Christoph Ksenofontov, S. Schlicher, M. Bauer and K. Heinze, *Chem. Commun.*, 2019, **55**, 4615–4618.

3 S. Wolf and H. Plenio, *J. Organomet. Chem.*, 2009, **694**, 1487–1492.

4 T. Dröge and F. Glorius, *Angew. Chem. Int. Ed.*, 2010, **49**, 6940–6952.

Chapter 6: Experimental

6.1 Standard operating techniques

The preparation, purification and reactions of the complexes described were carried out under an atmosphere of dry N_2 or Ar gas using standard Schlenk-line techniques. All reactions were mechanically stirred and monitored by IR spectroscopy where relevant. The substrate *N*(2-propyn-1-yl)benzamide,[1] and precursors $[CpFeMe(CO)_2]$,[2] $[Et_3O][BF_4]$,[3] $[M(cod)Cl]_2$ [M = Rh, Ir],[4,5] and [Au(tht)Cl][6] were prepared according to literature procedures. Aluminium oxide 60 (particle size 0.05 – 0.15 mm) or silica gel 60 (particle size 0.0063 – 0.200 mm) was used as resin for all column chromatography separations as specified. Anhydrous tetrahydrofuran (THF), diethyl ether (Et_2O), and *n*-hexane were distilled over sodium metal. Acetonitrile and dichloromethane (DCM) were distilled over CaH_2. All other reagents are commercially available and were used as received.

6.2 Characterization techniques

6.2.1 NMR spectroscopy

Nuclear magnetic resonance (NMR) spectra were recorded on Bruker Avance-III-300, Bruker Avance-III-400 and Bruker Avance-III-500 spectrometers using $CDCl_3$, CD_2Cl_2, THF-*d8* and C_6D_6 as solvents at 25 °C. The NMR spectra were recorded for ^1H at 300.13, 400.13 and 500.13 MHz, and for $^{13}C\{^1H\}$ at 75.48, 100.63 and 125.78 MHz. The ^{19}F NMR spectrum of complex **17**$^+$ was recorded at 376.46 MHz. The chemicals shifts were recorded as δ (in ppm), using deuterated solvent signals for internal references. The $CDCl_3$, CD_2Cl_2, THF-*d8* and C_6D_6 solvents were respectively assigned at 7.2600, 5.3200, 1.7300 and 7.1600 ppm for δH, and at 77.160, 54.00, 25.370 and 128.060 ppm for δC. 2D NMR techniques (COSY, HSQC) were employed to assign signals that were otherwise ambiguous.

6.2.2 Infrared spectroscopy

Infrared spectroscopy was performed on a PerkinElmer Spectrum FT-IR spectrophotometer over the range 4000 – 600 cm^{-1}. Solution IR spectra were recorded in CH_2Cl_2 using a NaCl cell with a path length of ca. 1.0 mm.

6.2.3 Melting point measurements

Melting points were measured with a Stuart SMP10 melting point apparatus.

6.2.4 X-ray crystallography

All crystals for single-crystal X-ray diffraction were grown by slow diffusion of *n*-hexane into a concentrated CH_2Cl_2 solution of the carbene complex at 4 °C. Single crystal X-ray diffraction data for complexes **10**, **12**, **18** – **22**, **24**, **26** – **32**, **34**, and **35** were collected at 173 K while data for **11** was collected at 150 K. XRD data for complexes **10**, **19**, **24**, **26**, **28** – **32**, **34**, and **35** were collected on a Bruker Apex II CCD diffractometer, while data for complexes **11**, **12**, **20**, **21**, **22**, and **27** were collected using a Bruker Venture D8 Photon CMOS diffractometer, with a graphite-monochromated Mo-K_α (λ = 0.71073 Å) radiation using an Oxford Cryostream 600 cooler. All data reductions were carried out using the program SAINT+, version 6.02[7] and empirical absorption corrections were made using SADABS.[7] Space group assignments were made using *XPREP.*[7] The structures were solved in the *WinGX*[8] Suite of programs, using intrinsic phasing through *SHELXT*[9] and refined using full-matrix least-squares/difference Fourier techniques on F^2 using *SHELXL-2017*.[9] All C-bound H atoms were placed at idealized positions and refined as riding atoms with isotropic parameters 1.2 times those of their parent atoms. The amine-H atom positions in **21**, **22**, **30** – **32**, **34**, and **35** were located and were refined. All diagrams and publication material were generated using OLEX2,[10] *ORTEP-3*,[8] and *PLATON*.[11] Experimental details of the X-Ray analyses are provided in Tables 6.1 – 6.3 below.

Table 6.1 Crystal data and summary of data collection and refinement for rhodium(I) FCCs **10**, **11**, and **12**

Crystal data for:	**10**	**11**	**12**
Chemical formula	$C_{19}H_{27}ClNORh$	$C_{21}H_{26}ClORhRu$	$C_{13}H_{15}ClNO_3Rh$
M_r	423.77	533.85	371.62
Crystal system	Monoclinic	Monoclinic	Monoclinic
Space group	$P2_1/c$	$P2_1/n$	$P2_1/c$
Temperature (K)	173	150	173
a (Å)	15.1355(8)	7.2519(4)	11.9906(5)
b(Å)	9.3853(4)	17.1093(9)	10.1632(4)
c (Å)	12.7973(7)	15.5569(9)	13.8171(6)
α (°)	90	90	90
β (°)	92.231(2)	94.663(2)	114.701(11)
γ (°)	90	90	90
V (Å^3)	1816.49(16)	1923.83(18)	1529.73(11)
Z	4	4	4
Radiation type	Mo $K\alpha$		
μ (mm^{-1})	1.091	1.788	0.683
Crystal size (mm)	0.498 × 0.412 × 0.102	0.268 × 0.178 × 0.060	0.114 × 0.078 × 0.057
Absorption correction			
T_{min}, T_{max}	0.619, 0.746	0.540, 0.631	0.900, 0.950
No. of reflections			
measured	10879	119483	33904
independent	3386	7421	2893
observed [I> 2σ(I)]	2859	5748	2291
R_{int}	0.0387	0.0813	0.0783
(sin θ/λ)$_{max}$ (Å^{-1})	0.606	0.773	0.481
Refinement			
$R[F^2> 2\sigma(F^2)]$	0.0295	0.0278	0.0267
$wR(F^2)$	0.0721	0.0507	0.0605
S	1.032	1.057	1.051
No. of reflections	3386	7421	2893
No. of parameters	211	227	174
No. of restraints	0	0	0
H-atom treatment	Constrained	Constrained	Constrained
Δρ$_{max}$, Δρ$_{min}$ (e Å^{-3})	0.69, -0.34	0.60, -0.79	0.41, -0.34

Table 6.2 Crystal data and summary of data collection and refinement for iridium(I) FCCs **18** – **22**, and **24**

Crystal data for:	**18**	**19**	**20**	**21**	**22**	**24**
Chemical formula	$C_{19}H_{27}ClIrNO$	$C_{19}H_{21}ClIrO_4Re$	$C_{21}H_{26}ClFeIrO$	$C_{15}H_{14}ClFeIrO_3$	$C_{20}H_{30}ClIrN_2$	$C_{22}H_{29}ClFeIrN$
M_r	513.06	727.423	577.92	525.76	526.11	590.96
Crystal system	Monoclinic	Orthorhombic	Orthorhombic	Monoclinic	Triclinic	Triclinic
Space group	$P2_1/c$	$P2_12_12_1$	$Pca2_1$	$P2_1/c$	P-1	P-1
Temp.(K)	173	173	173	173	173	173
a (Å)	15.0771(4)	7.1772(2)	23.4785(9)	9.5567(4)	9.7515(7)	7.621(4)
b(Å)	9.4273(2)	13.6484(4)	7.3046(3)	7.4257(3)	10.6457(7)	10.8953(6)
c (Å)	12.7543(3)	20.3481(6)	22.6327(9)	22.3102(9)	11.2922(8)	12.7852(7)
α (°)	90	90	90	90	64.293(2)	109.228(2)
β (°)	92.1530	90	90	95.626(2)	82.960(2)	93.019(2)
γ (°)	90	90	90	90	71.201(2)	95.009(2)
V (Å^3)	1811.57(7)	1993.24(10)	3881.5(3)	1575.54(11)	999.69(12)	994.89(9)
Z	4	4	8	4	2	2
Radiation type	Mo $K\alpha$					
μ (mm^{-1})	7.522	12.891	7.741	9.532	6.815	7.550
Crystal size (mm)	0.311 × 0.296 × 0.086	0.182× 0.167 × 0.053	0.261× 0.087 × 0.064	0.291 × 0.216 × 0.102	0.426 × 0.228 × 0.183	0.263 × 0.202 × 0.106
Absorption correction						
T_{min}, T_{max}	0.206, 0.697	0.177, 0.629	0.341, 0.845	0.097, 0.272	0.185, 0.405	0.621, 0.948
No. of reflections						
Measured	29663	36910	73073	30710	45043	30244
Independent	4376	4825	9376	8184	4811	4788
observed [I> 2σ(I)]	3859	4261	8669	6656	4628	4537
R_{int}	0.0343	0.0750	0.0628	0.0741	0.0269	0.0280
(sin θ/λ)$_{max}$ (Å^{-1})	0.660	0.661	0.660	0.665	0.661	0.660
Refinement						
$R[F^2> 2\sigma(F^2)]$	0.0144	0.0245	0.0309	0.0502	0.0115	0.0154
$wR(F^2)$	0.0324	0.0522	0.0633	0.1414	0.0267	0.0357
S	1.042	1.005	1.032	1.078	1.115	1.139
No. of reflections	4376	4825	9376	8184	4628	4788
No. of parameters	211	237	454	182	225	274
No. of restraints	0	0	1	0	0	96

H-atom treatment	Constrained	Constrained	Constrained	Constrained	Mixed	Constrained
$\Delta\rho_{max}$, $\Delta\rho_{min}$ (e Å^{-3})	0.63, -0.55	1.78, -0.88	1.67, -1.11	2.68, -1.65	1.90, -0.60	2.29, -1.80

Table 6.3 Crystal data and summary of data collection and refinement for gold(I) FCCs **26** – **32**, **34** and **35**

Crystal data for:	**26**	**27**	**28**	**29**	**30**	**31**	**32**	**34**	**35**
Chemical formula	$C_{14}H_{16}Au_2Cl_2O_2S_2$	0.5($C_{28}H_{32}Au_4Cl_4O_8$), 0.5($C_2H_4Cl_2$)	$C_{11}H_{15}AuClNO$	$C_{13}H_{14}AuClFeO$	$C_8H_{11}AuClNO$	$C_{12}H_{18}AuClN_2$	$C_{14}H_{17}AuClFeN$	$C_{13}H_{21}AuClN_3$	$C_{15}H_{21}AuClFeN_2$, $C_{15}H_{20}AuClFeN_2$, $CHCl_3$, Cl
M_r	745.22	798.03	409.66	474.51	369.59	422.70	487.55	451.74	1189.02
Crystal system	Triclinic	Orthorhombic	Orthorhombic	Orthorhombic	Monoclinic	Monoclinic	Orthorhombic	Monoclinic	Monoclinic
Space group	*P*-1	*P*nma	*P*na2$_1$	*P*ca2$_1$	*P*2$_1$/*c*	*P*2$_1$/*c*	*P*2$_1$2$_1$2$_1$	*P*2$_1$/*c*	*P*2$_1$/*n*
Temperature (K)	173	173	173	173	173	173	173	173	173
a (Å)	7.7154(4)	10.1229(6)	7.339(8)	16.9502(4)	8.512(3)	14.4677(9)	7.2466(4)	15.7593(16)	10.7145(3)
b(Å)	10.5169(7)	6.4642(4)	15.5386(17)	7.3598(2)	17.155.(8)	8.4912(5)	13.6643(5)	10.7545(11)	18.4675(5)
c (Å)	12.8618(8)	32.0692(19)	10.7564(11)	10.4161(2)	7.7212(3)	22.2849(14)	14.1747(9)	9.2841(9)	19.2118(5)
α (°)	68.742(3)	90	90	90	90	90	90	90	90
β (°)	79.844(3)	90	90	90	116.430(16)	92.979(3)	90	101.503(4)	93.5689(14)
γ (°)	77.354(3)	90	90	90	90	90	90	90	90
V (Å^3)	943.62(10)	2095.2(2)	1226.7(2)	1299.41(5)	1008.35(7)	2734.0(3)	1431.42(15)	1541.9(3)	3794.07(18)
Z	2	4	4	4	4	8	4	4	1
Radiation type	Mo *K*α								
μ (mm^{-1})	16.035	14.514	12.185	12.578	14.808	10.934	11.418	9.702	8.910
Crystal size (mm)	0.2× 0.097 × 0.092	0.401× 0.3 × 0.19	0.174 × 0.153 × 0.14	0.219 × 0.214 × 0.042	0.321 × 0.214 × 0.105	0.23 × 0.205 × 0.038	0.343 × 0.085 × 0.066	0.563 × 0.112 × 0.06	0.513 × 0.219 × 0.036
Absorption correction									
T_{min}, T_{max}	0.213, 0.518	0.053, 0.164	0.057, 0.190	0.146, 0.901	0.087, 0.305	0.225, 0.760	0.063, 0.644	0.378, 0.746	0.059, 0.775

No. of reflections									
measured	20010	23083	11184	18202	10720	44099	14445		61787
independent	4698	2818	2962	3202	2509	6816	3561	4383	9431
observed [$I > 2\sigma(I)$]	3772	2724	2151	2883	2107	5484	3458	3814	7645
R_{int}	0.0415	0.0244	0.0978	0.0343	0.0484	0.0501	0.0282		0.0426
$(\sin\theta/\lambda)_{max}$ ($Å^{-1}$)	0.668	0.6672	0.6604	0.6668	0.6670	0.6679	0.6676	0.6604	0.6681
Refinement									
$R[F^2 > 2\sigma(F^2)]$	0.0278	0.0274	0.0387	0.0175	0.0266	0.0280	0.0157	0.0362	0.0245
$wR(F^2)$	0.0493	0.0636	0.0877	0.0304	0.0640	0.0550	0.0367	0.0976	0.0490
S	1.080	1.343	0.937	0.836	1.035	1.035	1.029	1.165	1.020
No. of reflections	4698	2818	2962	3202	2509	6816	3561	4383	9431
No. of parameters	201	151	139	154	110	295	164	168	410
No. of restraints	0	0	1	1	0	0	0	0	0
H-atom treatment	Constrained	Constrained	Constrained	Constrained	Constrained	Constrained	Constrained	Constrained	Contrained
$\Delta\rho_{max}$, $\Delta\rho_{min}$ (e $Å^{-3}$)	0.92, -0.84	0.89, -2.35	2.33, -0.94	0.64, -0.51	1.23, -1.76	3.00, -0.75	0.64, -0.68	1.58, -1.52	1.54, -0.90

6.2.5 Mass spectrometry

Mass spectral analyses were performed on a Bruker Compact Q-TOF mass spectrometer (Bruker Daltonics, Bremen, Germany) with a positive electron spray as the ionization technique by direct infusion at 0.3 mL min^{-1}. The *m/z* values were measured in the range of 50 – 1000 in acetonitrile. Prior to analysis, the instrument was calibrated with sodium formate (5 mM) in resolution mode.

6.2.6 Elemental analysis

Elemental analyses were carried out using an Elementar varioELcube CHNS-O analyser.

6.2.7 Cyclic voltammetry

Electrochemical studies of rhodium(I) complexes **10** and **11** were carried out using Metrohm µAutolab type III potentiostat linked to a computer using GPES Electrochemistry software, in conjunction with a three-electrode cell. The working electrode was a glassy carbon disc (3.0 mm diameter) and the counter electrode was a platinum wire. The reference was a non-aqueous Ag/Ag^+ electrode separated from the test solution by a fine porosity frit. Solutions in CH_2Cl_2 were 1.0×10^{-3} mol dm^{-3} in the test compound and 0.1 mol dm^{-3} in $[N^nBu_4][PF_6]$ as the supporting electrolyte. Under these conditions, $E^{\circ\prime}$ for the redox couple $[Fe(\eta\text{-}C_5Me_5)_2]^{0/1+}$, added to the test solutions as internal standard, is -0.54 V. All E_p^{ox}, E_p^{red} and $E^{\circ\prime}$values are at scan rates of 100 mV s^{-1}. The obtained cyclic voltammograms (CVs) of **10** and **11** are presented in Figure 6.1 (a) and (b), respectively.

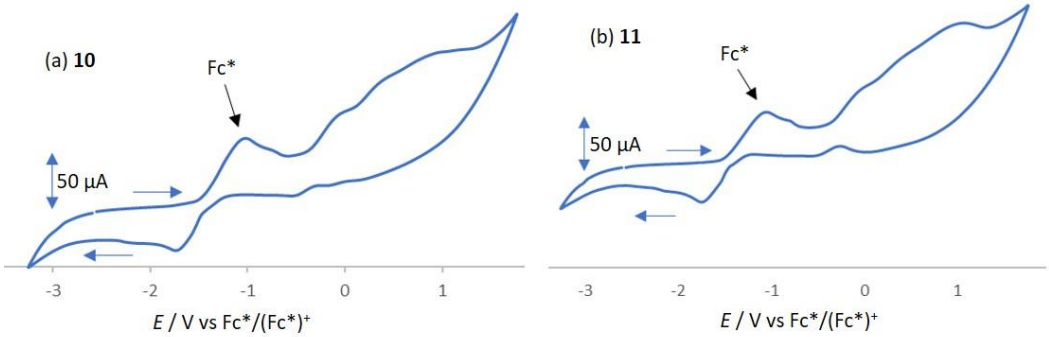

Figure 6.1 CVs of Rh(cod) complexes **10** (a) and **11** (b) in CH_2Cl_2 at a scan rate of 100 mV/s with 0.1 M $[N^nBu_4][PF_6]$ as a supporting electrolyte.

For the gold(I) FCCs **30** – **35**, electrochemical experiments were carried out on a BioLogic SP-50 voltammetric analyser using platinum wires as counter and working electrodes and a 0.01 M $Ag/AgNO_3$ electrode as reference electrode. The cyclic voltammetry measurements were carried out at scan rate of 50–100 mV s^{-1} using 0.1 M $[N^nBu_4][B(C_6F_5)_4]$ or 0.1 M $[N^nBu_4][PF_6]$ as supporting electrolytes in MeCN. Potentials are referenced to the $[Fe(\eta\text{-}C_5H_5)_2]^{0/1+}$ couple (between $E_{½}$ = 85 mV and 140 mV under the experimental conditions). CVs of Fc-substituted gold(I) aminocarbene complexes **32** and **35** are displayed in Figure 6.2 (a) and (b), respectively.

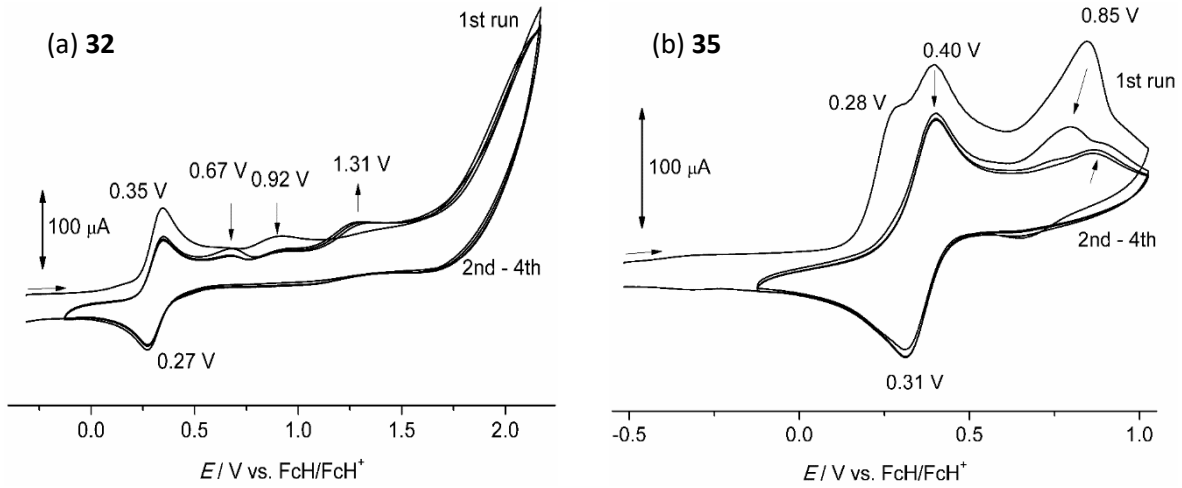

Figure 6.2 Cyclic voltammograms of gold(I) Fc-aminocarbene complexes **32** (a) and **35** (b) in MeCN at a scan rate of 100 mV/s with 0.1 M $[N^nBu_4][PF_6]$ as a supporting electrolyte.

6.2.8 EPR spectroscopy

X-band CW EPR spectra were measured on a Miniscope MS 300 at 77 K cooled by liquid nitrogen in a finger Dewar and at 298 K (Magnettech GmbH, Berlin, Germany). *g* factors are referenced to external Mn^{2+} in ZnS (*g* = 2.118, 2.066, 2.027, 1.986, 1.946, 1.906). Simulations of EPR spectra were performed with EasySpin (v 5.0.0) for MatLab (R2016b).[12] Quantification of the EPR signals was performed *via* an adapted literature procedure.[13,14] For quantification measurements, EPR tubes with an internal diameter of 2.0 mm were used. The calibration curve was determined using commercially available tetraphenylporphyrinato copper(II) (CuTPP) as standard. The samples were prepared in a glovebox under argon, and the EPR tubes were filled with 400 µL of the solution and sealed with Critoseal. They were inserted 10.4 cm (measured at the top of the Teflon holder) into the EPR spectrometer. Four concentrations (*c* = 1.67, 0.84, 0.42 and 0.21 mm) in THF were used for the calibration. The settings for the calibration curve and the sample EPR spectra were as follows: temperature = 298 K, field = 2999 G, sweep = 2498 G, sweep time = 60 s, modulation = 2000 mG, MW attenuation = 10 db, and number of passes = 3. The double integral of the experimental, baseline corrected spectra was plotted against the concentration. The resulting calibration (linear regression; $y = (1.45\pm0.07)\times10^5\times c(\text{mm})-(0.19\pm0.05)\times10^5\times c(\text{mm})$; $R^2 = 0.9939$) was used to quantify the experimental spectra of **32**/**35** after oxidation with Magic Blue.

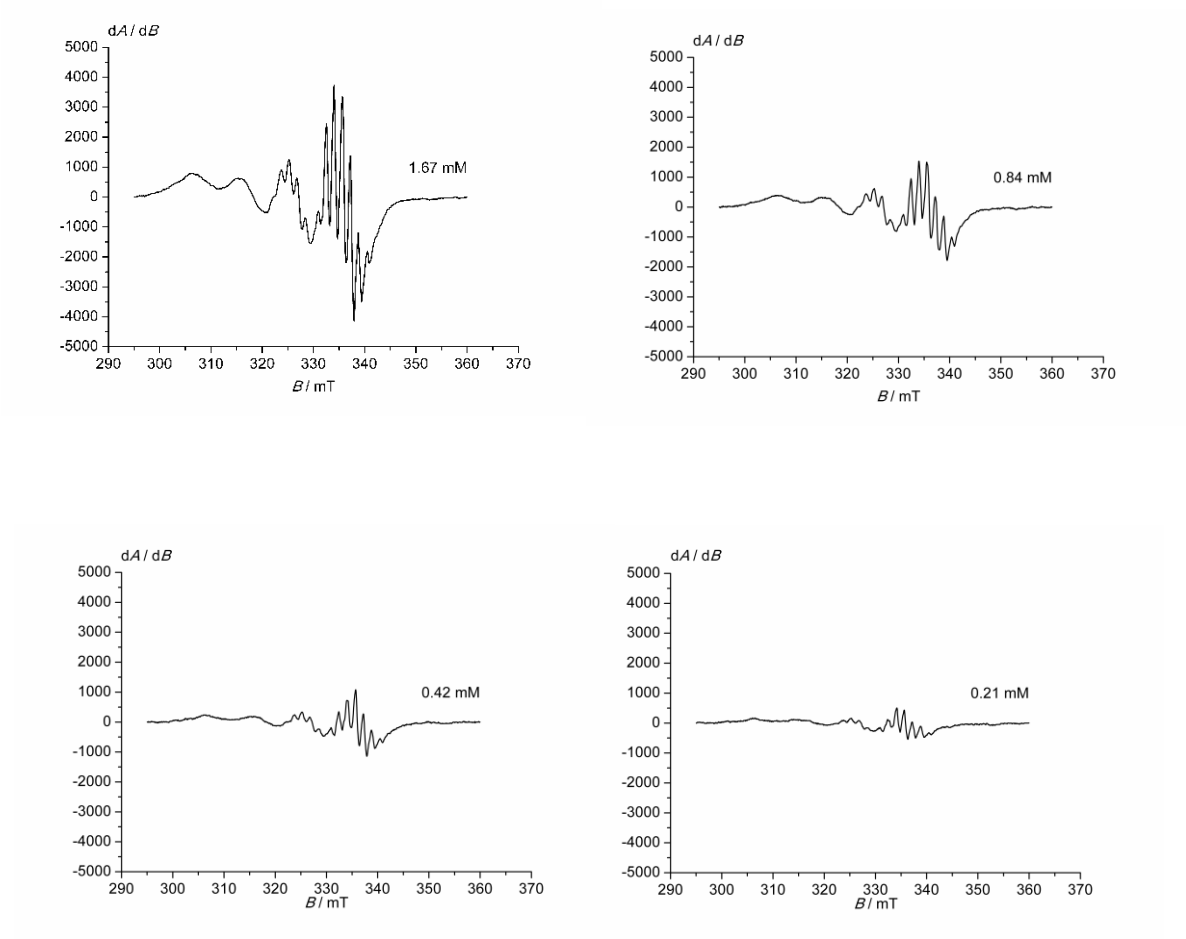

Figure 6.3 X-band EPR spectra of Cu(TPP) in THF at different concentrations

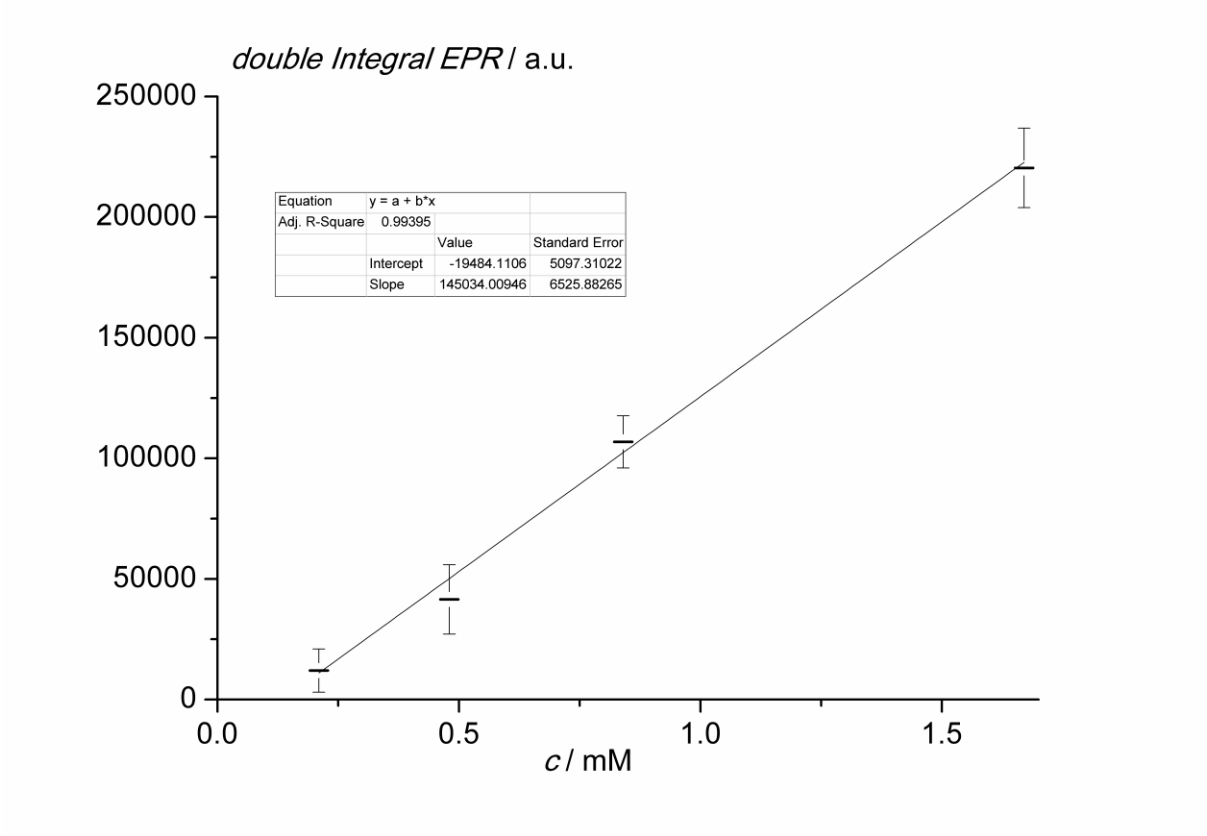

Figure 6.4 Linear regression of the double integral of the EPR resonances of Cu(TPP) versus concentration

6.2.9 DFT calculations

Density functional theory calculations were carried out using the ORCA program package (version 4.0.1).[15] All calculations were performed using the B3LYP functional[16–18] and employ the RIJCOSX approximation.[19,20] Relativistic effects were calculated at the zeroth order regular approximation (ZORA) level.[21] The ZORA keyword automatically invokes relativistically adjusted basis sets. To account for solvent effects, a conductor-like screening model (CPCM) modelling dichloromethane was used in all calculations.[22,23] Geometry optimizations were performed using Ahlrichs' split-valence triple-ξ basis set ZORA-def2-TZVP.[24] The auxiliary basis set for General-purpose Coulomb fitting SARC/J decontracted def2/J up to Kr was used.[25] The segmented all-electron relativistically contracted (SARC) auxiliary basis set beyond Kr, SARC-ZORA-TZVP, was used for gold and a special grid of 7 (default 4).[21,26–28] Atom-pairwise dispersion correction was performed with the Becke-Johnson damping scheme (D3BJ).[29,30] The presence of energy minima was checked by numerical frequency calculations.

6.3 General procedures for the catalytic reactions

6.3.1 Hydroformylation of 1-octene

The rhodium-catalyzed hydroformylation reactions were carried out in triplicate, in 90 ml stainless steel pipe reactors. Each reactor was charged with the catalyst precursor (5.096 $X10^{-3}$ mmol), the substrate: 1-octene (0.805 g, 7.175 mmol), and the internal standard: *n*-decane (0.204 g, 1.435 mmol) all dissolved in toluene (5 ml). The reactor was sealed, purged three times with N_2(g) and twice with syngas (1:1, CO/H_2) before heating to the desired temperature, under the desired syngas pressure. Once the reaction time was reached, the reactor was depressurized and the reaction mixture was allowed to cool to room temperature before analysing using gas chromatography. Authentic aldehyde and *iso*-octene standards were used for the confirmation of the products afforded.

6.3.2 Transfer hydrogenation of acetophenone

The iridium-catalyzed transfer hydrogenation reactions were done under an argon atmosphere in thick glass reaction tubes fitted with a greasless high-vacuum stopcock. In a typical reaction, the schlenk tube was charged with a solution of acetophenone (2.0 mmol, 230 µL) in *iso*-propanol (4 mL), base (42 µL, 0.01 mmol of a 0.24 M KOH solution in *iso*-propanol), internal standard (*n*-decane, 100 µL), and the iridium precatalyst (0.002 mmol, 0.1 mol %). The mixture was stirred at 82 °C for the required number of hours. Conversions were determined by gas chromatography analysis under the following conditions: column temperature 35 °C (2 min) to 220 °C at 20 °C/min with a flow rate of 1 mL/min using ultrapure He as carrier gas.

6.3.3 Intramolecular oxazoline synthesis

The gold-catalyzed cyclization reactions were done under an argon atmosphere in NMR tubes and in the absence of light. In a typical reaction, the tube was charged with a solution of *N*(2-propyn-1-yl)bezamide (0.10 mmol, 0.016 g) in the specified solvent (CD_2Cl_2 or THF-d_8), internal standard (1,4-di-*tert*-butylbenzene, 0.10 mmol, 0.019 g), gold complex (0.001 mmol, 1.0 mol%) and the oxidant magic blue (1.25 x 10^{-3} mmol, 1.00 x 10^{-3} g). The mixture was shaken and left standing for the required time period. All catalytic reactions were monitored by ^{1}H NMR spectroscopy at the beginning of the reaction (before addition of the gold complex and Magic Blue, T_0) and 24 hours after catalytic activation (T_{24}). In a typical reaction, catalytic activity of the investigated gold complex (in terms of percentage conversion/ yield) was calculated by integration values of the NC**H**$_2$ signal (green annotation in the T_0 and T_{24} ^{1}H NMR spectra) indicated in Figures 6.5 and 6.6, respectively.

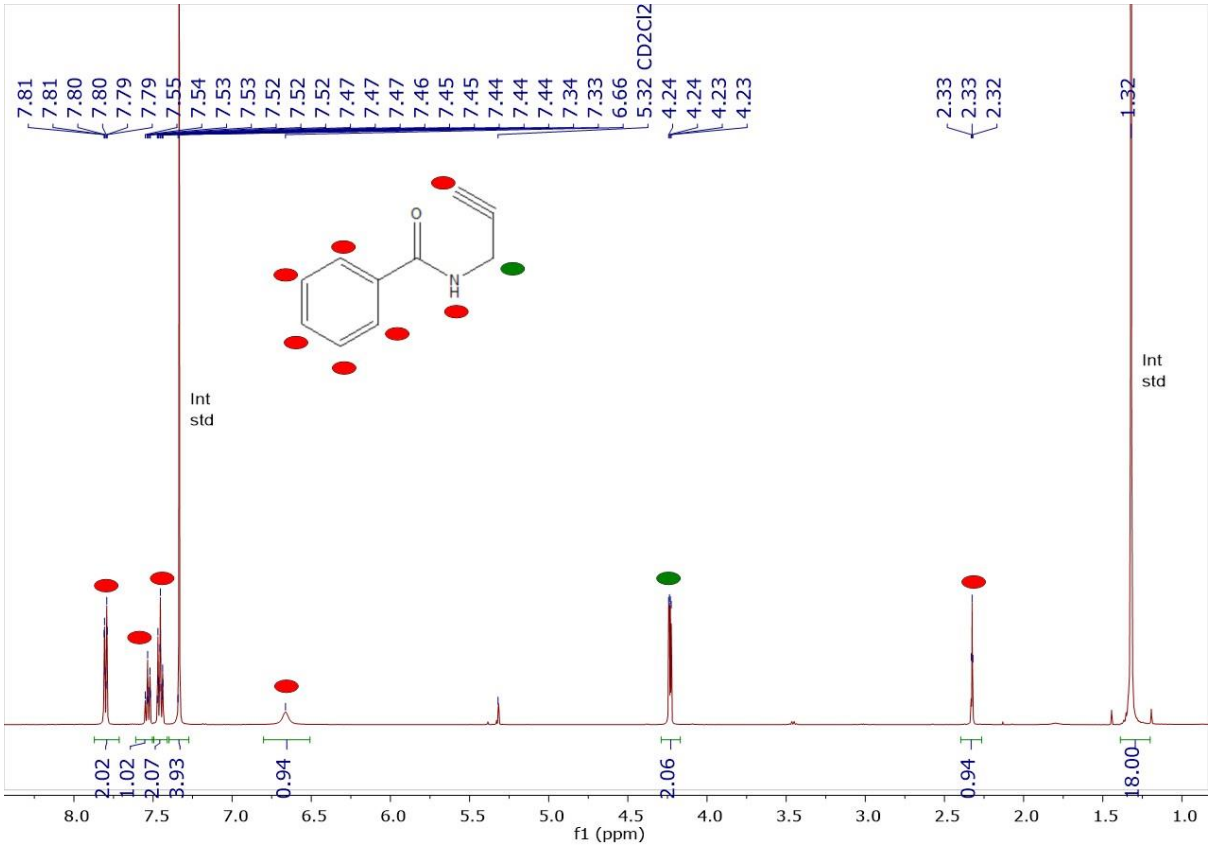

Figure 6.5 A model ^{1}H NMR spectrum of intramolecular oxazoline synthesis at T_0.

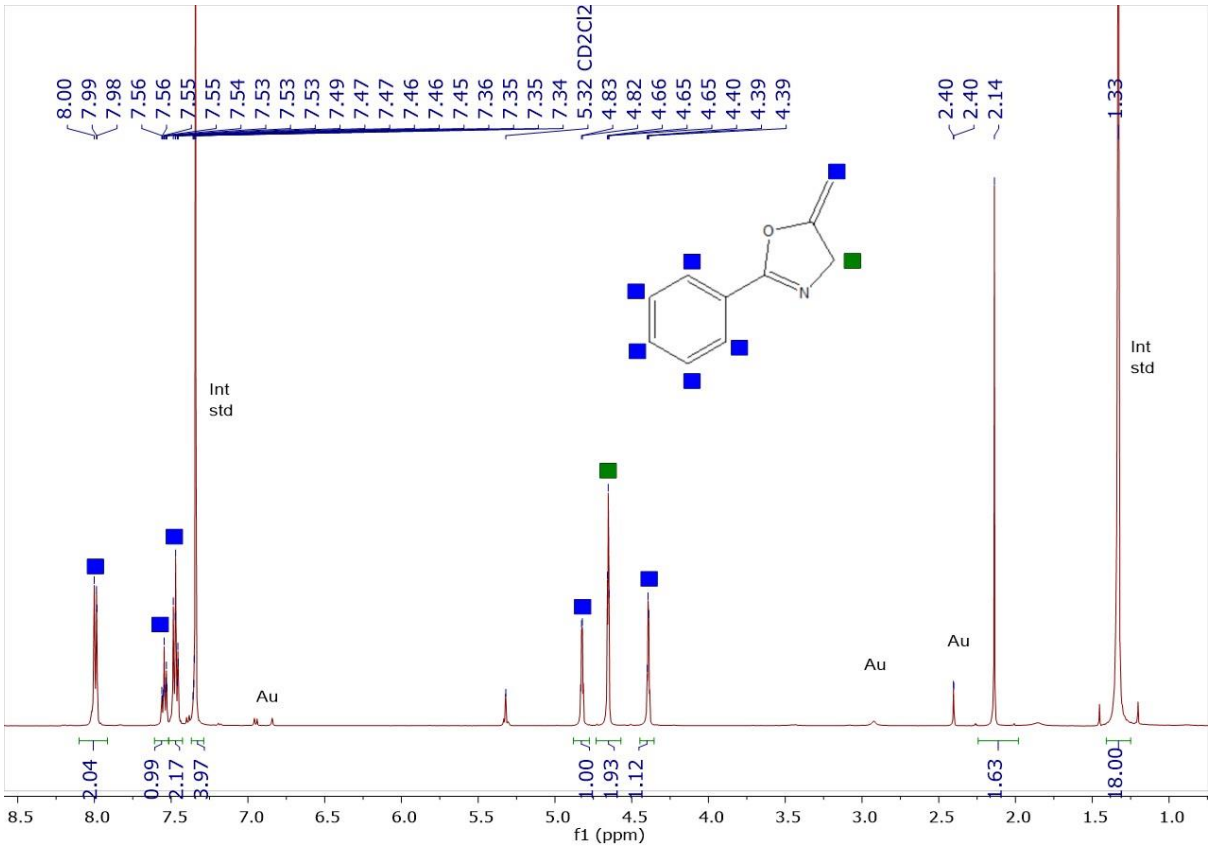

Figure 6.6 A model ^{1}H NMR spectrum of intramolecular oxazoline synthesis at T_{24}.

6.3.4 Intermolecular oxazoline synthesis

These reactions were done similarly to the intramolecular reactions described in section 6.3.3 above, using benzaldehyde and methyl *iso*cyanoacetate instead of the *N*(2-propyn-1-yl)bezamide substrate. All catalytic runs were done in the specified deuterated solvent in a high-pressure NMR tube, using 5 mol% gold(I) complexes and 2.5 mol% NEt_3 (with respect to the substrates). In all cases, 25 µL (0.245 mmol) benzaldehyde, 22 µL (0.245 mmol) methyl *iso*cyanoacetate substrates and 46.6 mg (0.245 mmol) 1,4-di-*tert*-butylbenzene internal standard were employed. Due to the anbiguty of the results, and lack of computational data to infer a reaction mechanism, only the intramolecular cylization results have been further investigated and discussed in this study. All data obtained from the intermolecular reactions is tabulated in Table 6.4 below.

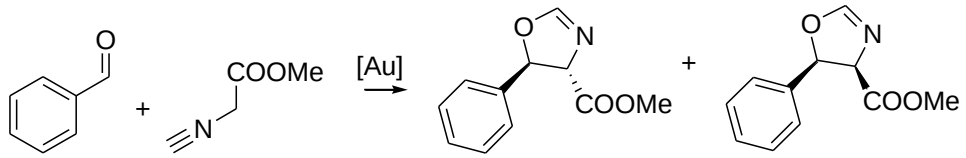

Scheme 6.1 Schematic representation of the gold-catalyzed intermolecular oxazoline synthesis described in Section 6.3.4

Table 6.4 Intermolecular oxazoline synthesis results of gold(I) precatalysts **26** – **33**, and **35**.

Entry	**[cat] no.**	**Loading (mol%)**	**Additive (mol%)**			**solvent**	**Temp. (°C)**	**% conversion**	**% yield**	***Cis/ trans***
			$AgPF_6$	**NEt_3**	**MB**					
1	**32**	5	-	-	-	CD_2Cl_2	40	32	18	8/10
2	**32**	5	-	-	-	THF-d_8	40	40	15	2/13
3	**32**	5	-	-	-	CD_2Cl_2	RT	0	0	0
4	**32**	5	-	-	-	THF-d_8	68	61	41	13/28
5	**32**	10	-	-	-	THF-d_8	68	66	48	15/33
6	**32**	5	5	-	-	THF-d_8	68	66	46	12/34
7	**32**	5	5	10	-	THF-d_8	68	95	94	16/78
8	**32**	5	-	10	-	THF-d_8	68	96	91	18/73
9	**-**	-	-	10	-	THF-d_8	68	68	48	6/42
10	**-**	-	-	2.5	-	THF-d_8	68	28	5	0/5
11	**32**	5	-	2.5	-	THF-d_8	68	91	89	22/67
12	**32**	5	-	2.5	-	THF-d_8	RT	100	100	18/80
13	**32**	5	-	-	-	THF-d_8	RT	4	2	0/2

14	**32**	1	-	2.5	-	THF-d_8	RT	62	51	10/41
15	**-**	-	-	2.5	-	THF-d_8	RT	3	1	0/1
16	**32**	1	-	2.5	1	THF-d_8	RT	42	24	4/20
17	**32**	1	-	-	1	THF-d_8	RT	15	0	0
18	**32**	1	-	2.5	1	CD_2Cl_2	RT	18	0	0
19	**32**	1	-	-	1	CD_2Cl_2	RT	5	0	0
20	**29**	1	-	-	1	CD_2Cl_2	RT	0	0	0
21	**32**	5	5	10	-	THF-d_8	68	95	94	16/78
22	**-**	-	5	10	-	THF-d_8	68	98	57	4/53
23	**33**	5	-	2.5	-	THF-d_8	68	92	87	23/64
24	**28**	5	-	2.5	-	THF-d_8	68	76	47	13/34
25	**27**	5	-	2.5	-	THF-d_8	68	75	56	16/40
26	**26**	5	-	2.5	-	THF-d_8	68	87	44	14/30
27	**29**	5	-	2.5	-	THF-d_8	68	65	54	14/40
28	**30**	5	-	2.5	-	THF-d_8	68	84	65	19/46
29	**31**	5	-	2.5	-	THF-d_8	68	92	79	26/53
30	**35**	5	-	2.5	-	THF-d_8	68	95	94	22/72

6.4 Cartesian coordinates of optimized geometries

30^+

1	-2.315076000	-1.968996000	-1.617501000
1	-2.359606000	-4.452945000	-1.409125000
1	-0.715130000	-2.576672000	-1.204602000
1	-0.208716000	4.582055000	0.407677000
6	-1.736897000	-2.465059000	-0.833604000
6	-2.339477000	-3.829243000	-0.514876000
6	0.306253000	3.657946000	0.201328000
1	2.258445000	4.097259000	-0.704576000

6	1.543450000	3.371823000	-0.355356000
8	-0.350863000	2.523450000	0.524284000
1	-3.363354000	-3.732093000	-0.147509000
1	-1.728438000	0.339914000	-0.482291000
1	-1.753749000	-4.348422000	0.246463000
6	1.656825000	1.987915000	-0.369895000
6	0.459556000	1.487242000	0.166729000
7	-1.145056000	-0.262610000	0.094843000
1	2.473423000	1.387204000	-0.734115000
6	-1.711553000	-1.575776000	0.407313000
6	0.026317000	0.146839000	0.433941000
1	-2.720484000	-1.402018000	0.783326000
1	-1.106890000	-2.013794000	1.199642000
79	1.391662000	-0.783318000	1.536974000
17	2.817071000	-2.075448000	2.791007000

31^{+}

1	0.059404000	4.381369000	-4.926144000
1	-2.123285000	4.366041000	-4.464020000
1	1.292658000	3.971263000	-3.722121000
6	0.300481000	4.385020000	-3.867080000
1	-2.047334000	2.593877000	-4.437382000
6	-2.006712000	3.497104000	-3.823263000
1	0.267465000	5.413533000	-3.499091000
7	-0.703213000	3.585522000	-3.169764000

1	-2.804630000	3.480139000	-3.088141000
6	-0.447830000	2.974126000	-1.996956000
1	1.485565000	3.931266000	-1.679476000
1	-2.305312000	1.834408000	-1.948241000
6	0.764328000	3.229007000	-1.293300000
6	-1.390130000	2.067852000	-1.428632000
6	1.008523000	2.611852000	-0.094000000
6	-1.132535000	1.470435000	-0.225549000
1	1.917897000	2.843474000	0.443527000
1	-1.856183000	0.791499000	0.203709000
6	0.072012000	1.719783000	0.461410000
1	2.172487000	0.616519000	1.233396000
6	0.308937000	1.102840000	1.772644000
7	1.489536000	0.611679000	1.986152000
79	-1.136278000	1.193833000	3.140152000
1	2.726975000	-0.671618000	3.032693000
6	1.961080000	0.067956000	3.263762000
1	1.119268000	-0.435556000	3.737149000
1	3.348452000	1.661809000	3.669562000
6	2.511400000	1.166645000	4.168675000
1	1.730742000	1.918138000	4.313177000
17	-2.806453000	1.325759000	4.740613000
1	3.744297000	-0.138251000	5.396549000
6	2.952368000	0.604524000	5.516111000
1	2.116105000	0.126761000	6.031674000

1	3.332244000	1.401153000	6.156977000

32^{+}

1	-0.512380000	-0.028339000	-3.039620000
1	1.386903000	-1.799666000	-3.739093000
6	-0.331241000	-0.981594000	-2.570866000
6	0.661434000	-1.925846000	-2.951633000
1	3.481896000	0.015821000	-1.647313000
6	-1.027253000	-1.512618000	-1.444182000
1	-1.832837000	-1.037754000	-0.908812000
6	0.580605000	-3.031838000	-2.069246000
1	1.241177000	-3.883990000	-2.064355000
6	2.842170000	-0.187302000	-0.803433000
6	-0.455988000	-2.780617000	-1.135509000
26	0.968542000	-1.238361000	-0.962918000
1	1.449113000	1.542050000	-0.835348000
1	-1.697528000	2.485015000	-0.677688000
6	1.757076000	0.614771000	-0.379496000
1	3.577618000	-2.166799000	-0.102703000
1	-3.372494000	3.023683000	-0.642066000
6	2.888486000	-1.345575000	0.010830000
1	-0.733696000	-3.416729000	-0.310791000
6	-2.443544000	3.004007000	-0.071094000
1	-2.106703000	4.034590000	0.064175000
6	1.113965000	-0.055595000	0.717994000

6	1.825312000	-1.282407000	0.940278000
1	-2.974362000	1.277949000	1.119309000
1	0.401518000	2.280218000	1.077556000
6	-2.652867000	2.312035000	1.271025000
1	1.577377000	-2.021421000	1.684152000
6	-0.064906000	0.374845000	1.474733000
7	-0.267270000	1.656614000	1.517928000
1	-3.447476000	2.807821000	1.833256000
6	-1.413182000	2.312777000	2.161585000
79	-1.305375000	-0.972402000	2.263829000
1	-1.099019000	3.330815000	2.388750000
1	-1.608514000	1.787900000	3.095201000
17	-2.782006000	-2.554509000	3.090030000

[33-N_2]$^+$

1	1.642037000	3.493317000	0.144684000
1	0.864031000	2.064088000	0.884792000
1	-5.330865000	0.130722000	-1.836960000
6	0.875574000	2.730502000	0.022000000
7	1.168533000	1.959085000	-1.152020000
6	-4.795896000	0.185302000	-0.903919000
1	-5.685101000	-1.203082000	0.527192000
6	-4.942778000	-0.460054000	0.290619000
8	-3.765942000	1.054521000	-0.858886000
1	-2.080361000	2.560192000	-1.118616000

6	-3.931907000	0.048160000	1.138133000
6	-3.222376000	0.975345000	0.410304000
7	-1.624453000	2.558502000	-0.212924000
1	-3.734587000	-0.224164000	2.161608000
6	-0.493937000	3.454617000	-0.069514000
6	-2.102458000	1.783079000	0.741920000
1	-0.588489000	4.023774000	0.854655000
1	-0.499638000	4.140611000	-0.912940000
79	-1.310129000	1.677904000	2.573347000
17	-0.408343000	1.548295000	4.702990000
6	0.654625000	0.623689000	-1.298374000
1	0.330875000	0.233890000	-0.338524000
1	-0.190294000	0.647006000	-1.998483000
1	1.427258000	-0.008318000	-1.739689000
6	1.949754000	2.540683000	-2.211578000
1	3.008980000	2.456741000	-1.937050000
1	1.775630000	2.006173000	-3.141072000
1	1.708545000	3.598861000	-2.308035000

[33-N_2]$^+$

1	-1.845459000	5.031618000	-1.993760000
1	-0.174296000	5.455561000	-1.526160000
1	1.363361000	1.549123000	1.550102000
6	-1.005772000	4.775114000	-1.349795000
7	-0.579087000	3.437523000	-1.662266000

6	0.294359000	1.445176000	1.631366000
1	-0.183963000	-0.472957000	2.557294000
6	-0.508877000	0.457506000	2.124202000
8	-0.439851000	2.476166000	1.168251000
1	-3.494053000	4.707098000	0.195552000
6	-1.835012000	0.908524000	1.949910000
6	-1.777439000	2.153839000	1.361083000
7	-2.651971000	4.207069000	0.443710000
1	-2.740265000	0.392607000	2.222114000
6	-1.429137000	4.931234000	0.136025000
6	-2.844426000	3.008818000	0.968706000
1	-0.625372000	4.637107000	0.798324000
1	-1.632543000	5.991739000	0.273079000
79	-4.722092000	2.325511000	1.152442000
17	-6.887761000	1.512846000	1.312400000
6	0.819364000	3.105343000	-1.593431000
1	1.287124000	3.647265000	-0.773615000
1	0.943141000	2.031509000	-1.485585000
1	1.289007000	3.429130000	-2.531503000
6	-1.519796000	2.468210000	-2.157921000
1	-1.382286000	2.384497000	-3.244520000
1	-1.310544000	1.493251000	-1.719672000
1	-2.536883000	2.790351000	-1.956866000

[33-Au-N_2]$^+$

1	0.638596000	2.619467000	-1.361761000
1	1.883455000	3.350087000	-0.339566000
1	-5.612169000	0.671538000	-0.230153000
6	1.155868000	2.535806000	-0.408827000
7	1.915367000	1.274700000	-0.404792000
6	-4.655090000	0.177906000	-0.241934000
1	-4.928590000	-1.932250000	-0.732097000
6	-4.276917000	-1.111247000	-0.486693000
8	-3.584283000	0.950476000	0.034910000
1	-1.932476000	2.542625000	0.451152000
6	-2.870120000	-1.139466000	-0.352813000
6	-2.471216000	0.137728000	-0.032645000
7	-1.092948000	1.972879000	0.461912000
1	-2.220303000	-1.990171000	-0.476245000
6	0.157720000	2.677627000	0.731080000
6	-1.190554000	0.694956000	0.215689000
1	0.574052000	2.327661000	1.675594000
1	-0.089654000	3.729348000	0.846147000
79	0.408845000	-0.528113000	0.196123000
17	2.040964000	-2.187160000	0.248280000
6	2.964758000	1.224667000	0.623962000
1	2.542028000	1.427235000	1.603917000
1	3.424526000	0.242174000	0.620409000
1	3.713007000	1.987352000	0.388318000
6	2.402106000	0.896995000	-1.738705000

1	3.095222000	1.668141000	-2.089537000
1	2.918143000	-0.056076000	-1.677301000
1	1.562504000	0.826421000	-2.424998000

[34-anilinyl]$^{+}$ with H-bond

1	-6.602915000	-0.226020000	2.308091000
1	-7.550804000	-0.897741000	0.968046000
6	-6.686269000	-0.290537000	1.220343000
1	-6.807486000	0.701377000	0.798265000
1	-5.020884000	1.609590000	1.282291000
7	-5.499553000	-0.944725000	0.676027000
1	-6.348927000	-2.765294000	1.188780000
6	-4.242592000	1.109035000	0.728914000
1	-4.648098000	-2.871035000	0.702541000
1	-2.990533000	2.821606000	0.734727000
6	-5.599397000	-2.391012000	0.497699000
6	-4.383079000	-0.260424000	0.361749000
6	-3.096398000	1.793210000	0.417246000
6	-3.313584000	-0.894947000	-0.334900000
6	-2.045148000	1.159184000	-0.271218000
1	-5.915488000	-2.612989000	-0.524715000
1	-1.837745000	3.442332000	-1.329608000
1	-3.400830000	-1.921849000	-0.651662000
6	-2.174955000	-0.197539000	-0.628809000
1	0.936577000	3.924033000	-0.649846000

7	-0.921975000	3.064749000	-1.065306000
6	-0.798296000	1.876316000	-0.570698000
1	-0.887570000	4.383222000	-3.877872000
1	-1.364603000	-0.686190000	-1.151661000
6	0.150709000	4.000367000	-1.398218000
1	0.570002000	3.713997000	-2.363561000
79	0.919826000	0.965188000	-0.144987000
6	-1.418466000	5.309139000	-3.658042000
1	-0.820901000	6.149605000	-4.044046000
1	-2.368444000	5.287534000	-4.192020000
6	-0.446377000	5.403475000	-1.433759000
7	-1.673662000	5.430347000	-2.225601000
17	2.880861000	-0.174291000	0.343849000
1	-0.698506000	5.704458000	-0.415506000
1	0.314697000	6.103092000	-1.808179000
1	-3.413603000	6.560020000	-2.490458000
6	-2.476203000	6.613500000	-1.935612000
1	-2.704228000	6.653982000	-0.870177000
1	-1.963057000	7.546121000	-2.217780000

$[34\text{-}N_2]^+$

1	-6.940744000	0.798211000	0.849942000
1	-7.638782000	-0.782452000	0.478240000
6	-6.853227000	-0.083424000	0.211307000
1	-6.996303000	0.220239000	-0.827749000

1	-5.364360000	1.778683000	-0.483208000
7	-5.561422000	-0.736718000	0.393358000
1	-6.552873000	-2.439075000	1.059868000
6	-4.427800000	1.260786000	-0.349262000
1	-4.963594000	-2.197387000	1.795955000
1	-3.347307000	2.932932000	-0.997024000
6	-5.535211000	-2.115314000	0.869440000
6	-4.416313000	-0.087159000	0.114139000
6	-3.262480000	1.916404000	-0.635164000
6	-3.150436000	-0.716434000	0.263813000
6	-1.996555000	1.296126000	-0.488673000
1	-5.090153000	-2.778981000	0.124756000
1	-1.642216000	3.735320000	-1.128061000
1	-3.088485000	-1.736479000	0.608647000
6	-1.996160000	-0.042443000	-0.035182000
1	1.078600000	3.379292000	-2.069817000
7	-0.773698000	3.216386000	-1.159666000
6	-0.749941000	1.940061000	-0.794436000
1	3.343896000	3.188024000	-0.319303000
1	-1.046385000	-0.548907000	0.079267000
6	0.386324000	3.990271000	-1.495199000
1	0.079926000	4.854378000	-2.079966000
79	1.030465000	1.006923000	-0.671755000
6	3.486676000	4.146873000	-0.811040000
1	4.422076000	4.609847000	-0.498570000

1	3.536348000	3.985588000	-1.895735000
6	1.118849000	4.481284000	-0.184533000
7	2.389800000	5.032115000	-0.504507000
17	3.135533000	0.022683000	-0.521419000
1	0.502415000	5.226732000	0.312306000
1	1.256877000	3.606550000	0.451082000
1	2.463517000	6.527170000	-1.950959000
6	2.512135000	6.423510000	-0.859028000
1	1.706647000	6.994915000	-0.406648000
1	3.482421000	6.797004000	-0.531872000

[34-Au-N_2]$^+$

1	-6.483751000	0.877086000	1.333325000
1	-7.571647000	0.227901000	0.101287000
6	-6.591830000	0.663632000	0.267379000
1	-6.533089000	1.603840000	-0.285424000
1	-4.555522000	1.972947000	0.823134000
7	-5.576202000	-0.278927000	-0.187742000
1	-7.084601000	-1.619211000	-0.691626000
6	-3.832672000	1.265701000	0.447802000
1	-5.586469000	-2.391799000	-0.159675000
1	-2.223884000	2.514836000	0.987132000
6	-6.001971000	-1.561482000	-0.734980000
6	-4.266828000	0.026651000	-0.105136000
6	-2.501348000	1.574088000	0.528410000

6	-3.265502000	-0.875411000	-0.557002000
6	-1.503471000	0.679974000	0.075018000
1	-5.689352000	-1.668312000	-1.776474000
1	-0.397228000	2.972933000	0.145767000
1	-3.542717000	-1.824957000	-0.986672000
6	-1.937280000	-0.556031000	-0.453078000
1	1.642672000	3.764929000	0.449155000
7	0.286995000	2.232693000	0.245988000
6	-0.105457000	0.986574000	0.154238000
1	4.999699000	1.274345000	-0.009468000
1	-1.199806000	-1.264304000	-0.810276000
6	1.665381000	2.678911000	0.411543000
1	2.055982000	2.321526000	1.364322000
79	1.236817000	-0.516638000	0.182656000
6	4.128427000	0.703185000	0.325745000
1	4.383676000	-0.348952000	0.402101000
1	3.813853000	1.070752000	1.298845000
6	2.557673000	2.251311000	-0.748960000
7	3.047202000	0.869886000	-0.655374000
17	2.518598000	-2.476729000	0.342751000
1	2.013048000	2.359693000	-1.684400000
1	3.428772000	2.912941000	-0.780408000
1	3.687597000	-0.742372000	-1.830017000
6	3.381103000	0.291144000	-1.963332000
1	2.512349000	0.339282000	-2.614855000

1	4.202492000	0.861307000	-2.409223000

[35-Au-N_2]$^+$

1	-0.367826000	0.797927000	-2.719328000
1	1.188835000	-1.156265000	-3.723482000
6	-0.350435000	-0.229388000	-2.394064000
6	0.472234000	-1.263876000	-2.925657000
1	3.510993000	-0.172148000	-1.749798000
6	-1.116203000	-0.784100000	-1.333471000
1	-1.818315000	-0.249649000	-0.714271000
6	0.213481000	-2.455066000	-2.190487000
1	0.702565000	-3.404832000	-2.332978000
6	2.901847000	-0.362242000	-0.881293000
6	-0.765759000	-2.159692000	-1.201528000
26	0.911512000	-0.976500000	-0.932921000
1	1.925878000	1.606864000	-0.538031000
6	2.065035000	0.580449000	-0.240440000
1	3.258263000	-2.533564000	-0.501166000
6	2.765497000	-1.617363000	-0.220789000
1	-1.160267000	-2.846414000	-0.470530000
7	-1.872972000	0.549298000	4.000849000
6	1.393942000	-0.096251000	0.841676000
6	1.831910000	-1.472713000	0.827117000
1	-0.195148000	1.736350000	4.356569000
1	0.834324000	2.310643000	1.380940000

6	-1.166417000	1.834450000	3.876228000
1	1.511914000	-2.240807000	1.511765000
6	0.300413000	0.397824000	1.625927000
7	0.136771000	1.682360000	1.764634000
1	-1.746657000	2.581976000	4.426293000
6	-0.984077000	2.327064000	2.447899000
79	-0.999359000	-0.955904000	2.348368000
1	-1.891901000	2.197910000	1.858594000
1	-0.763034000	3.390730000	2.478644000
17	-2.355415000	-2.789313000	2.869272000
6	-3.309432000	0.638488000	3.699682000
1	-3.784352000	1.289851000	4.439541000
1	-3.462986000	1.053098000	2.707324000
1	-3.747628000	-0.353379000	3.748149000
6	-1.611529000	-0.111669000	5.287621000
1	-2.121211000	-1.070229000	5.306777000
1	-0.541461000	-0.255884000	5.411096000
1	-1.990141000	0.521949000	6.095848000

[35-Fe]$^{+}$

1	0.003950000	1.052897000	-2.898029000
1	0.893439000	-1.327142000	-3.780999000
6	-0.295663000	0.086505000	-2.526918000
6	0.162409000	-1.172146000	-3.003890000
1	3.517205000	-0.862543000	-1.524781000

6	-1.199799000	-0.158377000	-1.450832000
1	-1.711989000	0.587248000	-0.865441000
6	-0.453989000	-2.188096000	-2.231050000
1	-0.262954000	-3.246146000	-2.312728000
6	2.817610000	-0.826009000	-0.704987000
6	-1.291696000	-1.568632000	-1.269654000
26	0.676489000	-0.883611000	-0.960945000
1	2.365316000	1.342846000	-0.563507000
6	2.198899000	0.341273000	-0.200785000
1	2.537916000	-2.977492000	-0.209081000
6	2.294912000	-1.945756000	-0.012093000
1	-1.863291000	-2.073145000	-0.507658000
7	-2.037341000	4.501636000	2.151329000
6	1.273782000	-0.056060000	0.826064000
6	1.338355000	-1.487079000	0.921995000
1	-0.579690000	4.219696000	0.692313000
1	1.615715000	2.346511000	1.356568000
6	-1.100401000	3.638598000	1.455012000
1	0.748236000	-2.094610000	1.588139000
6	0.374657000	0.789780000	1.614048000
7	0.739221000	2.028697000	1.758761000
1	-1.613877000	2.808158000	0.940533000
6	-0.064086000	3.055171000	2.420729000
79	-1.350618000	0.065494000	2.309899000
1	0.610728000	3.833276000	2.770389000

1	-0.545080000	2.590863000	3.278578000
17	-3.384519000	-0.763915000	3.042446000
6	-3.044528000	3.736356000	2.880105000
1	-3.674094000	3.135827000	2.203361000
1	-2.576939000	3.057362000	3.591987000
1	-3.687558000	4.418554000	3.436421000
6	-2.669596000	5.449644000	1.241179000
1	-3.324916000	6.113569000	1.806160000
1	-1.907962000	6.053202000	0.746394000
1	-3.274920000	4.949377000	0.466975000

[35-Fe]$^{+}$ with H-bond

1	-0.653455000	0.317236000	-3.003910000
1	0.907322000	-1.724555000	-3.805141000
6	-0.595572000	-0.655609000	-2.544074000
6	0.218107000	-1.739700000	-2.976352000
1	3.329856000	-0.132817000	-1.853558000
6	-1.300271000	-1.078676000	-1.377853000
1	-1.985557000	-0.484539000	-0.795949000
6	0.015866000	-2.824818000	-2.086780000
1	0.534346000	-3.769736000	-2.115932000
6	2.731035000	-0.291081000	-0.970900000
6	-0.915294000	-2.420875000	-1.097996000
26	0.740062000	-1.112081000	-1.018535000
1	1.552230000	1.588369000	-0.851243000

6	1.781085000	0.616212000	-0.444976000
1	3.274399000	-2.366782000	-0.379585000
6	2.697433000	-1.475153000	-0.194454000
1	-1.238556000	-3.008495000	-0.254024000
7	0.102144000	4.533401000	1.177384000
6	1.142702000	-0.013321000	0.677906000
6	1.715903000	-1.321928000	0.811904000
1	-1.675894000	3.621891000	0.612212000
1	0.746202000	2.399072000	1.169285000
6	-1.163066000	3.896386000	1.535350000
1	1.434164000	-2.054446000	1.550185000
6	0.073070000	0.521880000	1.529093000
7	0.045546000	1.812395000	1.629899000
1	-1.828627000	4.565445000	2.099272000
6	-0.924618000	2.629684000	2.351329000
79	-1.244586000	-0.730025000	2.350442000
1	-0.514380000	2.856133000	3.336704000
1	-1.842592000	2.062534000	2.482831000
17	-2.779019000	-2.249645000	3.193083000
6	0.697726000	5.254391000	2.298596000
1	0.065746000	6.092006000	2.632638000
1	0.853899000	4.586283000	3.145150000
1	1.667553000	5.652259000	1.999301000
6	-0.039691000	5.401875000	0.013819000
1	0.936646000	5.802320000	-0.261160000

1	-0.430412000	4.830096000	-0.828456000
1	-0.717153000	6.249443000	0.203111000

[36-Au-Cp]$^{+}$

1	-0.791984000	-3.073017000	-1.937270000
1	1.418656000	-4.484168000	-1.331517000
6	-0.339284000	-3.146505000	-0.961721000
6	0.843196000	-3.882711000	-0.645352000
1	2.571032000	-1.182778000	-2.638012000
6	-0.782265000	-2.481693000	0.217904000
6	1.135625000	-3.672938000	0.731604000
1	1.972198000	-4.087397000	1.272214000
6	2.214995000	-0.801651000	-1.694821000
6	0.139031000	-2.798588000	1.264258000
26	1.101609000	-1.851812000	-0.267475000
1	0.150067000	-0.100983000	-2.188504000
1	-0.657909000	3.807217000	1.399021000
6	0.937818000	-0.229494000	-1.464979000
1	3.913850000	-1.229825000	-0.309214000
1	-2.124328000	4.682072000	1.833499000
6	2.928584000	-0.820127000	-0.462399000
1	0.110790000	-2.417346000	2.272563000
6	-1.465069000	3.865757000	2.132611000
1	-1.025515000	4.124942000	3.099216000
6	0.857963000	0.129887000	-0.073486000

6	2.110735000	-0.239943000	0.538038000
1	-2.674252000	2.308394000	1.242972000
1	0.618084000	1.476235000	2.009020000
6	-2.237726000	2.553386000	2.215114000
1	2.352212000	-0.157175000	1.585238000
6	-0.374327000	0.405177000	0.649367000
7	-0.282782000	1.083689000	1.756358000
1	-3.068552000	2.648265000	2.918815000
6	-1.390429000	1.371856000	2.676598000
79	-2.043265000	-0.636438000	0.110504000
1	-0.943274000	1.572584000	3.650252000
1	-1.996976000	0.471865000	2.759344000
17	-4.123625000	-1.500956000	-0.606539000

[37-Au-Cp]$^{+}$

1	-1.207882000	-2.062581000	-2.056077000
1	0.564009000	-4.086218000	-1.933799000
6	-0.771956000	-2.465623000	-1.156213000
6	0.179643000	-3.528802000	-1.094035000
1	2.534716000	-0.991100000	-2.589929000
6	-1.002065000	-1.992941000	0.167646000
6	0.541422000	-3.714971000	0.269924000
1	1.248592000	-4.438088000	0.645103000
6	2.304692000	-0.751772000	-1.564543000
6	-0.178602000	-2.759152000	1.050213000

26	0.972014000	-1.769888000	-0.314196000
1	0.496170000	0.550416000	-1.749132000
6	1.229668000	0.063998000	-1.127947000
1	3.844704000	-1.901911000	-0.426504000
6	3.003440000	-1.227760000	-0.418394000
1	-0.087465000	-2.620794000	2.115742000
6	1.266880000	0.112314000	0.310504000
6	2.383362000	-0.694582000	0.738142000
1	0.150933000	3.307840000	3.546230000
1	1.425239000	0.988013000	2.640553000
6	-0.786229000	2.783951000	3.349286000
1	2.652349000	-0.913097000	1.758829000
6	0.162323000	0.528638000	1.161293000
7	0.448945000	0.896873000	2.377233000
1	-1.103284000	3.054167000	2.327201000
6	-0.520378000	1.279975000	3.399919000
79	-1.729265000	0.090929000	0.534631000
1	-0.114088000	1.001771000	4.371212000
1	-1.426783000	0.705042000	3.228185000
17	-3.958461000	-0.076738000	-0.230484000
7	-1.762692000	3.189847000	4.348030000
6	-3.119963000	2.804643000	3.976247000
6	-1.688383000	4.622892000	4.606849000
1	-2.394331000	4.887351000	5.395196000
1	-0.683266000	4.887590000	4.937659000

1	-1.929947000	5.225998000	3.715506000
1	-3.810159000	3.104156000	4.765343000
1	-3.197202000	1.724816000	3.855793000
1	-3.441842000	3.279695000	3.034594000

[37-Au-Cp]$^{+}$ with H-bond

1	-0.793386000	-3.300630000	-1.685512000
1	1.543188000	-4.495717000	-1.080463000
6	-0.283936000	-3.247172000	-0.737007000
6	0.963856000	-3.866777000	-0.422872000
1	2.408200000	-1.291645000	-2.762327000
6	-0.707548000	-2.495282000	0.396229000
6	1.314868000	-3.498244000	0.906311000
1	2.206367000	-3.799965000	1.433550000
6	2.066017000	-0.834196000	-1.848432000
6	0.288410000	-2.641851000	1.410569000
26	1.095281000	-1.794720000	-0.262925000
1	-0.062786000	-0.328453000	-2.309401000
6	0.762196000	-0.326349000	-1.616449000
1	3.848717000	-0.994680000	-0.511512000
6	2.831071000	-0.670563000	-0.658181000
1	0.285478000	-2.166486000	2.378432000
6	0.715400000	0.174632000	-0.268179000
6	2.016622000	-0.041225000	0.315036000
1	-1.327768000	3.676488000	2.266823000

1	0.475355000	1.714035000	1.715196000
6	-1.177691000	2.935880000	3.054324000
1	2.298741000	0.173513000	1.333055000
6	-0.502757000	0.446763000	0.482160000
7	-0.403782000	1.237797000	1.508567000
1	-1.913551000	3.139917000	3.846951000
6	-1.448015000	1.551511000	2.478121000
79	-2.103246000	-0.775362000	0.170640000
1	-1.452637000	0.787439000	3.256945000
1	-2.414861000	1.520742000	1.976704000
17	-4.101905000	-1.953153000	-0.298541000
7	0.198505000	3.058686000	3.528201000
6	0.433554000	2.315258000	4.760699000
6	0.592933000	4.454174000	3.674982000
1	1.644057000	4.506648000	3.961159000
1	0.465191000	4.974908000	2.725615000
1	0.001726000	4.979662000	4.442241000
1	1.480880000	2.412928000	5.046769000
1	0.221698000	1.255552000	4.618815000
1	-0.189997000	2.682648000	5.591685000

[37-Au-$C_{Carbene}$]$^{+}$

1	-0.752879000	-3.070796000	-1.733436000
1	1.394195000	-4.590886000	-1.181887000
6	-0.244033000	-3.118642000	-0.784456000

6	0.904886000	-3.914569000	-0.498651000
1	2.986453000	-1.515440000	-2.538662000
6	-0.576111000	-2.349376000	0.372740000
6	1.294518000	-3.651790000	0.845148000
1	2.129177000	-4.096193000	1.364331000
6	2.534642000	-1.024563000	-1.691846000
6	0.386557000	-2.687607000	1.380171000
26	1.308328000	-1.893156000	-0.252153000
1	0.518100000	-0.432379000	-2.467034000
6	1.234122000	-0.449526000	-1.662132000
1	4.095289000	-1.222369000	-0.103847000
6	3.123201000	-0.865281000	-0.404154000
1	0.444493000	-2.255701000	2.366420000
6	1.010466000	0.078794000	-0.343559000
6	2.199254000	-0.174222000	0.426354000
1	-2.142166000	1.328193000	2.746013000
1	0.736506000	2.096262000	1.064006000
6	-2.478870000	1.887295000	1.873043000
1	2.333577000	0.060499000	1.470152000
6	-0.265048000	0.622087000	0.127793000
7	-0.182057000	1.712799000	0.870519000
1	-3.161074000	2.672558000	2.218431000
6	-1.299025000	2.580566000	1.223259000
79	-1.862959000	-0.756089000	0.436909000
1	-1.615518000	3.133253000	0.335816000

1	-0.921709000	3.309979000	1.938024000
17	-3.899876000	-2.239051000	-0.178438000
7	-3.237607000	0.946902000	1.015623000
6	-3.777492000	1.599619000	-0.192116000
6	-4.359988000	0.422231000	1.824856000
1	-4.915132000	-0.301681000	1.238144000
1	-3.965304000	-0.067649000	2.713008000
1	-5.015317000	1.245959000	2.127106000
1	-4.386002000	0.875310000	-0.728947000
1	-2.967162000	1.922145000	-0.840726000
1	-4.394370000	2.462944000	0.079667000

6.5 References

1 G. C. Senadi, W.-P. Hu, J.-S. Hsiao, J. K. Vandavasi, C.-Y. Chen and J.-J. Wang, *Org. Lett.*, 2012, **14**, 4478–4481.

2 R. D. Gorsich, *J. Am. Chem. Soc.*, 1962, **84**, 2486–2491.

3 H. Meerwein, *Org. Synth.*, 1966, **46**, 113.

4 D. E. Giordano, G.; Crabtree, R. H.; Heintz, R.M.; Forster, D.; Morris, in *Inorganic Syntheses*, ed. R. J. Angelici, Wiley & Sons, Inc., New york, 28th edn., 1991, pp. 88–89.

5 J. Choudhury, S. Podder and S. Roy, *J. Am. Chem. Soc.*, 2005, **127**, 6162–6163.

6 C. Huerta-Aguilar, J. M. Talamantes Gómez, P. Thangarasu, I. Camacho-Arroyo, A. González-Arenas, J. Narayanan and R. Srivastava, *Appl. Organomet. Chem.*, 2013, **27**, 578–587.

7 Bruker, APEX-3, SAINT+, Version 6.02 (Includes XPREP and SADABS), Bruker AXS Inc., Madison, Wisconsin, USA, 2016.

8 L. J. Farrugia, *J. Appl. Crystallogr.*, 2012, **45**, 849–854.

9 G. M. Sheldrick, *Acta Crystallogr. Sect. C Struct. Chem.*, 2015, **71**, 3–8.

10 O. V Dolomanov, L. J. Bourhis, R. J. Gildea, J. A. K. Howard and H. Puschmann, *J. Appl. Crystallogr.*, 2009, **42**, 339–341.

11 A. L. Spek, *Acta Crystallogr. Sect. D*, 2009, **65**, 148–155.

12 S. Stoll and A. Schweiger, *J. Magn. Reson.*, 2006, **178**, 42–55.

13 A. Neidlinger, T. Kienz and K. Heinze, *Organometallics*, 2015, **34**, 5310–5320.

14 G. R. Eaton, S. S. Eaton, D. P. Barr and R. T. Weber, in *Quantitative EPR*, Springer, 2010, pp. 25–36.

15 F. Neese, *WIREs Comput. Mol. Sci.*, 2012, **2**, 73–78.

16 A. D. Becke, *J. Chem. Phys.*, 1993, **98**, 5648–5652.

17 C. Lee, W. Yang and R. Parr, *Phys. Rev. A*, 1988, **38**, 3098.

18 B. Miehlich, A. Savin, H. Stoll and H. Preuss, *Chem. Phys. Lett.*, 1989, **157**, 200–206.

19 F. Neese, F. Wennmohs, A. Hansen and U. Becker, *Chem. Phys.*, 2009, **356**, 98–109.

20 R. Izsák and F. Neese, *J. Chem. Phys.*, 2011, **135**, 144105.

21 D. A. Pantazis, X.-Y. Chen, C. R. Landis and F. Neese, *J. Chem. Theory Comput.*, 2008, **4**, 908–919.

22 V. Barone and M. Cossi, *J. Phys. Chem. A*, 1998, **102**, 1995–2001.

23 S. Miertuš, E. Scrocco and J. Tomasi, *Chem. Phys.*, 1981, **55**, 117–129.

24 F. Weigend and R. Ahlrichs, *Phys. Chem. Chem. Phys.*, 2005, **7**, 3297–3305.

25 F. Weigend, *Phys. Chem. Chem. Phys.*, 2006, **8**, 1057–1065.

26 D. A. Pantazis and F. Neese, *J. Chem. Theory Comput.*, 2009, **5**, 2229–2238.

27 D. A. Pantazis and F. Neese, *Theor. Chem. Acc.*, 2012, **131**, 1292.

28 D. A. Pantazis and F. Neese, *J. Chem. Theory Comput.*, 2011, **7**, 677–684.

29 S. Grimme, *J. Chem. Phys*, 2010, **132**, 1–19.

30 S. Grimme, S. Ehrlich and L. Goerigk, *J. Comput. Chem.*, 2011, **32**, 1456–1465.